SCUOLA DI DOTTORATO

UNIVERSITÀ DEGLI STUDI DI MILANO-BICOCCA

Dipartimento di / Department of Earth and Environmental Sciences

Dottorato di Ricerca in / PhD program: School of Chemical, Geological and Environmental Sciences Ciclo / Cycle XXXIII

Curriculum in Terrestrial and Marine Environmental Sciences

STUDY ON THE BIO-INTERACTION AND TOXIC EFFECTS OF PARTICLES EMITTED FROM DIFFERENT SOURCES: CONTRIBUTION TO RISK MANAGEMENT

Cognome / Surname: **ZERBONI** Nome / Name: **ALESSANDRA**

Matricola / Registration number: **775228**

Tutore / Tutor: Prof.ssa MARIA LUCE FREZZOTTI

Tutore esterno/External tutor: Ing. SIMONE CASADEI

Supervisore/Supervisor: Prof. PARIDE MANTECCA

Coordinatore / Coordinator: Prof.ssa MARIA LUCE FREZZOTTI

ANNO ACCADEMICO / ACADEMIC YEAR 2019/2020

We rise, we fall. We may rise by falling.

Defeat shapes us. Our only wisdom is tragic,

known too late, and only to the lost.

GUY DAVENPORT

CONTENTS

This thesis was submitted to the PhD School of Chemical, Geological and Environmental Sciences, University of Milano-Bicocca, as the final fulfilment of the requirements to obtain the PhD degree. The work presented was carried out in the years 2017-2020 in the laboratory of Prof. Paride Mantecca at the Department of Earth and Environmental Sciences, (DISAT)- POLARIS research centre (Polveri in Ambiente e Rischio per la Salute) University of Milano-Bicocca, Italy, in collaboration with INNOVHUB SSI (Fuels Department) Milan, Italy, under the co-supervision of Ing. Simone Casadei. I additionally spent a visiting period during the last year of PhD at the Consumer Products Safety Unit of the European Commission's Joint Research Centre, Ispra (VA), Italy.

ABSTRACT

Due to cardiovascular and respiratory diseases, air pollution remains a global issue for the 21st century. There is an urgent need to establish the real impact of Particulate Matter (PM) on human health by including the analysis of sources, size distribution, physico-chemical (P-chem) composition, and toxicological mechanisms. Increasing *in vitro* data for establishing pathways of toxicity in human cell lines exposed to specific air pollutants from rigorously characterized emission sources, could help to improve scientifically sound approaches in health risk characterizations, which finally may result in regulatory actions potentially more effective to protect public health. The aim of this thesis was to study the *in vitro* effects of particles emitted from different combustion sources using human lung cells, focusing on the relationship between the PM P-chem attributes and the cellular and molecular pathways that drive the toxicity. *In vitro* models, representative of the human respiratory system, were used to study the bio-interaction and toxicological effects of particles. Different exhaust particles were compared, with special emphasis on fine and ultrafine Particles (UFPs), namely Diesel exhaust particles (DEPs) from old and new generation vehicles and on particles emitted from the combustion of solid biomass fuels for residential heating. The emissions from vehicles and biomass-propelled stoves, as well as the PM collection, were performed in collaboration with INNOVHUB SSI (Fuels Department), while the P-chem characterization and toxicological studies were carried out in the Department of Earth and Environmental Sciences (DISAT)- POLARIS research centre (Polveri in Ambiente e Rischio per la Salute) and at the Consumer Products Safety Unit of the European Commission's Joint Research Centre. The results of this work show that testing different material sampled in realistic conditions allows evaluating how the toxicity of particles may vary in relation to the source. These data suggest that oxidative stress and inflammatory cytokines releases are crucial events after DEP exposure, which can also lead to vascular endothelial activation. Comparing an old generation diesel vehicle

without DPF (Diesel Particulate Filter) and last generation (or “Euro 6”) one during regeneration of DPF, we proved that Euro 6 is less powerful in activating the biological response, and it is characterized by different metal composition and less concentration of Polycyclic Aromatic Hydrocarbons (PAHs) than the old generation engine, although the exhaust emission from Euro 6 during DPF regeneration is characterized by a higher number of nucleation-mode particles. DEP emitted from an old generation diesel vehicle was confirmed as a very hazardous component of the urban PM, even when compared to Combustion derived particles (CDPs) from wood burning. However, the possible consequences on human health from chronic exposure to the wood CDPs should not be excluded. Moreover, the co-exposure effects of Metal Oxide Nanoparticles (NPs), representative of non-exhaust sources, and DEP were also evaluated. The co-exposure with DEP can either reduce the toxicity of NPs or enhance it. This finding indicates that the possible interaction of different hazardous airborne particles and the toxicity deriving from the mixture effects should be evaluated. In addition, this thesis highlights the significance to evaluate the contribution to PM of emission sources commonly poorly considered in the risk assessment, as latest-generation diesel vehicles and CDPs from biomass burning. The results presented in this work offer a contribution to our understanding of the physic-chemical properties and biological outcomes of particulate most relevant to public health, underlining the importance to evaluate different sources of PM, including exhaust, non-exhaust, and the potential co-exposure of both.

RIASSUNTO

L'inquinamento atmosferico rimane un problema globale per il 21 °secolo, in quanto causa di malattie cardiovascolari e respiratorie. È urgente stabilire il reale impatto del particolato (PM) sulla salute umana includendo l'analisi delle fonti, la distribuzione delle dimensioni, la composizione fisico-chimica (P-chem) e i meccanismi tossicologici. L'aumento dei dati *in vitro* per stabilire i meccanismi di tossicità utilizzando linee cellulari umane esposte a specifici inquinanti atmosferici da fonti di emissione rigorosamente caratterizzate, potrebbe aiutare a validare approcci scientifici nella caratterizzazione dei rischi per la salute, che alla fine possono determinare azioni normative potenzialmente più efficaci per proteggere la salute pubblica. Lo scopo di questa tesi è stato quello di studiare gli effetti *in vitro* delle particelle emesse da diverse fonti di combustione utilizzando cellule polmonari umane, concentrandosi sulla relazione tra le caratteristiche P-chem del PM e i processi cellulari e molecolari che inducono la tossicità. Sono stati utilizzati modelli *in vitro* rappresentativi del sistema respiratorio umano per studiare la bio-interazione e gli effetti tossicologici delle particelle. Sono state confrontate diverse particelle derivate da combustione, con particolare attenzione alle particelle fini e ultrafini (UFPs), ovvero le particelle emesse allo scarico di veicoli di vecchia e nuova generazione diesel (DEP) e alle particelle emesse dalla combustione di biomassa solida per il riscaldamento residenziale. Le emissioni dei veicoli e delle stufe a biomasse, così come la raccolta del PM, sono state eseguite in collaborazione con INNOVHUB SSI (Area Combustibili), mentre la caratterizzazione P-chem e gli studi tossicologici sono stati effettuati presso il Dipartimento di Scienze della Terra e dell'Ambiente (DISAT) - Centro di ricerca POLARIS (Polveri in Ambiente e Rischio per la Salute) e presso l'Unità Consumer Products Safety del Centro Comune di Ricerca della Commissione Europea. I risultati di questo lavoro mostrano che testare diversi materiali campionati in condizioni realistiche consente di valutare come la tossicità delle particelle possa variare in relazione alla fonte. Questi dati suggeriscono che lo stress ossidativo e

il rilascio di citochine infiammatorie sono eventi cruciali dopo l'esposizione a DEP, che possono anche portare all'attivazione dell'endotelio vascolare. Confrontando un veicolo diesel di vecchia generazione senza DPF (Diesel Particulate Filter) e uno di ultima generazione (o "Euro 6") durante la rigenerazione del DPF abbiamo dimostrato che il DEP Euro 6 determina una minore risposta biologica, ed è caratterizzato da diversa composizione metallica e minore concentrazione di Idrocarburi Policiclici Aromatici (IPA) rispetto a quello emesso allo scarico del veicolo di vecchia generazione, sebbene le emissioni da Euro 6 durante la rigenerazione del DPF siano caratterizzate da un maggior numero di particelle in modalità nucleazione. Il DEP emesso da un veicolo diesel di vecchia generazione si è confermato essere un componente molto pericoloso del PM urbano, anche rispetto alle particelle derivate dalla combustione (CDPs) di legna. Tuttavia, non si devono escludere possibili conseguenze sulla salute umana derivanti dall'esposizione cronica alle CDPs da biomassa. Inoltre, sono stati valutati anche gli effetti della co-esposizione di nanoparticelle di ossido di metallo (NPs), rappresentative dell'inquinamento non combustivo in miscela con DEP. La co-esposizione con DEP può ridurre la tossicità delle NPs o aumentarla. Questo risultato indica che è necessario valutare la possibile interazione di diverse particelle pericolose presenti in atmosfera e la tossicità derivante dagli effetti della loro miscela. Inoltre, questo lavoro evidenzia l'importanza di valutare il contributo al PM da parte di fonti di emissione generalmente poco considerate nella valutazione del rischio, come le emissioni allo scarico dei veicoli diesel di ultima generazione e le CDPs da combustione di biomasse. I risultati presentati in questa tesi offrono un contributo alla nostra comprensione delle proprietà fisico-chimiche e dei risultati biologici di particolato più rilevanti per la salute pubblica, sottolineando l'importanza di valutare diverse fonti di PM, incluse fonti da processi combustivi, non-combustivi e la potenziale co-esposizione ad entrambi.

FOREWORD

The impact of air pollution on health has been studied by the world scientific community over the last decades and has become part of the political debate due to the adverse consequences on public health. PM is the most harmful form of air pollution, especially the fine an ultrafine fraction, due to their ability to penetrate deep into the lungs, blood streams and brain. To recognize the toxicity of different air pollutants for human populations, and to develop an environmental health policy, it is necessary to analyse and monitor the toxic effects of exposure to PM from different sources. It is pivotal to identify the most toxic PM present in the environment, and the chemical compositions that trigger the most dangerous biological effects, in order to concentrate efforts to reduce these components through regulatory policy. All the aspects regarding the mechanisms of toxicity of the different component of PM are not yet entirely clear, and the increasing data provided by *in vitro* studies may serve as the basis for the characterization of biomarkers in the exposed population. Application of these biomarkers for risk assessment can be extremely helpful as predictive tools for public health. Research, in fact, has the strong social responsibility of providing up-to-date results and guarantee their relevance to environmental policy.

CHAPTER I

INTRODUCTION

The first chapter is divided into four parts. It presents the definition of air pollution, composition, and sources, and frames the scenario in which the topic of the thesis is developed. The next part is devoted to the description of the health effects of particulate matter (PM), while highlighting the cellular mechanisms involved in the toxicity of PM. The chapter also presents a brief overview to the relation between air quality and COVID-19 Pandemic.

1.1 ATMOSPHERIC POLLUTION

Word health organization (WHO) defines air pollution as the contamination of either indoor or outdoor environments by any chemical, physical, or biological agent that modifies the natural characteristics of the atmosphere. Tropospheric air pollution has a long history and is caused by solid and liquid particles and certain gases that are suspended in the air. From at least the 13th century up to the mid-20th century, the problems of air pollution were largely correlated with high concentrations of soot particles and sulphur dioxide (SO_2). With the industrial growth the levels of air pollution increased in the developing areas of the word. Major constituents of outdoor air pollutants include ozone, carbon monoxide (CO), volatile organic compounds (VOCs), nitrogen oxides (NO_x), sulphur oxides (SO_x), and particulate matter (PM), derived from common by-products of traffic emissions, industrial processes and power plants (Finlayson and Pitts; 1997). Biomass burning for cooking or heating and all the processes that release gases or particles are primary contributors to air pollution in developing countries (Li et al., 2021). PM is the solid component of air pollution

with a combination of particles that vary in both size and chemical composition. Before industrialization PM derived mainly from natural sources, crustal and burning of biomass, with the development of automotive transport the anthropogenic contribution to PM became predominant. All the gaseous, and particles are diluted into the atmosphere, processed and transported depending on weather condition (Zhang et al., 2018). According to Klimont and colleagues global emission of PM have not undergone particular change between 1990 and 2010, but there were different regional trends, in fact while in North America, Pacific regions and Europe there was a reduction in emission by 30 to over 50 %, in Asia and Africa there was an increase by about 30% (Klimont et al., 2016). According to the EEA report 2019 the main sectors contributing to air pollution in Europe are: transport, commercial, energy, industry, agriculture, and waste. In the period 2015-2017 about 8 % of the urban population in the EU-28 was exposed to levels above the EU annual limit value of $PM_{2.5}$ (25 µg/m^3), and approximately 77 % was exposed to concentrations exceeding the WHO air quality guidelines (AQG) value (10 µg/m^3) for $PM_{2.5.}$

1.1.1 PM Physico-Chemical properties

Particulate matter is a complex mixture of small particles and liquid droplets (Pope and Dockery; 2006). PM is composed of different components, including acids (such as nitrates and sulphates), metals, organic chemicals, and soil or dust particles. It is convenient to classify the particles by their generation process and aerodynamic diameter. According to the sources PM can be classified as primary, emitted directly from an emission source, or secondary, generated by PM precursors, which are pollutant that are partly transformed into particles by photo-chemical reactions in the atmosphere (European Environment Agency (EEA)).

The aerodynamic properties of the particles are used as a parameter to classify PM based on their size distribution. Atmospheric particles have widely variable shapes, conventionally the size of such irregularly shaped particles is expressed in terms of an

aerodynamic equivalent diameter (Dae), which is defined as the diameter of a sphere of density of 1 g/cm^3.

Different terminology is used to define particles with respect to their size. Total suspended particulates (TSP) correspond to all suspended particles in the air, regardless of size. Particles having an aerodynamic diameter less than 10 μm are named coarse particles or PM_{10}. Those having an aerodynamic diameter less than 2.5 μm are called fine particles or $PM_{2.5}$. Ultrafine particles, or PM $_{0.1}$ are particles with an aerodynamic diameter less than 0.1 μm. Whitby proposed that physical size distributions of particles can be well characterized by a trimodal model consisting of three log-normal distribution (Whitby, 1978). The atmospheric aerosol may be thought in terms of three particle groups: coarse mode particles (> 1 μm in diameter), accumulation mode particles (about 0.1 to 1.0 μm in diameter, although accumulation mode PM may include 1 to 2.5 μm diameter size range at high relative humidity), and ultrafine particles (< 0.1 μm in diameter). Moreover, a four modal distribution has been proposed (Figure 1), dividing the ultra-fine particles into the nucleation region (< 10 nm), and the Aitken region (10 to 100 nm) (USEPA, 2004). Coarse particles are generated by mechanical mechanism or re-suspended material, these particles have a short atmospheric life, except on windy days. Accumulation mode contains particles formed due to the coagulation of particles smaller than 0.1 μm and from the condensation of vapours onto existing particles. They might derive also directly through the incomplete combustion of oil, wood, coal, petrol, and other fuels. Fine particles have long atmospheric life, until they are ultimately lost through wet deposition. Particles extending from 0.01 to 0.1 μm are usually formed from volatile precursors and are lost mainly by coagulation with larger particles. The nucleation and Aitken mode particles account for a significant atmospheric of particles number, but due to their small sizes, they rarely account to the total mass. This suggests that number concentration is better than mass concentration for the evaluation of climate and health effects of particulate, although the number concentration of ultrafine particles is not a metric included in European policies for air quality assessment (Dinoi et al; 2020).

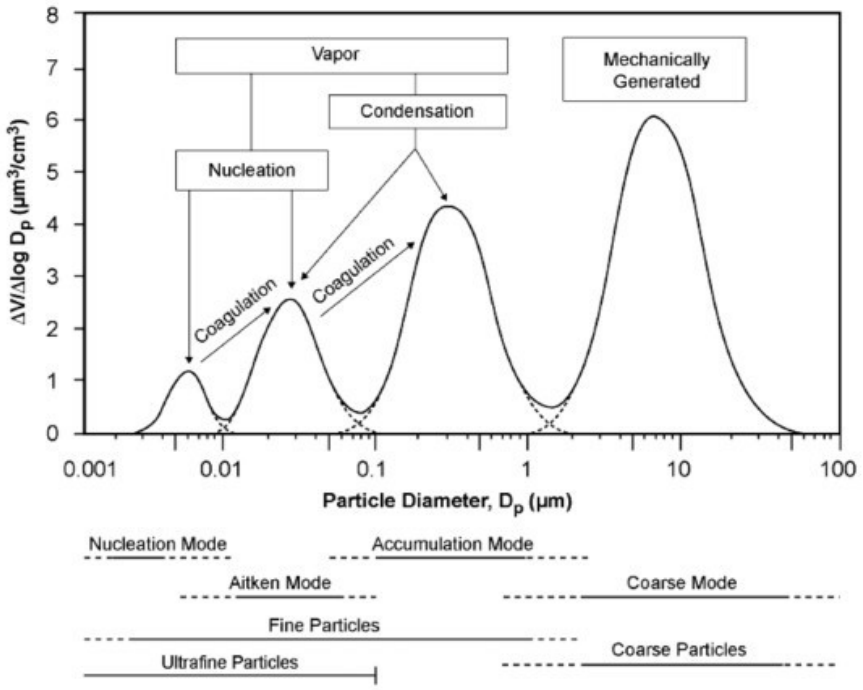

Figure 1: Idealized modal classification; coarse, accumulation, Aitken and nucleation modes. Particles Diameter (D_p) is expressed in micrometers (μm). (USEPA, 2004).

Coarse, fine and ultrafine PM are generated by distinct processes and are characterized of different size but also different chemical composition. A large fraction of ambient PM contains significant amounts of elemental carbon (EC) and organic carbon (OC), metals, inorganic ions and organic species, as polycyclic aromatic hydrocarbons (PAHs), but also biological components (pollens and spores) (Pope and Dockery; 2006). Most metals in the atmosphere are found in almost all aerosol size fractions, but usually fine particles carry higher concentrations of toxic metals than coarse particles (Bi et al., 2006)(K. Zhang et al., 2018). PAHs are formed during the incomplete combustion of organic matter, for example, oil, wood, and gasoline, and consist of two or more fused benzene rings. PAHs adsorbed on the surfaces of combustion-generated particles may lead to chemical transformations and to the consequent generation of products more polar than the parent PAHs (Seinfeld, and Pandis; 1998). Particles emitted from different sources may present a different chemical composition also in relation to location and season, in fact differences in meteorology and topography influence particles concentrations, composition and properties (Graham et al., 2020).

1.1.2 Emission sources

At the urban level anthropogenic sources are often more important than natural ones; this is particularly the case of city centres and heavily industrialized sites. The chemical characteristic of the emitted particles is determined by their origin, and the production mechanisms are responsible for their size and shape.

In the following paragraphs the most important sources of fine and ultrafine particles will be described, which have been investigated in this thesis, and that might be divided into exhaust sources and non-exhaust sources.

I. Exhaust sources

Exhaust particles are generated as result of a combustion of fuels such as diesel fuel, petrol, natural gas, fuel oil, coal, or wood. Two of the most relevant sources of exhaust particles in residential areas are: diesel exhaust particles and biomass combustion derived particles (CDPs).

Motor vehicles powered by diesel engines, have often been cited as a leading source of ambient ultrafine particles (UFPs), indeed diesel exhaust particles (DEP) consists of fine particles including a high number of ultrafine particle (Argyropoulos et al., 2016)(Mili et al; 2018). DEP are composed of a centre core of elemental carbon and adsorbed organic compounds including PAHs and nitro-PAHs, sulphate, nitrate, metals, and other trace elements. According to Kittelson engine aerosols can be described by three size modes (Figure 2) (Kittelson; 1998).

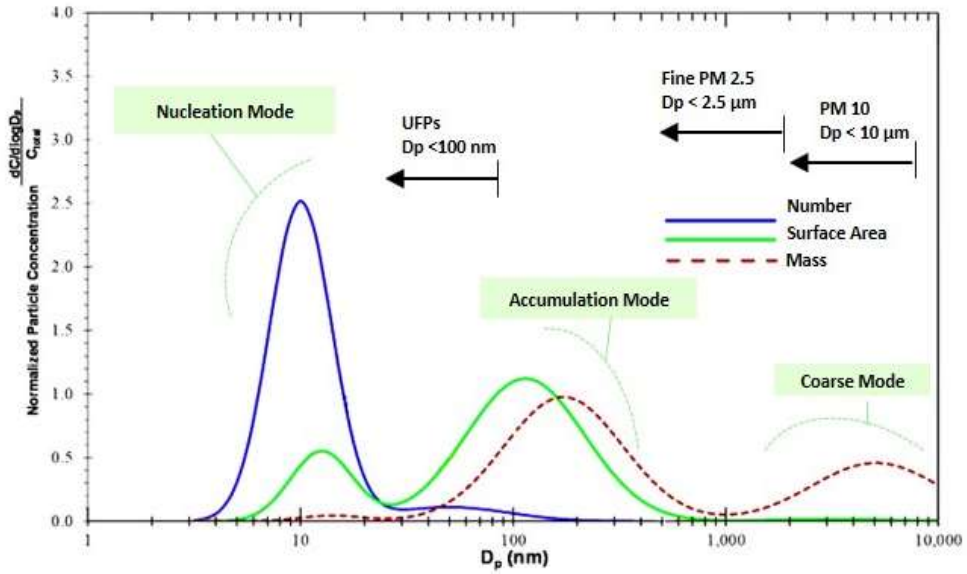

Figure 2: Tri-modal particles size distribution using different particles metric (number, surface area and mass). Particles Diameter (D_p) is expressed in nanometres (nm). Modified from (Baldauf et al., 2016).

Most of the particles mass is concentrated in the accumulation mode (diameter range 0.1—0.3 µm) and is characterized of carbonaceous agglomeration and absorbed materials residue. The nuclei mode (diameter range 0.005—0.05 µm) usually consists of volatile organic and sulphur compounds and may also contain metals and solid carbon. The nuclei mode generally contains 1—20% of the particle mass and more than 90% of the particle number carbon, so by number almost all the particles emitted by a diesel engine are ultrafine particles (Kittelson; 1998). Within a DEP sample we can find particles with different shapes, (i.e. spherulites, chains/clusters, spherules, flake), observable using electron microscopy. Aggregation properties of particles can change as a result of sample preparation, such as wetting and sonication for toxicological studies (Bérubé et al., 1999).

In last years, due to the increasingly strengthened exhaust emissions regulation, the combustion strategies have been improved developing new exhaust after-treatment systems to reduce the particles emitted from diesel engines (e.g. diesel particulate filter). In the European Union, the important regulatory steps for light-duty vehicles are typically referred to as Euro 1, Euro 2, Euro 3, Euro 4, Euro 5 and Euro 6. The production of the emitted DEP depends on complicated physical and chemical processes. Moreover, the properties of particulate matter emitted by diesel exhaust are determined by combined contributions of oxidation, soot nucleation and aggregation processes in the combustion

chamber. The physicochemical characteristics of emitted particles are essential to further understand their formation process and oxidation reactivity (Pfau et al., 2018)(Wang et al; 2019). A deeper understanding of DEP physicochemical properties allow to reduce more efficiently the emission, and this aspect is also important in the evaluation of the impact of DEP on environment and on human health.

Biomass is the first fuel used by humanity and it played a pivotal role in the economy of the middle of the 18th century, then biomass was replaced by fossil fuels, which became predominant due to the higher energy content (Abbasi and Abbasi; 2010). Biomass fuels are still extensively used for home heating and cooking, especially in developing countries (Streets et al; 2003), but its employ has grown in the last years also in the developed countries for residential heating, as consequence of the lower costs and also due to a general effort in improving the use of renewable energy sources and for the reduction of greenhouse gases emissions. Biomass combustion emissions, in contrast to emissions from diesel engine, are rising and expected to become the major source of primary particulate matter emissions (Sigsgaard et al., 2015). Biomass energy is perceived as a carbon-neutral source of energy, but its role in environmental pollution is controversial, in fact it is still unclear whether the consumption of biomass energy reduces CO_2 emissions (Danish and Wang; 2019). Anthropogenic biomass combustion comprises agricultural combustion and the combustion for heat generation (e.g., in domestic boilers, wood stoves and fireplaces). The adverse impact of domestic biomass combustion on local PM mass concentration is conspicuous, because such emissions are mostly unregulated, and the combustion process in residential heating appliances is incomplete (Saarikoski et al., 2008). Furthermore, such combustion lead to the emissions of gaseous pollutants, such as CO, CO_2, NO_x, heavy metals (i.e. Pb, Cu, Fe, Zn, and Hg, etc.), PAHs and other harmful compounds (Kukkonen et al., 2019)(Capistrano et al; 2017). The combustion conditions, included the furnace type, fuel, and the operation conditions determined the mass, number, and size of the emitted particles (Tiwari et al; 2014). The particles emitted from biomass burning are mostly in the fine and ultrafine size range, typically more than 80% are smaller than 1μm, with mean particle size typically around 0.1μm, while a small fraction of particles (~10%) is part of coarse mode (Nussbaumer et al., 2001). Scanning and transmission electron microscopy analysis have shown a variety of morphologies in combustion particles, such as chain

aggregates, solid irregulars, and spherical shape. There is a tendency towards more complicated shapes at extreme oxidation environments, with higher combustion efficiencies and temperatures, conversely, spherical particles without observable nuclei are more often correlated with smouldering combustion (Reid et al., 2005).

II. Non-exhaust emission:

Non-exhaust related emissions include particles produced from non-exhaust traffic sources such as tyres, brakes, clutches and road surface wear or particles present in the environment and resuspended in the wake of passing traffic. The wear of brakes produces typically coarse particles, but the high temperatures associated with brake components typically lead to the generation of UFPs. Different materials are used for these components, and previous works have reported Fe, Cu, Zn, Sn, Sb to be the most abundant heavy metals in the brake lining (Grigoratos and Martini, 2015). Metals are also present in tyre wear particles, especially Zn and Cd (Adamiec et al; 2016). In traffic areas, non-exhaust emission represents a major source for many of these metals into ambient air, especially Zn and Cu (AQEG, 2019). Zinc represents almost 1% by weight of the material from which the tyre tread is made and its release has been recognized as an important source of Zn in the environment(Blok; 2005)(Smolders and Degryse; 2002). Brake lining wear and crustal material are considered the only significant sources of Cu in the environment, estimated brake lining wear to be responsible for 69% of Cu of PM_{10} (Thorpe and Harrison; 2008).

Moreover, nanomaterials employed in industrial processes and unintentionally released in the environment fall into the categories of non-exhaust anthropogenic sources of particulate, contributing to air pollution, especially in the industrialized sites.

The EU adopted a definition of a nanomaterial in 2011 (Recommendation on the definition of a nanomaterial (2011/696/EU)), which defined nanomaterial as: "*A natural, incidental or manufactured material containing particles, in an unbound state or as an aggregate or as an agglomerate and where, for 50 % or more of the particles in the number size distribution, one or more external dimensions is in the size range 1 nm - 100 nm.".*

In the last years nanotechnology has led to the increased production of nanomaterials in a broad range of fields such as automotive, energy, electronics, biomedical and cosmetics (Piccinno et al; 2012). Due to the intensive use of nanoparticles in commercial products, the possible contamination of the environment and the risk of potentially adverse effects in natural systems should be considered. The nanoparticles can pollute the environment through the incorrect management of industrial waste and improper disposal of products by the users. Current environmental laws and occupational health guidelines are based on the nominal chemical composition of the material and not specifically for nanosized particles. For this reason, the potential occupational health, and environmental effects of these nanosized particles are a public health concern.

In addition, co-occurring contaminants can interact with nanoparticles(Bundschuh et al., 2018). In fact nanoparticles can potentially interact with pre-existing contaminants leading to biological effects that are poorly understood (Deng et al., 2017).

1.2 HUMAN EXPOSURE TO PARTICULATE MATTER

Exposure could be defined as the interaction between air pollutant and a target (e.g., human respiratory tract), and it is the key to linking the pollution source and adverse health effects. Health effects of air pollution depend on both doses received by a human being (host) and the susceptibility of the host. The host susceptibility to pollutant effects depends on various factors such as health conditions, age, gender and ethnicity. Dose, which is the amount of substance that reach a target organ or tissue, depends not only on exposure but also on host-parameters such as respiratory rate, and metabolic rate, for this reason it is not easy to determine the exposure dose for a whole population. The contact between a pollutant and a target depends on two critical aspects of the exposure: the concentration in a specific microenvironment and the contact duration in the microenvironment (Zhang and Lioy; 2002). Although the WHO has established average annual levels of 10 μg /m^3, almost the entire world population is exposed to $PM_{2.5}$ concentrations above this limit (WHO, 2018). Many studies have highlighted this calculating personal and background

exposure in specific site (Hoek; 2017). For example in a recent study the detected $PM_{2.5}$ concentration in the central area of Singapore varied from 22.2 to 46.2 μg/m^3 (Tran et al; 2020). In another study the $PM_{2.5}$ background daily concentration detected in Milan, have a mean value of 75.94 μg/m^3, in this study the authors concluded that the relationship between personal exposure to PM and reference measurements indicate that background values represent a proper proxy for personal exposure (Borgini et al., 2011).

PM may enter the human body through different mechanisms: inhalation, dermal absorption and ingestion (Thompson; 2018), but inhalation definitely results the most impacting one.

1.2.1 The respiratory system, main target of particulate matter.

Inhalation is the primary route of exposure to PM. The respiratory tract is characterized of a large internal surface area that is directly exposed to 10,000 to 20,000 liters of ambient air, making it a potential target site for PM. Moreover, due to the thin barrier between inhaled air and the pulmonary bloodstream, the respiratory tract is also a potential portal of entry into the blood stream (Watson et al; 1988). The human airway is often described by three regions, the head airways (nose, mouth, pharynx, and larynx), the tracheobronchial region (TCB), and the alveolar region. Particle size and shape, breathing rate, lung volume, respiration volume, and health condition of a person determined the aerosol deposition of the inhalable aerosols (diameter<10 μm) in the different regions of respiratory apparatus. Regional deposition is an essential factor for assessing the potential hazards posed by inhaled particles. The most important mechanisms of particles deposition in the respiratory system are inertial impaction, gravitational settling, and diffusion (Hinds; 1999).

Breath air containing particles passed from the head airways into the trachea, bronchus and finally into the bronchioles. The essential role of head airways and TCB regions is to increase the temperature and relative humidity of the air and to remove the particles through the mucociliary clearance, which is the primary innate defence mechanism of the lung (Ostrowski and Bennett; 2006). Nevertheless, small, non-hygroscopic particles, may

be able to avoid this mechanism and penetrate deeper in the lungs. After the TCB region, exchange of gases between the air and blood occurs within the alveoli. Beyond the size also the charge of the particles influences their cellular uptake. Particles with cationic surface charges are preferentially taken up into macrophages or epithelial cells and prevented from the rapid translocation pathways, nevertheless, particles with anionic, zwitterionic, or polar surfaces can be successfully translocated (Thompson; 2018). Evidence proves also that a fraction of insoluble ultrafine particles can be translocated from lungs into the blood circulatory system (Burch; 2002). Evidence also exists that the nervous system can be targeted by insoluble ultrafine particles (Kao et al., 2012)(Oberdörster et al., 2004). For quantify exposure to particles is possible to measure the lung deposited surface area (LDSA), which is one of the most relevant physical parameters. This metric considers the deposition efficiency of particles in different compartments of the lung (Geiss et al; 2016).

Since *in vivo* models for the determination of particle deposition in the lung are expensive and not well standardized, there is an arising interest for computational models. One of the most important examples of models is the single path models of the International Commission on Radiological Protection (ICRP) for deposition and retention of inhaled radioactive particles (ICRP, 1994). Another model has been created by the National Council on Radiation Protection and Measurements (NCRP) (NCRP, 1997). Moreover, multi-path models have been developed to give a more realistic lung-modelling, an example for this models is the Multiple Path Particle Dosimetry model (MPPD) (Fröhlich; 2016).

1.2.2 Health effects of particulate matter.

Air pollution represents a significant threat to health worldwide (Burnett et al., 2018)(Cohen et al., 2017). As reported by WHO in addition to the existing evidence that air pollution causes lung cancers, stroke, heart disease, chronic obstructive pulmonary disease and childhood pneumonia recent studies evidence that air pollution is a causative factor for dementia and a risk factor for low birth weight and poor lung development in children (WHO, 2018).

A recent paradigm for the study of the health effects of air pollution is the Exposome. The Exposome is a model to include the totality of human environment (non-genetic)(Vrijheid; 2014), which constitutes a novel progress towards the development of "next generation exposure assessment" of environmental chemicals and their mixtures. The concept of the exposome was elaborated for giving a more complete environmental exposure assessment in epidemiological studies (Wild; 2012). EXPOsOMICS is one of the first considerable European Union funded project on the exposome that aims to develop a new approach to the evaluation of exposure to environmental pollutants. The project focuses on the exposure assessment at the personal and population levels and employ multiple "omic" technologies (genomics, transcriptomics, proteomics) for the analysis of biological samples (internal markers of external exposures) (Vineis et al., 2017).

PM is deemed one of the most dangerous to health and moreover, problems persist with high atmospheric concentrations. After thoroughly reviewing the scientific literature, the International Agency for Research on Cancer (IARC), classified diesel engine particles and PM as carcinogenic to humans (Group 1) (IARC; 2012) (IARC, 2013). Toxicological studies have shown that PM comprises fractions that elicit different types and degrees of harmful effects, indicating a role for both chemical composition (such as transition metals and combustion-derived primary and secondary organic particles) and physical properties (particle number, size and surface area) (Cassee et al, 2013). Between the organic component of PM, PAHs, which are aryl hydrocarbon receptor (AHR) ligands, may contribute to worsen disease states (O'Driscoll et al., 2018).

As explained above, particles small in diameter can get deep into the lung and for this reason pose the greatest health problems. UFPs, indeed, respect to largest particles, have a greater predicted pulmonary deposition, larger surface area, higher potential to induce pulmonary inflammation and enhanced oxidant capacity (Shah et al., 2008).

PM is associated with respiratory toxicity both in *in vitro* and *in vivo* studies. Exposure to PM has been implicated in oxidative stress and inflammation as mechanisms that lead to development of lung damage and cardiovascular alterations (Aztatzi-Aguilar et al., 2018). It triggers the development and exacerbation of different diseases of the respiratory system, such as asthma and chronic obstructive pulmonary disease (COPD) (Karakatsani et al., 2012). PM can generate ROS and some oxidative metabolite, it can induce damage at

DNA level and potentially lead to cancer development (Kim et al., 2017). The carcinogenicity potential of PM may act through its combined effects on suppression of DNA, repair and increase of DNA replication errors (Mehta et al., 2008). Moreover, there is a robust correlation between PM and the deaths caused due to cardiovascular diseases (Pope et al., 2004) and several pathways have been identified that can explain this link. The theory of a direct pathway supposes that $PM_{2.5}$, especially UFPs, directly translocate into the blood stream and target distal organs. Two other hypotheses theorize the existence of two indirect pathways. One is mediated by pulmonary oxidative stress and inflammatory response, which is chronic and occurs after several hours or days of inhalation. Another indirect pathway is the interaction on the autonomic nervous system via specific lung receptor (Du et al., 2016). PM induces adverse cardiovascular conditions, including myocardial infarction, atherosclerosis, hypertension, heart rate variability, thrombosis, and coronary heart disease due to both direct or indirect mechanisms of action (Nelin et al., 2012). Exposure to fine and ultrafine PM fraction may also lead to neurological pathology. Following inhalation, PM may reach the brain through entry into pulmonary capillaries or directly through the olfactory mucosa of the nasopharyngeal region and subsequent translocation along axons of the olfactory nerve directly into the olfactory bulb of the brain (Oberdörster et al., 2004). Long-term exposure to high concentrations of PM seems to decrease the brain volume and increase the concentration of inflammatory markers (Wright and Ding; 2016).

To investigate human exposure, it is pivotal to have a valid and sensitive characterization of individual exposure to PM. The National Institutes of Health Biomarkers Definitions Working Group defined a biomarker as *"A characteristic that is objectively measured and evaluated as an indicator of normal biological processes, pathogenic processes, or pharmacologic responses to a therapeutic intervention."* (Atkinson et al., 2001). The utility of a biomarker must be assessed by demonstrating an association between the exposure and the biological change of interest. A valid marker must be both sensitive and specific to a certain exposure. Sensitivity indicates how responsive the biomarker is to changes in exposure; a sensitive biomarker would react also to small changes in PM levels. Moreover, a specific biomarker will be modulated only in association with a certain PM exposure and not change otherwise (Elvidg et al; 2013). Multiple biomarkers may mark relevant

intermediate steps leading to health outcomes after PM exposure. Important biomarker of PM human exposure includes: metabolites of pollutants; DNA and protein adduct; biomarkers of oxidative stress; biomarkers of systemic inflammation (cytokine, proteins involved in the coagulation cascade and lymphocyte proliferation); telomere length; intercellular adhesion molecule and DNA methylation (Yang et al; 2017). Gong and colleagues reported that changes in biomarker levels associated with increases in UFPs and $PM_{2.5}$ in an exposed population could be comparable in magnitude, nevertheless, UFPs and $PM_{2.5}$ probably affect pathophysiological pathways independently (Gong et al., 2014). This underlines the importance of including the ultrafine fraction of particulate matter in control policies to protect human health.

1.3 CELL TOXICITY MECHANISMS INDUCED BY PARTICULATE MATTER

1.3.1 *In vitro* models

In the last three decades, considerable efforts have been made towards using less animal tests and performing alternative methods in scientific research. Alternative tests are methods that reduce, refine and replace the use of animals for biological studies (3Rs principles)(Knight; 2008)(Richmond; 2002)(Lorenzetti et al., 2011). A wide range of non-animal techniques is available, these include *in silico* and *in vitro* methods, which provide mechanistic information on toxic effects of chemicals (Sewell et al., 2017). *In vitro* models are methods based on isolated living cells in culture and represent the starting point in biological research. The *in vitro* assays are applicable for the use in support of environmental toxicology, where they act as a complementary method for the study of biological mechanisms, for analyse xenobiotic-induced effect correlation and risk assessment (Poteser; 2017). *In vitro* assays may be used to identify important biomarkers of effects, and thus these models may be employed for biomonitoring studies.

The use of human airway and alveolar cell cultures is a reliable method for study the toxic potential of particulate matter or nanoparticles on the respiratory system. After adequate characterisation and validation, such models may be helpful alternatives to *in vivo*

experiments with animals. The most used human airway epithelial cell lines are the Calu-3, 16HBE14o- and BEAS-2B, while the cell line A549 is one of the most widely used type of alveolar cells. In many cell cultures models a monolayer of cells is immersed in medium and particles are directly added suspended in liquid. In the last years more advanced models have been developed, in which particles can be nebulised on the cells using an exposition chamber with an integrated aerosol generator. Beside the simple cell monolayers, new 3D cell culture models, including co-cultures of different cell types, have been introduced, to be more physiologically relevant (Rothen-Rutishauser et al; 2008). Air–liquid interface (ALI) is the most representative method of respiratory cells culture, in which cells are supplied with medium from the basolateral side, while the apical side is facing air (Fröhlich et al; 2018).

1.3.2 Cellular response pathways

Cellular response pathways, when sufficiently perturbed by stressors, result in toxicity pathways and eventually lead to adverse health outcomes. The cellular stress responses to environmental signals involve multiple and complex communication pathways and signal transductions processes that aim to re-establish homeostasis. PM is known to mediate toxic effects (e.g. oxidative stress, inflammation, DNA damage and genotoxicity), however if too much damage has been provided cell death process must occurred (Poteser; 2017). A schematic representation of some pathways activated after exposure to PM and the consequent outcomes is shown in Figure 3.

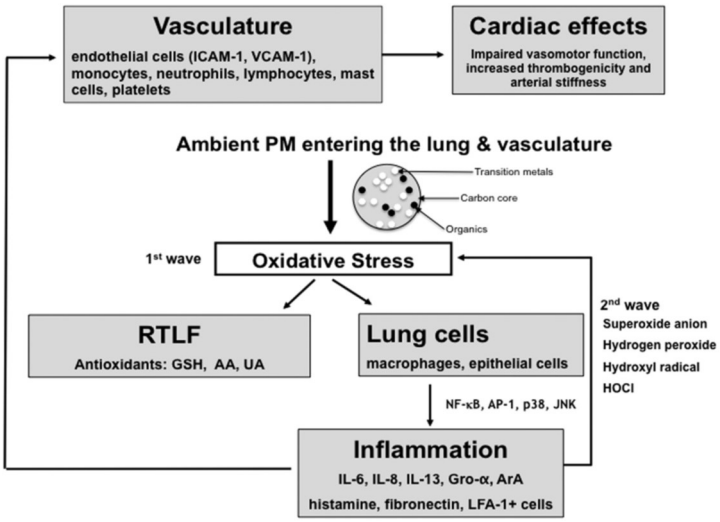

Figure 3: Biological pathways linking PM exposure with oxidative stress and inflammation in the lung and cardio vasculature (Kelly and Fussell, 2015).

Of specific interest for this thesis are the toxic effects of the UFPs and NPs, which potentially induce the worst effects on human health. There are different mechanisms, described below, by which PM (including UFPs) and NPs may impact on cells.

- **Oxidative Stress**: the ability to generate ROS and to induce oxidative stress stands at the base of the PM and NPs mechanisms of toxicity (Tseng et al; 2017) (Manke et al 2013). The oxidative stress phenomenon results from an imbalance between the production of ROS and a biological system's capacity to detoxify the reactive intermediates or repair the resulting damage. *In vitro* studies have shown that the NP- and PM-mediated oxidative stress results in: **1)** increase in the production of molecules involved in the detoxification of a wide variety of oxidant species, such as the oxidised glutathione (GSSG) (Lasagni et al. 2015); **2)** activation of oxidative stress-responsive transcription factors, such as NF-κB which leads to the transcription of key pro-inflammatory genes (Weng et al., 2018); **3)** specific proteins synthesis, such as the pro-inflammatory intracellular mediators (cytokine release) (Ji et al., 2018) and the antioxidants proteins e.g., Heme oxygenase 1(HO-1), glutathione peroxidase (GPx), and superoxide dismutase (SOD) (Lasagni et al. 2015).
  In combustion derived PM, PAHs play a pivotal role in the induction of oxidative stress, in fact they bind the cytosolic aryl hydrocarbon receptor and induce phase I metabolization

enzymes cytochrome P450 1A1 (CYP1A1) and cytochrome P450 1A2 (CYP1A2)(Shimada and Fujii-Kuriyama; 2004). HO-1 expression, a sensitive marker for oxidative stress, is directly correlated with the high organic carbon and PAHs content of PM (Kamalvand et al., 2003). For what concerns the metal-based NPs, they can elicit free radical-mediated toxicity via Fenton-type reactions, although few studies have reported the direct toxicity of NPs without causing ROS (Manke et al., 2013). There are critical determinants involved in the production of ROS as consequence of nanotoxicity, which include: shape, size, particle surface, surface positive charges, particle dissolution, metal ion release from NPs, aggregation (Fu et al; 2014).

- **Inflammation:** inflammation is one of the most central processes required in defence of animal cells against adverse stimuli. This process is characterized by the release of pro-inflammatory mediators (cytokines) by alveolar macrophages and pulmonary epithelial cells. Cytokines perform pleiotropic functions and are generally recognized as inflammatory-related biomarkers. The most relevant cytokines involved in PM induced inflammatory process and frequently detected at mRNA and protein levels are: GM-CSF; IL-1 α; IL-1β; IL-6; IL-8; MIP-2; TNF- α (Mitschik et al., 2008) (Fujii et al., 2001). These proteins are up regulated when macrophages or phagocytic cell lines are incubated with PM. Interleukins 6 and 8 (IL-6 and IL-8) are well known and widely studied pro-inflammatory cytokines, which have been studied both in relation to PM and DEP exposure and that seem to be induced via p38, Akt, and NF-κB signaling pathways (J. A.Kim et al., 2016) (Y.-M. Kim et al., 2005). The oxidative stress and the direct particle interaction stimulate an increase in intracellular Ca^{2+} levels that may also cause activation of NF-κB (Brown et al; 2000). In addition Calcium signalling events may drive the production of ROS leading to a positive feedback mechanism, the induction of these pathway may activate inflammatory gene as well as increase antioxidant production (Donaldson and Stone., 2003). Studies on metal oxide NPs suggest that the inflammatory effects could arise from both the NPs themselves and from soluble ions release. Experiments on monocultures of epithelial and bronchial cells, proved that NPs determined inflammatory response (Hsiao and Huang., 2011), moreover in co-culture models of air-blood barrier (ABB) NPs has shown to induce

activation of endothelial cells, which released pro-inflammatory mediators (IL-6, IL-8) (Bengalli et al; 2017).

- **Genotoxicity:** several studies have considered DNA damage as an endpoint for the effects of PM. Urban PM, as well as particles derived from diesel engine and from biomass combustion have shown to induce genotoxic effects (Tapanainen et al., 2011) (Danielsen et al; 2008) (Carero et al; 2001). Genotoxicity biomarkers (e.g., phosphorylation of histone H2AX as a marker of double-stranded breaks) are sensitive parameters that make possible a complementary approach for the environmental evaluation of carcinogenic compounds. PAHs play a pivotal role in genotoxicity and elicit their effects through metabolic activation by cytochrome P450s enzymes which induce the formation of a covalent binding between reactive electrophilic substances and the nucleophilic sites in DNA and generate adduct. It has already been shown that DNA adducts are implicated at early stages of carcinogenesis process (Ewa and Danuta, 2017). The extent of damage to DNA by organic extract of $PM_{2.5}$ seems to be higher than for water-soluble extract, and the organic extract genotoxicity is greater for the sample containing also higher concentrations of PAHs (Mohseni et al., 2017) (Billet et al., 2018). Acute DNA damage is known to trigger cell cycle arrest, enabling increased DNA repair time, or resulting in cell death (Dasika et al., 1999). It has been reported that fine PM may induce cell cycle alterations and consequent increased frequency of cells with micronuclei (Longhin et al., 2013). Insufficient DNA repair may, in the long-term, lead to the accumulation of mutations which contribute to carcinogenesis (Mroz et al., 2008) (Lahtz and Pfeifer, 2011). Increased attention is being placed on the study of metal NPs potential genotoxicity, indeed many metal NPs were found to induce chromosomal aberrations, oxidative DNA damage, DNA strand breaks and mutations (Xie et al., 2011). Mroz and colleagues reported that PM and their NPs constituent, cause ROS and induce DNA damage, activating p53 and proteins related to DNA repair. The hypothetical pathway associated with DNA damage by NPs is shown in figure 4 (Mroz et al., 2008).

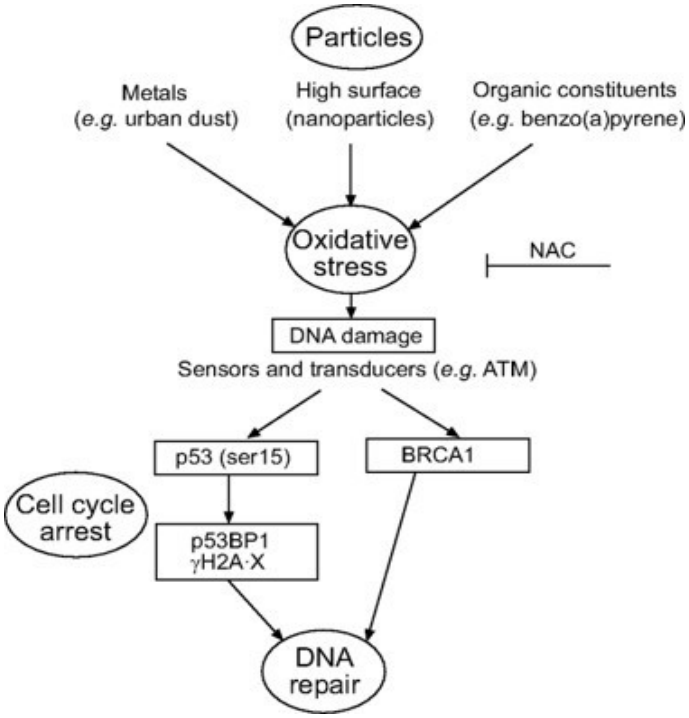

Figure 4: Pathway of DNA damage induce by NPs (Mroz et al., 2008).

- **Cell death:** a deep understanding of molecular mechanism of cells death are essential in toxicological studies. Exposure to PM can trigger the major mechanism of cell death, different studies indicate that the mechanisms by which PM causes cell death involve an inflammatory-related cascade, oxidative stress, and DNA damage (Thomson et al., 2015) (Longhin et al., 2016) (Gasparotto et al., 2013).

  The main forms of cells death are apoptosis, autophagy, and necrosis.

  The cytotoxic effects of PM an NPs exposure may lead to apoptosis in cells (Montiel-Dávalos et al. 2010) (Park et al. 2008). Apoptosis is a highly regulated physiological cell death process. There are two main apoptotic pathways: the extrinsic or death receptor pathway, which is TNF-α-related, and the intrinsic or the mitochondria-regulated pathway. Both pathways have been studied in relation to PM exposure (Dagher et al., 2006). Upadhyay and colleagues reported that PM causes alveolar epithelial apoptosis by mechanisms that involve the mitochondria-regulated death pathway and the generation of iron-derived free radicals (Upadhyay et al., 2003). According to Chin and colleagues, after PM exposure TNF-

α mediates apoptosis and the MAPK pathway may have an important role in regulating this pathway (Chin et al., 1998). In a recent study it has been proved that subcellular structures, including endoplasmic reticulum, and mitochondria are susceptible to oxidative stress and calcium overload induced by PM: these may lead to apoptosis in endothelial cells exposed to PM (Wang et al. 2020). Autophagy is a highly conserved eukaryotic cellular recycling process that decomposes folded proteins, protein complexes and dysfunctional organelles (Parzych and Klionsky 2014). The cytoplasmic materials are sequestered into an ‘‘autophagosomes’’, which is a double-membrane vesicle, and are subsequently fused with lysosomes to form autolysosomes and are degraded by lysosomal hydrolases. Autophagy has been considered an adaptive response to stress, supporting cellular homeostasis, and found to be activated during several pathogenic conditions, as well as the execution of a caspase-independent cell death (Hurley and Young 2017). Autophagy is involved in PM-induced airway epithelial injury (Chen et al. 2016). Cells exposure to DEP stimulated a significant increase of the autophagic flux, in terms of LC3-II level (Chen et al. 2016). Moreover, autophagy is also related to endothelial dysfunction and consequence atherosclerosis, in fact DEP-induced oxidative stress plays a central role in the initiation of both autophagy and apoptosis causing endothelial dysfunction (Wang et al.2017). Also, NPs may induce autophagy, and this pathway seems to be protective for apoptosis (Shen et al. 2019).

Many types of necrosis, both accidental and programmed, share common morphological features, which lead to cell lysis and release of the cytoplasmic contents into the extracellular space (Berghe et al., 2014). Commonly necrosis cell death is a minor contributor in PM exposure, but when an intense inflammation response occurred, the upregulation of cytokines and exacerbation ROS production was shown to be involved in a caspase-independent and necrosis (Peixoto et al., 2017). It has been reported that NPs induced necrosis in cells and that the cytotoxic effects of NPs are related to their physico-chemical properties (Mohammadinejad et al. 2019).

1.4 AIR POLLUTION AND COVID-19 PANDEMIC

In the context of a dissertation on atmospheric particulate, the relationship between air quality and the novel coronavirus disease (COVID-19) pandemic deserves a mention. COVID-19, caused by the severe acute respiratory syndrome coronavirus 2 (SARS-CoV-2), has rapidly developed into a pandemic throughout the world in the last year.

The measures to limit the infection of people, hence the general lockdown, have led to beneficial temporally reductions in PM concentrations (Kumar et al., 2020),(Briz-Redón et al., 2021), indeed the global action to mitigate the pandemic have led to switching off most PM emission sources, which should give the opportunity to reflect regarding potential control systems and regulations for improved air quality in next years.

Moreover, the populations located in areas with higher PM concentrations seem to be more predisposed to severe manifestations of the COVID-19 disease. In fact, long-term exposure to atmospheric pollution increases vulnerability to the most severe COVID-19 outcomes (Wu et al., 2020). In Italy, Lombardy and Emilia Romagna regions are two areas with both the highest level of virus lethality in the world and with a high level of PM concentration. Conticini and colleagues reported that the high level of pollution in that regions should be considered a co-factor of the high lethality registered in northern Italy (Conticini et al. 2020). Also Gupta and colleagues reported that exists a positive correlation between the level of PM in a specific region and the lethality related to COVID-19, indeed past chronic exposures to high level of $PM_{2.5}$, is found to significantly correlate with present COVID-19 mortality per unit reported cases (Gupta et al., 2020). Since air is a vehicle through which microbial agents can move in the atmosphere, it has been hypothesized that COVID-19 could also have an airborne transmission and PM could act as a carrier through the aerosol and enter human organism during nasal inhalation (Borisova and Komisarenko, 2020). The correlation between air pollution and COVID-19 severity could be viewed merely as the passive result of a carrier action of virus by PM, however, one should acknowledge that PM air pollution is also a primary cause of chronic systemic and airway inflammation (Dadvand et al., 2014). It is important to recognize that short-term effects of air pollution are usually proinflammatory, while chronic exposure can cause immune dysregulation. The

physio pathological overlap between PM-driven inflammatory cytokine production and the cytokine storm in patients with COVID-19 might suggest a boosting action on the SARS-CoV-2 evolution of disease. In fact, pathological pathways provoked by PM partially overlaps with that induced by COVID-19. SARS-CoV-2 coronavirus can stimulate a type-I interferon-mediated innate immune response, which is accompanied by dysregulated secretion of IL-6 (McGonagle et al., 2020), in a similar way PM triggers the release of proinflammatory cytokines (included IL-6) from alveolar macrophages, inducing an acceleration of arterial thrombosis (Menendez, 2020). Studies have proved that alveolar macrophages from people living in highly polluted areas have a reduced innate immune capacity, which is proportional to the amount of phagocytosed PM (Wang et al, 2020). Chronic fine particles exposure may contribute to the variation in morbidity and mortality observed in COVID-19 infections due to disrupted immune response characterized by hypothalamic–pituitary–adrenal (HPA) axis disruption (Deek, 2020). In addition, exposure to fine PM can interfere with Human innate immune molecule LL37 destruction of viruses and may reduce effective immune signalling modulation by LL37(Crane-Godreaur et al, 2020).

The correlation between COVID-19 and PM concentration should require further investigation, but this potential correlation supports the need for environmental policies that would not only reduce the impact of pollution on human health but might help mitigate the negative effects of another future pandemic.

1.5 BIBLIOGRAPHY

Abbasi, T., & Abbasi, S. A. (2010). Biomass energy and the environmental impacts associated with its production and utilization. *Renewable and Sustainable Energy Reviews*, *14*(3), 919–937. https://doi.org/10.1016/j.rser.2009.11.006

Adamiec, E., Jarosz-Krzemińska, E., & Wieszała, R. (2016). Heavy metals from non-exhaust vehicle emissions in urban and motorway road dusts. *Environmental Monitoring and Assessment*, *188*(6), 1–11. https://doi.org/10.1007/s10661-016-5377-1

Air Quality Expert Group. (2019). *Non-Exhaust Emissions from Road Traffic*. Retrieved from https://uk-air.defra.gov.uk/

Argyropoulos, G., Samara, C., Voutsa, D., Kouras, A., Manoli, E., Voliotis, A., … Eleftheriadis, K. (2016). Concentration levels and source apportionment of ultrafine particles in road microenvironments. *Atmospheric Environment*, *129*, 68–78. https://doi.org/10.1016/j.atmosenv.2016.01.009

Atkinson, A. J., Colburn, W. A., DeGruttola, V. G., DeMets, D. L., Downing, G. J., Hoth, D. F., … Zeger, S. L. (2001). Biomarkers and surrogate endpoints: Preferred definitions and conceptual framework. *Clinical Pharmacology & Therapeutics*, *69*(3), 89–95. https://doi.org/10.1067/mcp.2001.113989

Aztatzi-Aguilar, O., Valdés-Arzate, A., Debray-García, Y., Calderón-Aranda, E., Uribe-Ramirez, M., Acosta-Saavedra, L., … De Vizcaya-Ruiz, A. (2018). Exposure to ambient particulate matter induces oxidative stress in lung and aorta in a size- and time-dependent manner in rats. *Toxicology Research and Application*, *2*, 239784731879485. https://doi.org/10.1177/2397847318794859

B. R'Mili, A. Boreave, A. Meme, P. Vernoux, M. Leblanc, et al. . (2018). Physico-Chemical Characterization of Fine and Ultrafine Particles Emitted during Diesel Particulate Filter Active Regeneration of Euro5 Diesel Vehicles Physico-chemical characterization of fine and ultrafine particles emitted during 1 DPF active regenerat. *Environmental Science&Technology*,*52(5),* pp.3312-3319. https://doi.org/10.1021/acs.est.7b06644ï

Baldauf, R. W., Devlin, R. B., Gehr, P., Giannelli, R., Hassett-Sipple, B., Jung, H., … Walker, K. (2016). Ultrafine particle metrics and research considerations: Review of the 2015 UFP workshop. *International Journal of Environmental Research and Public Health*, *13*(11), 1–21. https://doi.org/10.3390/ijerph13111054

Bengalli, R., Gualtieri, M., Capasso, L., Urani, C., & Camatini, M. (2017). Impact of zinc oxide nanoparticles on an in vitro model of the human air-blood barrier. *Toxicology Letters*, *279*, 22–32. https://doi.org/10.1016/j.toxlet.2017.07.877

Bérubé, K. A., Jones, T. P., Williamson, B. J., Winters, C., Morgan, A. J., & Richards, R. J. (1999). Physicochemical characterisation of diesel exhaust particles: Factors for assessing biological activity. *Atmospheric Environment*, *33*(10), 1599–1614. https://doi.org/10.1016/S1352-2310(98)00384-7

Bi, X., Feng, X., Yang, Y., Qiu, G., Li, G., Li, F., … Jin, Z. (2006). Environmental contamination of heavy metals from zinc smelting areas in Hezhang County, western Guizhou, China. *Environment International*, *32*(7), 883–890. https://doi.org/10.1016/j.envint.2006.05.010

Billet, S., Landkocz, Y., Martin, P. J., Verdin, A., Ledoux, F., Lepers, C., … Courcot, D. (2018). Chemical characterization of fine and ultrafine PM, direct and indirect genotoxicity of PM and their organic extracts on pulmonary cells. *Journal of Environmental Sciences (China)*, *71*, 168–178. https://doi.org/10.1016/j.jes.2018.04.022

Blok, J. (2005). Environmental exposure of road borders to zinc. *Science of the Total Environment*, *348*(1–3), 173–190. https://doi.org/10.1016/j.scitotenv.2004.12.073

Borgini, A., Tittarelli, A., Ricci, C., Bertoldi, M., De Saeger, E., & Crosignani, P. (2011). Personal exposure to PM2.5 among high-school students in Milan and background measurements: The EuroLifeNet study. *Atmospheric Environment*, *45*(25), 4147–4151. https://doi.org/10.1016/j.atmosenv.2011.05.026

Borisova, T., & Komisarenko, S. (2020). Air pollution particulate matter as a potential carrier of SARS-CoV-2 to the nervous system and/or neurological symptom enhancer: arguments in favor. *Environmental Science and Pollution Research*, 1–7. https://doi.org/10.1007/s11356-020-11183-3

Briz-Redón, Á., Belenguer-Sapiña, C., & Serrano-Aroca, Á. (2021). Changes in air pollution during

COVID-19 lockdown in Spain: A multi-city study. *Journal of Environmental Sciences (China)*, *101*, 16–26. https://doi.org/10.1016/j.jes.2020.07.029

Bundschuh, M., Filser, J., Lüderwald, S., McKee, M. S., Metreveli, G., Schaumann, G. E., … Wagner, S. (2018). Nanoparticles in the environment: where do we come from, where do we go to? *Environmental Sciences Europe*, *30*(1). https://doi.org/10.1186/s12302-018-0132-6

Burch, W. M. (2002). Passage of inhaled particles into the blood circulation in humans. *Circulation*, *106*(20), 411–414. https://doi.org/10.1161/01.cir.0000037134.24080.42

Burnett, R., Chen, H., Szyszkowicz, M., Fann, N., Hubbell, B., Pope, C. A., … Spadaro, J. V. (2018). Global estimates of mortality associated with longterm exposure to outdoor fine particulate matter. *Proceedings of the National Academy of Sciences of the United States of America*, *115*(38), 9592–9597. https://doi.org/10.1073/pnas.1803222115

Capistrano, S. J., van Reyk, D., Chen, H., & Oliver, B. G. (2017). Evidence of biomass smoke exposure as a causative factor for the development of COPD. *Toxics*, *5*(4), 1–16. https://doi.org/10.3390/toxics5040036

Carero, A. D. P., Hoet, P. H. M., Verschaeve, L., Schoeters, G., & Nemery, B. (2001). Genotoxic effects of carbon black particles, diesel exhaust particles, and urban air particulates and their extracts on a human alveolar epithelial cell line (A549) and a human monocytic cell line (THP-1). *Environmental and Molecular Mutagenesis*, *37*(2), 155–163. https://doi.org/10.1002/em.1023

Cassee, F. R., Héroux, M. E., Gerlofs-Nijland, M. E., & Kelly, F. J. (2013, December). Particulate matter beyond mass: Recent health evidence on the role of fractions, chemical constituents and sources of emission. *Inhalation Toxicology*, Vol. 25, pp. 802–812. https://doi.org/10.3109/08958378.2013.850127

Cohen, A. J., Brauer, M., Burnett, R., Anderson, H. R., Frostad, J., Estep, K., Forouzanfar, M. H. (2017). Estimates and 25-year trends of the global burden of disease attributable to ambient air pollution: an analysis of data from the Global Burden of Diseases Study 2015. *The Lancet*, *389*(10082), 1907–1918. https://doi.org/10.1016/S0140-6736(17)30505-6

Conticini, E., Frediani, B., & Caro, D. (2020, June 1). Can atmospheric pollution be considered a

co-factor in extremely high level of SARS-CoV-2 lethality in Northern Italy? *Environmental Pollution*, Vol. 261, p. 114465. https://doi.org/10.1016/j.envpol.2020.114465

Crane-Godreau, M. A., Clem, K. J., Payne, P., & Fiering, S. (2020). Vitamin D Deficiency and Air Pollution Exacerbate COVID-19 Through Suppression of Antiviral Peptide LL37. Frontiers in Public Health, 8. https://doi.org/10.3389/fpubh.2020.00232

Dadvand, P., Nieuwenhuijsen, M. J., Agustí, À., De Batlle, J., Benet, M., Beelen, R., … Garcia-Aymerich, J. (2014). Air pollution and biomarkers of systemic inflammation and tissue repair in COPD patients. *European Respiratory Journal*, *44*(3), 603–613. https://doi.org/10.1183/09031936.00168813

Danielsen, P. H., Loft, S., & Møller, P. (2008). DNA damage and cytotoxicity in type II lung epithelial (A549) cell cultures after exposure to diesel exhaust and urban street particles. *Particle and Fibre Toxicology*, *5*. https://doi.org/10.1186/1743-8977-5-6

Danish, & Wang, Z. (2019). Does biomass energy consumption help to control environmental pollution? Evidence from BRICS countries. *Science of the Total Environment*, *670*, 1075–1083. https://doi.org/10.1016/j.scitotenv.2019.03.268

Dasika, G. K., Lin, S. C. J., Zhao, S., Sung, P., Tomkinson, A., & Lee, E. Y. H. P. (1999). DNA damage-induced cell cycle checkpoints and DNA strand break repair in development and tumorigenesis. *Oncogene*, *18*(55), 7883–7899. https://doi.org/10.1038/sj.onc.1203283

Deek, S. A. (2020). Chronic exposure to air pollution implications on COVID-19 severity. Medical Hypotheses, 145, 110303. https://doi.org/10.1016/j.mehy.2020.110303

Deng, R., Lin, D., Zhu, L., Majumdar, S., White, J. C., Gardea-Torresdey, J. L., & Xing, B. (2017, May 28). Nanoparticle interactions with co-existing contaminants: joint toxicity, bioaccumulation and risk. *Nanotoxicology*, Vol. 11, pp. 591–612. https://doi.org/10.1080/17435390.2017.1343404

Dinoi, A., Conte, M., Grasso, F. M., & Contini, D. (2020). Long-term characterization of submicron atmospheric particles in an urban background site in Southern Italy. *Atmosphere*, *11*(4), 1–15. https://doi.org/10.3390/atmos11040334

Donaldson, K., & Stone, V. (2003). Current hypotheses on the mechanisms of toxicity of ultrafine

particles. *Annali Dell'Istituto Superiore Di Sanita*, *39*(3), 405–410.

Du, Y., Xu, X., Chu, M., Guo, Y., & Wang, J. (2016). Air particulate matter and cardiovascular disease: The epidemiological, biomedical and clinical evidence. *Journal of Thoracic Disease*, Vol. 8, pp. E8–E19. https://doi.org/10.3978/j.issn.2072-1439.2015.11.37

Elvidge, T., Matthews, I. P., Gregory, C., & Hoogendoorn, B. (2013, January 1). Feasibility of using biomarkers in blood serum as markers of effect following exposure of the lungs to particulate matter air pollution. *Journal of Environmental Science and Health - Part C Environmental Carcinogenesis and Ecotoxicology Reviews*, Vol. 31, pp. 1–44. https://doi.org/10.1080/10590501.2013.763575

Ewa, B., & Danuta, M. Š. (2017, August 1). Polycyclic aromatic hydrocarbons and PAH-related DNA adducts. *Journal of Applied Genetics*, Vol. 58, pp. 321–330. https://doi.org/10.1007/s13353-016-0380-3

Finlayson-Pitts, B. J., & Pitts, J. N. (1997). Tropospheric air pollution: Ozone, airborne toxics, polycyclic aromatic hydrocarbons, and particles. *Science*, *276*(5315), 1045–1052. https://doi.org/10.1126/science.276.5315.1045

Fröhlich, E. (2018, November 5). Comparison of conventional and advanced in vitro models in the toxicity testing of nanoparticles. *Artificial Cells, Nanomedicine and Biotechnology*, Vol. 46, pp. 1091–1107. https://doi.org/10.1080/21691401.2018.1479709

Fröhlich, E., Mercuri, A., Wu, S., & Salar-Behzadi, S. (2016). Measurements of deposition, lung surface area and lung fluid for simulation of inhaled compounds. *Frontiers in Pharmacology*, Vol. 7. https://doi.org/10.3389/fphar.2016.00181

Fu, P. P., Xia, Q., Hwang, H. M., Ray, P. C., & Yu, H. (2014, March 1). Mechanisms of nanotoxicity: Generation of reactive oxygen species. *Journal of Food and Drug Analysis*, Vol. 22, pp. 64–75. https://doi.org/10.1016/j.jfda.2014.01.005

Fujii, T., Hayashi, S., Hogg, J. C., Vincent, R., & Van Eeden, S. F. (2001). Particulate matter induces cytokine expression in human bronchial epithelial cells. *American Journal of Respiratory Cell and Molecular Biology*, *25*(3), 265–271. https://doi.org/10.1165/ajrcmb.25.3.4445

Geiss, O., Bianchi, I., & Barrero-Moreno, J. (2016). Lung-deposited surface area concentration

measurements in selected occupational and non-occupational environments. *Journal of Aerosol Science*, *96*, 24–37. https://doi.org/10.1016/j.jaerosci.2016.02.007

Gong, J., Zhu, T., Kipen, H., Wang, G., Hu, M., Guo, Q., … Zhang, J. (2014). Comparisons of ultrafine and fine particles in their associations with biomarkers reflecting physiological pathways. *Environmental Science and Technology*, *48*(9), 5264–5273. https://doi.org/10.1021/es5006016

Graham, A. M., Pringle, K. J., Arnold, S. R., Pope, R. J., Vieno, M., Butt, E. W., … McQuaid, J. B. (2020). Impact of weather types on UK ambient particulate matter concentrations. *Atmospheric Environment: X*, *5*, 100061. https://doi.org/10.1016/j.aeaoa.2019.100061

Grigoratos, T., & Martini, G. (2015). Brake wear particle emissions: a review. *Environmental Science and Pollution Research*, *22*(4), 2491–2504. https://doi.org/10.1007/s11356-014-3696-8

Gupta, A., Bherwani, H., Gautam, S., Anjum, S., Musugu, K., Kumar, N., … Kumar, R. (2020). Air pollution aggravating COVID-19 lethality? Exploration in Asian cities using statistical models. *Environment, Development and Sustainability*, 1–10. https://doi.org/10.1007/s10668-020-00878-9

Hinds, W. C. (1999). Aerosol Technology: Properties, Behavior, and Measurement of Airborne Particles, 2nd Edition | Wiley. Retrieved November 11, 2020, from https://www.wiley.com/en-us/Aerosol+Technology%3A+Properties%2C+Behavior%2C+and+Measurement+of+Airborne+Particles%2C+2nd+Edition-p-9780471194101

Hoek, G. (2017, December 1). Methods for Assessing Long-Term Exposures to Outdoor Air Pollutants. *Current Environmental Health Reports*, Vol. 4, pp. 450–462. https://doi.org/10.1007/s40572-017-0169-5

Hsiao, I. L., & Huang, Y. J. (2011). Effects of various physicochemical characteristics on the toxicities of ZnO and TiO2 nanoparticles toward human lung epithelial cells. *Science of the Total Environment*, *409*(7), 1219–1228. https://doi.org/10.1016/j.scitotenv.2010.12.033

Hyo Jeong Kim, R., Gi Choi, M., Kyun Park, M., & Rok Seo, Y. (2017). Predictive and Prognostic Biomarkers of Respiratory Diseases due to Particulate Matter Exposure. *JOURNAL OF*

CANCER PREVENTION, *22*(1). https://doi.org/10.15430/JCP.2017.22.1.6

IARC. (2012). *IARC: DIESEL ENGINE EXHAUST CARCINOGENIC*. https://doi.org/10.1093/jnci/djs034

IARC. (2013). *PRESS RELEASE N° 221 IARC: Outdoor air pollution a leading environmental cause of cancer deaths*. Retrieved from http://www.iarc.fr/en/publications/books/sp161/index.php

ICRP, 1994. Human Respiratory Tract Model for Radiological Protection. ICRP Publication 66. Ann. ICRP 24 (1-3). (1994). *ICRP. Human Respiratory Tract Model for Radiological Protection.* (C. P. A. I. 66., Ed.).

Ji, J., Upadhyay, S., Xiong, X., Malmlöf, M., Sandström, T., Gerde, P., & Palmberg, L. (2018). Multi-cellular human bronchial models exposed to diesel exhaust particles: Assessment of inflammation, oxidative stress and macrophage polarization. *Particle and Fibre Toxicology*, *15*(1), 1–16. https://doi.org/10.1186/s12989-018-0256-2

Kamalvand, G., Pinard, G., & Ali-Khan, Z. (2003). Heme-oxygenase-1 response, a marker of oxidative stress, in a mouse model of AA amyloidosis. *Amyloid*, *10*(3), 151–159. https://doi.org/10.3109/13506120308998997

Kao, Y. Y., Cheng, T. J., Yang, D. M., Wang, C. T., Chiung, Y. M., & Liu, P. S. (2012). Demonstration of an olfactory bulb-brain translocation pathway for ZnO nanoparticles in rodent cells in vitro and in vivo. *Journal of Molecular Neuroscience*, *48*(2), 464–471. https://doi.org/10.1007/s12031-012-9756-y

Karakatsani, A., Analitis, A., Perifanou, D., Ayres, J. G., Harrison, R. M., Kotronarou, A., … Katsouyanni, K. (2012). Particulate matter air pollution and respiratory symptoms in individuals having either asthma or chronic obstructive pulmonary disease: A European multicentre panel study. *Environmental Health: A Global Access Science Source*, *11*(1). https://doi.org/10.1186/1476-069X-11-75

Kelly, F. J., & Fussell, J. C. (2015). Linking ambient particulate matter pollution effects with oxidative biology and immune responses. *Annals of the New York Academy of Sciences*, *1340*(1), 84–94. https://doi.org/10.1111/nyas.12720

Kim, J. A., Cho, J. H., Park, I.-H., Shin, J.-M., Lee, S.-A., & Lee, H.-M. (2016). Diesel Exhaust Particles Upregulate Interleukins IL-6 and IL-8 in Nasal Fibroblasts. *PLOS ONE*, *11*(6), e0157058. https://doi.org/10.1371/journal.pone.0157058

Kim, Y.-M., Reed, W., Lenz, A. G., Jaspers, I., Silbajoris, R., Nick, H. S., & Samet, J. M. (2005). Ultrafine carbon particles induce interleukin-8 gene transcription and p38 MAPK activation in normal human bronchial epithelial cells. *American Journal of Physiology-Lung Cellular and Molecular Physiology*, *288*(3), L432–L441. https://doi.org/10.1152/ajplung.00285.2004

Kittelson, D. B. (1998). Engines and nanoparticles: a review. *J. Aerosol Sci. Vol.*, *29*(5/6), 575–588. https://doi.org/10.1016/S0021-8502(97)10037-4

Klimont, Z., Kupiainen, K., Heyes, C., Purohit, P., Cofala, J., Rafaj, P., … Schöpp, W. (2016). Global anthropogenic emissions of particulate matter including black carbon. *Atmospheric Chemistry and Physics Discussions*, (October), 1–72. https://doi.org/10.5194/acp-2016-880

Knight, A. (2008). Non-Animal Methodologies within Biomedical Research and Toxicity Testing. *Experimentation Collection*. Retrieved from https://www.wellbeingintlstudiesrepository.org/acwp_arte/84

Kukkonen, J., López-Aparicio, S., Segersson, D., Geels, C., Kangas, L., Kauhaniemi, M., … Brandt, J. (2019). The influence of residential wood combustion on the concentrations of PM_{2.5} in four Nordic cities. *Atmospheric Chemistry and Physics Discussions*, 1–53. https://doi.org/10.5194/acp-2019-564

Kumar, P., Hama, S., Omidvarborna, H., Sharma, A., Sahani, J., Abhijith, K. V., … Tiwari, A. (2020). Temporary reduction in fine particulate matter due to 'anthropogenic emissions switch-off' during COVID-19 lockdown in Indian cities. *Sustainable Cities and Society*, *62*, 102382. https://doi.org/10.1016/j.scs.2020.102382

Lahtz, C., & Pfeifer, G. P. (2011). Epigenetic changes of DNA repair genes in cancer. *Journal of Molecular Cell Biology*, *3*(1), 51–58. https://doi.org/10.1093/jmcb/mjq053

Lasagni Vitar, R. M., Tau, J., Reides, C. G., Berra, A., Ferreira, S. M., & Llesuy, S. F. (2015). Evaluation of oxidative stress markers in human conjunctival epithelial cells exposed to diesel exhaust particles (DEP). *Investigative Ophthalmology and Visual Science*, *56*(12),

7058–7066. https://doi.org/10.1167/iovs.15-16864

Li, T., Liu, B., Bi, X., Wu, J., Zhang, Y., & Feng, Y. (2021). Size and chemical characteristics of particles emitted from typical rural biomass cookstoves in North China. *Atmospheric Research*, *249*. https://doi.org/10.1016/j.atmosres.2020.105295

Longhin, E., Holme, J. A., Gutzkow, K. B., Arlt, V. M., Kucab, J. E., Camatini, M., & Gualtieri, M. (2013). Cell cycle alterations induced by urban PM2.5 in bronchial epithelial cells: Characterization of the process and possible mechanisms involved. *Particle and Fibre Toxicology*, *10*(1), 63. https://doi.org/10.1186/1743-8977-10-63

Lorenzetti, S., Altieri, I., Arabi, S., Balduzzi, D., Bechi, N., Cordelli, E., … Mantovani, A. (2011). Innovative non-animal testing strategies for reproductive toxicology: The contribution of Italian partners within the EU project ReProTect. *Annali Dell'Istituto Superiore Di Sanita*, *47*(4), 429–444. https://doi.org/10.4415/ANN_11_04_16

Manke, A., Wang, L., & Rojanasakul, Y. (2013). Mechanisms of nanoparticle-induced oxidative stress and toxicity. *BioMed Research International*, Vol. 2013. https://doi.org/10.1155/2013/942916

McGonagle, D., Sharif, K., O'Regan, A., & Bridgewood, C. (2020). The Role of Cytokines including Interleukin-6 in COVID-19 induced Pneumonia and Macrophage Activation Syndrome-Like Disease. *Autoimmunity Reviews*, *19*(6), 102537. https://doi.org/10.1016/j.autrev.2020.102537

Mehta, M., Chen, L. C., Gordon, T., Rom, W., & Tang, M. shong. (2008). Particulate matter inhibits DNA repair and enhances mutagenesis. *Mutation Research - Genetic Toxicology and Environmental Mutagenesis*, *657*(2), 116–121. https://doi.org/10.1016/j.mrgentox.2008.08.015

Menendez, J. A. (2020). Metformin and SARS-CoV-2: Mechanistic lessons on air pollution to weather the cytokine/thrombotic storm in COVID-19. *Aging*, *12*(10), 8760–8765. https://doi.org/10.18632/aging.103347

Mitschik, S., Schierl, R., Nowak, D., & Jörres, R. A. (2008). Effects of particulate matter on cytokine production in vitro: A comparative analysis of published studies. *Inhalation Toxicology*, *20*(4), 399–414. https://doi.org/10.1080/08958370801903784

Mohseni Bandpi, A., Eslami, A., Shahsavani, A., Khodagholi, F., Aliaghaei, A., & Alinejad, A. (2017). Water-soluble and organic extracts of ambient PM $_{2.5}$ in Tehran air: assessment of genotoxic effects on human lung epithelial cells (A549) by the Comet assay. *Toxin Reviews*, *36*(2), 116–124. https://doi.org/10.1080/15569543.2016.1259634

Mroz, R. M., Schins, R. P. F., Li, H., Jimenez, L. A., Drost, E. M., Holownia, A., … Donaldson, K. (2008). Nanoparticle-driven DNA damage mimics irradiation-related carcinogenesis pathways. *European Respiratory Journal*, *31*(2), 241–251. https://doi.org/10.1183/09031936.00006707

NCRP. (1997). Report No. 125 – Deposition, Retention and Dosimetry of Inhaled Radioactive Substances. Retrieved November 14, 2020, from Bethesda, MD website: https://ncrponline.org/shop/reports/report-no-125-deposition-retention-and-dosimetry-of-inhaled-radioactive-substances-1997/

Nelin, T. D., Joseph, A. M., Gorr, M. W., & Wold, L. E. (2012, February 5). Direct and indirect effects of particulate matter on the cardiovascular system. *Toxicology Letters*, Vol. 208, pp. 293–299. https://doi.org/10.1016/j.toxlet.2011.11.008

Nussbaumer, T., Braun, C., Burtscher, H., Livbjerg, H., Jokiniemi, J., Ebert, F., … Schmatloch, V. (2001). Aerosols from biomass combustion. In *International Seminar by IEA Bioenergy Task*.

O'Driscoll, C. A., Gallo, M. E., Hoffmann, E. J., Fechner, J. H., Schauer, J. J., Bradfield, C. A., & Mezrich, J. D. (2018). Polycyclic aromatic hydrocarbons (PAHs) present in ambient urban dust drive proinflammatory T cell and dendritic cell responses via the aryl hydrocarbon receptor (AHR) in vitro. *PLOS ONE*, *13*(12), e0209690. https://doi.org/10.1371/journal.pone.0209690

Oberdörster, G., Sharp, Z., Atudorei, V., Elder, A., Gelein, R., Kreyling, W., & Cox, C. (2004). Translocation of inhaled ultrafine particles to the brain. *Inhalation Toxicology*, *16*(6–7), 437–445. https://doi.org/10.1080/08958370490439597

Ostrowski, L. E., & Bennett, W. D. (2006). Cilia and Mucociliary Clearance. *Encyclopedia of Respiratory Medicine, Four-Volume Set*, 466–470. https://doi.org/10.1016/B0-12-370879-6/00079-X

Pfau, S. A., Rocca, A. La, Haffner-Staton, E., Rance, G. A., Fay, M. W., Brough, R. J., & Malizia, S.

(2018). *Comparative nanostructure analysis of gasoline turbocharged direct injection and diesel soot-in-oil with carbon black*. https://doi.org/10.1016/j.carbon.2018.06.050

Piccinno, F., Gottschalk, F., Seeger, S., & Nowack, B. (2012). Industrial production quantities and uses of ten engineered nanomaterials in Europe and the world. *Journal of Nanoparticle Research*, *14*(9). https://doi.org/10.1007/s11051-012-1109-9

Pope, C. A., Burnett, R. T., Thurston, G. D., Thun, M. J., Calle, E. E., Krewski, D., & Godleski, J. J. (2004). Cardiovascular Mortality and Long-Term Exposure to Particulate Air Pollution: Epidemiological Evidence of General Pathophysiological Pathways of Disease. *Circulation*, *109*(1), 71–77. https://doi.org/10.1161/01.CIR.0000108927.80044.7F

Pope, C. A., & Dockery, D. W. (2006). Health effects of fine particulate air pollution: Lines that connect. *Journal of the Air and Waste Management Association*, *56*(6), 709–742. https://doi.org/10.1080/10473289.2006.10464485

Poteser, M. (2017a). Cell-based in vitro models in environmental toxicology: a review. *Biomonitoring*, *4*(1), 11–26. https://doi.org/10.1515/bimo-2017-0002

Poteser, M. (2017b). Cell-based in vitro models in environmental toxicology: a review. *Biomonitoring*, *4*(1), 11–26. https://doi.org/10.1515/bimo-2017-0002

Reid, J. S., Eck, T. F., Christopher, S. A., Koppman, R., Dubovik, O., Eleuterio, D. P., … Zhang, J. (2005). A review of biomass burning emissions part III: Intensive optical properties of biomass burning particles. *Atmospheric Chemistry and Physics*, *5*(3), 827–849. https://doi.org/10.5194/acp-5-827-2005

Richmond, J. (2002). Refinement, reduction, and replacement of animal use for regulatory testing: Future improvements and implementation within the regulatory framework. *ILAR Journal*, *43*(SUPPL.), S63–S68. https://doi.org/10.1093/ilar.43.suppl_1.s63

Rothen-Rutishauser, B., Blank, F., Mühlfeld, C., & Gehr, P. (2008). In vitro models of the human epithelial airway barrier to study the toxic potential of particulate matter. *Expert Opinion on Drug Metabolism and Toxicology*, *4*(8), 1075–1089. https://doi.org/10.1517/17425255.4.8.1075

Saarikoski, S. K., Sillanpää, M. K., Saarnio, K. M., Hillamo, R. E., Pennanen, A. S., & Salonen, R. O.

(2008). Impact of biomass combustion on urban fine particulate matter in Central and Northern Europe. *Water, Air, and Soil Pollution*, *191*(1–4), 265–277. https://doi.org/10.1007/s11270-008-9623-1

Seinfeld, J., Pandis, S. (1998). Atmospheric Chemistry and Physics: from Air Pollution to Climate Change. *Wiley-Interscience, NewYork*. Retrieved from https://www.academia.edu/35730031/ATMOSPHERIC_CHEMISTRY_AND_PHYSICS_From_Air_Pollution_to_Climate_Change_SECOND_EDITION

Sewell, F., Aggarwal, M., Bachler, G., Broadmeadow, A., Gellatly, N., Moore, E., … Burden, N. (2017, August 15). The current status of exposure-driven approaches for chemical safety assessment: A cross-sector perspective. *Toxicology*, Vol. 389, pp. 109–117. https://doi.org/10.1016/j.tox.2017.07.018

Shah, A. P., Pietropaoli, A. P., Frasier, L. M., Speers, D. M., Chalupa, D. C., Delehanty, J. M., … Frampton, M. W. (2008). Effect of inhaled carbon ultrafine particles on reactive hyperemia in healthy human subjects. *Environmental Health Perspectives*, *116*(3), 375–380. https://doi.org/10.1289/ehp.10323

Shimada, T., & Fujii-Kuriyama, Y. (2004, January). Metabolic activation of polycyclic aromatic hydrocarbons to carcinogens by cytochromes P450 1A1 and 1B1. *Cancer Science*, Vol. 95, pp. 1–6. https://doi.org/10.1111/j.1349-7006.2004.tb03162.x

Sigsgaard, T., Forsberg, B., Annesi-Maesano, I., Blomberg, A., Bølling, A., Boman, C., … Brunekreef, B. (2015). Health impacts of anthropogenic biomass burning in the developed world. *European Respiratory Journal*, *46*(6), 1577–1588. https://doi.org/10.1183/13993003.01865-2014

Smolders, E., & Degryse, F. (2002). Fate and effect of zinc from tire debris in soil. *Environmental Science and Technology*, *36*(17), 3706–3710. https://doi.org/10.1021/es025567p

Streets, D. G., Yarber, K. F., Woo, J. H., & Carmichael, G. R. (2003). Biomass burning in Asia: Annual and seasonal estimates and atmospheric emissions. *Global Biogeochemical Cycles*, *17*(4). https://doi.org/10.1029/2003gb002040

Tapanainen, M., Jalava, P. I., Mäki-Paakkanen, J., Hakulinen, P., Happo, M. S., Lamberg, H., … Hirvonen, M. R. (2011). In vitro immunotoxic and genotoxic activities of particles emitted

from two different small-scale wood combustion appliances. *Atmospheric Environment*, *45*(40), 7546–7554. https://doi.org/10.1016/j.atmosenv.2011.03.065

Thompson, J. E. (2018a). Airborne Particulate Matter: Human Exposure and Health Effects. In *Journal of Occupational and Environmental Medicine* (Vol. 60). https://doi.org/10.1097/JOM.0000000000001277

Thompson, J. E. (2018b). Airborne Particulate Matter: Human Exposure and Health Effects. In *Journal of Occupational and Environmental Medicine* (Vol. 60). https://doi.org/10.1097/JOM.0000000000001277

Thorpe, A., & Harrison, R. M. (2008). Sources and properties of non-exhaust particulate matter from road traffic: A review. *Science of the Total Environment*, *400*(1–3), 270–282. https://doi.org/10.1016/j.scitotenv.2008.06.007

Tiwari, M., Sahu, S. K., Bhangare, R. C., Yousaf, A., & Pandit, G. G. (2014). Particle size distributions of ultrafine combustion aerosols generated from household fuels. *Atmospheric Pollution Research*, *5*(1), 145–150. https://doi.org/10.5094/APR.2014.018

Tran, P. T. M., Ngoh, J. R., & Balasubramanian, R. (2020). Assessment of the integrated personal exposure to particulate emissions in urban micro-environments: A pilot study. *Aerosol and Air Quality Research*, *20*(2), 341–357. https://doi.org/10.4209/aaqr.2019.04.0201

Tseng, C. Y., Wang, J. S., & Chao, M. W. (2017, October 1). Causation by Diesel Exhaust Particles of Endothelial Dysfunctions in Cytotoxicity, Pro-inflammation, Permeability, and Apoptosis Induced by ROS Generation. *Cardiovascular Toxicology*, Vol. 17, pp. 384–392. https://doi.org/10.1007/s12012-016-9364-0

USEPA, U. S. E. P. A. (2004). Air Quality Criteria for Particulate Matter October 2004, Volume 2. *Air Quality Criteria for Particulate Matter*, *II*(October), 1148. Retrieved from file:///C:/Users/Laíssa/Downloads/VOL_II_FINAL_PM_AQCD_OCT2004.PDF

Vineis, P., Chadeau-Hyam, M., Gmuender, H., Gulliver, J., Herceg, Z., Kleinjans, J., … Wild, C. P. (2017). The exposome in practice: Design of the EXPOsOMICS project. *International Journal of Hygiene and Environmental Health*, *220*(2), 142–151. https://doi.org/10.1016/j.ijheh.2016.08.001

Vrijheid, M. (2014). EThe exposome: A new paradigm to study the impact of environment on health. *Thorax*, *69*(9), 876–878. https://doi.org/10.1136/thoraxjnl-2013-204949

Wang, X., Wang, Y., Bai, Y., Wang, P., & Zhao, Y. (2019). An overview of physical and chemical features of diesel exhaust particles. *Journal of the Energy Institute*, *92*(6), 1864–1888. https://doi.org/10.1016/j.joei.2018.11.006

Wang, Baoming, Hui Chen, Yik Lung Chan, and Brian G. Oliver. 2020. "Is There an Association between the Level of Ambient Air Pollution and COVID-19?" American Journal of Physiology-Lung Cellular and Molecular Physiology 319(3): L416–21. https://journals.physiology.org/doi/10.1152/ajplung.00244.2020

Watson, A. Y., Bates, R. R., & Kennedy, D. (1988). *Biological Disposition of Airborne Particles: Basic Principles and Application to Vehicular Emissions*. Retrieved from https://www.ncbi.nlm.nih.gov/books/NBK218161/

Weng, C. M., Lee, M. J., He, J. R., Chao, M. W., Wang, C. H., & Kuo, H. P. (2018). Diesel exhaust particles up-regulate interleukin-17A expression via ROS/NF-κB in airway epithelium. *Biochemical Pharmacology*, *151*, 1–8. https://doi.org/10.1016/j.bcp.2018.02.028

Whitby, K. T. (1978). The physical characteristics of sulfur aerosols. *Atmospheric Environment (1967)*, *12*(1–3), 135–159. https://doi.org/10.1016/0004-6981(78)90196-8

WHO. (2018). Health, environment and climate change. Road map for an enhanced global response to the adverse health effects of air pollution. *Seventy-First World Health Assembly*, *2016*(April), 1–8.

Wild, C. P. (2012, February 1). The exposome: From concept to utility. *International Journal of Epidemiology*, Vol. 41, pp. 24–32. https://doi.org/10.1093/ije/dyr236

World Health Organization. (2018). Exposure to ambient air pollution from particulate matter for 2016. *World Health Organization*, (April), 6. Retrieved from www.who.int/airpollution/data.%0Ahttps://www.who.int/airpollution/data/AAP_exposure_Apr2018_final.pdf?ua=1

Wright, J., & Ding, Y. (2016). Pathophysiological effects of particulate matter air pollution on the central nervous system. *Environmental Disease*, *1*(3), 85. https://doi.org/10.4103/2468-

5690.191932

Wu, X., Nethery, R. C., Sabath, B., Braun, D., Dominici, F., & James, C. (2020). *Exposure to air pollution and COVID-19 mortality in the United States: A nationwide cross-sectional study*. https://doi.org/10.1101/2020.04.05.20054502

Xie, H., Mason, M. M., & Wise, J. P. (2011). Genotoxicity of metal nanoparticles. *Reviews on Environmental Health*, *26*(4), 251–268. https://doi.org/10.1515/REVEH.2011.033

Yang, L., Hou, X. Y., Wei, Y., Thai, P., & Chai, F. (2017). Biomarkers of the health outcomes associated with ambient particulate matter exposure. *Science of the Total Environment*, *579*, 1446–1459. https://doi.org/10.1016/j.scitotenv.2016.11.146

Zhang, B., Jiao, L., Xu, G., Zhao, S., Tang, X., Zhou, Y., & Gong, C. (2018). Influences of wind and precipitation on different-sized particulate matter concentrations (PM2.5, PM10, PM2.5–10). *Meteorology and Atmospheric Physics*, *130*(3), 383–392. https://doi.org/10.1007/s00703-017-0526-9

Zhang, J. J., & Lioy, P. J. (2002). Human exposure assessment in air pollution systems. *TheScientificWorldJournal*, *2*, 497–513. https://doi.org/10.1100/tsw.2002.119

Zhang, K., Chai, F., Zheng, Z., Yang, Q., Zhong, X., Fomba, K. W., & Zhou, G. (2018). Size distribution and source of heavy metals in particulate matter on the lead and zinc smelting affected area. *Journal of Environmental Sciences (China)*, *71*, 188–196. https://doi.org/10.1016/j.jes.2018.04.018

CHAPTER II

AIMS AND METHODOLOGY

Exposure to air pollution especially to PM remains a major health risk. PM toxicity occurs primarily by fine and ultrafine particles due to their physical and chemical properties. However, toxicity mechanisms of PM are not fully recognized. Therefore, to contribute to fulfil this gap of knowledge and to better understand how air pollution impacts the human heath, toxicological studies were performed. The general aim of this thesis is to compare different sources of fine-ultrafine particles linking their *in vitro* effects to the particles size, physical and chemical properties. The research is focussed on diesel exhaust particles (DEP) of old and new generation diesel vehicles, as well on standard DEP (NIST Standard Reference Materials); on metal oxide NPs, representative of non-exhaust sources of pollutants, themselves and in mixture with DEP and on particles derived from combustion of biomass for residential heating.

2.1 SPECIFIC AIMS OF THE THESIS

- Relatively few studies have been conducted with mixtures of toxicants affecting the respiratory system. The cumulative risk assessment should be based on the evaluation of combined effects derived from the exposures to different PM sources. Objectives of the first part of the research was to analyse the combined *in vitro* effects of a standard DEP (SRM 2975) and commercial metal oxides NPs (ZnO, CuO), representative of non-exhaust sources of PM, on alveolar cells line and investigate the adverse outcome pathways activated by particles themselves and by the mixtures of DEP and NPs.

The major hypothesis was that NPs-mixture exposure can result in different cellular toxicity than the single counterpart (addressed in chapter III and IV).

- Diesel exhaust particles (DEP) are responsible for both respiratory and cardiovascular effects. However, many questions are still unravelled and the mechanisms behind the health effects induced by the exposure to DEP need further investigations. Furthermore, different emission sources can lead to diverse biological responses, thus the aim of this study was to compare the effects induced by three different DEPs: two standard reference materials (SRM 1650b and 2975) and one DEP directly sampled from a Euro 4 vehicle without DPF, to investigate the DEP-induced responses on the epithelial and endothelial cells separately, as well as their interplay in the resulting inflammatory effects and how these effects change in relation to the chemical composition of DEP. The major hypothesis was that different DEP chemical composition can lead to different biological effects and also that it is possible to study the response of endothelial cells indirectly exposed to particles (addressed in chapter V).

- In order to meet Euro 6 standards, new diesel vehicles must be equipped with after-treatment systems, such as Diesel Particulate Filter (DPF). Not only the old generation, but also the new generation diesel vehicles can potentially represent an important health hazard as well, in fact DPF requires to be regenerated regularly to clean the filter, which causes diesel vehicles to 'spill out' large amounts of particulate matter in the environment for a few minutes. Aim of this study was to compare an old diesel vehicle without DPF (Euro 3) and latest generation (or "Euro 6") one during the regeneration of DPF, for evaluating how the differences between an old and a new diesel vehicle may change the modal-particles emission, the physical-chemical characteristics and the hazard effects of DEP using bronchial cell line. The major hypothesis was that the evolution of diesel engines and of the technologies of after-treatment systems have led to a modification of DEP emitted and of the consequent toxicological effects (addressed in paper VI).

- Combustion derived particles (CBPs) have been linked to several adverse health effects, including lung cancer. Diesel exhaust particles (DEP) and particles derived from biomass burning are two of the major exhaust-sources of fine and ultrafine CBPs in urban areas. The aim of the present study was to characterise and compare the PM emitted from a mobile (diesel vehicle) and a fixed (wood burning) exhaust source, with respect to their physicochemical properties and biological effects, included inflammation, genotoxicity and gene expression response of bronchial cells exposed to Euro 3 DEP and particles derived from biomass combustion. The hypothesis was that the biological effects that may occur following exposure to biomass-derived PM are comparable to those observed for particles originated from traffic sources. (addressed in paper VII).

2.2 METHODOLOGY

To achieve the objectives reported before, different materials and techniques were used, here the methodology approach is briefly reported, materials and methods are explained in detail in the next chapters.

A schematic illustration of the methodology approach is presented in figure 1

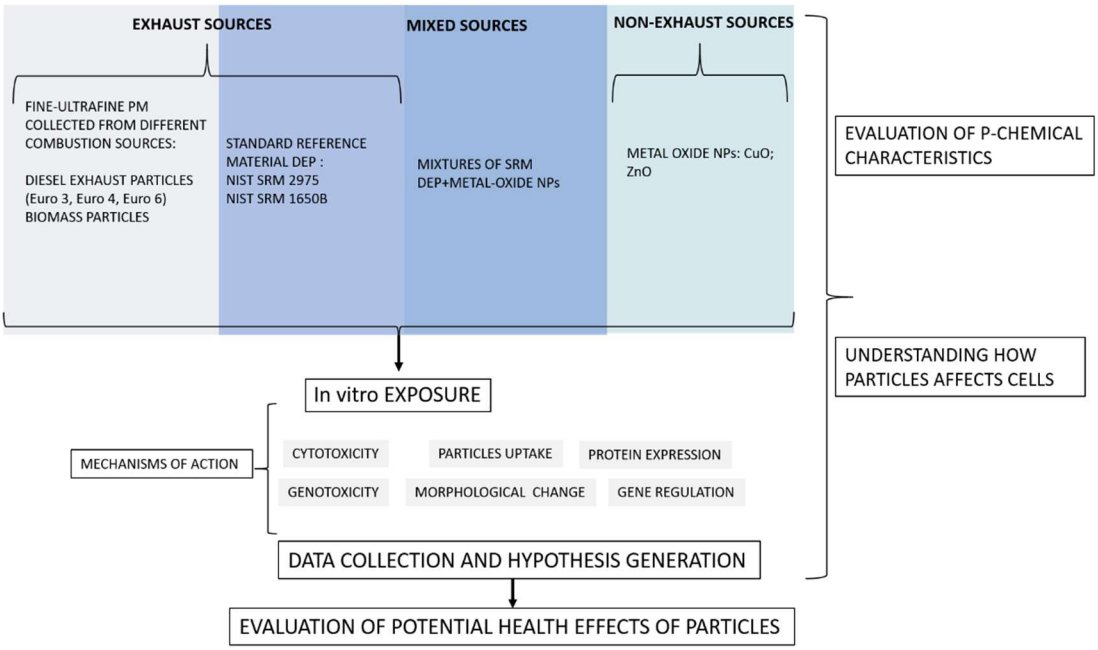

Figure 1: Schematic representation of research design.

The particles selected for these studies are representative of the main sources of exhaust fine and ultrafine particles (DEP and biomass CDPs) and of non-exhaust sources (CuO and ZnO NPs). Standard materials are very useful for studying the *in vitro* effects, having well-defined properties, in fact in many studies the NIST Standard Reference Material SRM® DEP have been used to confirm the toxic potential of DEP and to investigate the molecular mechanisms activated after its exposure. However, the use of particulates directly collected from different emission sources, applying methods to select a specific

dimensional fraction, gives the possibility to better characterize the particles based on their source and this provides a more realistic condition of environmental exposure. Metal-Oxide NPs were used as model particles representative of non-exhaust sources, in fact Cu and Zn, which in the environment are transformed in their oxide forms, are important pollutants derived from brakes, tyres, clutches and road surface wear. However, sampling of fine and ultrafine particles from direct sources presents some limitations. In fact, the difficulty to collect large quantities of material limits the use of such materials for P-chemical characterization and *in vitro* toxicology experiments. This is particularly the case of DEP collected from DPF regeneration of Euro 6 vehicle, which requires to force the regeneration in laboratory conditions that are not always easily achievable. After particles collections, filters were preserved at −20 °C until particles extraction, that was done by sonication in the bath-type sonicator. Particle suspensions were then dried into a desiccator, weighed with a microbalance and stored at - 20 °C until use for experiments. Furthermore, the extraction yield via sonication of the particulates from the filters is generally 70% with consequent loss of sampled material.

- **Particles used for the studies**:

Reference materials: two standard reference materials from the NIST were used: DEP SRM 1650b and 2975 (Diesel Particle NIST® SRM®, Sigma Aldrich), which derive from the exhaust emission of a heavy engine and a light duty, respectively.

Commercial NPs: CuO (CAS 1317-38-0) and ZnO (CAS 1314-13-2) NPs, with size <50 nm, were purchased from Sigma-Aldrich (Sigma-Aldrich, Milan, Italy).

Fine and ultrafine particles: DEP Euro 3, 4 and 6 and biomass CDPs were sampled on Teflon filters (Whatman, Maidstone, UK) using a high sample flow rate cascade impactor (Dekati® DGI-1570, Finland), that allows to collect particles based on the mass size distribution of the PM fraction. Teflon filters were placed in the last stage of the impactor, stage cut-point of 0.1 µm, for Euro 4 and in the stage cut-point 2.5 µm for Euro 3 and Euro 6 to collect as much particles as possible. DEP Euro 3 and Euro 4 without DPF were run on a chassis dynamometer following a driving cycle named “URBAN” Artemis Driving Cycle, which was chosen to be representative of urban driving, while DEP from a Euro 6 were sampled over

a DPF regeneration phase. Euro 6 vehicle was run on a chassis dynamometer, following the standard homologation Worldwide harmonized Light vehicles Driving Cycle (WTLC) to force DPF regeneration.

Biomass CDPs, produced from a stove (Piazzetta Model e920, 8 kW) fuelled with beech wood were sampled on Teflon filters after dilution of flue gases with clean air, using the Gravimetric Impactor to remove bigger aggregates (stage cut-point of 2.5 µm).

A graphical representation of particles sampling is reported in Figure 2.

Filters from diesel and biomass combustion, were preserved at −20 °C after sampling and until chemical characterization or particles extraction for biological tests.

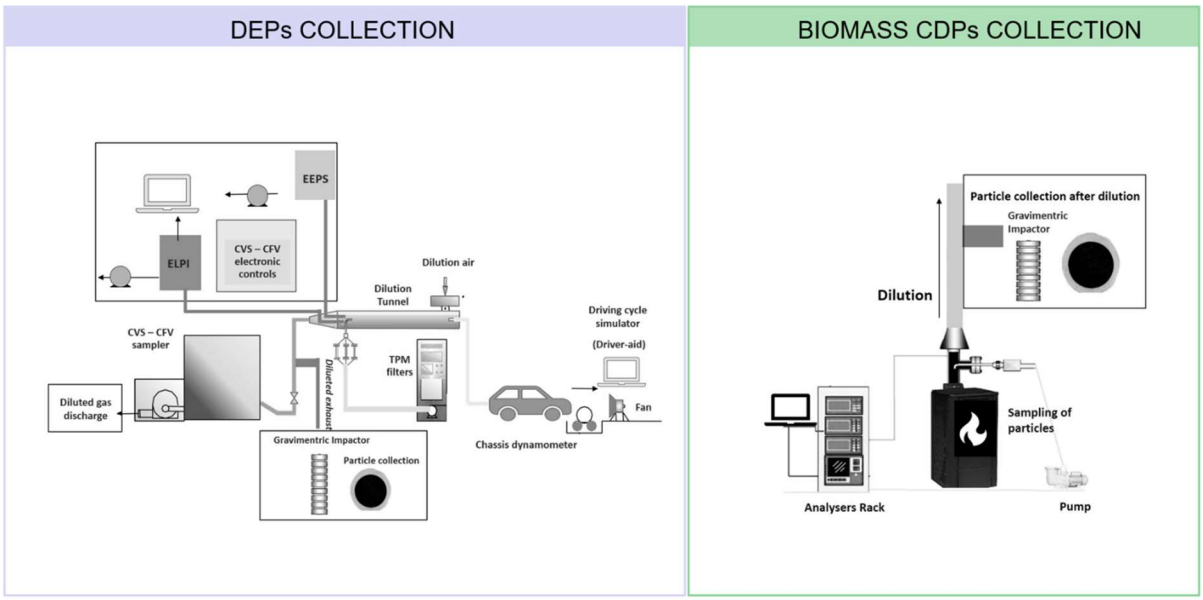

Figure 2: Graphical representation of particles collection of DEPs from diesel vehicle and of CDPs emitted from a stove fuelled with biomass.

- **P-chemical characterisation of particles**:

Particles were characterized for their morphological (shape and size) and chemical (organic and inorganic composition) properties. Transmission electron microscopy (TEM) was used in order to characterize the particles morphology and TEM/STEM EDX spectra were acquired to evaluate elemental composition. Metal and polycyclic aromatic hydrocarbon

(PAHs) content were quantified through Inductively Coupled Plasma Mass Spectrometry (ICP-MS) and Chromatography with mass spectrometry (GC-MS), respectively. The particles hydrodynamic size was measured using a dynamic light scattering (DLS) technique. The ionic dissolution of the NPs themself and in mixture with DEP was also evaluated. The dissolution of the ZnO and CuO NPs in the cell medium was determined by quantifying the Zn^{2+} and Cu^{2+} in solution by inductively coupled plasma-optic emission spectroscopy (ICP-OES) after ultrafiltration of particle suspensions.

- **Toxicological analyses**: to predict the *in vitro* bio-interaction and effects of the particles at the level of the respiratory system, appropriate cell lines were used*:* Human Alveolar Basal Epithelial cells (A549), Human Bronchial Epithelial Cells (BEAS-2B) and Human Pulmonary Microvascular Endothelial Cells (HPMEC-ST1.6R). A549 cells derived from the human lung adenocarcinoma, this cells present a type II pneumocyte-like phenotype and are characterized by the presence of hydrophilic surfactant-associated and lamellar bodies (Murgia et al. 2014). This cell line is a good model, wildly used in the research to test PM and NPs cytotoxic effects (He et al., 2017)(Deng et al., 2013)(Zhang et al., 2018). BEAS-2B cells are immortalized, but non-tumorigenic, human epithelial bronchial cells obtained from a non-cancerous individual and transfected with DNA sequences of an adenovirus, the *Simian Virus* 40 (Ad12-SV40)(Reddel et al., 1988). The cells conserve the ability to undergo squamous differentiation in response to serum. BEAS-2B is a valid model for study the toxicological effects of PM and allow to study differentiation and carcinogenesis process (Zhou et al., 2016)(Chi et al., 2018). HPMEC-ST1.6R are endothelial cells deriving from the pulmonary microcirculation. Cells were generated by co-transfection with a plasmid encoding for hTERT and the SV40 large T-antigen. They exhibit several unique specific characteristics that define endothelial cells including platelet endothelial cell adhesion molecule, von Willebrand factor and the adhesion molecules (Krump-Konvalinkova et al., 2001). HPMEC-ST1.6R cells co-cultured with alveolar epithelial cells are able to differentiate an air-blood barrier *in vitro* model useful for study the effects of PM and NPs (Bengalli et al., 2013).

  Cells were exposed to particles in a submerge condition, using concentrations of particles reflecting as much as possible the human exposure in polluted urban area. In fact, a critical aspect in the *in vitro* studies is testing concentrations representative of real exposure

conditions. For this reason, it is necessary to reconcile the in vivo exposures with the particles concentrations in cell cultures. Basing on literature data, the doses selected for the toxicological studies, mimic an exposure scenario similar to that of an urban area, where winter daily PM concentrations can exceed 70 μg/m^3(Li et al. 2003).

In vitro studies with monocultures of human lung cells shed deeper knowledge on the cellular mechanisms by which PM induce toxicity, but this model presents some limitation, in fact studying the toxicity of PM or NPs in only one cell line can under-or overestimate its induced adverse effects (Kasurinen et al., 2018). For this reason, in this thesis, lung models involving both epithelial and vascular endothelial cells have been used in addition to *in vitro* monoculture models. Different biological endpoints were investigated (e.g., oxidative stress; inflammation; cell death; DNA damage) and the obtained results provide a focus on the biological responses induced by fine-ultrafine particles on lung cells.

2.3 BIBLIOGRAPHY

Bengalli, R., Mantecca, P., Camatini, M., & Gualtieri, M. (2013). Effect of nanoparticles and environmental particles on a cocultures model of the air-blood barrier. *BioMed Research International*, *2013*. https://doi.org/10.1155/2013/801214

Chi, Y., Huang, Q., Lin, Y., Ye, G., Zhu, H., & Dong, S. (2018). Epithelial-mesenchymal transition effect of fine particulate matter from the Yangtze River Delta region in China on human bronchial epithelial cells. *Journal of Environmental Sciences (China)*, *66*, 155–164. https://doi.org/10.1016/j.jes.2017.05.002

Deng, X., Zhang, F., Rui, W., Long, F., Wang, L., Feng, Z., Chen, D., & Ding, W. (2013). PM2.5-induced oxidative stress triggers autophagy in human lung epithelial A549 cells. *Toxicology in Vitro*, *27*(6), 1762–1770. https://doi.org/10.1016/j.tiv.2013.05.004

He, T., Long, J., Li, J., Liu, L., & Cao, Y. (2017). Toxicity of ZnO nanoparticles (NPs) to A549 cells and A549 epithelium in vitro: Interactions with dipalmitoyl phosphatidylcholine (DPPC). *Environmental Toxicology and Pharmacology*, *56*, 233–240. https://doi.org/10.1016/j.etap.2017.10.002

Kasurinen, S., Happo, M. S., Rönkkö, T. J., Orasche, J., Jokiniemi, J., Kortelainen, M., Tissari, J., Zimmermann, R., Hirvonen, M. R., & Jalava, P. I. (2018). Differences between co-cultures and monocultures in testing the toxicity of particulate matter derived from log wood and pellet combustion. *PLoS ONE*, *13*(2). https://doi.org/10.1371/journal.pone.0192453

Krump-Konvalinkova, V., Bittinger, F., Unger, R. E., Peters, K., Lehr, H. A., & Kirkpatrick, C. J. (2001). Generation of human pulmonary microvascular endothelial cell lines. *Laboratory Investigation*, *81*(12), 1717–1727. https://doi.org/10.1038/labinvest.3780385

Li, N., Hao, M., Phalen, R. F., Hinds, W. C., & Nel, A. E. (2003). Particulate air pollutants and asthma. A paradigm for the role of oxidative stress in PM-induced adverse health effects. *Clinical Immunology (Orlando, Fla.)*, *109*(3), 250–265.

http://www.ncbi.nlm.nih.gov/pubmed/14697739

Murgia, X., De Souza Carvalho, C., & Lehr, C. M. (2014). Overcoming the pulmonary barrier: New insights to improve the efficiency of inhaled therapeutics. In *European Journal of Nanomedicine* (Vol. 6, Issue 3, pp. 157–169). Walter de Gruyter GmbH. https://doi.org/10.1515/ejnm-2014-0019

Reddel, R. R., Ke, Y., Gerwin, B. I., McMenamin, M. G., Lechner, J. F., Su, R. T., Brash, D. E., Park, J.-B., Rhim, J. S., & Harris, C. C. (1988). Transformation of Human Bronchial Epithelial Cells by Infection with SV40 or Adenovirus-12 SV40 Hybrid Virus, or Transfection via Strontium Phosphate Coprecipitation with a Plasmid Containing SV40 Early Region Genes. *Cancer Research*, *48*(7).

Zhang, Y., Darland, D., He, Y., Yang, L., Dong, X., & Chang, Y. (2018). Reduction of PM2.5 toxicity on human alveolar epithelial cells A549 by tea polyphenols. *Journal of Food Biochemistry*, *42*(3). https://doi.org/10.1111/jfbc.12496

Zhou, W., Tian, D., He, J., Wang, Y., Zhang, L., Cui, L., Jia, L., Zhang, L., Li, L., Shu, Y., Yu, S., Zhao, J., Yuan, X., & Peng, S. (2016). Repeated PM2.5 exposure inhibits BEAS-2B cell P53 expression through ROS-Akt-DNMT3B pathway-mediated promoter hypermethylation. *Oncotarget*, *7*(15), 20691–20703. https://doi.org/10.18632/oncotarget.7842

CHAPTER III

MIXTURES EFFECTS OF DIESEL EXHAUST AND METAL OXIDE NANOPARTICLES IN HUMAN LUNG A549 CELLS.

Airborne ultrafine particles (UFPs) mainly derive from combustion sources (e.g., diesel exhaust particles—DEP), abrasion sources (non-exhaust particles) or from the unintentional release of engineered nanoparticles (e.g., metal oxide nanoparticles—NPs), determining human exposure to UFPs mixtures. The aim of the present study was to analyse the combined in vitro effects of DEP and metal oxide NPs (ZnO, CuO) on human lung A549 cells. The mixtures and the relative single NPs (DEP, ZnO, CuO) were characterized by transmission electron microscopy (TEM), dynamic light scattering (DLS) and inductively coupled plasma-optic emission spectroscopy (ICP-OES). Cells were exposed for different times (3–72 h) to mixtures of standard DEP at a subcytotoxic concentration and ZnO and CuO at increasing concentrations. At the end of the exposure, the cytotoxicity was assessed by 3-(4,5-Dimethylthiazol-2-yl)-2,5-Diphenyltetrazolium Bromide (MTT) and clonogenic tests, the pro-inflammatory potential was evaluated by interleukin-8 (IL-8) release and the cell morphology was investigated by fluorescence and transmission electron microscopy. The obtained results suggest that the presence of DEP may introduce new physico-chemical interactions able to increase the cytotoxicity of ZnO and to reduce that of CuO NPs.

This chapter is a published paper *"Zerboni A, Bengalli R, Baeri G, Fiandra L, Catelani T, Mantecca P. Mixture Effects of Diesel Exhaust and Metal Oxide Nanoparticles in Human Lung A549 Cells, Nanomaterials (Basel). 2019;9(9):1302. Published 2019 Sep 11. doi:10.3390/nano9091302."*

Graphical abstract

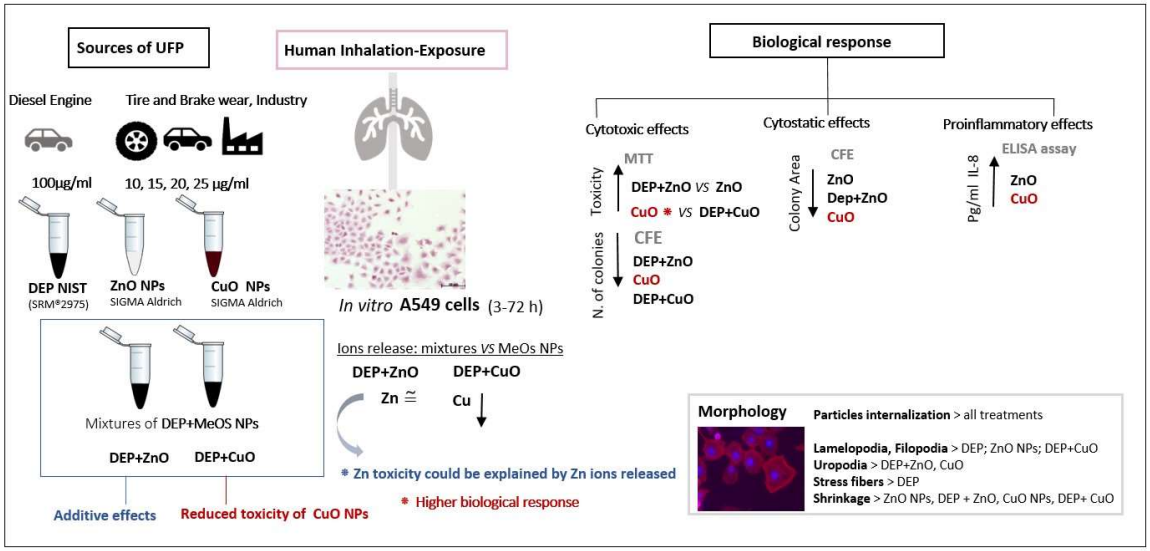

1.Introduction

Several epidemiological studies show an increase in respiratory and cardiac morbidity and mortality due to the exposure to particulate matter (PM), especially related to pulmonary and cardiovascular diseases (Pope et al. 2002). PM is a mixture of particles suspended in the air and is subdivided in PM_{10}, $PM_{2.5}$, and ultrafine particles (UFPs) (<10 µm, <2.5 µm, and <0.1 µm, respectively) according to its "aerodynamic equivalent diameter". Nowadays, UFPs are the fraction of inhalable particles that largely impact on human health, since they can deeply penetrate in the respiratory system, reaching the profound lungs, where they interact with the alveolar epithelium, potentially cross the respiratory barrier and eventually reach secondary target organs (Möller et al. 2008). In the recent years, increasing attention has been paid to the monitoring of UFP personal exposure (Wallace

and Ott 2011), as well as to the experimental studies aimed at discovering the UFsP toxicological impact.

Combustion processes represent the main sources of UFPs, especially in urban areas. Among them, diesel exhaust particles (DEP), which are composed of a carbonaceous core and adsorbed organic compounds, including polycyclic aromatic hydrocarbons (PAHs), metals, and other trace elements (H.-E. Wichmann 2007), are the emissions that mainly contribute to urban PM. Another source of UFPs are derived from non-exhaust sources, coming from tire and brake wearing (Adamiec, Jarosz-Krzemińska, and Wieszała 2016) or from the unintentional release of engineered nanoparticles (NPs) in the environment. Since the exposure to DEP and to non-exhaust particles occurs simultaneously, it is inevitable to consider their possible interaction in biological systems. DEP toxicity has been studied both *in vitro* and in vivo and in 2012, the International Agency for Research on Cancer concluded that DEP is a carcinogen (Group I) (Bacchetta et al. 2012). Exposure to diesel exhaust is widespread all over the world and, in the last few years, the issue of health effects derived from DEP exposure was dealt with by national and international emission regulations for light duty vehicles emission. Non-exhaust particles derive from abrasive sources, which include tire and brake wear and abrasion of the road surface. Trace metals are an important source emitted by the above-mentioned processes in the urban environment (Abu-Allaban et al. 2003). The most abundant metals originating from brake wear are: Fe, Cu, Zn, Sn, and Sb (Grigoratos and Martini 2015), which mainly contribute to the non-exhaust fraction of PM. After Fe, Cu is the second element which is more representative of NPs emitted by brake wear (Gasser et al. 2009), while zinc-based nanoparticles (Zn-NPs) mainly derive from tire wear (Harrison et al. 2012; Hjortenkrans, Bergbäck, and Häggerud 2007). Most of the metals are subject to corrosion either at room temperature or at high-temperatures and, by means of atmospheric oxidation, it is possible to produce passivating oxide layers on elemental metal Cu and Zn (Samal 2016). Metal oxides may have surface properties similar to their element counterparts (Walkowicz et al. 2018). Along with the extensive NPs industrial and medical application, especially of metal oxide nanoparticles (MeO), an accidental release in the environment of NPs could also occur during production and disposal operations. Nevertheless, even an unintentional exposure to these particles can occur, since they are present in everyday life goods, including textiles, food packaging,

cosmetics, and paintings (Lu et al. 2015). Finally, NPs have also been employed as engine fuel additives as an improvement in the abatement of greenhouse gases (Park et al. 2008). All of this evidence shows that, upon release and emission of nanomaterials (NMs) in the environment, these compounds may interact with other chemicals/contaminants, including metals and PAHs, that could lead to the occurrence of mixture effects and different toxicity on exposed organisms or *in vitro* systems. Furthermore, an initial classification of the possible NM–chemical interactions has been proposed by Naasz and colleagues (Naasz et al. 2018), which also studied the transition of these interactions into specific biological effects.

In order to understand the possible mixture's effects of DEP and non-exhaust particles we chose CuO NPs and ZnO NPs as representative MeO NPs. Studies showed that CuO NPs induce oxidative stress and cytotoxicity on airway epithelial cells (Ahamed et al. 2010; Fahmy and Cormier 2009), mostly through the Trojan horse mechanism and consequent cellular death or autophagy (Moschini et al. 2013).

Other works demonstrate that ZnO NPs are toxic to different mammalian cells, thanks to their tendency to release in the cellular medium, free zinc ions, which exert their toxic effect in exposed cells (Buerki-Thurnherr et al. 2013).

Although several studies have been conducted on the toxicity of MeO NPs, the aspect regarding their potential interactions with other air pollutant UFPs, in particular DEP, has still been poorly investigated. Many works have studied the toxicity of DEP. In vivo and in *vitro* studies report that DEP induced changes in markers of inflammation, including cytokines (Schwarze et al. 2013; Stenfors et al. 2004), oxidative stress and DNA damage (Douki et al. 2018). Nevertheless, in our recent studies we demonstrated that different DEPs may induce different *in vitro* effects on the base of the chemical composition (PAHs and metals) (Bengalli et al. 2019).

The aim of the present study is to analyse the combined *in vitro* effects of a standard DEP (SRM® 2975) and commercial metal oxides NPs (ZnO, CuO), on human lung cells A549 as a model of the respiratory system.

A549 cells derive from a human pulmonary adenocarcinoma and show properties such as surfactant production and transport-like AT-II cells in vivo, secrete cytokines, and perform phase I and phase II xenobiotic biotransformation similar to lung tissue (Castell, Donato, and Gómez-Lechón 2005; Fröhlich and Salar-Behzadi 2014). For these reasons, they are the

most representative cell line for lung tissue and are used for the screening of nanoparticles in inhalation toxicology. Furthermore, different regulatory frameworks for the safety evaluation of NMs, including the Organisation for Economic Co-operation and Development (OECD) Working Party on Manufactured Nanomaterials (WPMN) and the NANoReG project. A549 cells have been used as main the cell model common for several biological endpoints, making it a promising candidate cell model for regulation of *in vitro* testing of NPs.

Of relevant importance is to understand if ZnO NPs and CuO NPs may interact with DEP and how this may contribute in modifying the toxic effects. For this purpose, a set of tests was employed to evaluate dose-response cytotoxicity, colony forming efficiency (CFE), inflammatory response and morphology changes, and data were discussed in relation to the physicochemical *properties* of particles. More robust data regarding how single particles and mixtures elicit their effects may contribute to improving the hazard risk assessment of accidentally released UFPs and engineered NMs.

2. Materials and Methods

2.1. Preparation of the Particle Suspensions

Commercial CuO (CAS 1317-38-0) and ZnO (CAS 1314-13-2) NPs, with size <50 nm, were purchased from Sigma-Aldrich (Sigma-Aldrich, Milan, Italy). Standard Diesel

Exhaust Particles (DEP) were purchased from the National Institute of Standard and Technology (NIST) (SRM®2975) (Sigma-Aldrich). Following preparation protocols already set up in our lab (Longhin et al. 2016; Moschini et al. 2013), NPs and DEP were weighed in a micro-balance (Sartorius, Goettingen, Germany) in sterile condition, under a laminar flow hood, suspended in sterile ultrapure water, and sonicated in an ultrasonic bath (SONICA Soltec, Milano, Italy) for 10 min.

DEP (2 mg/mL) was sonicated with a probe-type sonicator until it reached energy 3 kJ/s (Bandelin Sonopuls, Berlin, Germany), in order to obtain a well-dispersed suspension of particles. Suspensions were stored at room temperature, while DEP was stored at –20 °C for a period no longer than 15 days. The mixtures were freshly prepared before the experiments using a sub cytotoxic concentration of DEP (100 μg/mL) and increasing concentrations of CuO and ZnO NPs (10, 15, 20, 25 μg/mL). Mixtures were sonicated in the

ultrasonic bath (SONICA Soltec) for 10 min. The mixtures are indicated as DEP + CuO and DEP + ZnO and were produced by mixing DEP at 100 µg/mL with metal oxide NPs to achieve the final concentrations of CuO and ZnO used for the single NPs.

2.2. Physico-Chemical Characterization of the Particle Suspensions

2.2.1. Transmission Electron Microscopy (TEM)

To study the particles' morphology, primary size, and agglomeration state, a drop (5 µL) of the following particle suspensions was added in ultrapure water: DEP at 100 µg/mL, CuO and ZnO at 20 µg/mL, and mixtures of DEP (100 µg/mL) and CuO or ZnO (20 µg/mL) were pipetted onto Formvar®-coated 200 mesh copper grids. The excess of water was gently blotted by filter paper. Once dried, grids were observed under the TEM Jeol JEM-1220 (JEOL, Tokyo, Japan) operating at 80 kV, equipped with a charged-coupled device (CCD) camera.

2.2.2. Dynamic Light Scattering (DLS)

The particles hydrodynamic size and surface charge were measured using a dynamic light scattering (DLS) (Malvern Zetasizer, Malvern, UK) technique, at a scattering angle of θ = 90°. ZnO, DEP + ZnO, CuO, and DEP + CuO mother suspensions were prepared using the method previously described, then diluted in Milli-Q water at a concentration of 100 µg/mL of DEP and 20 µg/mL of NPs.

2.2.3. Inductively Coupled Plasma-Optic Emission Spectroscopy (ICP-OES)

The dissolution of the ZnO and CuO NPs in the cell medium was determined by quantifying the Zn^{2+} and Cu^{2+} in solution by inductively coupled plasma-optic emission spectroscopy (ICP-OES) after ultrafiltration of particle suspensions. Briefly, ZnO, CuO, and the mixtures DEP + CuO and DEP + ZnO were suspended in cell culture medium at a final metal oxide concentration of 20 µg/mL and incubated for 3 and 24 h at 37 °C. Then, before the analysis, the solutions were ultra-filtrated at 4000 g for 30 min, using centrifuge tubes, VIVASPIN, with a molecular weight cut-off of 10,000 Da (Sartorius StedimBiotech GmbH, Goettingen, Germany). The solution obtained from the ultrafiltration was then analysed by ICP-OEC (Optima 7000 DV; PerkinElmer,Waltham, MA, US).

2.3. Cell Culture and Treatments

Human alveolar epithelial cells, A549 (ATCC® CCL-185, American Type Culture Collection, Manassas, VA, US), were grown at 37 °C, 5% CO_2, and maintained in OptiMEM medium (Gibco, Life Technologies, Monza, Italy) supplemented with 10% heat-inactivated fetal bovine serum (FBS, Gibco) and 1% Penicillin/Streptomycin (Euroclone, Pero, Italy). For the experiments, cells (passages from 7 to 30), were seeded at a concentration of 1.6×10^4 cells/cm^2 on 6-well plates (Corning®) and grown up for 24 h. At the optimal confluence (80%), the culture medium was replaced with OptiMEM (1% FBS) and cells were exposed, directly adding particles suspension into the medium for different times of exposure (3, 24, 48, and 72 h) depending upon the different biological endpoints investigated. Experiments were assessed in at least three independent replicates.

2.4. Biological Responses: Cytotoxicity Assays

2.4.1. Cell Viability: MTT Assay

For the 3-(4,5-Dimethylthiazol-2-yl)-2,5-Diphenyltetrazolium Bromide (MTT) assay, A549 cells were treated to DEP 100 µg/mL, CuO NPs, and ZnO NPs to 10, 15, 20 and 25 µg/mL, and a mixture of DEP 100 µg/mL + NPs (CuO or ZnO) at the concentration of 10, 15, 20 and 25 µg/mL. At the end of exposure at different time points (3 h, 24 h and 48 h), cells were rinsed with phosphate-buffered saline (PBS) and then MTT (Sigma Aldrich) solution, prepared in OptiMEM 10% FBS at a concentration of 0.3 mg/mL, was added to the cells and incubated for 3 h.

After the conversion of the substrate to a chromogenic product by metabolically active cells, the medium was removed and the purple MTT formazan crystals were solubilized with dimethyl sulfoxide (DMSO, Euroclone, Pero, Italy). The absorbance of each sample was measured with a multiplate reader spectrophotometer (Infinite 200Pro, TECAN, Männedorf, Switzerland) at 570 nm, using 690 nm as a reference wavelength. Cell viability, proportional to absorbance, was reported as relative decrease compared to the absorbance resulting from the control, considered as 100% of viable cells. Data are presented as mean ± standard error (SE) of at least three independent experiments.

2.4.2. Colony Forming Efficiency Assay

The colony forming efficiency (CFE) assay is schematized in Supplementary Materials (Table S1). On Day 1, 200 A549 cells were seeded in 3 mL of OptiMEM 10% FBS in Petri dishes (Corning®, 60 mm diameter). According to Ponti and colleagues (Jessica Ponti et al. 2014), after 24 h (Day 2), particle suspensions were added to the cells directly in the culture medium. Cells were treated with DEP 100 µg/mL, CuO NPs and ZnO NPs 10 and 20 µg/mL, and mixtures of DEP 100 µg/mL + NPs (CuO or ZnO) at concentrations of 10 and 20 µg/mL. Cells were treated for 24 h (from Day 2 to Day 3) and for 72 h (from Day 2 to Day 5). On Day 3 (24 h) and on Day 5 (72 h) the treatment was removed and replaced with fresh OptiMEM 10% FBS and cells were cultured for further 48 h (Day 8). At Day 8, the medium was removed and the colonies were fixed using a solution of 4% (*v/v*) formaldehyde in PBS, then stained using 0.4% (*v/v*) of Crystal Violet (Sigma Aldrich) 15% in aqueous ethanol for 5 min and washed several times with Milli-Q water. After drying, colonies were counted under a stereomicroscope, Carl Zeiss Stemi SV6 (Carl Zeiss SpA, Milano, Italy), and the percentage of the Colony Forming Efficiency (% CFE) was calculated as follows:

$$\%\mathrm{CFE} = \frac{\text{average of number of colonies in treatment}}{\text{average of number of colonies in the control}} \times 100$$

In this work, cell colonies containing more than 20 cells were deemed adequate for the counting. Additionally, the area of the colonies was measured by AxioVision Real 4.8 software (Carl Zeiss Solutions, Jena, Germany) and expressed as μm^2. To obtain this supplementary information on the colonies' area, each plate was analysed by using the stereomicroscope. Experiments were performed in triplicate and parallel tests were performed in duplicate.

2.5. Quantification of Cytokine IL-8 Release

At the end of particles exposure (3 h and 24 h), cell culture media were collected and centrifuged at 10,000 rpm for 6 minutes to remove cell debris and particles suspended in the medium. The final supernatants were stored at −80 °C until analysis. IL-8 protein levels were determined according to the manufacturer's instructions (IL-8, Life Technologies). The absorbance of each sample was measured by a multiplate reader (Infinite 200Pro, TECAN) at the wavelength of 450 nm and the amount of proteins in pg/mL was calculated based on standard curves. Data were expressed as pg/mL and experiments were performed in at least triplicate.

2.6. Morphological Analysis

2.6.1. Fluorescence Microscopy

For the staining, A549 cells were fixed with 4% paraformaldehyde and, after washing with PBS, cytoskeleton actin was marked with rhodamine-phalloidin (1:150, Cytoskeleton Inc., Denver, CO, US). Nuclei were counter-stained with DAPI (4',6-diamino-2-phenylindole, 1:100, Molecular Probes, Life Technologies). Finally, the slides were mounted with VECTASHIELD® Antifade mounting medium (Vector Laboratories Inc., Burlingame, CA, US). The images were acquired with a reverse microscope (Carl Zeiss Axio Observer) and processed with the Zeiss ZEN (Blue edition) software.

2.6.2. Transmission Electron Microscopy

For transmission electron microscopy analysis, cells cultured in 6-well plates and exposed to the different NPs as described above, were trypsinized, washed in PBS, and immediately fixed for 45 minutes in a 2% glutaraldehyde solution prepared in the same medium. Subsequently, cells were centrifuged for 10 min at 13,000 rpm in order to obtain a pellet, and fixative solution was replaced with 2% glutaraldehyde solution prepared in 0.1 M phosphate buffer (PB). After 1 hour of fixation, cell pellets were washed with PB 0.1 M and post-fixed for 1 h in 1% Osmium Tetroxide solution prepared in PB 0.1 M. After several washes in PB 0.1 M, samples were transferred in Milli-Q water and then incubated overnight at 4 °C in 1% Uranyl Acetate aqueous solution. Finally, samples were dehydrated in ascendant with a series of alcohols, transferred in a final concentration of propylene oxide, and then embedded in Epon resin. After resin polymerization at 60 °C for 48 h, samples were cut with Rickert-Jung ultramicrotome and ultra-thin sections (70 nm) were collected on TEM grids. Samples were observed with a Jeol JEM 1220 Transmission Electron Microscope (JEOL, Japan), operating at 80 kV acceleration voltage and equipped with a

Lheritier LH72WA-digital camera, and by a Zeiss SEM-FEG Gemini 500, operating at 30 kV in scanning transmission electron microscopy (STEM) mode (Zeiss, Germany).

2.7. Statistical Analysis

All the experiments were performed in independent triplicates, and data were reported as mean ± standard error (SE), if not otherwise specified. Statistical analyses were performed using One-Way ANOVA or unpaired *t*-test and relative post-hoc analysis with Sigma Stat 3.2. Values of $p < 0.05$ were considered statistically significant.

3. Results

3.1. Characterization of Nanoparticle (NP) Mixtures

TEM analysis showed that the different particles suspended in solution form aggregates (Figure 1). The DEP sample showed a chain composition, typical of soot. In a mixture with NPs, DEP forms particle aggregates with a chain structure too (Figure 1A, B). The single NPs of CuO (Figure 1C) and ZnO (Figure 1D) are also distinguishable in the mixtures DEP + CuO (Figure 1A) and DEP + ZnO (Figure 1B), since the NPs, being composed of heavy elements, are more electrodense compared to DEPs which are composed mainly of Carbon atoms. ZnO NPs showed an irregular shape and aggregates are composed of particles of similar size (Figure 1D), with jagged edges. Size distribution ranges from 10 to 40 nm with a mean diameter of 38 nm (Bengalli et al. 2017). TEM analysis revealed that CuO NPs also have an irregular shape (Figure 1C), especially with spherical and rod-like particles. The size distribution ranges from 10 to 50 nm and mean diameter of 34 nm (Moschini et al. 2013).

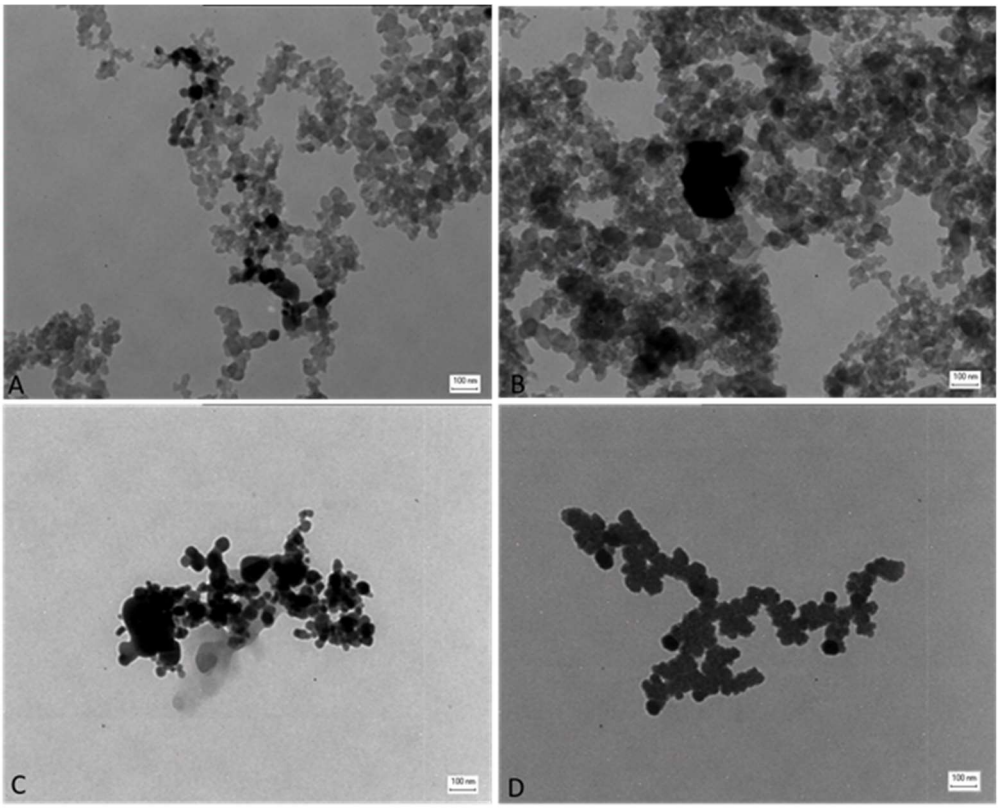

Figure 1. Morphological characterization of nanoparticles (NPs) and mixtures**.** Transmission electron microscopy (TEM) images of mixtures of: diesel exhaust particles (DEP) (100 µg/mL) and CuO (20 µg/mL) (A), DEP (100 µg/mL) and ZnO (20 µg/mL) (B), single NPs of: CuO NPs (C), ZnO NPs (D). Scale bars = 100 nm.

DLS analysis (Table 1) showed that the hydrodynamic diameter of all the particles increased when in culture medium compared to the data obtained in Milli-Q water, thanks to the tendency of NPs to form bigger aggregates in these media, due to the protein corona phenomenon. Nevertheless, the analysis in cell culture medium confirmed that the particles' aggregates fall in the nanometric range. CuO NPs show a mean hydrodynamic diameter (z-average) higher than the other particles (464.67 ± 2 nm). DEP particles had the lower Polydispersity Index (PdI = 0.21 ± 0.01 in Opti-MEM) (Table 1), and therefore they were the more stable in the medium. Data showed that in culture cell medium, in the presence of DEP, the z-average is lowered for both CuO and ZnO NPs.

The data regarding ζ-Potential measurements in Milli-Q water (Table 1) showed positive potentials for ZnO and CuO NPs respectively, 25 ± 0.13 and 12 ± 0.6 mV, and negative potentials for their respective mixtures (–19 ± 0.21 mV for DEP + ZnO and –18 ± 0.09 for DEP + CuO). This behaviour could reflect the tendency of these NPs to have a poor stability in Milli-Q and to aggregate, since their surface charge does not allow a strong repulsion.

DEP instead have a negative ζ-potential (−35 ± 0.52 mV) (Table 1) that indicates the stability of this suspension.

	ZnO	DEP + ZnO	CuO	DEP + CuO	DEP (2975)
Milli-Q Z-average ± SE (nm)	275.7 ± 9	179.7 ± 2	208.43 ± 2	217.07 ± 3	263.03 ± 3
PdI	0.361	0.352	0.209	0.223	0.29
Opti-MEM 1% FBS Z-average ± SE (nm)	314.38 ± 204	207.37 ± 7	464.67 ± 2	275.7 ± 3	320.8 ± 6
PdI	0.63	0.52	0.35	0.22	0.21
Milli-Q Z-potential ± SE (mV)	25 ± 0.13	−19 ± 0.21	12 ± 0.6	−18 ± 0.09	−35 ± 0.52

Table 1. Dynamic light scattering (DLS) analyses of CuO and ZnO NPs and mixtures. Z-average and PdI (polidispersity index) of particles suspended in Milli-Q water and in culture medium, as well as ζ-potential in water, are presented. For the analyses, CuO and ZnO NPs at the concentration of 20 μg/mL were used, while for the mixtures, a suspension of 100 μg/mL of DEP and 20 μg/mL of NPs were prepared. For the analyses of DEP, the concentration of 100 μg/mL was used.

ICP data (Table 2) show that the metal ions dissolution in cell medium is higher for ZnO NPs and for mixtures DEP + ZnO. In Table 2, the percentages of released ions are reported, and it is clear that dissolution was not complete for any of the particle suspensions. The release of Zn ions occurs with a higher percentage (69%) after 24 h of incubation with ZnO NPs, rather than the mixture of DEP + ZnO (62%). The release of Cu ions results is higher with the single NPs of CuO (43.3%) after 24 h of incubation, compared to the DEP + CuO mixture (26.7%). At 24 h, it is evident that the presence of DEP in both mixtures reduced the ions release.

	ZnO	DEP + ZnO	CuO	DEP + CuO
3 h ppm Zn	9.36 ± 1.1	8.3 ± 0.3	0.1 ± 0.0	0.1 ± 0.0

3 h % Zn	51.2%	51.5%	0%	0%
24 h ppm Zn	11.1 ± 0.1	10.0 ± 0.1	nd	nd
24 h % Zn	69.4%	62.5%	nd	nd
3 h ppm Cu	nd	nd	2.4 ± 0.1	2.4 ± 0.1
3 h % Cu	0%	0%	14.7%	14.5%
24 h ppm Cu	nd	nd	7.1 ± 0.2	4.4 ± 0.2
24 h % Cu	0%	0%	43.3%	26.7%

Table 2. Inductively coupled plasma-optic emission spectroscopy (ICP-OES) analysis of metal dissolution from CuO and ZnO NPs and mixtures. The release of ions was evaluated after 3 and 24 h of incubation of NPs (20 μg/mL) and mixtures with DEP (100 μg/mL of DEP and 20 μg/mL of NPs) in cell culture medium. Data were expressed as concentration in ppm ± SE. In the table, percentage of dissolute ions after 3 and 24 h in medium, calculated on the base of ICP-OES analysis, is presented. * nd = not detected.

3.2. Cytotoxic Effects

Results from the MTT assay performed at 3, 24 and 48 h after exposure to increasing concentrations (0, 10, 15, 20 and 25 μg/mL) of NPs and respective mixtures are reported in Figure 2. No significant decrease in cell viability was induced after 3 h of exposure to all the NPs tested, whereas a significant dose-dependent decrease of cell viability was observed after 24 h of exposure to CuO NPs at concentrations of 15, 20 and 25 μg/mL (Figure 2C). Interestingly, both ZnO and DEP + ZnO NPs at 24 h and 48 h induced a significant reduction of cells viability at the dose 25 μg/mL (Figure 2A, B). After 48 h of exposure, it is noteworthy that with the mixture, a partial recovery of cell viability was noticed. A strong cytotoxicity was observed after CuO NPs exposure (Figure 2C). At 24 h, a dose-dependent reduction in cell viability is evident, while at 48 h almost all cells resulted as not viable for CuO NPs doses ≥10 μg/mL. The mixtures of DEP + CuO also induced a significant decrease of viability with respect to the control, but at a lower extent compared to the effects induced by the single CuO NPs (Figure 2D). DEP exposure did not induce a significant viability reduction (Figure S1).

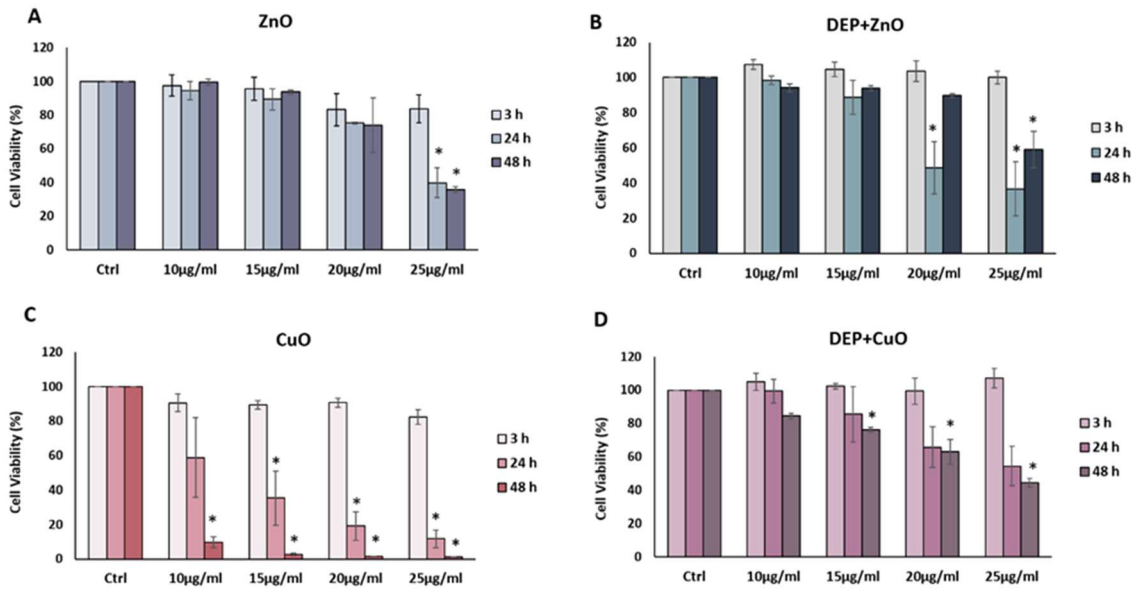

Figure 2. Cell viability: MTT assay**.** Histograms represent the percentage, with respect to control cells (Ctrl, 100%), of viable cells after the exposure to: 10, 15, 20, 25 µg/mL ZnO NPs (A), DEP 100 µg/mL + ZnO 10, 15, 20, 25 µg/mL (B), 10, 15, 20, 25 µg/mL CuO NPs (C), and DEP 100 µg/mL + CuO 10, 15, 20, 25 µg/mL (D). Data show the mean ±SE (n = 3). *Statistically significant with respect to the control according to One Way ANOVA; $p < 0.05$. Post hoc test: Tukey Test.

Figure 3 shows the percentage of CFE in treatment compared to control cells. After 24 h of exposure (Figure 3A), CFE confirmed the cytotoxicity of CuO NPs at the concentrations of 10 and 20 µg/mL, with a % CFE of about 50% and 14%, respectively. No colonies were detected after 72 h of exposure (Figure 3C).

A dose-dependent reduction of % CFE was also observed after exposure to DEP + CuO after 24 h (64% at 10 µg/mL; 35% at 20 µg/mL) and a higher reduction of colonies after 72 h, comparable to the effects of single CuO NPs. ZnO NPs induced a decrease of CFE, (82% at 10 µg/mL; 75% at 20 µg/mL) after 24 h, albeit not significant, while 20 µg/mL DEP + ZnO mixture induced a significant reduction of colonies at the same time point. After 72 h, ZnO NPs seemed to induce a recovery of colonies, in fact the % of CFE was higher compared to the results obtained after 24 h. The mixture DEP + ZnO induced a reduction of CFE (95% at 10 µg/mL, 89% at 20 µg/mL), slightly lower with respect to the single ZnO NPs. At 72 h, also with the mixture DEP + ZnO, a slight recovery was noticed. DEP induced 87% CFE after 24 h and 86% after 72 h of exposure (Figure S2).

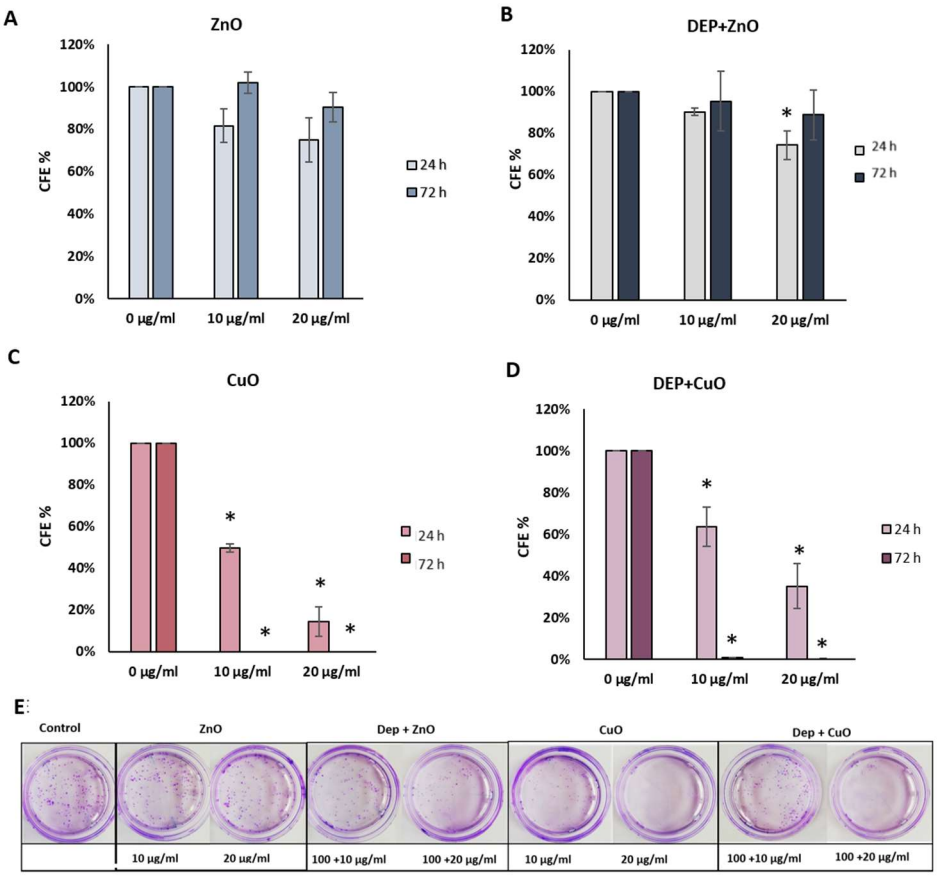

Figure 3. Colony forming efficiency (CFE) assay. Histograms represent the percentage of CFE calculated after the exposure for 24 h and 72 h to 10 and 20 µg/mL of ZnO (A), DEP 100 µg/mL + ZnO 10, 20 µg/mL (B), 10 and 20 µg/mL of CuO (C) and DEP 100 µg/mL + CuO 10, 20 µg/mL (D). Figure (E) shows the images of the Petri related to one experiment where cells were treated for 24 h. Data show the mean ± SE (n = 3). * Statistically significant with respect to the control according to One Way ANOVA; $p < 0.05$. Post hoc test: Tukey Test.

3.3. Cytostatic Effects

The analysis of the mean surface area of the colonies was conducted in order to identify those treatments able to induce a cytostatic effect, which determines an inhibition of cell growth, and so a reduction in the colony area after 24 h of treatment. The results, expressed as the mean area of ten colonies counted, showed a decrease of the colony size after exposure to ZnO at the doses of 10 and 20 µg/mL and with DEP + ZnO at 20 µg/mL (Figure 4). Mixtures of DEP + CuO induced only a slight decrease in colony at both

concentrations tested. The strongest cytostatic effect was observed for CuO NPs at 20 µg/mL. DEP alone did not induce a cytostatic effect compared to control cells (Figure S3).

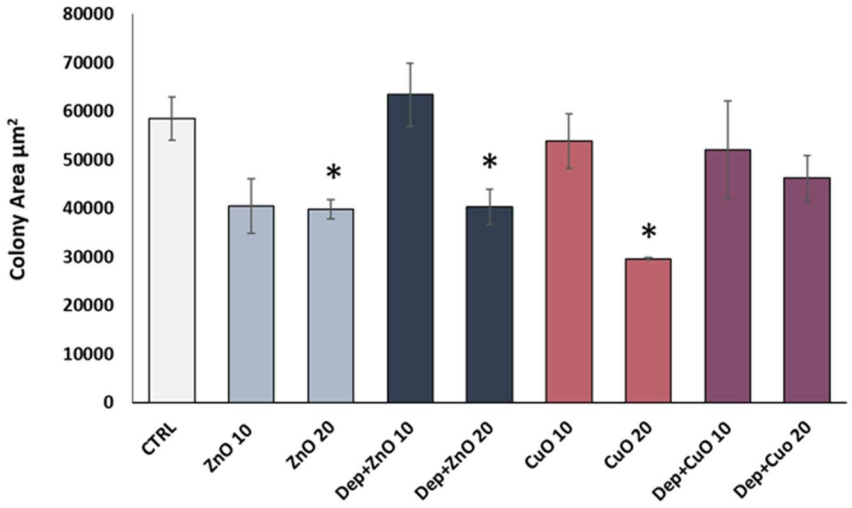

Figure 4. Cytostatic effect. Histograms represent the mean surface area (±SE) of A549 cell colonies treated for 24 h to ZnO NPs, DEP + ZnO mixture, CuO NPs and DEP + CuO mixture. * Statistically significant with respect to the control according to un-paired t test; $p < 0.05$.

3.4. Pro-Inflammatory Effects

The IL-8 release was investigated in order to evaluate the pro-inflammatory response related to NPs' and mixtures' exposure. ZnO and CuO NPs induced more IL-8 release compared to their respective mixtures with DEP. Data showed a significant increase in the release of IL-8 after exposure to ZnO NPs at 25 µg/mL (9.6-fold increase) (Figure 5A) and to CuO NPs at 10 µg/mL (15-fold increase) (Figure 5B) compared to control cells. DEP + ZnO mixture induced an increase in IL-8 release comparable to the one promoted by ZnO NPs, although no statistically significant values were reached. Interestingly, the CuO NP-induced inflammatory response seemed to be completely rescued by the presence of diesel particles (Figure 5B). DEP alone did not determine an increase in IL-8 release from exposed A549 cells (Figure S4). In addition, to confirm these results, we reported the pg/mL of IL-8 in relation to the total amount of proteins (mg) of each sample (Figure S5). Since the release of cytokines can occur at earlier time points, the amount of IL-8 secreted after 3 h of

exposure to the different NPs and mixtures was assessed. A slight, though not significant, tendency of increased IL-8 release after treatment with ZnO and CuO (at the doses 20 and 25 µg/mL) at an earlier time point (3 h) was observed (Figure S6).

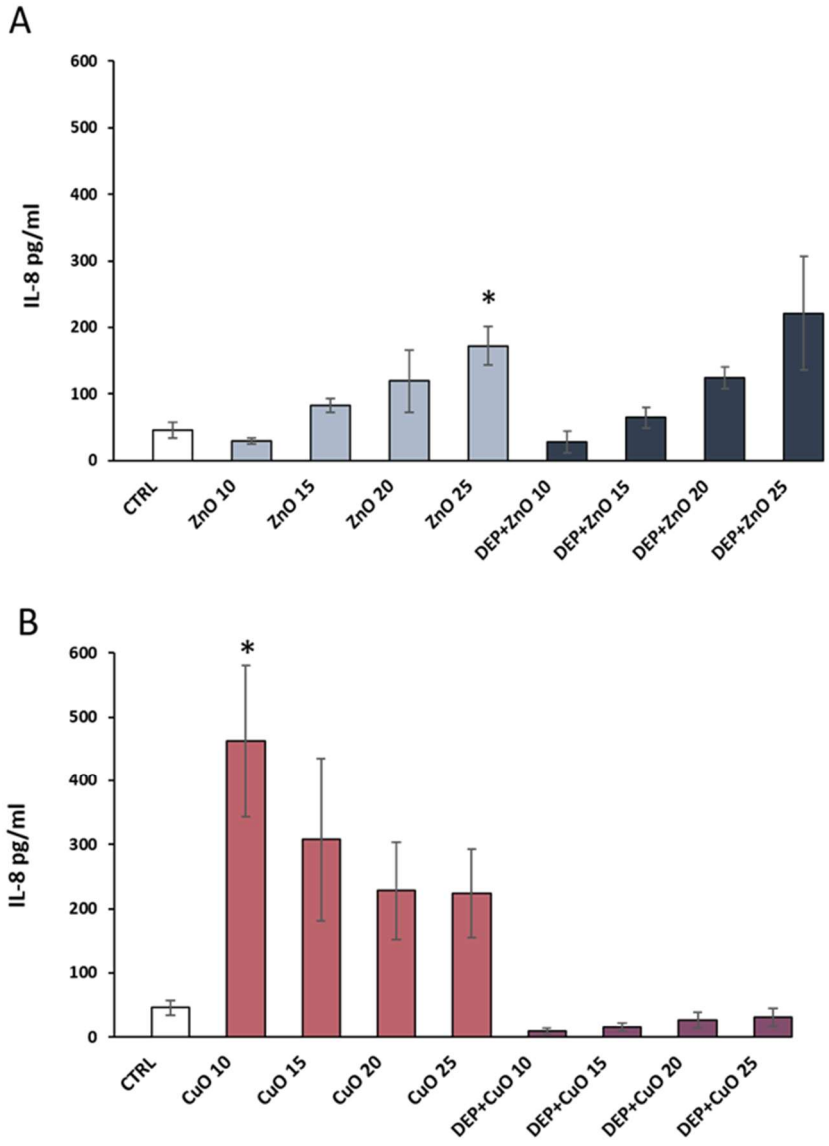

Figure 5. Inflammatory response. The release of the pro-inflammatory cytokine IL-8 was evaluated in A549 supernatants after the exposure for 24 h to 0, 10, 15, 20, and 25 µg/mL of ZnO (A) and CuO (B) NPs alone and mixed with DEP (100 µg/mL). Data are presented as pg/mL and the histograms represent the mean ±SE of at least three independent experiments. * Statistically significant according to the un-paired t test; $p < 0.05$.

3.5. Cells Morphology

3.5.1. Electron Microscopy

Data from electron microscopy analysis showed the internalization of particles in A549 cells after 24 h of exposure (Figure 6). ZnO NPs were not taken up by cells very efficiently, only a few large cytoplasmic vesicles were observed containing cell debris and particulate material (Figure 6B and Figure S7). Although A549 are considered not-phagocytic cells, after the exposure to the DEP + ZnO mixture, phagocytosis processes consisting in protrusions of the cell membrane that engulf particles agglomerates have been detected (Figure 6C) and a large amount of particles was observed in several large endocytic vesicles and multivesicular bodies (Figure S7). The single DEP particles were efficiently internalized and ended up in cytoplasmic multivesicular bodies (Figure 6D). This suggests that in combination with DEP, the ZnO NPs uptake might have been improved. Figure 6E shows an agglomerate of CuO NPs in lysosomes, and the presence of swollen mitochondria (M) with loss of cristae is also noticeable. Cells exposed to the DEP + CuO mixture displayed particles internalized in a phagosome and were characterized by a similar altered ultrastructure (Figure 6F).

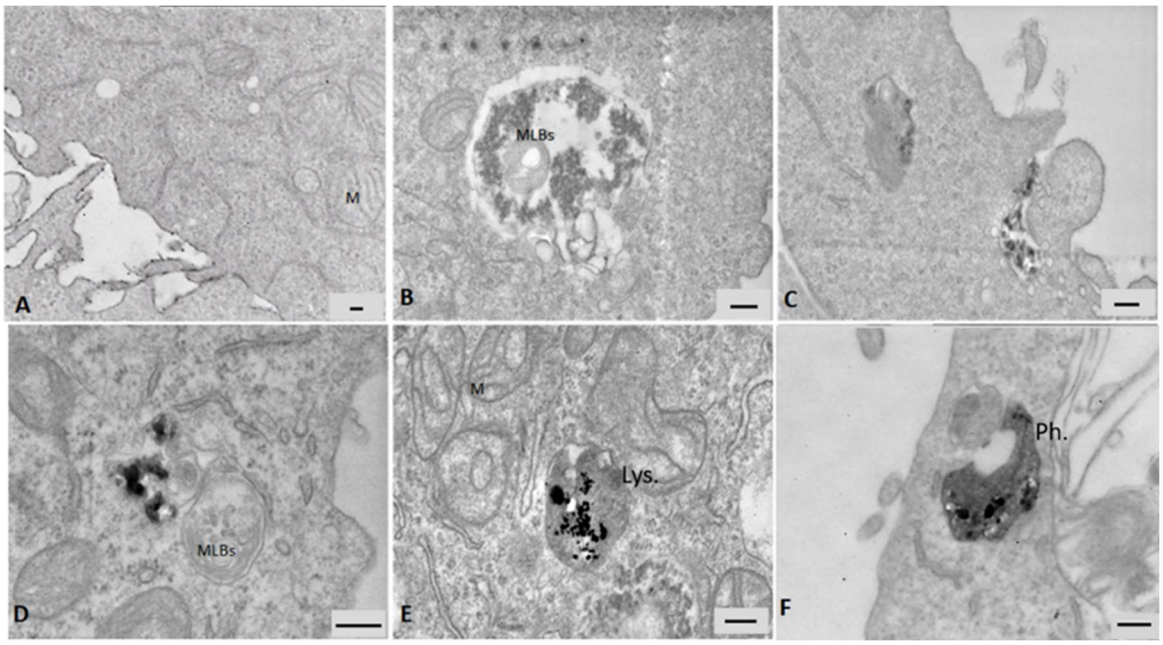

Figure 6. TEM analyses of A549 cells after 24 h of exposure to particles. (A) Ultrastructure of a control cell, scale bar = 150 nm. (B) ZnO (20 µg/mL) agglomerates internalized in large cytoplasmic vesicle, scale bar = 200 nm. (C) DEP (100 µg/mL) + ZnO (20 µg/mL) phagocytosis in cells, scale bar = 200 nm. (D) Internalization of DEP (100 µg/mL), scale bar = 200 nm, (E) CuO (20 µg/mL) agglomerates internalized in lysosome (Lys.), scale bar = 200 nm. (F) DEP (100 µg/mL) + CuO (20 µg/mL) internalized in a phagosome (Ph.), scale bar = 200 nm. M = mitochondria, MLBs = Multilamellar bodies.

3.5.2. Fluorescence Microscopy

Fluorescence microscopy imaging of actin cytoskeleton shows that all the treatments induced a change in the regular shape of A549 cells, which have a uniform cobblestone appearance (Figure 7A). Protrusions of plasma membrane, such as lamellipodia and filopodia, are evident in cells exposed to DEP (Figure 7B), ZnO NPs (Figure 7C) and DEP + CuO mixture (Figure 7F). Stress fibres were evident in cells exposed to DEP (Figure 7B). Data also confirmed the CuO NPs cytotoxicity (Figure 7E), since a significantly lower number of viable cells with regular morphology was observed. Cells exposed to ZnO (Figure 7C) and CuO NPs (Figure 7E) appeared shrunken, as morphological evidence of cell death, and with uropodia as evidence of polarization and cells locomotion. Similar morphological alterations were appreciable in ZnO and DEP + ZnO-exposed cells, although the actin cytoskeleton of the cells exposed to the mixture appeared even more disorganized (Figure 7C,D). On the contrary, the cytoskeletal and nuclear morphology of the DEP + CuO-exposed

cells resulted as more preserved with respect to the severely altered structures observed in the CuO NPs-exposed cells (Figures 7E,F).

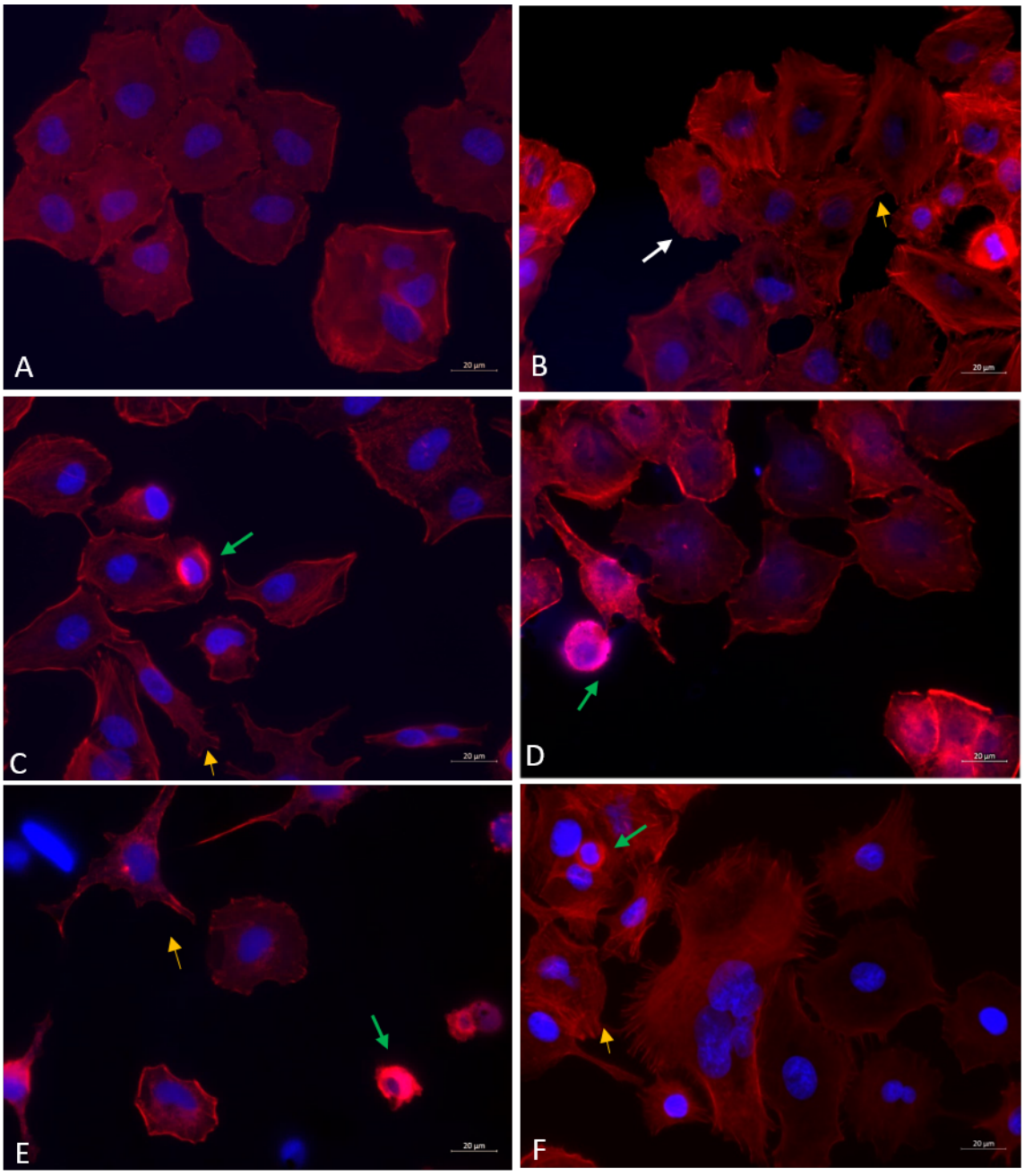

Figure 7. Fluorescence microscopy images of actin cytoskeleton. Control cells (A), DEP 100 µg/mL (B), ZnO 20 µg/mL (C), DEP + ZnO 20 µg/mL (D), CuO 20 µg/mL (E), DEP + CuO 20 µg/mL (F). Scale bar = 20 µm. White arrow: stress fibres, Orange arrow: microspikes (filopodia), Yellow arrow: lamellipodia, Green arrow: shrunk cells, Blue arrow: uropodia.

4. Discussion

There is a great concern about the health risk associated with air pollution, especially to UFPs. The issue concerning UFPs emissions and the related health risk have been dealt with in the last year by regulating the circulation of the vehicle and by improving the technology of abatement systems for Diesel engine emissions. Europe has developed Euro standards which have continuously been lowered since 1993 with the Euro 1 to Euro 6, respectively (Reşitoğlu et al.2015).

Nevertheless, in addition to the exhaust source of pollution, there are also non-exhaust ones, which represent an important origin of particles in the nanometric range. Vehicles contribute to non- exhaust during the mechanical processes associated with driving, especially brake and tire wear. Furthermore, metal-based NPs are also used as fuel additives, such as cerium oxide and zinc oxide nanoparticles applied in order to mitigate the emission of particulates and greenhouse gases in the atmosphere (Arul et al. 2009).

Moreover, growing industrial activity based on nanotechnology represents an additional source of UFPs that covers different classes of compounds, including MeO (Charitidis et al. 2014). Since in the real conditions the population is exposed to a mixture of different particles, it is possible that the co-exposure to these mixtures can lead to a different toxicity compared to the well-known biological responses induced by the single compounds. Generally, there is a unanimous consensus on the necessity to demonstrate if the addition of NMs in the environment may alter the intrinsic toxicity of particles emitted in the exhaust (Park et al. 2008). A recent work showed that the co-exposure to benzo(a)pyrene (B(a)P) and silica nanoparticle (Si-NPs) synergistically potentiated the toxicological effects on endothelial cells, including DNA damage, oxidative stress, cell cycle arrest at the G2/M check point, and apoptosis (Asweto et al. 2017).

In this perspective, the hazard assessment of NMs interactions with airborne UFPs has been addressed here by a range of *in vitro* assays, aimed to evaluate the toxicity of two commonly used MeO NPs, CuO and ZnO, alone and in mixtures with standard diesel exhaust particulates derived from a light duty engine. DEP SRM®2975 was used at the

concentration of 100 μg/mL (corresponding to 10 μg/cm^2), which is a sub cytotoxic dose typically used in *in vitro* experiments for assessing DEP effects in lung cells (Lawal et al. 2015; Tseng et al. 2016).

The morphological characterization of particles confirmed that they are in the nanometric range, with a tendency to agglomerate. DLS analysis showed that the hydrodynamic diameter for all particles increases in the culture medium. The CuO NPs formed the largest aggregates (465 nm), while the DEP + ZnO mixture formed the smallest aggregates with a hydrodynamic diameter of 207 nm. Data showed that in cell culture medium, the z-average is lowered for both CuO and ZnO NPs when in a mixture with DEP. We suppose that, in the cell culture media, the presence of DEP interferes with the NPs state of agglomeration, reducing it, with possible consequences on the interactions among NPs and cells. Since surface charge could be related to variation in their electrostatic interaction, we measured the ζ-potential of these particles. Obtained data showed that ZnO and CuO NPs have a charge of +25 mV and +12 mV respectively, while the values for DEP + ZnO and DEP + CuO mixtures are −19 mV and −18 mV, respectively. In both cases, the charge values were not sufficient to allow a repulsion between particles and data to justify the tendency of NPs to form aggregates. Several studies demonstrated that the dissolution of metal particles in the culture medium or in the biological environment/fluids resulted in the release of ions, which play a main role in their toxicity. Our results showed that the percentage of ions released by DEP + ZnO (62.5%) after 24 h of incubation in medium is similar to that of the single ZnO NPs (69.4%), unlike DEP + CuO, which instead showed a reduced percentage of released ions (26.7%) compared to the single CuO NPs (43.3%). While the release of Zn^{2+} ions from ZnO NPs seemed to not be influenced by the interaction with DEP, our data point out that diesel particles may somehow interact with CuO NPs, limiting the ions dissolution from their surface, thus reducing the bioavailability of free CuO NPs and Cu^{2+} ions. Of course, such speculation is worthy of additional physico-chemical studies.

The *in vitro* toxicity study has been performed on human lung A549 cells exposed to single particles or mixtures and the results have been interpreted considering the NP physico-chemical behaviour. The cytotoxicity was investigated using MTT, a standard metabolic assay based on a simple colorimetric reaction, but limited by the possible interference of absorbance with particles (Holder et al. 2012) and CFE assay. CFE has the advantage to be a label-free test, since it is a non-colorimetric and non-fluorescent assay, thus avoiding the

possible interference with the particles. In addition, by using the CFE assay, it is possible to analyse particle-induced cytostatic effects that lead to the reduction in the colony area. Moreover, the CFE assay has been recognized as a reliable and standardized method for the *in vitro* toxicity assessment of NMs (Jessica Ponti et al. 2014).

The combined results from the MTT and CFE assays showed that the more cytotoxic particles were the CuO NPs, which, after 24 h of exposure at concentration of 20 µg/mL, induced a cell mortality over 80%. A comparable toxic effect has been reported in previous studies, in which CuO NPs resulted as more cytotoxic compared to other MeO NPs and carbon nanotubes (Karlsson et al. 2008). Furthermore, a study on A549 cells exposed to the same CuO NPs showed that CuO resulted as cytotoxic at lower concentrations of exposure and that the effects were due to the modality of cell–particle interactions (Moschini et al. 2013).

As CuO NPs, the DEP + CuO mixture induced cytotoxicity on A549 cells in a time- and concentration-dependent manner, even though cytotoxicity in the mixture was lower, probably due to the interaction between DEP and CuO NPs. The cytotoxicity measured by MTT for ZnO NPs and the DEP mixture showed a kind of synergic effect between DEP and ZnO NPs. Indeed, the DEP + ZnO induced an enhanced response with respect to the single particle at the dose 20 µg/mL after 24 h of exposure (Figure 2). A similar trend was found also comparing CFE data from 24 h of exposure and 72 h and this effect was probably due to a change in dynamic toxicity and uptake of NPs. With the CFE assay, this recovery is also evident after treatment with ZnO NPs alone after 72 h (Figure 3).

Nevertheless, it is noticeable that the presence of both NPs in the two different mixtures with DEP enhanced the toxicity of the environmental UFPs. DEP did not affect cytotoxicity, but in co-exposure with MeO NPs, a decreased cell viability was observed at both 24 h and 72 h. The augmented biological effects of DEP + CuO, compared to DEP alone, are supported by the work of Guo et al., in which the authors showed a synergistic effect on protein oxidation after the co-exposure to the elemental carbon of PM (carbon black, CB) and Fe_2O_3 NPs on lung epithelial cells (Guo et al. 2009). In the cited work, the authors proposed that when transition metal oxide NPs, such as Fe_2O_3 NPs, but also others, and CB are simultaneously internalized, the CB particles may reduce the bioavailable Fe^{3+} ions within the cells and that lysosomal acidification plays a crucial role in the mechanism. We suggest that this process could be similar for DEP + CuO co-exposure. Nevertheless, Guo

and co-workers also suggested that synergistic effects of Fe_2O_3 NPs and CB are due to the reduction of Fe^{3+} ions by the carbon black particles attributed to the reactive functional groups on the carbon surface. However, in our work, even if the oxidative potential was not investigated, CuO NPs alone were more toxic compared to the DEP + CuO mixture and that could probably be due to the more bioavailability of extracellular Cu^{2+} ions and to intracellular Cu^{2+} ions derived from lysosomal acidification after CuO NPs uptake (Trojan horse mechanism). Furthermore, it is important to mention that DEPs have different physicochemical properties from CB particles and that the PAHs and metals adsorbed on the carbonaceous core of particles may interact differently with MeO with respect to elemental carbon (CB). Previous works have indeed confirmed the possible interactions of MeO NPs with PAHs, such as B(a)P (Asweto et al. 2017), or with organometallic cation (Yu et al. 2015).

Furthermore, our data suggest that Cu^{2+} ions release is reduced by the presence of DEP with a corresponding reduction of cytotoxicity of the mixture (27% after 24 h) compared with the single NPs of CuO (43% after 24 h), probably due to an interaction between particles that affects the superficial charge of CuO and the ions release. Although other studies have demonstrated that CuO cytotoxicity depends mostly on its intracellular solubility (Studer et al. 2010), it has also been reported that extracellular dissolution of Cu^{2+} ions from CuO NPs could contribute to NPs cytotoxicity on A549 cells and this effect depends on NPs size and modes of entry of NPs (Wongrakpanich et al. 2016). Regarding ZnO NPs, their cellular toxicity could be explained by the Zn^{2+} ions released from ZnO NPs in the cellular medium solution (Deng et al. 2009) and that Zn^{2+} ions also induce inflammatory responses (Vandebriel and De Jong 2012), in accordance with our results.

The high percentages of Zn^{2+} ions released by the ZnO NPs and DEP + ZnO mixture, compared to CuO NPs alone and in mixture, support the hypothesis that ions dissolution contributes to ZnO toxicity, as previously demonstrated (Cho et al. 2011). The slightly different response towards the DEP + ZnO mixture with respect to the individual NPs of ZnO could be attributed to the possible different mechanisms of interaction and endocytosis of DEP + ZnO NPs aggregates, compared to the single ZnO NPs (Figure 6 and Figure S7).

These data about zinc ions' contribution to cellular toxicity, augmented by the simultaneous exposure with carbonaceous particles, are in accordance with the work of

Wilson and colleagues, in which co-exposure to CB and $ZnCl_2$ induced a significant release of TNF-a compared to $ZnCl_2$ alone (Wilson et al. 2007). Furthermore, previous works on PM with different content of metals, in particular zinc, showed that PM enriched with Zn resulted as more toxic compared to other samples (Uski et al. 2015), and that the depletion of zinc ions by chelating agents determined a reduction of the cytotoxic effects (Marchetti et al. 2019). A change in the toxic kinetics of ZnO NPs in mixture with DEP could explain the recovery of viability after the cytotoxicity peak at 24 h of exposure. We suppose that, after 24 h, the survived fraction of cells is able to make cellular replication and for this reason, an increased cell viability was observed. Moreover, contrary to CuO- and DEP + CuO-exposed ones, the DEP + ZnO-exposed cells did not show severe ultrastructural lesions, which may support the capability of them to survive the Zn-mediated insult, and even the elimination of the internalized particles through exocytosis may not be excluded. Nevertheless, these aspects about toxicity kinetics require further investigation.

The inflammatory response was indeed promoted by ZnO NPs and the respective mixture at the highest dose when toxicity occurs. On the contrary, CuO NPs induced IL-8 release in the lung epithelial cells already at sub-toxic concentrations (10 μg/mL), as previously observed by Mantecca et al. (Mantecca et al. 2017). The co-exposure of CuO with DEP resulted in a significant decrease of IL-8 release compared to CuO NPs alone, and DEP themselves did not promote the release of this protein. These data evidenced once again the interference between these two different particles in inducing the biological responses. A reduction of IL-8 after winter Milan $PM_{2.5}$, which is the major source of combustion particles derived from diesel emissions, has already been reported in a previous work (Longhin et al. 2018), in which the authors suggested that the observed effect was accompanied by altered organization of the actin filaments, that actively participate in the motility of secretory granules (Schmoranzer and Simon 2003). Other pro-inflammatory cytokines are very useful markers for understanding the inflammatory response related to NPs and UFPs exposure. In our work, the release of TNF-α, after 24 h of exposure to all treatments, was also investigated, but in our model, the release of this protein was very low, and we did not notice remarkable variation in cells exposed to the NPs with respect to the control (data not shown).

Our data on actin cytoskeleton alteration underlined that all the treatments induced an alteration of cells regular morphology and a more elongated morphology of cytoskeleton

was evident compared to the typical shape of unexposed cells. Exposure to CuO NPs resulted in an accentuated morphological alteration, disorganization of the cytoskeleton and shrinkage of cells, as evidence of cell death. Cells treated with DEP alone and in mixture with CuO NPs showed more presence of filipodia, while uropodia and actin bundles were visible after exposure to ZnO NPs, alone and in mixture, and to CuO NPs. These data confirm that the exposure to engineered NPs could cause cellular cytoskeletal disturbance (Ispanixtlahuatl-Meráz et al.2018), with consequences in the alteration in proteins involved in cell migration (Vuong et al. 2016).

In the presence of DEP, enhanced plasma membrane ruffling and presence of stress fibres were observed, in accordance with previous data on bronchial cells exposed to fine PM (Dornhof et al. 2017).

Data from the TEM analysis confirmed that all the tested particles are internalized by lung cells. ZnO NPs are visible in cellular vesicles after the invagination of the cellular plasma membrane. The presence of multilamellar bodies enlighten the hypothesis that autophagy is one of the key events involved on the response to MeO NPs, and it may act as a survival mechanism by targeting harmful components to the lysosomes for degradation, as already supported by different *in vitro* works (Halamoda Kenzaoui et al. 2012). However, this aspect needs further investigations. As expected, the presence of CuO NPs in lysosomes after 24 h of exposure has confirmed data from the literature (Moschini et al. 2013; Wang et al. 2012). Mitochondria were also compromised by this treatment. Interestingly, agglomerates of DEP + CuO NPs are visible in phagosome, suggesting a different kinetics of this mixture compared to single CuO NPs. As a matter of fact, at a prolonged time of exposure, 48 h for MTT and 72 h for CFE assay, DEP + CuO mixtures were more toxic compared to at the 24 h time point.

These results showed that MeO NPs in mixture with airborne UFPs could differently affect lung cell toxicity, evidencing the importance to test the possible synergistic or antagonistic effects of different environmental particles. Furthermore, CuO NPs resulted as the more cytotoxic NPs in this study, also able to induce cytotoxicity, inflammatory response, cytostatic effect and cellular morphological changes.

It is likely that the interaction of DEP with ZnO and CuO NPs may interact and change the surface reactivity between environmental UFPs and engineered NPs. Furthermore, this interaction is influenced by the kind of NPs. DEP enriched in Zn^{2+} are more toxic than DEP

and ZnO NPs alone, while CuO NPs could be adsorbed on DEP surface, reducing the bioavailability of Cu^{2+} with consequent reduced toxic effects compared to single CuO NPs. However, the co-exposure to MeO NPs and DEP highly increases the toxicity of carbon-based UFPs.

Recently, the Air Liquid Interface (ALI) exposure systems received considerable attention as an alternative method to the submerged system in studying the biological effects of engineered NPs (Fizeșan et al. 2019; Lenz et al. 2013) and DEP (Klein et al. 2017; Loxham et al. 2015). However, the widespread adoption of ALI systems is still limited by the minimal efficiency of particles deposition and by the complex strategy needed to characterize the composition of the particles delivered to the cells. In the future, ALI exposure to NPs and UFPs would be the preferable reference standard, since it more closely mimics a real exposure scenario. The cellular responsiveness to NPs and UFPs at the aerosol/airborne phase could vary a lot with respect to submerged conditions, as previously demonstrated by Lenz et al. (Lenz et al. 2013).

We suppose that, at the ALI, A549 cells would have different responses, especially towards DEP, as evidenced by previous authors (Fizeșan et al. 2018; Klein et al. 2017). Biological outcomes would be influenced by different bioavailability to O_2 and by a different interaction with NPs in the absence of a lining fluid (e.g., reduction of NPs agglomeration and different NPs uptake). Moreover, since free ions release from NPs will be avoid or reduced at ALI exposure, inflammatory response and oxidative stress could also be modulated. Further experimental evidences on NPs and UFPs mixture toxicity under ALI conditions should be generated to address such speculations.

5. Conclusions

In the light of providing experimental results more strictly reflecting real-life environmental conditions of exposure to outdoor and indoor NPs, the possible interaction of different hazardous airborne particles, and the final toxicity deriving from the mixture effects, should be considered. Different modes of action (MoA) have been proposed for the combined toxicity of DEP and MeO (i.e., ZnO and CuO) NPs. DEP usually exerts its toxic effects thanks to the compounds adsorbed onto the carbonaceous core, such as PAHs and metals, which trigger oxidative stress, inflammation, DNA damage and cytotoxicity. Similar mechanisms are also somehow evoked by MeO NPs, by direct internalization of NPs in cells or ions

dissolution. Our results are in accordance with previous studies, in which the different mechanisms of CuO and ZnO NPs and related ions have been demonstrated. Cu is a transition metal oxide that could generate ROS through the Fenton reaction, and the adverse cellular outcomes may even be worsened by the Trojan horse mechanism exerted by the NP forms. The extra- and intra-cellular release of Cu ions from the surface of the less soluble CuO NPs might have been limited by a sort of passivation effect exerted by DEPs, which can justify the lower toxicity of DEP + CuO. The ZnO NPs trigger cytotoxicity mainly thanks to the massive release of zinc ions, which seemed to be almost unaffected by the presence of DEP. The enhanced toxicity observed for the DEP + ZnO mixture was largely attributable to an increased NPs uptake by the lung epithelial cells.

We have previously demonstrated that the variable content of PAHs and metals in different DEPs is responsible for different biological responses in human bronchial cells (Bengalli et al. 2019). Since real environmental DEPs could have different chemical compositions, due to different driving cycles (e.g., on urban centres, highways etc.), combustion processes, and other external sources, it would be extremely interesting to analyse the effect of sampled DEP, enriched with metals coming from NPs-added fuels or NMs manufacturing sites.

Furthermore, it would be suitable to investigate if, by changing the physicochemical properties of NMs (e.g., size, chemical composition, surface properties, coating, and crystallinity), the co-exposure with environmental UFPs may modulate the biological responses. This aspect would be very useful in the design of safer NMs and should be incorporated in the nano-risk assessment frameworks.

3.1 BIBLIOGRAPHY

Abu-Allaban, Mahmoud et al. 2003. “Tailpipe, Resuspended Road Dust, and Brake-Wear Emission Factors from on-Road Vehicles.” *Atmospheric Environment* 37(37): 5283–93.

Adamiec, Ewa, Elżbieta Jarosz-Krzemińska, and Robert Wieszała. 2016. “Heavy Metals from Non-Exhaust Vehicle Emissions in Urban and Motorway Road Dusts.” *Environmental Monitoring and Assessment* 188(6).

Ahamed, Maqusood et al. 2010. “Genotoxic Potential of Copper Oxide Nanoparticles in Human Lung Epithelial Cells.” *Biochemical and Biophysical Research Communications* 396(2): 578–83. http://dx.doi.org/10.1016/j.bbrc.2010.04.156.

Arul, V, Mozhi Selvan, R B Anand, and M Udayakumar. 2009. “EFFECTS OF CERIUM OXIDE NANOPARTICLE ADDITION IN DIESEL AND DIESEL-BIODIESEL-ETHANOL BLENDS ON THE PERFORMANCE AND EMISSION CHARACTERISTICS OF A CI ENGINE.” 4(7). www.arpnjournals.com.

Asweto, Collins Otieno et al. 2017. “Combined Effect of Silica Nanoparticles and Benzo[a]Pyrene on Cell Cycle Arrest Induction and Apoptosis in Human Umbilical Vein Endothelial Cells.” *International Journal of Environmental Research and Public Health* 14(3).

Bacchetta, Renato et al. 2012. “Nano-Sized CuO, TiO_2 and ZnO Affect *Xenopus Laevis* Development.” *Nanotoxicology* 6(4): 381–98.

Bengalli, Rossella et al. 2017. “Impact of Zinc Oxide Nanoparticles on an in Vitro Model of the Human Air-Blood Barrier.” *Toxicology Letters* 279: 22–32.

Bnegalli, Rossella et al. 2019. “In Vitro Pulmonary and Vascular Effects Induced by Different Diesel Exhaust Particles.” *Toxicology Letters* 306: 13–24.

Buerki-Thurnherr, Tina et al. 2013. “In Vitro Mechanistic Study towards a Better Understanding of ZnO Nanoparticle Toxicity.” *Nanotoxicology* 7(4): 402–16.

Castell, José V, M Teresa Donato, and María José Gómez-Lechón. 2005. “Metabolism and Bioactivation of Toxicants in the Lung. The in Vitro Cellular Approach.” *Experimental and toxicologic pathology : official journal of the Gesellschaft fur Toxikologische Pathologie* 57 Suppl 1: 189–204.

Charitidis, Costas A. et al. 2014. “Manufacturing Nanomaterials: From Research to Industry.” *Manufacturing Review* 1: 11.

Cho, Wan Seob et al. 2011. “Progressive Severe Lung Injury by Zinc Oxide Nanoparticles; the Role of Zn2+dissolution inside Lysosomes.” *Particle and Fibre Toxicology* 8(1): 27. http://www.particleandfibretoxicology.com/content/8/1/27.

Deng, Xiaoyong et al. 2009. “Nanosized Zinc Oxide Particles Induce Neural Stem Cell Apoptosis.” *Nanotechnology* 20(11): 115101.

Dornhof, Regina et al. 2017. “Stress Fibers, Autophagy and Necrosis by Persistent Exposure to PM2.5 from Biomass Combustion” ed. Yi-Hsien Hsieh. *PLOS ONE* 12(7): e0180291.

Douki, Thierry et al. 2018. “Comparative Study of Diesel and Biodiesel Exhausts on Lung Oxidative Stress and Genotoxicity in Rats.” *Environmental Pollution* 235: 514–24.

Fahmy, Baher, and Stephania A. Cormier. 2009. “Copper Oxide Nanoparticles Induce Oxidative Stress and Cytotoxicity in Airway Epithelial Cells.” *Toxicology in Vitro* 23(7): 1365–71. http://dx.doi.org/10.1016/j.tiv.2009.08.005.

Fizeșan, Ionel et al. 2018. “Responsiveness Assessment of a 3D Tetra-Culture Alveolar Model Exposed to Diesel Exhaust Particulate Matter.” *Toxicology in Vitro* 53: 67–79.

Fizesan, Ionel et al. 2019. “In Vitro Exposure of a 3D-Tetraculture Representative for the Alveolar Barrier at the Air-Liquid Interface to Silver Particles and Nanowires.” *Particle and Fibre Toxicology* 16(1): 14.

Fröhlich, Eleonore, and Sharareh Salar-Behzadi. 2014. “Toxicological Assessment of Inhaled Nanoparticles: Role of in Vivo, Ex Vivo, in Vitro, and in Silico Studies.” *International Journal of Molecular Sciences* 15(3): 4795–4822.

Gasser, Michael et al. 2009. “Toxic Effects of Brake Wear Particles on Epithelial Lung Cells in Vitro.” *Particle and Fibre Toxicology* 6(1): 30. https://doi.org/10.1186/1743-8977-6-30.

Grigoratos, Theodoros, and Giorgio Martini. 2015. “Brake Wear Particle Emissions: A Review.” *Environmental Science and Pollution Research* 22(4): 2491–2504.

Guo, Bing, Rema Zebda, Stephen J Drake, and Christie M Sayes. 2009. “Synergistic Effect of Co-Exposure to Carbon Black and Fe2O3 Nanoparticles on Oxidative Stress in Cultured Lung Epithelial Cells.” *Particle and Fibre Toxicology* 6(1): 4.

H.-E. Wichmann. 2007. “Diesel Exhaust Particles.” *Inhalation Toxicology* 19:sup1: 241–44.

Halamoda Kenzaoui, Blanka, Catherine Chapuis Bernasconi, Seher Guney-Ayra, and Lucienne Juillerat-Jeanneret. 2012. “Induction of Oxidative Stress, Lysosome Activation and Autophagy by Nanoparticles in Human Brain-Derived Endothelial Cells.” *Biochemical Journal* 441(3): 813–21.

Harrison, Roy M. et al. 2012. “Estimation of the Contributions of Brake Dust, Tire Wear, and Resuspension to Nonexhaust Traffic Particles Derived from Atmospheric Measurements.” *Environmental Science and Technology* 46(12): 6523–29.

Hjortenkrans, David S.T., Bo G. Bergbäck, and Agneta V. Häggerud. 2007. “Metal Emissions from Brake Linings and Tires: Case Studies of Stockholm, Sweden 1995/1998 and 2005.” *Environmental Science and Technology* 41(15): 5224–30.

Holder, Amara L., Regine Goth-Goldstein, Donald Lucas, and Catherine P. Koshland. 2012. “Particle-Induced Artifacts in the MTT and LDH Viability Assays.” *Chemical Research in Toxicology* 25(9): 1885–92.

Ispanixtlahuatl-Meráz, Octavio, Roel P. F. Schins, and Yolanda I. Chirino. 2018. “Cell Type Specific Cytoskeleton Disruption Induced by Engineered Nanoparticles.” *Environmental Science: Nano* 5(2): 228–45.

Jessica Ponti, Agnieszka Kinsner-Ovaskainen, Hedvig Norlén, Sandrine Altmeyer, Cristina Andreoli, Alessia Bogni et al. 2014. “Interlaboratory Comparison Study of the Colony Forming Efficiency Assay for Assessing Cytotoxicity of Nanomaterials.” *Luxembourg: Publications Office of the European Union*: 76 pp. – 21.0 x 29.7 cm.

Karlsson, Hanna L, Pontus Cronholm, Johanna Gustafsson, and Lennart Mo. 2008. “Copper Oxide Nanoparticles Are Highly Toxic A Comparison between Metal Oxide Nanoparticles and Carbon Nanotubes - Chemical Research in Toxicology (ACS Publications).” : 1726–32.

Klein, Sebastian G. et al. 2017. “Endothelial Responses of the Alveolar Barrier in Vitro in a Dose-Controlled Exposure to Diesel Exhaust Particulate Matter.” *Particle and Fibre Toxicology* 14(1): 7.

Lawal, Akeem O. et al. 2015. “Heme Oxygenase-1 Protects Endothelial Cells from the Toxicity of Air Pollutant Chemicals.” *Toxicology and Applied Pharmacology* 284(3): 281–91.

Lenz, Anke-Gabriele et al. 2013. “Inflammatory and Oxidative Stress Responses of an Alveolar Epithelial Cell Line to Airborne Zinc Oxide Nanoparticles at the Air-Liquid Interface: A Comparison with Conventional, Submerged Cell-Culture Conditions.” *BioMed Research International* 2013: 1–12.

Longhin, Eleonora et al. 2016. “Physico-Chemical Properties and Biological Effects of Diesel and Biomass Particles.” *Environmental Pollution* 215: 366–75. http://www.ncbi.nlm.nih.gov/pubmed/27194366 (February 20, 2018).

Longhin, Eleonota et al. 2018. “Milan Winter Fine Particulate Matter (WPM2.5) Induces IL-6 and IL-8 Synthesis in Human Bronchial BEAS-2B Cells, but Specifically Impairs IL-8 Release.” *Toxicology in Vitro* 52: 365–73.

Loxham, Matthew et al. 2015. “The Effects on Bronchial Epithelial Mucociliary Cultures of Coarse, Fine, and Ultrafine Particulate Matter From an Underground Railway Station.” *Toxicological Sciences* 145(1): 98–107.

Lu, Pei Jia et al. 2015. “Analysis of Titanium Dioxide and Zinc Oxide Nanoparticles in Cosmetics.” *Journal of Food and Drug Analysis* 23(3): 587–94.

Mantecca, Paride et al. 2017. “Airborne Nanoparticle Release and Toxicological Risk from Metal-Oxide-Coated Textiles: Toward a Multiscale Safe-by-Design Approach.” *Environmental Science & Technology* 51(16): 9305–17.

Marchetti, Sara et al. 2019. “In Vitro Lung Toxicity of Indoor PM10 from a Stove Fueled with Different Biomasses.” *Science of the Total Environment* 649: 1422–33.

Möller, Winfried et al. 2008. “Deposition, Retention, and Translocation of Ultrafine Particles from the Central Airways and Lung Periphery.” *American Journal of Respiratory and Critical Care Medicine* 177(4): 426–32.

Moschini, Elisa et al. 2013. “The Modality of Cell–Particle Interactions Drives the Toxicity of Nanosized CuO and TiO2 in Human Alveolar Epithelial Cells.” *Toxicology Letters* 222(2): 102–16.

Naasz, Steffi, Rolf Altenburger, and Dana Kühnel. 2018. “Environmental Mixtures of Nanomaterials and Chemicals: The Trojan-Horse Phenomenon and Its Relevance for Ecotoxicity.” *Science of the Total Environment* 635: 1170–81.

Park, Barry et al. 2008. “Hazard and Risk Assessment of a Nanoparticulate Cerium Oxide-Based Diesel Fuel Additive - A Case Study.” *Inhalation Toxicology* 20(6): 547–66.

Pope, C. Arden et al. 2002. “Lung Cancer, Cardiopulmonary Mortality, and Long-Term Exposure to Fine Particulate Air Pollution.” *JAMA : the journal of the American Medical Association* 287(9): 1132.

Reşitoğlu, İbrahim Aslan, Kemal Altinişik, and Ali Keskin. 2015. “The Pollutant Emissions from Diesel-Engine Vehicles and Exhaust Aftertreatment Systems.” *Clean Technologies and Environmental Policy* 17(1): 15–27.

Samal, Sneha. 2016. “High-Temperature Oxidation of Metals.” In *High Temperature Corrosion*, InTech.

Schmoranzer, Jan, and Sanford M. Simon. 2003. “Role of Microtubules in Fusion of Post-Golgi Vesicles to the Plasma Membrane” ed. Juan Bonifacino. *Molecular Biology of the Cell* 14(4): 1558–69.

Schwarze, P E et al. 2013. “Inflammation-Related Effects of Diesel Engine Exhaust Particles: Studies on Lung Cells in Vitro.” *BioMed research international* 2013: 685142. http://www.ncbi.nlm.nih.gov/pubmed/23509760 (February 20, 2018).

Stefania Gottardo, Editors et al. 2017. “NANoREG Framework for the Safety Assessment of Nanomaterials.”

Stenfors, N. et al. 2004. “Different Airway Inflammatory Responses in Asthmatic and Healthy Humans Exposed to Diesel.” *European Respiratory Journal* 23(1): 82–86.

Studer, Andreas M. et al. 2010. “Nanoparticle Cytotoxicity Depends on Intracellular Solubility: Comparison of Stabilized Copper Metal and Degradable Copper Oxide Nanoparticles.” *Toxicology Letters* 197(3): 169–74. http://dx.doi.org/10.1016/j.toxlet.2010.05.012.

Van Teunenbroek, Tom. 2016. *NANoREG, a Common European Approach to the Regulatory Testing of Nanomaterials Final Report (Part 1)*.

Tseng, Chia Yi, Jhih Syuan Wang, and Ming Wei Chao. 2016. “Causation by Diesel Exhaust Particles of Endothelial Dysfunctions in Cytotoxicity, Pro-Inflammation, Permeability, and Apoptosis Induced by ROS Generation.” *Cardiovascular Toxicology*: 1–9.

Uski, O. et al. 2015. “Effect of Fuel Zinc Content on Toxicological Responses of Particulate Matter

from Pellet Combustion in Vitro." *Science of the Total Environment* 511: 331–40.

Vandebriel, Rob J., and Wim H. De Jong. 2012. "A Review of Mammalian Toxicity of ZnO Nanoparticles." *Nanotechnology, Science and Applications* 5(1): 61–71.

Vuong, Ngoc Q. et al. 2016. "Proteomic Changes in Human Lung Epithelial Cells (A549) in Response to Carbon Black and Titanium Dioxide Exposures." *Journal of Proteomics* 149: 53–63.

Walkowicz, Monika et al. 2018. "Impact of Oxidation of Copper and Its Alloys in Laboratory-Simulated Conditions on Their Antimicrobial Efficiency." *Corrosion Science* 140: 321–32.

Wallace, Lance, and Wayne Ott. 2011. "Personal Exposure to Ultrafine Particles." *Journal of Exposure Science and Environmental Epidemiology* 21(1): 20–30.

Wang, Zhenyu et al. 2012. "CuO Nanoparticle Interaction with Human Epithelial Cells: Cellular Uptake, Location, Export, and Genotoxicity." *Chemical Research in Toxicology* 25(7): 1512–21.

Wilson, Martin R. et al. 2007. "Nanoparticle Interactions with Zinc and Iron: Implications for Toxicology and Inflammation." *Toxicology and Applied Pharmacology* 225(1): 80–89.

Wongrakpanich, Amaraporn et al. 2016. "Size-Dependent Cytotoxicity of Copper Oxide Nanoparticles in Lung Epithelial Cells." *Environmental Science: Nano* 3(2): 365–74.

Yu, Yongbo et al. 2015. "Combined Toxicity of Amorphous Silica Nanoparticles and Methylmercury to Human Lung Epithelial Cells." *Ecotoxicology and Environmental Safety* 112: 144–52.

3.2 SUPPLEMENTARY DATA CHAPTER III

Supplementary table S1. Scheme describing CFE assay set-up.

DAY 1	DAY 2	DAY 3	DAY 4	DAY 5	DAY 6	DAY 7	DAY 8
Cell seeding	**Exposure T=0h**	**T=24 h**		**T=72 h**			**Fix and stain**

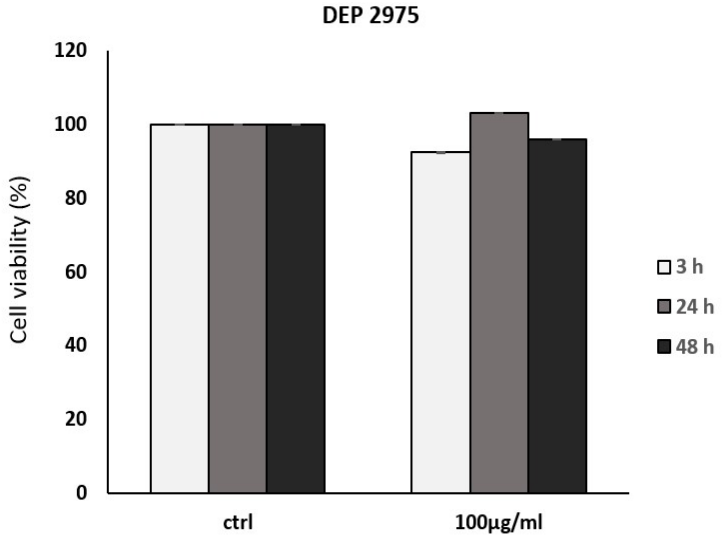

Figure S1. Cell viability of A549 after exposure to DEP. Histograms represent the percentage respect to control cells (100%) of viable cells after the exposure to DEP 100 µg/ ml. Data show the mean ± SE (n = 3).

Supplementary data S.2

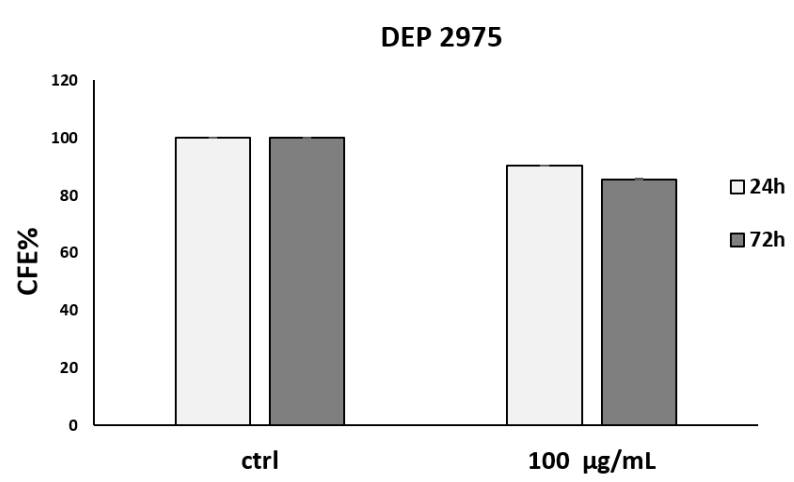

Figure S2. Colony forming efficiency (CFE) assay. Histograms represent the percentage of CFE calculated after the exposure to DEP 100 µg/mL. Data show the mean ± SE (n = 3).

Supplementary data S.3

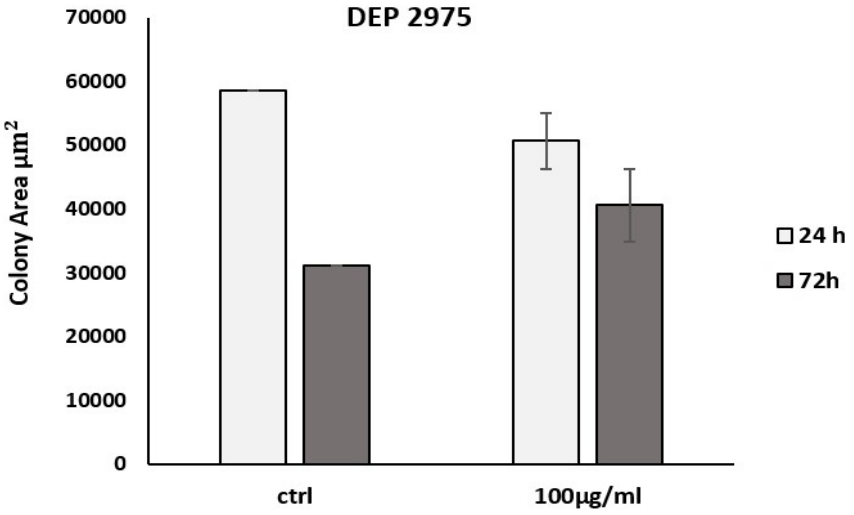

Figure S3. Analysis of the mean area of the colony. Mean of 10 counts, ± SE.

Supplementary data S.4

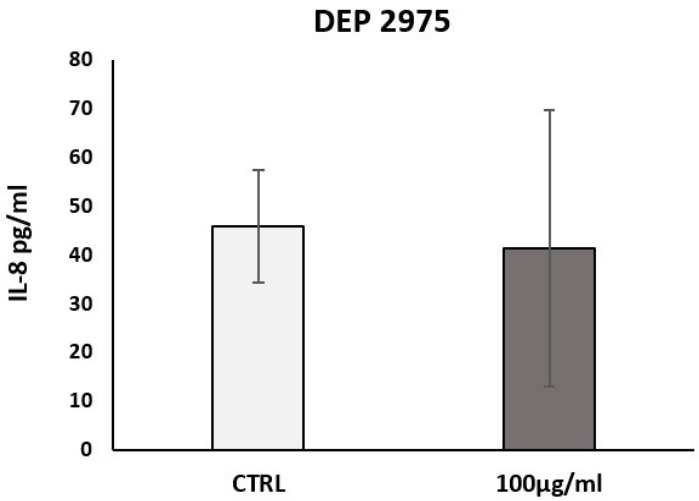

Figure S4. Inflammatory response. The release of the pro-inflammatory cytokine IL-8 was evaluated in A549 supernatants after the exposure for 24 h to DEP (100 µg/mL). Data are presented as pg/mL and the histograms represent the mean ± SE of at least three independent experiments.

Supplementary data S.5

A

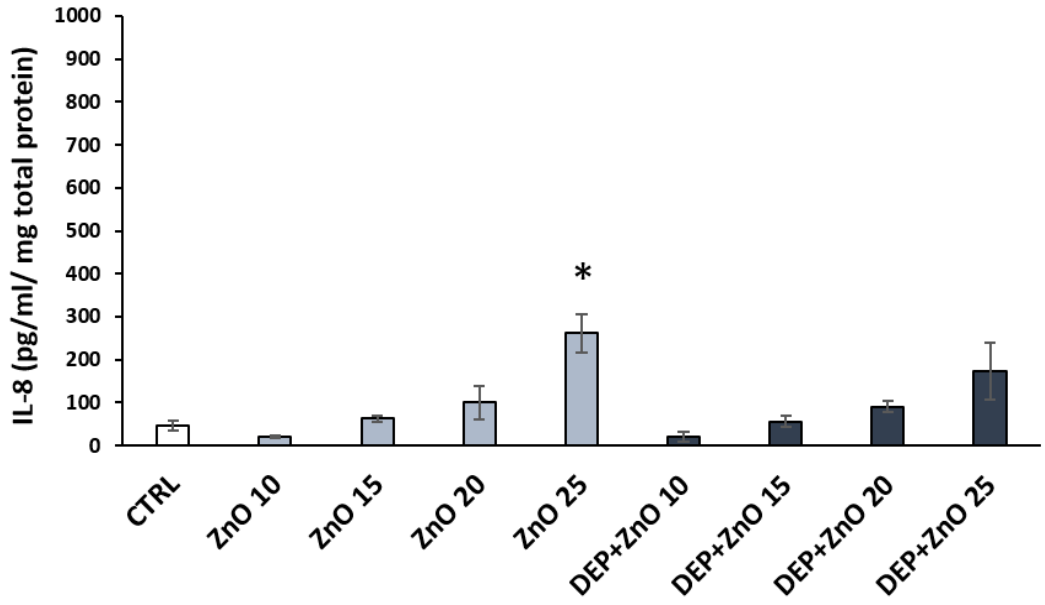

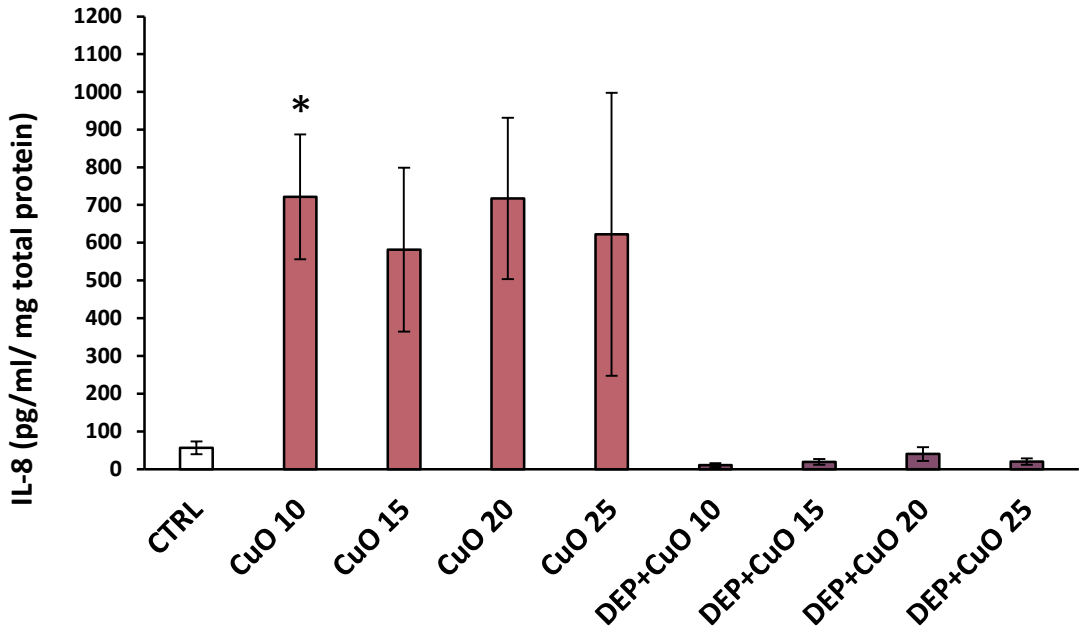

B

Figure S5. Inflammatory response at 24 h. The release of the pro-inflammatory cytokine IL-8 was evaluated in A549 supernatants after the exposure for 24 h to: A) ZnO (10, 15, 20 and 25 µg/mL) and ZnO+DEP (100 µg/mL); B) CuO (10, 15, 20 and 25 µg/mL) and CuO+DEP (100 µg/mL). Data were normalized to the total amount of protein (mg) in each sample measured by BCA (Bicinchoninic Acid) Protein Assay (Sigma Aldrich),

which is relate to the number of cells. Data are presented as pg/mL/mg total protein and the histograms represent the mean ± SE of at least three independent experiments.

Supplementary data S.6

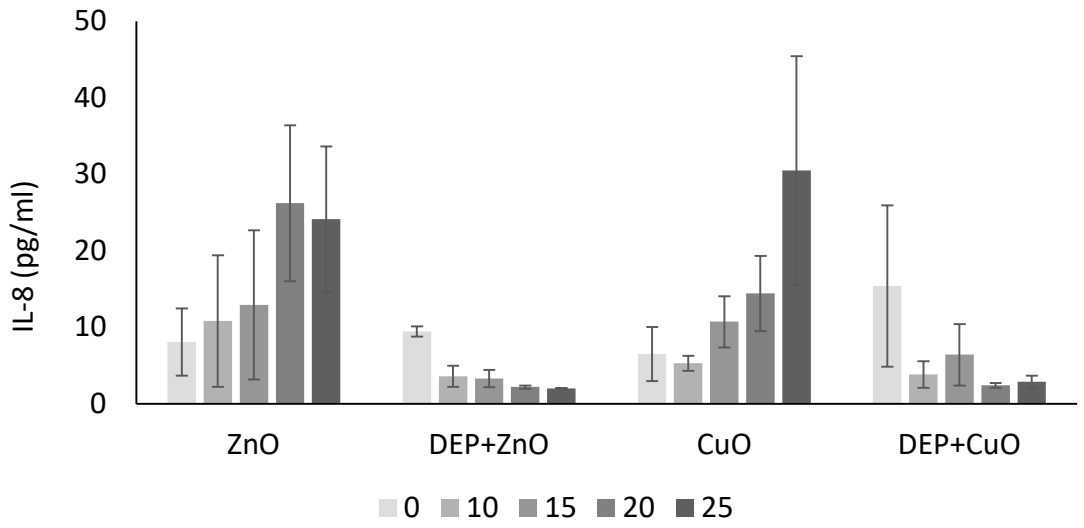

Figure S6. Inflammatory response at 3 h. The release of the pro-inflammatory cytokine IL-8 was evaluated in A549 supernatants after the exposure for 3h to 0, 10, 15, 20, 25 µg/mL of ZnO and CuO NPs alone and mixed with DEP (100 µg/mL). Data are presented as pg/mL and the histograms represent the mean ± SE of at least three independent experiments.

Supplementary data S.7

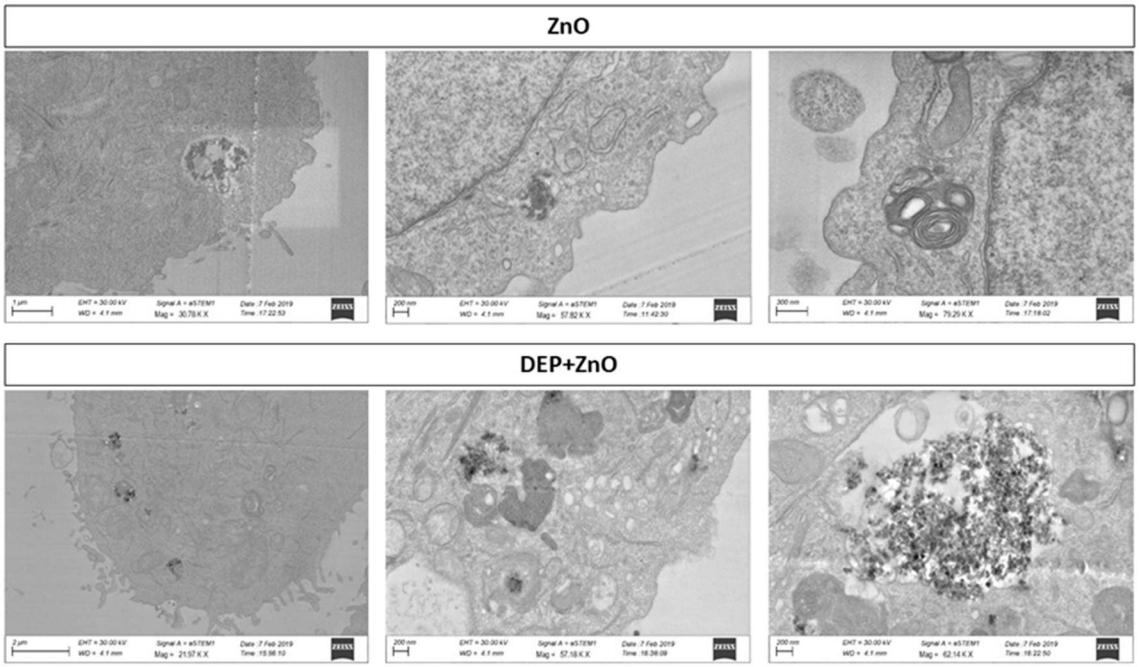

Figure S7. TEM images of A549 cells exposed to ZnO NPs (upper panel) and DEP + ZnO NPs (lower panel). Cells exposed to ZnO showed low NP uptake and only few multivesicular bodies with debris and particulate inclusions were observable in the cytoplasm; cells exposed to DEP + ZnO showed several and large vesicles containing cellular debris together with electron dense NPs. Cells were exposed for 24h to ZnO NPs at 20 µg/mL and DEP at 100 µg/mL..

CHAPTER IV

MIXTURE EFFECTS OF DIESEL EXHAUST AND METAL OXIDE NANOPARTICLES IN HUMAN LUNG A549 CELLS: CELLULAR MECHANISMS INVOLVED

Diesel exhaust particles (DEP) can act as a factor in triggering the development or progression of many respiratory chronic diseases. The assessment of pollutants toxicity in a more complex approach should be based on the evaluation of the combined effects of cumulative exposures to different particulate sources. In the present work, which constitutes the second part of a previously published paper, we aimed to investigate whether DEP, metal-oxide nanoparticles (MeO-NPs) and their mixtures could affect alveolar cells (A549) functionality and morphology. The research was focused on NPs induced apoptosis, necrosis, and autophagy and on their ability to modulate cell motility and migration. Autophagy and cell cycles were investigated by flow cytometry quantification of the autophagic biomarker LC3B and the microscopic analysis of LC3B in co-localization with lysosomes. Cells ultrastructure was then observed by TEM to confirm the presence of autophagosomes in treated cells. Changes in cell motility and migration were assessed by Transwell Migration assay and by the cytofluorimetric analysis of E-cadherin expression, after the exposure to single NPs or to mixtures of DEP+MeO-NPs. After Colony forming efficiency (CFE) assay four types of colonies were identified, based on their morphologies. Colonies were also stained for E-cadherin and cytoskeletal actin filaments to investigate the interaction among cells inside the colonies and how these interactions change after exposure to the single particles and their mixtures. The results obtained suggest NPs can either reduce the toxicity of DEP (CuO) or enhance it (ZnO), through a mechanism that may involve autophagy as cells response to stressor and as consequence of particles cellular uptake and which can determine modification of adhesion molecules (E-cadherin)

expression and consequentially of colonies' formation, morphology, and dimensions. These results evidence the importance to include in future research the investigation also of co-contaminant exposure during the health safety assessment of environmental pollutants.

1. Introduction

The inhalation of airborne ultrafine particles (UFPs, <0.1 µm diameter) is known to promote the insurgence and exacerbation of severe lung diseases, including chronic obstructive pulmonary disease (COPD), lung fibrosis and lung cancer (MacNee and Donaldson 2003). Humans have been exposed to airborne UFPs throughout all their evolutionary stages, but over the last century the exposure to these airborne particles has grown drastically (Sierra et al; 2016), due to the increase of new anthropogenic sources. Several epidemiological studies have suggested that the carcinogenic potential of particulate matter (PM) and UFPs, including diesel combustion-derived particles (CDPs), is mainly related to their small size and to the amount of polycyclic aromatic hydrocarbons (PAHs) and toxic metals that are adsorbed on the soot core of CDPs (Bangia et al; 2015) (Schenker; 1989). In urban areas two main sources of atmospheric pollution are ultrafine diesel exhaust particles (DEP) and non-exhaust particles from abrasive sources, which are enriched in metal content, especially in Cu, Zn, Fe, due to tire and break wear (Grigoratos and Martini 2015)(Adamiec et al; 2016). Furthermore, the increasing production of engineered nanoparticles (NPs), especially metal-oxide nanoparticles (MeO-NPs), such as copper and zinc oxide (CuO, ZnO) NPs developed for industrial, medical and research purposes, is an additional source of emitted particles in the nanosized range, that could lead to an increased exposure to humans to metal-based toxic compounds (Taghavi et al; 2013). The toxic nature of NPs varies widely depending on their amount, portals of entry and duration of exposure. The evaluation and collection of toxicity and exposure data is needed for the individual pollutants. However, humans are inevitably exposed to a mixture of pollutants that could coexist in the same environmental conditions. Despite this evidence, the co-exposure to co-contaminants, such as UFPs (e.g., DEP) and engineered NPs, has largely been ignored so far. Indeed, the interaction among UFPs and NPs and their possible agonist, antagonist or synergistic effects on biological systems are still poorly known. In a perspective of

cumulative risk assessment (CRA), it will be important to evaluate the possible interaction between different pollutants, acting on multiple pathways, that could lead to common or different health outcomes.

Recently, we presented a study on the combined *in vitro* effects of DEP and CuO and ZnO NPs on human lung A549 cells (Zerboni et al. 2019). Data showed that the co-exposure to DEP and NPs may induce physico-chemical interactions among the particles, with consequent increased cytotoxicity for ZnO NPs mixed with DEPs, and reduced effects for CuO NPs when in mixture with DEP. With the present work we explored some of the mechanisms that could drive the biological outcomes observed after the exposure of lung cells to mixtures DEP+CuO/ZnO mixtures and the relative single particles (DEP, ZnO, CuO).

Several mechanisms of toxicity have been proposed for both NPs and environmental UFPs, including oxidative stress, apoptosis, inflammatory response, DNA damage and cell cycle alteration, autophagy, lysosomal damage, and cell motility alteration (Donaldson and Stone 2003)(Manke et al; 2013)(Gao and Sang 2020)(Möller et al; 2002). Most of them have been extensively elucidated while some others are not yet fully investigated and understood.

Regarding NPs-induced mechanisms of cell death, several evidences reported the activation of the apoptotic pathway by CuO, ZnO and TiO_2 NPs, and by PM and ambient UFPs (S.-W. Wang et al; 2020)(Wilhelmi et al; 2012). Nevertheless, it is not the only pathway that could be activated by NPs: indeed, high doses could induce an irreversible cellular damage and consequent necrosis. Furthermore, there is a strict relation among necrosis, apoptosis and even autophagy.

Autophagy is a conserved catabolic pathway, stimulated by multiple forms of cellular stress, by which dysfunctional cellular components and aggregated proteins are delivered to the lysosomes for degradation (Kroemer et al. 2010). Recently, autophagy has been recognized as an important response in NPs-induced toxicity (R. J. Chen et al. 2020) and it can be triggered either by NPs-induced oxidative stress or by NPs uptake and compartmentalization in auto-phagolysosomes for degradation, acting as a survival mechanism in response to harmful compounds. However, an excess of autophagy may also lead to cell death. Thus, this mechanism has also been proposed as cellular key event in the framework of adverse outcome pathways (AOPs) related to lung fibrosis and acute lung toxicity (R. J. Chen et al; 2020).

Another mechanism of lung toxicity induced by UFPs is the dysregulation of cell motility and migration, that could lead to epithelial to mesenchymal transition (EMT). EMT is a biologic process that allows a polarized epithelial to acquire multiple changes that enable it to assume a mesenchymal cell phenotype, which includes enhanced migratory capacity, invasiveness, elevated resistance to apoptosis (Kalluri and Weinberg 2009). It is characterized by the downregulation of cellular epithelial markers (e.g., E-cadherin) and the upregulation of mesenchymal one (N-cadherin, Vimentin)(Gheldof and Berx; 2013).
Some observations indicate that autophagy and EMT are linked in a complex relationship: cells that undergo through EMT indeed require autophagy activation to survive during the metastatic spreading, but on the counterpart, autophagy could limit the activation of the EMT by acting as onco-suppressive signal (Gugnoni et al; 2016).

In this paper, we aimed to investigate whether DEPs, MeO-NPs and their mixtures could affect alveolar type II cells (A549) functionality and morphology by assessing cellular apoptosis and necrosis, oxidative stress response, and DNA damage. Then, our research was focused on NPs induced autophagy and, on their ability to modulate cells motility and migration. Autophagy was investigated through flow cytometry quantification of the autophagic biomarker LC3B (Tanida et al.2008) and the microscopic analysis of LC3B in co-localization with lysosomes. Cells ultrastructure was then observed by TEM to confirm the presence of autophagosomes in treated cells. Changes in cell motility and migration was assessed by Transwell Migration assay and through the cytofluorimetric analysis of E-cadherin expression, after the exposure to single NPs or to mixtures of DEP+MeO-NPs. Colony forming efficiency (CFE) assay was performed in our previous study to determine NPs and mixtures cytotoxic and cytostatic effects. However, CFE assay gives also additional information on the cell-cell interactions, intercellular junction and on the ability of cells to aggregates and form colonies. Here, a classification of the colonies, based on their shape and area, was performed. Colonies were also stained for E-cadherin and cytoskeletal actin filaments to investigate the interaction among cells inside the colonies. The results obtained suggest that the exposure to mixtures can result in different cellular toxicity compared to the single counterparts, evidencing the importance to include in future research the investigation also of co-contaminant exposure during the health safety assessment of environmental pollutants.

2. Material and methods

2.1. Particle Suspensions and mixtures preparation

Commercial CuO (< 50 nm, CAS 1317-38-0), ZnO (<50 nm, CAS 1314-13-2) NPs and Diesel Exhaust Particles (DEPs; NIST SRM®2975) were purchased by Sigma-Aldrich (Milan, Italy). Particles suspensions and mixtures were prepared as previously described (Zerboni et al. 2019). The mixtures were freshly prepared before use. A subcytotoxic concentration of DEPs (100 μg/mL) and two concentrations of CuO and ZnO NPs (10, and 20 μg/mL) were used basing on previous results.

The particle suspensions were named as followed:

- ZnO: suspension of ZnO NPs (final concentration 10 or 20 μg/mL)
- ZnO+DEP: mixture suspension of ZnO NPs (10 or 20 μg/mL) and DEP (100 μg/mL)
- CuO: suspension of CuO NPs (final concentration 10 or 20 μg/mL)
- CuO+DEP: mixture suspension of CuO NPs (10 or 20 μg/mL) and DEP (100 μg/mL)
- DEP: suspension of DEP particles (final concentration 100 μg/mL)

2.2. Cell cultures and treatments

Human alveolar epithelial cells, A549 (ATCC® CCL-185, American Type Culture Collection, Manassas, VA, US), were grown and maintained as previously reported (Zerboni et al., 2019, ref). For the experiments, cells were seeded at a concentration of 1.6×10^4 cells/cm^2 on 6-well plates (Corning®) and grown up for 24 h. At the optimal confluence (80-90%), the culture medium was replaced with fresh OptiMEM supplemented with 1% of fetal bovine serum (FBS) (Gibco, Life Technologies, Monza, Italy) and cells were treated by directly adding the different particles suspensions (ZnO, ZnO+DEP, CuO, CuO+DEP, DEP) into the medium. After 24 h of exposure, cells were processed for the different experimental endpoints. At least three independent experiments were performed for each biological response investigated.

2.3 Hoechst 33342/PI double staining

Apoptosis and necrosis induced by mixtures and single particles exposure were assessed by two assays: Propidium iodide (PI) and Hoechst 33342 (Hoechst) staining and Annexin V/PI kit.

Hoechst/PI staining allowed to distinguish viable, apoptotic, necrotic, and mitotic A549 cells after NPs and mixtures exposure. At least 300 cells per sample were counted under a fluorescence microscope (Zeiss-Axioplan, Carl Zeiss Microscopy GmbH, Jena, Germany) with a UV filter (365 nm) and scored as viable cells (H positive and PI negative cells, without special nuclear characteristic and an intact plasma membrane), necrotic cells (PI positive), apoptotic cells (bright H positive cells with fragmented nuclei) and mitotic cells (H positive with condensed chromosomes). Data are represented as the mean percentage ± standard error (SE) of the cell for each nuclear characteristic. The description of the Annexin V/PI evaluation of apoptotic and necrotic cells by cytofluorimetric analysis is described at paragraph 2.6.

2.4 Cytological Observation

2.4.1 A549 cell monolayers staining.

For morphological analysis, cells were seeded on a cover slide at a concentration of $1.5x10^5$ cells/well, cultured for 24 h and then exposed to particles for further 24 h. At the end of the treatment, cells were processed for hematoxylin-eosin (HE) staining as previously reported (Bengalli et al. 2019). The slides were observed using an optical microscope (Zeiss-Axioplan, Carl Zeiss Microscopy GmbH, Jena, Germany), and pictures were acquired using an AxioCam MRc5 digital camera and processed using AxioVision Real 4.8 software (Carl Zeiss Solutions, Jena, Germany).

For the evaluation of LC3B expression in acidic organelles (lysosomes), cells were incubated for 2 h with LysoTracker™ Red DND (Thermo Fisher) adding 75 nM of probe into the medium. After LysoTracker staining, cells were fixed fixed in 4% paraformaldehyde for 20 min and non-specific sites were blocked by incubating cells with cold PBST (PBS 1X with 0.1% Tween20; Sigma Aldrich) containing 2% bovine albumin serum (BSA). Then coverslips were incubated with a primary antibody rabbit anti-human LC3B (1:200 dilution, Cell

Signaling). Cells were subsequently washed with PBS and incubated with the secondary antibody Goat anti-Rabbit Alexa Fluor 488 (1: 500, Life Technologies) for 2h. Finally, coverslips were dried and observed under an inverted microscope AxioObserver Z1 Cell Imaging station (Carl-ZEISS Spa, Milano, Italy). Images were acquired by an MRc5 digital camera and elaborated with s ZEN 2.3 Blue edition software.

2.4.2 Colony forming efficiency (CFE): classification of colonies and morphological changes.

After Colony Forming Efficiency assay, performed as previously reported (Zerboni et al. 2019), cell adhesion and cytoskeleton organization of colonies was analysed after exposure for 24 h to 10 and 20 µg/mL of NPs or mixtures (100 µg/mL of DEP and 10-20 µg/mL od NPs). Cells, seeded on a Petri dishes (Corning®, 60 mm diameter), were processed for immunostaining by using primary antibody rabbit anti-human E-cadherin (1:200 dilution, Cell Signaling), and Goat anti-Rabbit Alexa Fluor 488 (1: 500, Life Technologies) as secondary antibody. In addition, cytoskeleton actin was marked by staining actin microfilaments with rhodamin phalloidine (1:40 dilution, Cytoskeleton Inc., Denver, CO, USA). Nuclei were counter-stained with DAPI (4', 6-diamino-2-phenylindole, 1:100, (Molecular Probes, Life Technologies, Monza, Italia). Colonies were then observed with AxioObserver Z1 Cell Imaging station. Colonies were classify based on four recurrent shape and morphological features:

Colony type A: a colony composed of a high-density cluster with close interactions between the cells (Supplementary, Figure S.4.1)

Colony type B: a colony characterized by a core of high-density cells and a uniform density distribution of cells all around. The colony seems to be composed by the union of two cells clusters (Supplementary, Figure S.4.2).

Colony type C: a colony characterized by a uniform distribution of cells and irregular borders (Supplementary, Figure S.4.3).

Colony type D: a colony composed of dispersed cells with an irregular distribution (Supplementary, Figure S.4.4).

2.5 Transmission Electron Microscopy (TEM)

For transmission electron microscopy analysis, cells were processed, after treatment with DEP (100 µg/ml), NPs (10 µg/ml) and mixtures as described in our previous work (Zerboni et al. 2019). Sample were observed with Jeol JEM 1220 Transmission Electron Microscope (JEOL, Japan), operating at 80kV acceleration voltage and equipped with a Lheritier LH72WA-digital camera and by a Zeiss SEM-FEG Gemini 500 operating at 30kV in STEM mode (Zeiss, Germany 2.6).

2.6 Cytofluorimetric Analysis

Cytofluorimetric analyses were performed using a Cytoflex flow cytometer and using the CytExpert software, to investigate particles and mixtures capability to induce ROS formation, to evaluate the expression of a marker of DNA damage (y-H2AX), to analyse the percentage of live, necrotic, or apoptotic cells (Annexin V/PI assay) and cells cycle progression and to investigate the expression of LC3B and E-Cadherin proteins in cells after the treatments.

In order to analyse the apoptosis process after exposure to particles, a Dead Cell Apoptosis Kit with Annexin V FITC and PI (Thermo Fischer) was used following the manufacturer's instructions. Briefly, cells were seeded and treated with either mixtures or single NPs as reported at paragraph 2.2. After 24h of exposure, cells were harvested, centrifuged for 6 min at 1200 rpm, suspended in fresh medium (100 µL) and incubated with Annexin V and propidium iodide (PI) for 10 min at RT in the dark, after vortexing. The quantification of the population of apoptotic, late apoptotic, and necrotic cells was analysed through flow cytometry (Cytoflex). Data were expressed as mean percentage ± SE of cells for each cell population. At least three independent experiments were performed.

The cell cycle progression of cells exposed to particles and mixtures was investigated after 24 h of exposure by DNA-staining. Cells were trypsinized, collected and pooled with the harvested medium, centrifuged at 1200 rpm for 6 min, fixed in 90% cold ethanol and stored at −20 °C until analysis.

For the analysis, cells were centrifuged at 1600 rpm for 6 min to discharge ethanol, samples were resuspended in PBS supplemented with RNAse DNAse-free (1 mg/mL, Sigma-Aldrich, Italy) and incubated for 30 minutes. Finally, the fluorescent dye PI was added to stain DNA

of cells for 7 min in the dark. Fluorescence was measured by flow cytometer (CytoFLEX, Beckman Coulter GmbH, Krefeld, Germany) using 617 nm band pass filters. For the analysis, cells in different cell cycle phases (subG0; G1; S; G2/M) were selected and analysed as mean percentage of cells in each phase.

For ROS detection, A549 cells were pre-incubated for 20 min with the probe Carboxy-2',7'-Dichlorofluorescein Diacetate (carboxy-DCFDA, 5 µM, Life Technologies) and incubated with NPs for 180 min. After incubation, cells were detached, centrifuged at 1200 rpm for 6 min, re-suspended in 500 µL of PBS and analyzed in the FITC channel by flow cytometry (CytoFLEX) with the software CytoExpert. The signal from unloaded samples (cells without the probe carboxy-DCFDA) was evaluated as reference to assess cells and NPs' autofluorescence. These values were then subtracted from the values to DCFDA stained samples. The capability of particles and mixtures to induce the expression of phospho-histone H2AX (y-H2AX), as marker of DNA double-strands breaks (DSBs) were evaluate by probing exposed and control cells with the rabbit mAb anti-yH2AX Alexa Fluor 488 Conjugate (Cell Signaling). After 24 h of exposure to particles, cells were detached, washed in PBS, fixed in 1% paraformaldehyde in PBS, suspended in 90% cold methanol and stored overnight at −20 °C before the analysis. Samples were then stained for y-H2AX following manufacturers' instructions and analysed at the CytoFLEX (Beckman Coulter) in the FITC channel.

Furthermore, the expression of specific protein was investigated by cytofluorimeter. Cells, after exposure to 10 µg/mL of NPs, 100 µg/mL of DEP and mixtures particles for 24 h, were harvested, fixed with paraformaldehyde 4% for 15 min, permeabilized with methanol 90%, and then stained with the antibody rabbit anti-human LC3B (1:400 dilution, Cell Signalling) and E-Cadherin (1:200 dilution, Cell Signaling). After 1 h of incubation in the appropriate buffer (0.5% bovine serum albumin in PBS 1X), cells were washed in buffer and then incubated for 60 min with secondary antibody AlexaFluor anti-rabbit 488 (1:200 dilution, Life Technologies). After washing, cells were resuspended in PBS and analysed by the CytoFLEX in the FITC channel.

2.7 Cell migration Assay

Cells migration after the exposure to individual NPs and to mixtures, was assessed using a Cell Migration Assay Kit (Cell Biolab CytoSelects ^{TM}). Briefly 2.2x 10^4 cells were seeded on the apical side of an insert (Ø 8 µm) in cells free medium, treated with particles (DEP 100 µg/mL, NPs 10 µg/mL and mixtures) and incubated for 24 h at 5% CO_2, 37° C.I In the basal side of the inserts was add 1.5 mL of OptiMEM with 10% of FBS. After the incubation time, non-invasive cells in the apical side of the insert were removed with a cotton-tipped swab. Then, inserts were transferred to a well containing a Cell Staining Solution and incubate for 10 minutes. The insert was then transfer to an empty well adding an Extraction solution and incubate for 10 minutes. The extraction solution was then transfer to a 96-weel plate and OD was measured by a multiplate reader (Infinite 200Pro, TECAN) at the wavelength of 560 nm.

2.8 Statistical Analysis

The data represent the mean ± standard error of the mean (SE) of at least three independent biological experiments. Statistical analyses were performed using GraphPad Prism software, using unpaired t-test, one-way or two-way ANOVA + post hoc test.

3. Results

3.1 Effects on cell viability and cell cycle alteration after exposure to mixtures and single NPs.

Cell viability of mixtures and single NPs and DEP were previously assessed through MTT assay (Zerboni et al. 2019). The previous data showed that CuO NPs induce high mortality, while the co-exposure with DEP reduced the toxicity of CuO. DEP+ZnO are slightly more toxic than ZnO NPs alone. However, the co-exposure enhances the toxicity in cells compared to samples treated only with DEP. The differences observed were due to the amount of Cu^{2+} and Zn^{2+} ions released from NPs, alone or in co-presence with DEP. Here we investigated the mechanisms of cell death induced by the different treatment.

The present study began with an investigation of the type of death induced by particles. Two different approaches were adopted: a microscopic analysis with Hoechst/PI staining and through the cytofluorimetric analysis of Annexin V/PI expression. A concentration of 20 μg/mL was previously chosen since it was the most effective one, but in order to investigate the mechanisms of action of particles and mixtures a lower concentration (10 μg/mL) was used for the further experiments. Data from Hoechst/PI staining confirmed the data from MTT test, showing that CuO NPs at high concentration (20 μg/mL) induced necrosis. An increase of necrotic cells, though not statistically significant, was observed also after the exposure to ZnO, DEP+ZnO and DEP+CuO (Supplementary materials, Figure S1). The H/PI method allows us to classify cells in apoptotic, mitotic and viable status basing on the nuclear morphology and in necrotic cells by incorporation of PI inside the cells. However, this method is based on cellular count under the microscope by the operator, and the analysis is less objective compared to MTT and other assays.

For this reason, Annexin V/PI double staining was performed in cell treated for 24 h with NPs at the concentration of 10 (Figure 1A) and 20 μg/mL (Figure 1B), either in mixture with DEP or as single NPs. To detect cell death, Annexin V/PI double staining kit was used in flow cytofluorimetric analyses. The Annexin V corresponding signal is a sensitive method for detecting cellular apoptosis, while propidium iodide (PI) is used to detect necrotic or late apoptotic cells, characterized by the loss of the integrity of the plasma and nuclear membranes. Data generated by flow cytometry are show in the Figure 1 and expressed as a percentage of cells in the different status (Viable, Apoptotic, Necrotic, Late Apoptotic). In our previous work, a concentration of 25 μg/mL of CuO and ZnO induced a strong cytotoxic effect after 24 h of exposure, which reduced considerably the number of viable cells. At the concentration of 10 μg/mL, CuO NPs increased the programmed cell death (apoptosis) and a significant reduction of viable cells was observed. At 20 μg/mL, CuO NPs determined the increase of necrotic cells, also in mixture with DEPs. This assay did not show an increase of dead cells after exposure to ZnO and DEP+ZnO, that was expected according to previous results from cytototoxicity test (MTT). Moreover HO/PI staining (Data show in Supplementary S.1), confirmed the significant induction of necrosis in cells exposed to CuO 20 μg/mL and after DEP+CuO, albeit to a lower extent. HO/PI staining also showed an

induction of necrosis after ZnO (20 µg/mL) and of both necrosis and apoptosis after DEP+ZnO exposure.

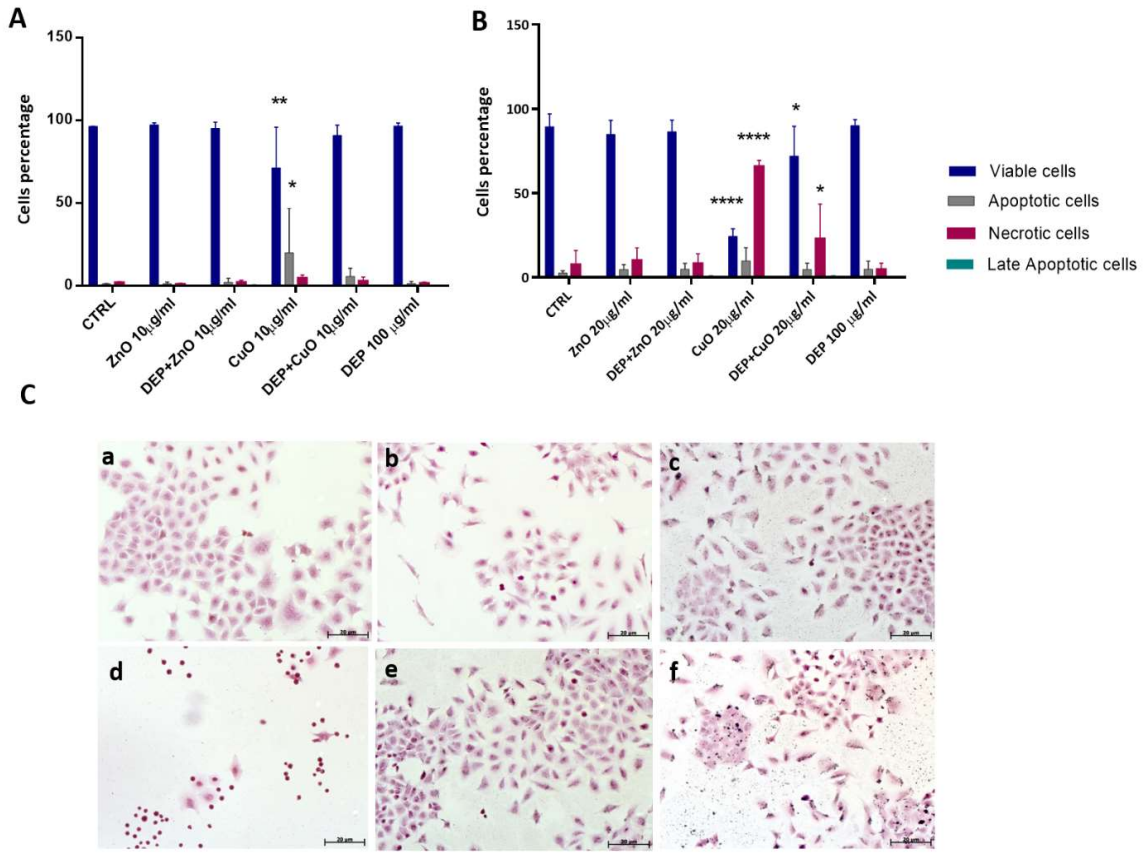

Figure 1. Cell death after particles and mixtures exposure. Panels A and B show flow cytometry analyses of cells stained with Annexin V and PI after exposure to ZnO and CuO NPs at 10 µg/mL (**A**) and 20 µg/mL (**B**), alone or in mixture with DEP (100 µg/mL). * Statistically significant with respect to the control according to One-Way Anova, ***p*<0.01 and **p*<0.05 ****< 0,0001 vs control. (**C**) Morphological analysis. Microscope images of A549 cells, stained with hematoxylin/eosin, (**a**)ctrl; (**b**)ZnO 20 µg/ml; (**c**)DEP+ZnO 20 µg/ml (**d**) CuO 20 µg/ml; (**e**) DEP+CuO 20 µg/ml; (f) DEP 100 µg/ml. Scalebar=20 µm.

Cell death has been described by a different set of both morphological and biochemical features, which collectively define this process (e.g. loss of cell volume or cell shrinkage and nuclear condensation)(Bortner and Cidlowski 2002). Cell morphology and particles interaction was investigated by optic microscopy on A459 cells exposed to NPs (20 µg/mL), DEP (100 µg/mL) and mixtures. The HE staining showed that diesel particles came in

contact with cells (Fig. 1.C), especially after DEP exposure, visible in the Figure.1, C.f). Exposed cells shown a slight increase in elongated cell morphologies with all treatments compared to control samples. The cytotoxic effects of CuO itself induced cell shrinkage, as shown in Figure 1.C.d.

Alterations of the cell cycle progression were evaluated after exposure of cells to particles and mixtures and are presented in Figure2.

A marked reduction in G1 phase cell percentage was evident after exposure to CuO 10 µg/mL, but also after exposure to DEP+CuO. A corresponding increase in the phases S and/or G2 was noticed, indicating an accumulation of cells cycle in late S and/or early G2. The ZnO NPs and their mixtures with DEP induced slight variation on cell cycle progression respect to the control, with a slight increase of percentage in phase S with ZnO 10 µg/mL and DEP+ZnO 10 µg/mL.

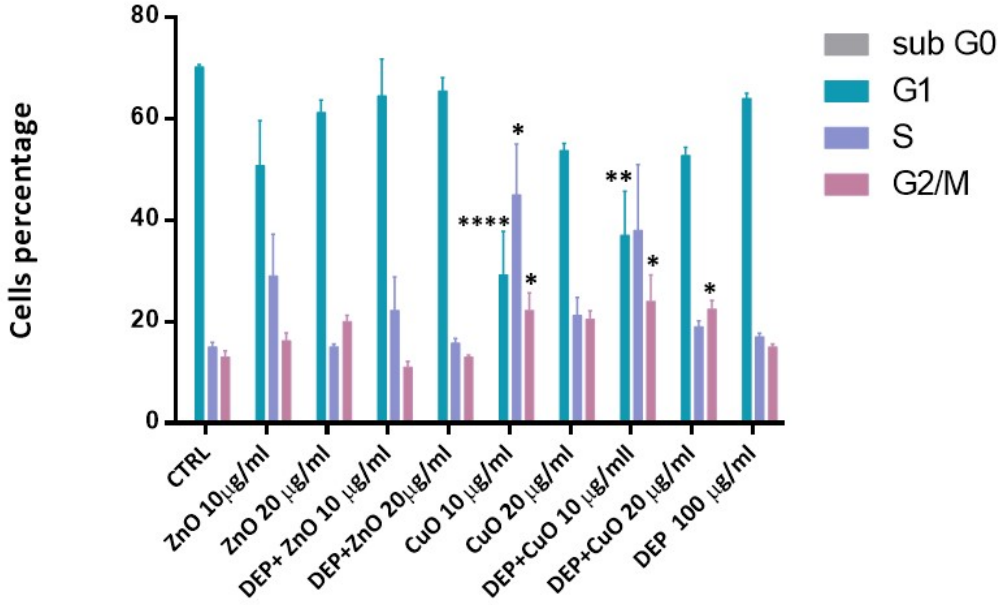

Figure 2: Cell cycle investigation. Cell percentage in each phase of the cycle after 24 h exposure to particles and mixtures (ZnO and CuO at 10 and 20 µg/mL). Statistical analysis was performed by One-way ANOVA with Dunnett's multiple comparisons tests. ***p*<0.01 and **p*<0.05 ****< 0,0001 vs control.

3.2 Cell-cell interaction and colonies' classification

Here we evaluated the migration of single cells after exposure to NPs (10 µg/mL), DEP and mixtures (Figure 3A) and the expression of E-Cadherin (Figure 3B) using cytofluorimetric analyses. A slight though not significant increase of migration was recognizable after all the treatments, except for CuO, compared to the control. Presumably, the high cytotoxicity induced by CuO NPs exposure, limited the number of migratory cells able to cross the transwell porous membrane. A downregulation of E-cadherin was evident after exposure of cells to ZnO, DEP+ZnO and CuO, suggesting that these tested substances interfere with the cellular contacts.

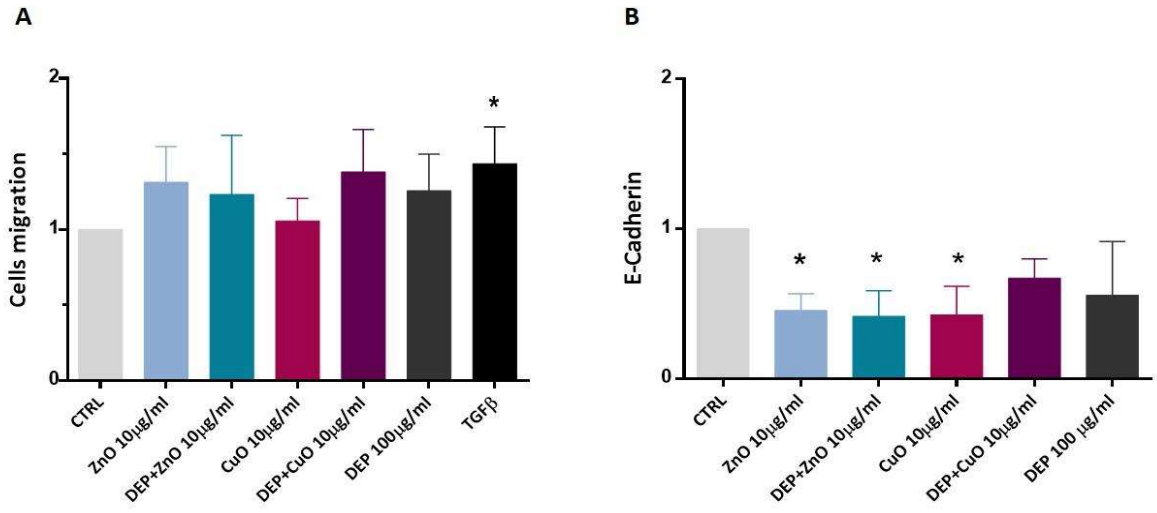

Figure 3. Cells migration and E-cadherin expression. Cell migration was evaluated in cells exposed to 10 µg/mL of ZnO and CuO and respective mixtures with DEP (100 µg/mL) (A), compared with untreated cells (CTRL) and with a positive control for migration (TGFβ), (A) (Data are presented as fold change respect to the control). At the same exposure concentration, the expression of E-Cadherin (Presented as fold change respect to the control). (B) was evaluated using a cytofluorimeter and data were expressed as fold change respect to the unexposed control. Data represent the mean ± SE of three independent experiments (n=3). *Statistically different respect to control sample; $p<0.05$, One-Way ANOVA + Bonferroni's post hoc test.

In addition, we established a method for A549 colonies classification utilizing images taken with a stereo microscope and fluorescence microscopy directly from cell culture dishes. On the basis of CFE assay of untreated cells, four different types of colonies (Figure 4) have been identified and this classification could be used as a parameter to evaluate DEP, NPs, and mixtures capability to affect the colonies phenotype. The different types of colonies were identified based on shape, cells distribution and cells-cells interactions. A deeper evaluation of colonies morphologies was done through an immunofluorescence investigation (Figure 4 A) (Supplementary S.4). The cytoskeleton and the adhesion between cells, as well the E-cadherin expression, appeared regular in colony type B and C, while in colony type A there is an overlap of cells, which limited the characterization of cytoskeleton and cell-cell adhesion. In colony type D cells presented altered cytoskeleton and reduced expression of E-Cadherin.

In figure 4 C are reported the percentage of the four different type of colonies after exposure for 24 h to particles. The analyses were done on three independent experiments and reported as percentage of colonies belonging to the four classes respect to the total colonies evaluated. Colony type D, which has a more disorganized morphology and more dispersed cells, was frequent after exposure to all the treatments, with a percentage around 20% with respect to the 10% present in control cells. This type of colony was prevalent after exposure to CuO (32% with 20 μg/mL and 38% with 10 μg/mL). On the other side, the percentage of colony types B and C, which presented high cells density, resulted decreased after exposure to CuO NPs. A slight reduction of colony C was also evident after exposure to DEP+ZnO and DEP+CuO mixtures. CuO at high concentration (20 μg/mL) also induced an increase of colony type A, which are colonies with a small diameter and cells very adherent to each other. This result fits with the evidenced strongest cytostatic effect observed for CuO NPs at 20 μg/mL in our previous work. In addition, the area (μm^2) of each colony type after treatment with particles was evaluated on three independent experiments (Supplementary data S.2), and these analyses confirm the reduction of the colonies' area after exposure of CuO and its mixtures, especially a significant decrease of colony type D area was evident.

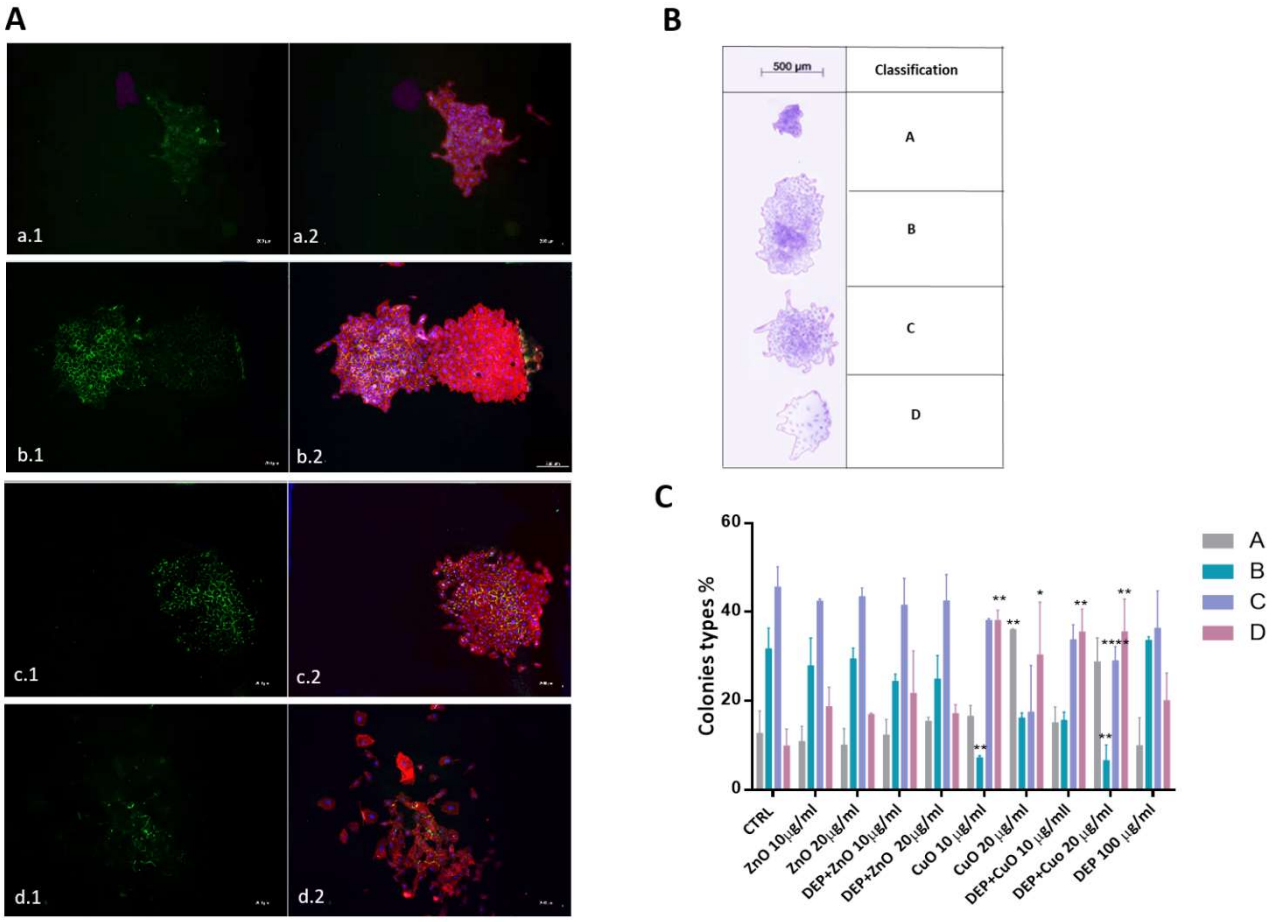

Figure 4: Colonies classification. Panel A show fluorescence microscope images of colonies stained for E-cadherin (a.1; b.1; c.1; d.1), phalloidin and DAPI (a.2; b.2; c.2; d.2). Colonies classification according to their shape and cellular contacts is shown in panel B. Histograms representing the percentage of colonies in the four groups (A, B, C, D) are represented in panel C . Statistical analysis was performed by One-way ANOVA with Dunnett's multiple comparisons tests. $^{**}p<0.01$ and $^{*}p<0.05$ ****< 0,0001 vs control.

3.3 Induction of autophagy

The induction of the autophagic mechanism, induced by NPs, either alone or in mixture with DEP, was here evaluated through the cytofluorimetric and microscopic analyses of LC3B biomarker and by TEM observation of autophagosomes presence in cells which have internalized the tested particles.

Data from cytofluorimetric analysis show that overall MeO-NPs, either alone or in co-exposure with DEP, increased the levels of LC3B expression in exposed cells (Figure 5 A), while DEP alone did not induce an increase of LC3B expression. A significant increase of the marker expression was observed with ZnO+DEP, CuO and CuO+DEP. Since autophagosome clearance depends on its fusion with lysosomes, the co-localization of LC3B puncta and lysosomes have been detected by immunofluorescence microscopy. To elucidate which particles can induce an autophagic response, we analysed these markers after exposure to NPs (10 µg/mL) alone and in mixtures with DEP for 24 h. ZnO NPs, CuO NPs and DEP+CuO mixture induced an increase of LC3B signalling and the LC3B puncta co-localize with lysosomes. Moreover, the ultrastructural analysis of cells exposed to particles shows that CuO NPs increased the intracellular formation of spherical structures with double layer membranes, which are features of an autophagosome (Figure 6).

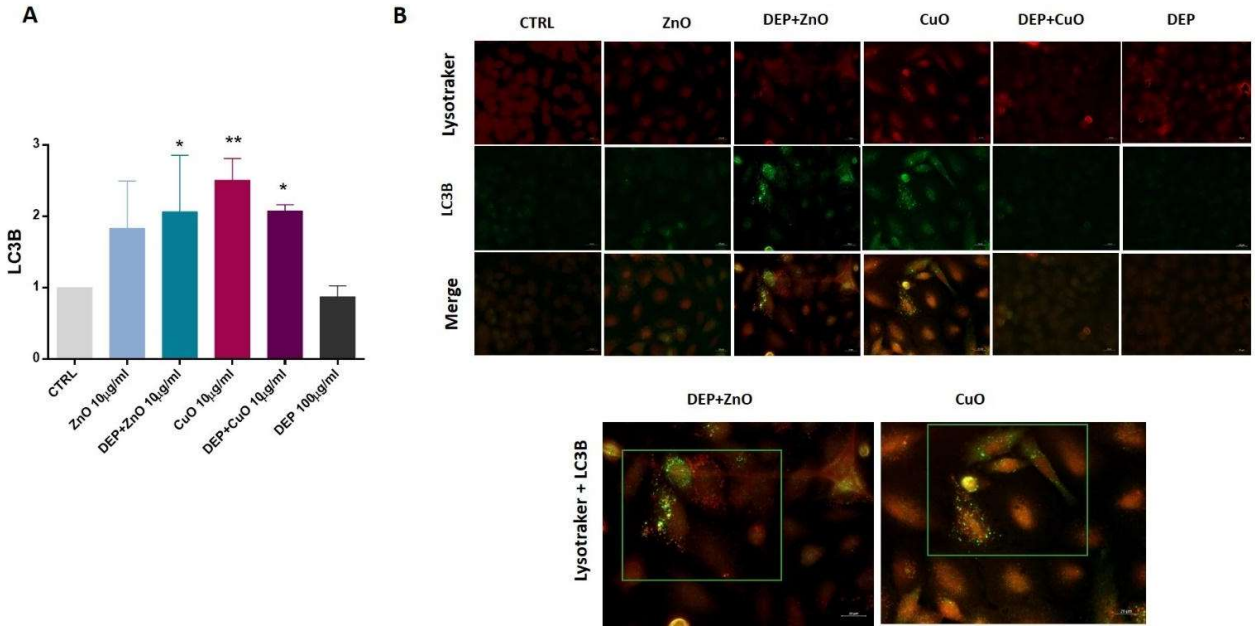

Figure 5. Autophagy detection by LC3B and co-localization with lysosomes. The expression of LC3B, as marker of autophagy was evaluated by cytofluorimetric analysis (A)in A549 cells exposed for 24h to ZnO and CuO NPs (10 µg/mL), alone or in mixture with DEP (100 µg/mL) and histograms represent the mean ± SE of the fold change of three independent experiments (n=3). In panel B are shown fluorescence microscopy images of A549 cells exposed to either MeO-NPs alone or mixtures and stained for lysosomes (Lysotracker, red) and LC3B (green). Merged figures indicate the colocalization of LC3B puncta with acidic organelles (highlighted images of cells exposed to DEP+ZnO and CuO NPs). Statistical analysis was performed by One-way ANOVA with Dunnett's multiple comparisons tests. **p<0.01 and *p<0.05.

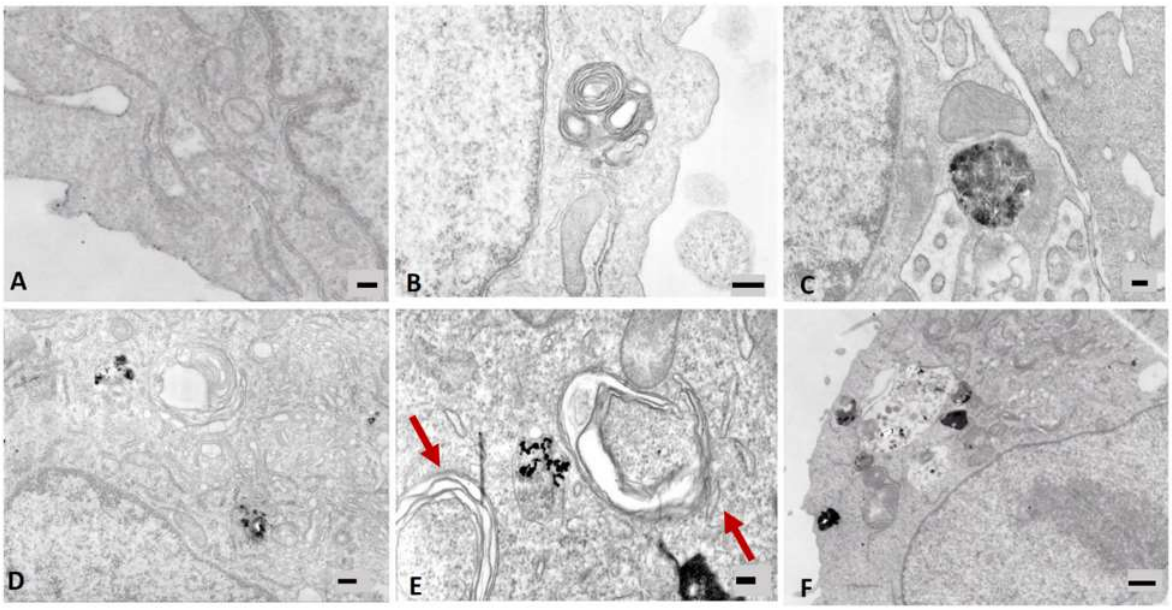

Figure 6. TEM analyses of A549 cells after 24 h exposure to particles. A: ctrl (100nm); **B:** ZnO 10 µg/mL (300 nm); **C:** DEP+ZnO 10 µg/mL (200 nm); **D:** DEP 100 µg/mL (300 nm); **E:** CuO 10 µg/mL (200nm); **F:** DEP+CuO 10 µg/ml (200nm). Red arrows indicate autophagosomes.

4- Discussion:

In real environmental condition it is quite difficult to distinguish background and incidental exposure to airborne nanomaterials, since the methods employed generally measure the presence of UFPs and do not differentiate between the various types of particles that may be present. Chemical risk assessment has usually focused on single stressors, also for what concerns air pollution, because the intense air pollution problems of the 20th century were determined by a limited number of chemicals, which were emitted in considerable quantities. Moreover, in the last years, beside the common air pollution sources (e.g., diesel exhaust particles and biomass burning), new emergent sources have been introduced, such as nanomaterials. It must be considered that the exposure to a single chemical/contaminants is an exception rather than the rule: indeed in everyday life, humans are exposed to a multitude of different stressors (Ragas et al. 2011). Nowadays, available data on the joint toxicity of environmental contaminants is very limited. In this perspective, we analysed how the *in vitro* effects of two widely use metal oxide nanomaterials (CuO and ZnO NPs) can change in concomitance with the presence of DEP. In a previous study from our group, the pivotal role of ions release from NPs in their toxic outcomes, and how this could change in co-presence of DEP, have been demonstrated (Zerboni et al. 2019). We observed that Cu ions release from the surface of soluble CuO NPs, was limited by a passivation effect of DEPs, which can explain the lower toxicity of DEP+CuO mixture. For what concerns ZnO NPs, they provoked cytotoxicity through the release of zinc ions, which seemed to be almost unaffected by the presence of DEP. The slight enhanced toxicity observed after lung cells exposure to DEP+ZnO mixture was correlated to an increased NPs uptake by the cells when in co-presence with DEP. Here, the analysis of the cellular mechanisms of death involved showed once again that CuO NPs are the most cytotoxic particles, and that they induce apoptosis at the lower concentration (10 µg/mL) and necrosis at the higher concentration (20 µg/mL) tested. Lai and colleagues reported that the expression of the apoptosis inhibitor proteins Bcl-2 and Mcl-1 resulted significantly decreased in A549 and BEAS-2B cells treated for 24 h with 10 µg/mL of CuO NPs. These observations confirm that CuO at low concentration induces apoptosis and it is in line with our results (Figure 1). The same authors also assumed a correlation between ROS generation after exposure to CuO NPs and the induction of autophagy (Lai et al. 2018).

At the tested conditions we were not able to detect any intracellular ROS generation, only DEP was able to induce a slight though not significant increase of ROS (Supplementary Data S.3 A). However, the induction of ROS and the consequent triggered toxicity by MeO-NPs is controversial. MeO-NPs biological effects could be either be ROS-dependent and independent (Manke et al; 2013b), and in the presence of NPs, the autophagic pathway could be activated by the compartmentalization of harmful compounds in lysosomes for degradation, acting as survival mechanism (Klionsky 2007). DNA damage by oxidative stress, here evaluated through the analysis of y-H2AX expression, was not observed, since the induction of ROS generation was not evidenced in our experimental conditions (Supplementary Data S.3 B). However, data from cell cycle analysis evidenced that the exposure to NPs significantly affected the normal progression of cells through the different cycle phases, with an evident arrest of cells in the S and G2/M phase when exposed to either CuO, DEP+CuO and at a less extend also ZnO and ZnO+DEP. These evidences support the hypothesis that NPs can alter DNA, consequently leading to mutations and cancer progression, by preventing cells to continue their cycle when DNA defects are detected at the specific checkpoints. Cell cycle can be indeed blocked or delayed in reaction to different genotoxic stresses, but also to structural dysfunctions of proteins (Longhin et al.2013).

Furthermore, our studies were focused on important mechanisms involved in the response to particles exposure and in the regulation of cancer progression: i) cell motility and cell-to-cell interaction and ii)autophagy (H. T. Chen et al. 2019).

Cell motility and the interaction among cells have a role in the maintenance of the homeostasis of the alveolar epithelium functionality in physiological conditions. Alteration of cells motility could also be due to downregulated expression of epithelial markers, such as E-cadherin that could lead to Epithelial-to-Mesenchymal Transition (EMT) (Loh et al. 2019). This process has been shown to be crucial in tumorigenesis, in addition to imparting a migratory and invasive capacity to cancer cells. The involvement of EMT as biological response to DEP exposure has been reported before by other authors, testing the toxicity of DEP on bronchial epithelial cells *in vitro*, a varying degree of expression of EMT-markers has been found (Rynning et al. 2018)(Grilli et al. 2018). In our study however DEP did not induce a significant downregulation of E-Cadherin or neither increased cells migration. Moreover, the morphology of A549 colonies exposed to DEP did not showed peculiar

variations with respect to control colonies, suggesting that in this experimental condition the cell-cell adhesion, by which cells interact and attach to neighbouring cells, was not compromised, as well as the process of colony formation. CuO NPs exposure on the other side induced a significant decrease of E-Cadherin expression and deeply changed the colonies phenotype, with an increased presence of colonies with less adherent cells, here identified as colony type D (Figure 4). This evidence enlighten that CuO NPs strongly reduce the adhesiveness of cells inside the colony and this phenomenon could be consequent to an augmented motility and invasiveness capability of cells exposed to such particles. A reduced E-cadherin expression was observed even in cells exposed to ZnO NPs and DEP+ZnO mixture, but not in cell expose to DEP+CuO. This evidence supports our previous results in which the biological effects exercised by CuO NPs was limited by the simultaneous presence of DEP, while DEP+ZnO mixture may lead to higher toxic outcomes compared to the single particles.

The choice to investigate carcinogenic related responses, such as cell motility and a marker of EMT in a tumoral cell line (A549) is for sure tricky and quite controversial. However, this cell line more likely reflects the target of the tested particles and *in vitro* studies about EMT and autophagy has been previously performed on these cell type (Rho et al. 2009)(D. Gao et al. 2019). However longer time of exposure and lower concentrations of NPs should be tested in order to investigate the carcinogenic process in this cell line in a more relevant manner.

Autophagy pathway has been studied before both relate to DEP and NPs exposure (Niranjan et al. 2020) (Jia, Hao, and Yang 2020). Moreover, DEP emitted from Euro 4 and Euro 5 engines was proved to induce a significant increase of the autophagic flux in bronchial epithelial cells (Colasanti et al. 2018). Moreover, some nanoparticle types, including metal based NPs, have been identified as a novel class of autophagy activators (Zabirnyk et al. 2007)(Lopes et al. 2016).

Nanoparticles can be commonly observed within the autophagosomes, suggesting that the activation of the autophagic pathway is prompted by the effort to sequester and destroy materials that enter into the cytoplasm (J. Wang et al. 2017). Microtubule-associated protein 1A/1B-light chain 3B (LC3B) is the most widely used marker of autophagosomes (Meyer et al. 2013), and it was here used as biomarker of autophagy.

Our results suggest that CuO NPs lead to the expression of some features connect to autophagic pathway, in particular the increase signal of LC3B marker, the presence of LC3 puncta co-localized with lysosomes and the formation of double membranes structure attributable to autophagosome formation, as confirmed also by TEM images. Furthermore, also the exposure to DEP+ZnO mixture induced the expression of LC3B marker of autophagy in treated cells.

The activation of the autophagy process is likely due the higher uptake of particles (CuO NPs and DEP+ZnO) in exposed A549 cells with respect to other NPs and mixtures (as reported in Zerboni et al., 2019) rather than due to oxidative stress, since in the tested conditions no ROS or oxidative damage was observed. Moreover, data from lysosomes and LC3B puncta colocalization and TEM strongly suggest that CuO NPs and DEP+ZnO mixture, once internalized in lung cells, are sequestered in auto-phagolysosomes for degradation as mechanism of survival against harmful compounds.

Our results in accordance with the study of Sun and co-workers (Sun et al. 2012), which showed that CuO NPs induce autophagic cell death in A549 cells. Evidences of the involvement of autophagy after exposure to ZnO NPs were reported in the study of Liu and co-worker, in which autophagy was identified as the main mechanisms of cell death involved in response to ZnO NPs(Liu et al. 2020). Altogether, these evidences confirm once again the less toxicological potential of CuO NPs when in mixture with DEP and the slightly higher potential of DEP+ZnO compared to ZnO NPs alone.

4. Conclusions

The assessment and mitigation of the effects of air pollutants is still a challenge for environmental policy and this topic should be addressed with a more complex approach, based on the evaluation of combined effects of cumulative exposures to different particulate sources. Furthermore, sophisticated sublethal endpoints linked to chronic toxicity should be considered. In the present work a simplified model of cumulative exposure has been simulated by exposing lung cells with single NPs and mixture of MeO-NPs and DEP. In this study we confirmed that the exposure to NPs-mixture can result in different cellular toxicity than the single NPs counterparts. NPs can either reduce the

toxicity of DEP (CuO) or enhance it (ZnO) through a mechanism that may involve autophagy as cells response to stressor and as consequence of particles cellular uptake. These results support the growing evidence that autophagy is a relevant molecular event in response to UFPs and NPs and that it should be investigated in the future researches for the definition of acute lung toxicity AOPs. On the other hand, a modification in cell-cell interaction of epithelial cells was observed. A new method for colonies identification and classification was proposed by the evaluation of colonies size and shape and by analysing cellular interactions inside the colony, through E-cadherin expression. This method could be used to understand how cell-cell interaction could be altered by particles exposure, giving insights about the contribution of particles interaction with lung cells to EMT and lung cancer progression. CuO individual particles and in mixtures with DEP, but also ZnO NPs and its mixtures at a lower extent, determined modification of adhesion molecules (E-cadherin) expression and consequentially of colonies' formation, morphology, and dimensions. Further investigations are needed to elucidate if other parameters can influence these results, such as dose of exposure, type of NPs, time of exposure and sub-chronic experiments. However, the present research, for the first time to our knowledge, point out how some relevant mechanisms, already known to be involved in response to environmental particles, could be differently activated when a co-exposure to different particulate sources occurs.

4.1 BIBLIOGRAPHY

Adamiec, Ewa, Elżbieta Jarosz-Krzemińska, and Robert Wieszała. 2016. "Heavy Metals from Non-Exhaust Vehicle Emissions in Urban and Motorway Road Dusts." *Environmental Monitoring and Assessment* 188(6): 1–11. https://link.springer.com/article/10.1007/s10661-016-5377-1).

Bangia, Komal S., Elaine Symanski, Sara S. Strom, and Melissa Bondy. 2015. "A Cross-Sectional Analysis of Polycyclic Aromatic Hydrocarbons and Diesel Particulate Matter Exposures and Hypertension among Individuals of Mexican Origin." *Environmental Health: A Global Access Science Source* 14(1): 51. http://ehjournal.biomedcentral.com/articles/10.1186/s12940-015-0039-2 .

Bortner, C. D., and J. A. Cidlowski. 2002. "Apoptotic Volume Decrease and the Incredible Shrinking Cell." *Cell Death and Differentiation* 9(12): 1307–10.

Chen, Hong Tao et al. 2019. "Crosstalk between Autophagy and Epithelial-Mesenchymal Transition and Its Application in Cancer Therapy." *Molecular Cancer* 18(1): 1–19.

Chen, Rong Jane et al. 2020. "The Current Understanding of Autophagy in Nanomaterial Toxicity and Its Implementation in Safety Assessment-Related Alternative Testing Strategies." *International Journal of Molecular Sciences* 21(7): 2387. /pmc/articles/PMC7177614/?report=abstract .

Colasanti, Tania et al. 2018. "Diesel Exhaust Particles Induce Autophagy and Citrullination in Normal Human Bronchial Epithelial Cells." *Cell Death and Disease* 9(11).

Donaldson, Ken, and Vicki Stone. 2003. "Current Hypotheses on the Mechanisms of Toxicity of Ultrafine Particles." *Annali dell'Istituto Superiore di Sanita* 39(3): 405–10. https://europepmc.org/article/med/15098562 .

Gao, Dongmei et al. 2019. "Role of Autophagy in Inhibiting the Proliferation of A549 Cells by Type III Interferon." *Cell Biology International* 43(6): 605–12. https://onlinelibrary.wiley.com/doi/abs/10.1002/cbin.11132 .

Gao, Rui, and Nan Sang. 2020. "Quasi-Ultrafine Particles Promote Cell Metastasis via HMGB1-

Mediated Cancer Cell Adhesion." *Environmental Pollution* 256: 113390.

Gheldof, Alexander, and Geert Berx. 2013. "Cadherins and Epithelial-to-Mesenchymal Transition." In *Progress in Molecular Biology and Translational Science*, Elsevier B.V., 317–36. https://pubmed.ncbi.nlm.nih.gov/23481201/ .

Grigoratos, Theodoros, and Giorgio Martini. 2015. "Brake Wear Particle Emissions: A Review." *Environmental Science and Pollution Research* 22(4): 2491–2504. /pmc/articles/PMC4315878/?report=abstract .

Grilli, Andrea et al. 2018. "Transcriptional Profiling of Human Bronchial Epithelial Cell BEAS-2B Exposed to Diesel and Biomass Ultrafine Particles." *BMC Genomics* 19(1): 302. https://bmcgenomics.biomedcentral.com/articles/10.1186/s12864-018-4679-9 (November 5, 2020).

Gugnoni, Mila et al. 2016. "Autophagy and Epithelial–Mesenchymal Transition: An Intricate Interplay in Cancer." *Cell Death and Disease* 7(12): e2520. /pmc/articles/PMC5260980/?report=abstract .

Jia, Lu, Shuang Li Hao, and Wan Xi Yang. 2020. "Nanoparticles Induce Autophagy via MTOR Pathway Inhibition and Reactive Oxygen Species Generation." *Nanomedicine* 15(14): 1419–35.

Kalluri, Raghu, and Robert A. Weinberg. 2009. "The Basics of Epithelial-Mesenchymal Transition." *Journal of Clinical Investigation* 119(6): 1420–28. /pmc/articles/PMC2689101/?report=abstract .

Klionsky, Daniel J. 2007. "Autophagy: From Phenomenology to Molecular Understanding in Less than a Decade." *Nature Reviews Molecular Cell Biology* 8(11): 931–37. www.nature.com/reviews/molcellbio .

Kroemer, Guido, Guillermo Mariño, and Beth Levine. 2010. "Autophagy and the Integrated Stress Response." *Molecular Cell* 40(2): 280–93. /pmc/articles/PMC3127250/?report=abstract .

Lai, Xiaofeng et al. 2018. "Intranasal Delivery of Copper Oxide Nanoparticles Induces Pulmonary Toxicity and Fibrosis in C57BL/6 Mice." *Scientific Reports* 8(1): 1–12.

http://dx.doi.org/10.1038/s41598-018-22556-7.

Liu, Zixuan et al. 2020. “Zinc Oxide Nanoparticles Effectively Regulate Autophagic Cell Death by Activating Autophagosome Formation and Interfering with Their Maturation.” *Particle and Fibre Toxicology* 17(1): 1–17. https://link.springer.com/articles/10.1186/s12989-020-00379-7 .

Loh, Chin Yap et al. 2019. “The E-Cadherin and N-Cadherin Switch in Epithelial-to-Mesenchymal Transition: Signaling, Therapeutic Implications, and Challenges.” *Cells* 8(10). /pmc/articles/PMC6830116/?report=abstract .

Longhin, Eleonora et al. 2013. “Cell Cycle Alterations Induced by Urban PM2.5 in Bronchial Epithelial Cells: Characterization of the Process and Possible Mechanisms Involved.” *Particle and Fibre Toxicology* 10(1): 1–19.

Lopes, Viviana R et al. 2016. “Dose-Dependent Autophagic Effect of Titanium Dioxide Nanoparticles in Human HaCaT Cells at Non-Cytotoxic Levels.” *Journal of Nanobiotechnology* 14: 22.

MacNee, W., and K. Donaldson. 2003. “Mechanism of Lung Injury Caused by PM10 and Ultrafine Particles with Special Reference to COPD.” In *European Respiratory Journal, Supplement*, European Respiratory Society, 47s-51s. https://erj.ersjournals.com/content/21/40_suppl/47s .

Manke, Amruta, Liying Wang, and Yon Rojanasakul. 2013a. “Mechanisms of Nanoparticle-Induced Oxidative Stress and Toxicity.” *BioMed Research International* 2013. /pmc/articles/PMC3762079/?report=abstract .

Meyer, Gregory et al. 2013. 19 Current Pharmaceutical Design *The Cellular Autophagy Markers Beclin-1 and LC3B-II Are Increased During Reper-Fusion in Fibrillated Mouse Hearts*.

Möller, Winfried et al. 2002. “Ultrafine Particles Cause Cytoskeletal Dysfunctions in Macrophages.” *Toxicology and Applied Pharmacology* 182(3): 197–207.

Niranjan, Niranjan et al. 2020. “Proliferation of Lung Epithelial Cells Is Regulated by the Mechanisms of Autophagy upon Exposure of Soots.” *bioRxiv Cell Biology*. http://biorxiv.org/cgi/content/short/2020.09.19.304725v1?rss=1&utm_source=researche

r_app&utm_medium=referral&utm_campaign=RESR_MRKT_Researcher_inbound.

Ragas, Ad M.J. et al. 2011. “Cumulative Risk Assessment of Chemical Exposures in Urban Environments.” *Environment International* 37(5): 872–81.

Rho, Jin Kyung et al. 2009. “Epithelial to Mesenchymal Transition Derived from Repeated Exposure to Gefitinib Determines the Sensitivity to EGFR Inhibitors in A549, a Non-Small Cell Lung Cancer Cell Line.” *Lung Cancer* 63(2): 219–26.

Rynning, Iselin et al. 2018. “In Vitro Transformation of Human Bronchial Epithelial Cells by Diesel Exhaust Particles: Gene Expression Profiling and Early Toxic Responses.” *Toxicological sciences : an official journal of the Society of Toxicology* 166(1): 51–64. https://academic.oup.com/toxsci/article/166/1/51/5054330 .

Schenker, M. B. 1989. “Epidemiologic Studies of Populations Exposed to Motor Vehicle Exhausts and Polycyclic Aromatic Hydrocarbons.” In *Assessment of Inhalation Hazards*, Springer Berlin Heidelberg, 293–300. https://link.springer.com/chapter/10.1007/978-3-642-74606-2_27 (December 16, 2020).

Sierra, M. I. et al. 2016. “The Effect of Exposure to Nanoparticles and Nanomaterials on the Mammalian Epigenome.” *International Journal of Nanomedicine* 11: 6297–6306. /pmc/articles/PMC5135284/?report=abstract .

Sun, Tingting et al. 2012. “Copper Oxide Nanoparticles Induce Autophagic Cell Death in A549 Cells” ed. Srinivasa M. Srinivasula. *PLoS ONE* 7(8): e43442. https://dx.plos.org/10.1371/journal.pone.0043442 .

Taghavi, Sayed Mohammad et al. 2013. “Effects of Nanoparticles on the Environment and Outdoor Workplaces.” *Electronic physician* 5(4): 706–70612. /pmc/articles/PMC4477780/?report=abstract .

Tanida, Isei, Takashi Ueno, and Eiki Kominami. 2008. “LC3 and Autophagy.” *Methods in Molecular Biology* 445: 77–88. https://pubmed.ncbi.nlm.nih.gov/18425443/.

Wang, Ji et al. 2017. “Silica Nanoparticles Induce Autophagy Dysfunction via Lysosomal Impairment and Inhibition of Autophagosome Degradation in Hepatocytes.” *International Journal of Nanomedicine* 12: 809–25. /pmc/articles/PMC5279829/?report=abstract .

Wang, Shih-Wei et al. 2020. “ZnO Nanoparticles Induced Caspase-Dependent Apoptosis in Gingival Squamous Cell Carcinoma through Mitochondrial Dysfunction and P70S6K Signaling Pathway.” *International Journal of Molecular Sciences* 21(5): 1612. https://www.mdpi.com/1422-0067/21/5/1612.

Wilhelmi, Verena et al. 2012. “Evaluation of Apoptosis Induced by Nanoparticles and Fine Particles in RAW 264.7 Macrophages: Facts and Artefacts.” *Toxicology in Vitro* 26(2): 323–34.

Zabirnyk, Olga, Maksym Yezhelyev, and Oleksandr Seleverstov. 2007. “Nanoparticles as a Novel Class of Autophagy Activators.” *Autophagy* 3(3): 278–81. https://www.tandfonline.com/doi/abs/10.4161/auto.3916 .

Zerboni, Alessandra et al. 2019. “Mixture Effects of Diesel Exhaust and Metal Oxide Nanoparticles in Human Lung A549 Cells.” *Nanomaterials* 9(9): 1–21.

4.2 SUPPLEMENTARY DATA CHAPTER IV

Supplementary data S.1

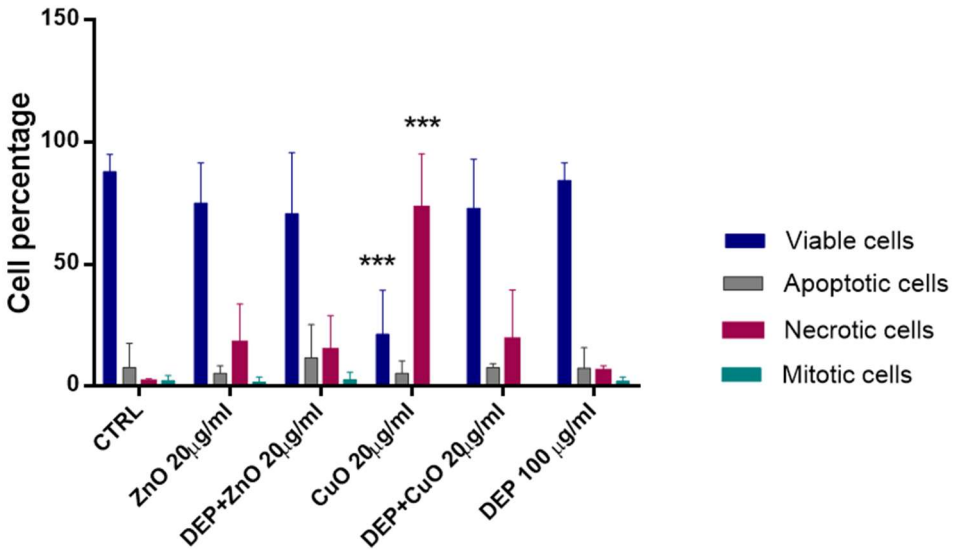

Figure S.1: Graphic representing the percentage of viable, apoptotic, necrotic, mitotic cells, according to Hoechst/PI staining, in control cells and cells exposed to ZnO; CuO (20µg/ml); DEP (100 µg/ml) and respective mixtures for 24 h. Statistical analysis was performed by One-way ANOVA with Dunnett's multiple comparisons tests. ***p< 0.0001 vs control.

Supplementary data S.2

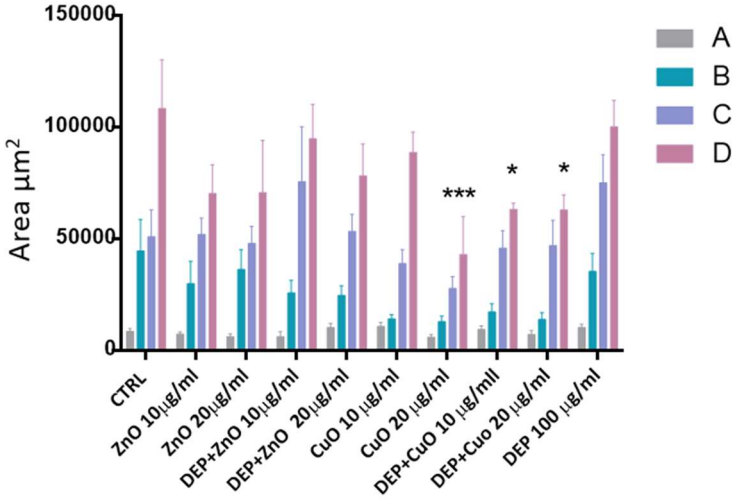

Figure S.2: Graphic representing the mean area of colonies (µm^2) divided in the four type (**A, B, C, D**) in control cells and cells exposed to ZnO; CuO (20µg/ml); DEP (100 µg/ml) and respective mixtures for 24 h.

Supplementary data S.3

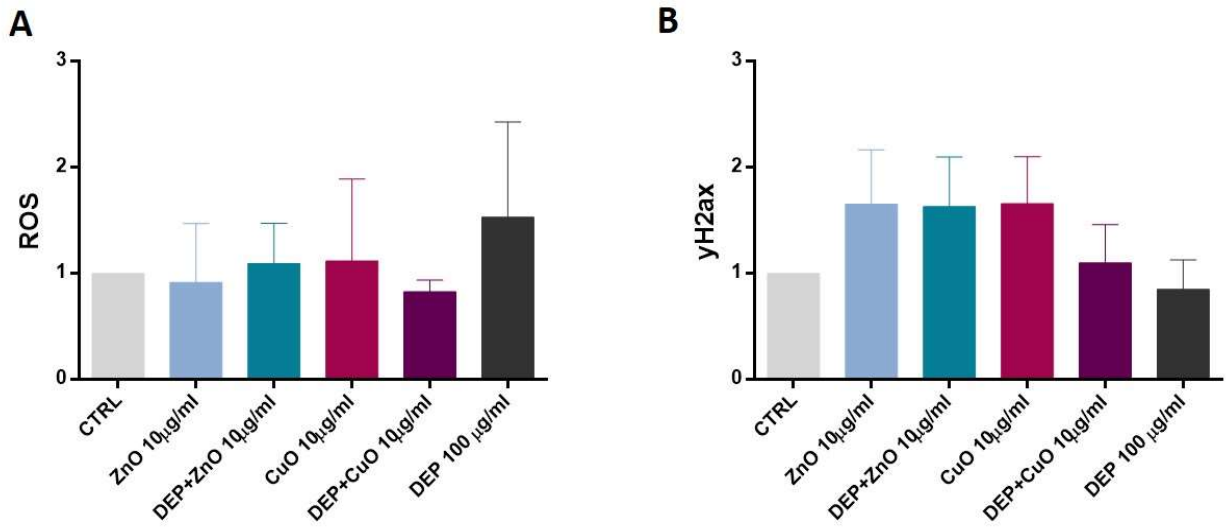

Figure S.3: (A) ROS and **(B)** γ-H2AX fold increase in cells exposed to ZnO and CuO NPs (10µg/mL); DEP (100 µg/mL) and DEP+ZnO and DEP+CuO (concentration of NPs: 10 µg/mL) mixtures for 24 h.

Supplementary data S.4: Colonies classification:

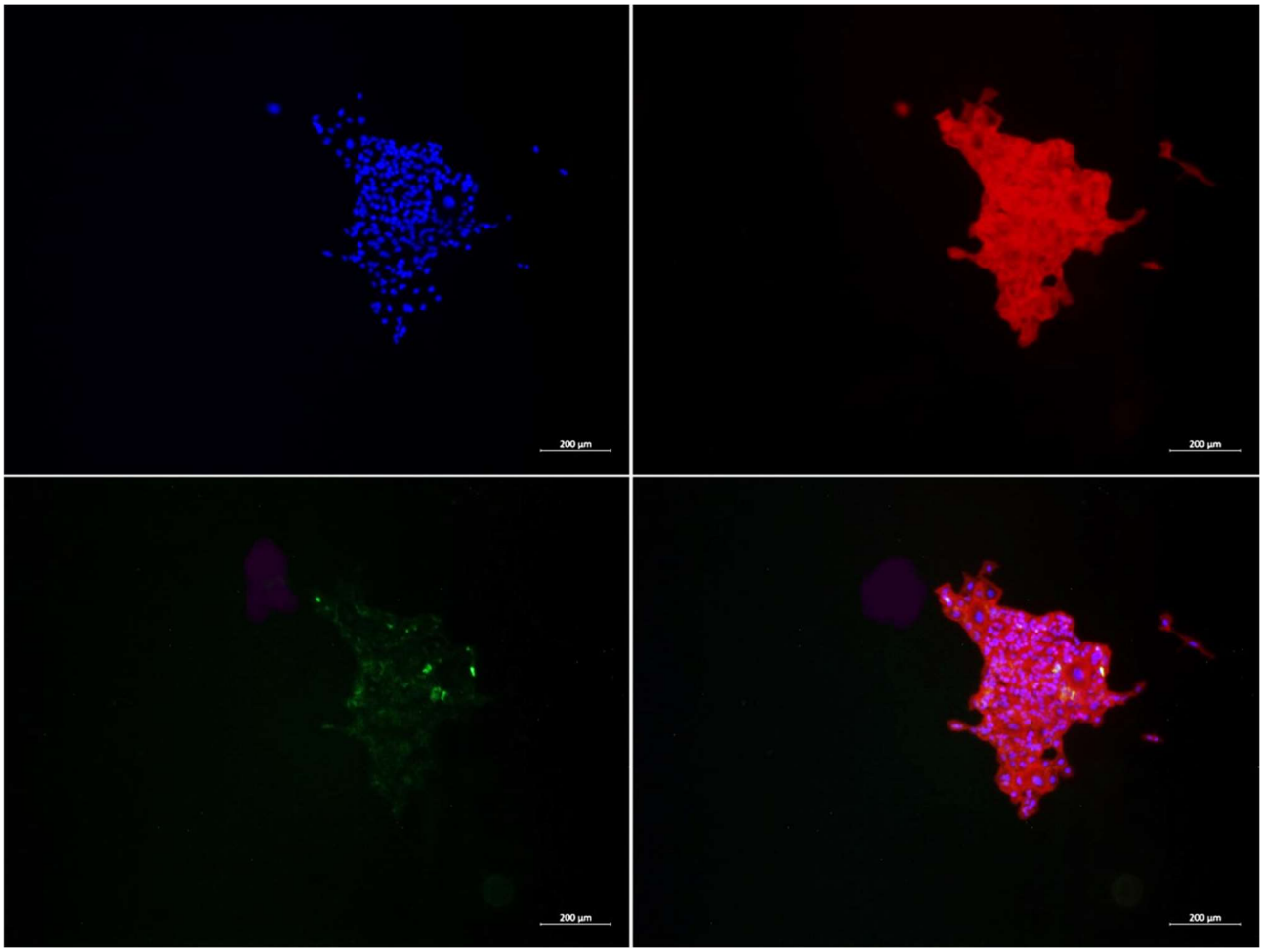

Figure S.4.1 Colony type A. Colonies' classification: E-cadherin (green), phalloidin rhodamine (red) and DAPI (blue) staining of colonies.

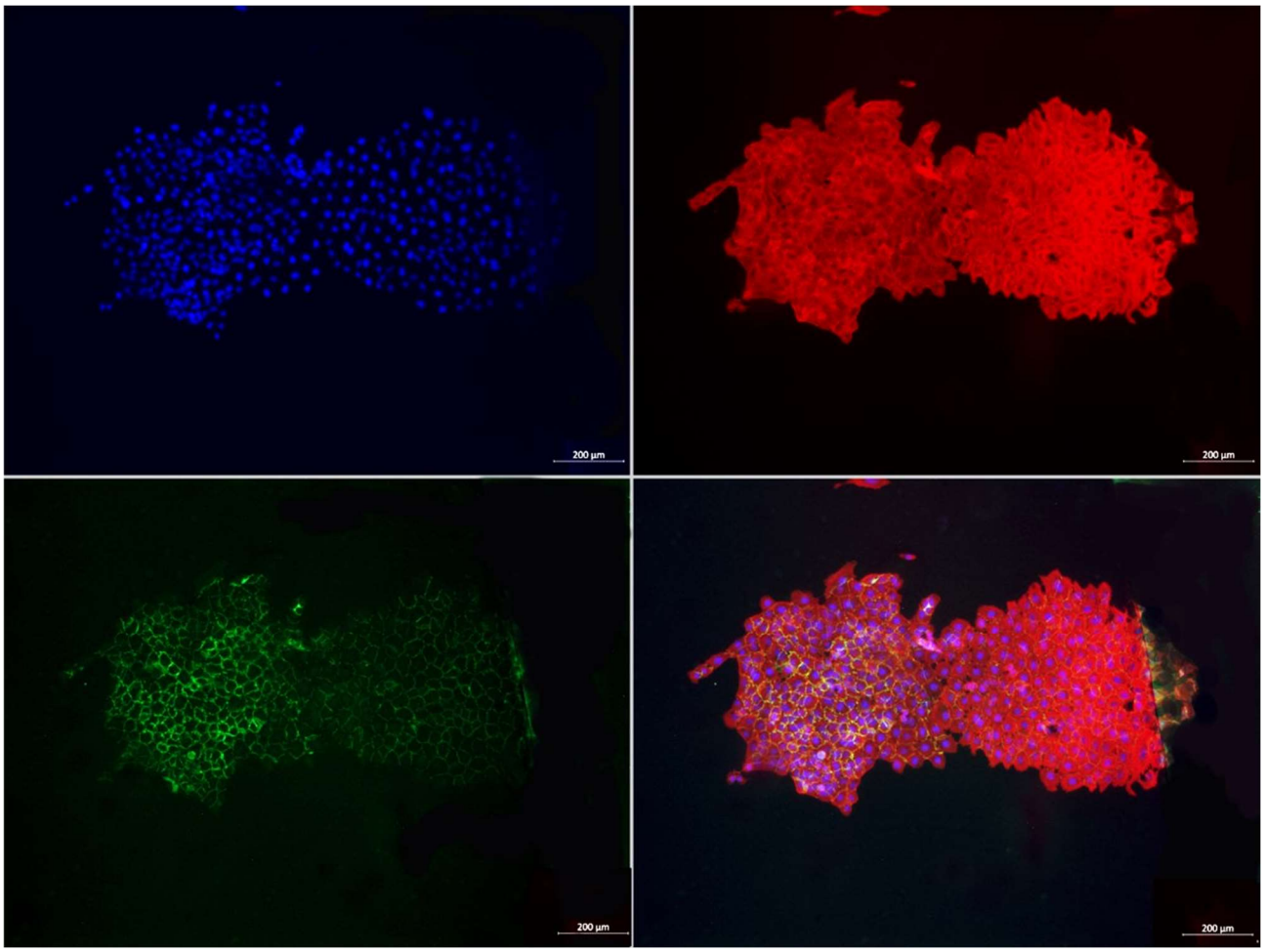

Figure S.4.2 Colony type B. Colonies' classification: E-cadherin (green), phalloidin rhodamine (red) and DAPI (blue) staining of colonies.

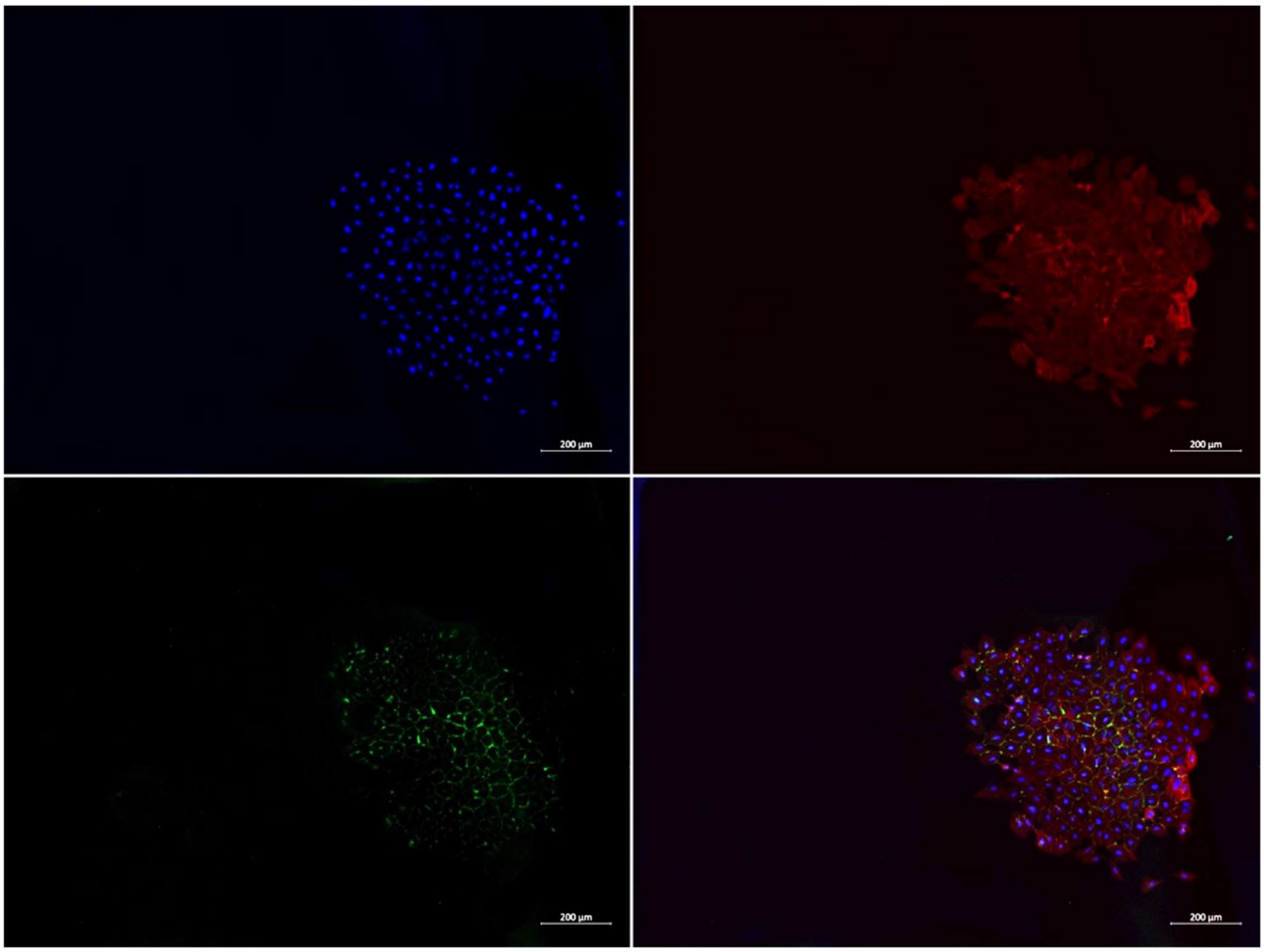

Figure S.4.3 Colony type C. Colonies' classification: E-cadherin (green), phalloidin rhodamine (red) and DAPI (blue) staining of colonies.

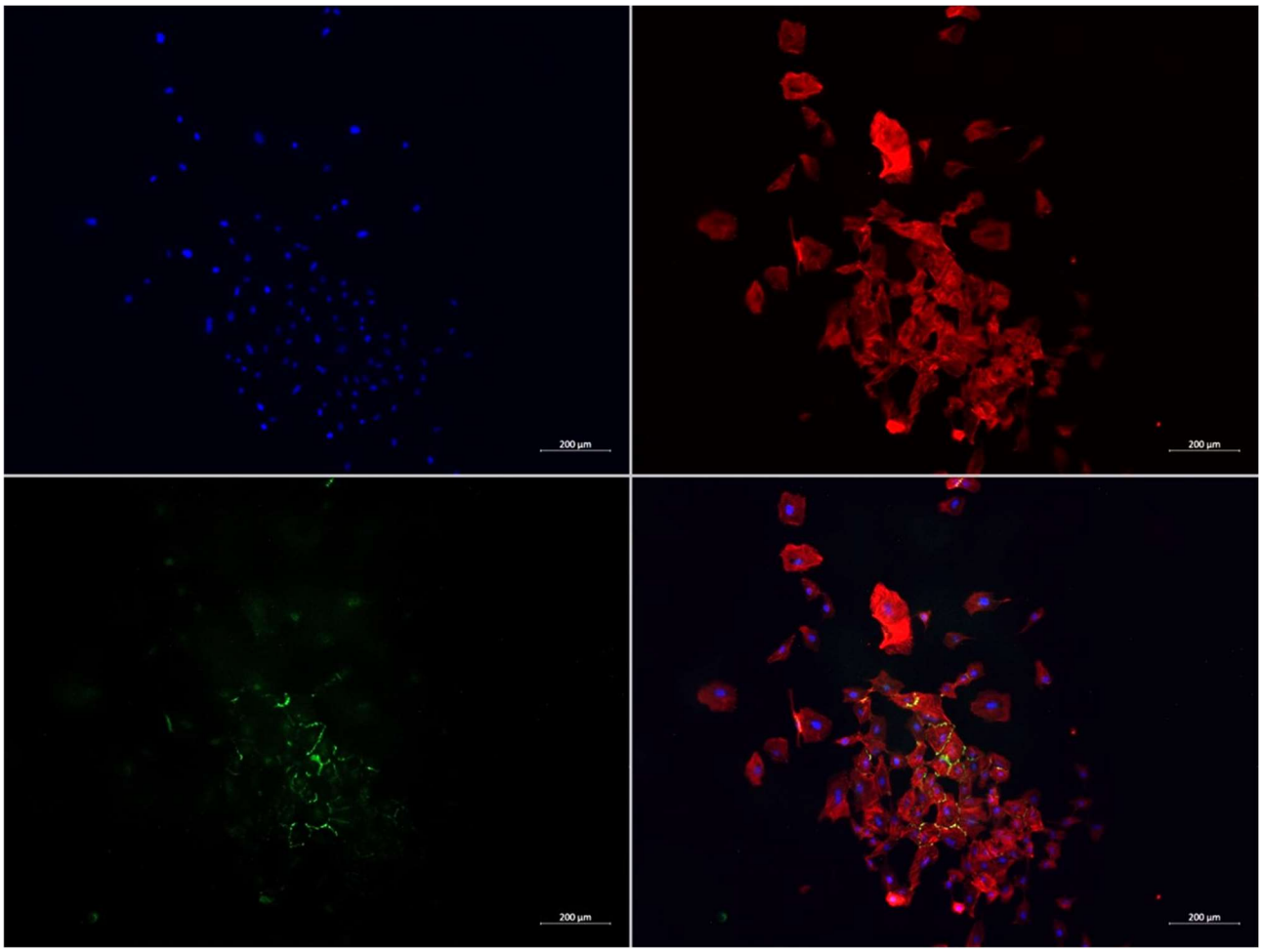

Figure S.4.4 Colony type D. Colonies' classification: E-cadherin (green), phalloidin rhodamine (red) and DAPI (blue) staining of colonies.

CHAPTER V

IN VITRO PULMONARY AND VASCULAR EFFECTS INDUCED BY DIFFERENT DIESEL EXHAUST PARTICLES

Diesel exhaust particles (DEP) are responsible for both respiratory and cardiovascular effects. However, many questions are still unravelled and the mechanisms behind the health effects induced by the exposure to ultrafine particles (UFPs) need further investigations. Furthermore, different emission sources can lead to diverse biological responses. In this perspective, here we have compared the effects of three DEPs, two standard reference materials (SRM 1650b and 2975) and one DEP directly sampled from a Euro 4 vehicle without Diesel Particulate Filter (DPF). For the biological investigations, different in vitro lung models involving both epithelial and vascular endothelial cells, were used. Cell viability, oxidative stress, inflammation, DNA damage and endothelial activation markers were investigated at sub-cytotoxic DEP doses.

The data obtained have shown that only DEP Euro 4, which had the major content of polycyclic aromatic hydrocarbons (PAHs) and metals, was able to induce oxidative stress, inflammation, and consequent endothelial activation, as demonstrated by the expression of adhesion molecules (ICAM-1 and VCAM-1) and the release of inflammatory markers (IL-8) from endothelial cells. Standard reference materials were not effective under our experimental conditions. These data suggest that oxidative stress, endothelial activation, and systemic inflammatory cytokines release are crucial events after DEP exposure and that the source of DEP emission, responsible of the particle chemical fingerprint, may have a key role in the resulting adverse biological outcomes.

This chapter is a published paper: " Bengalli, R.*, Zerboni, A*., Marchetti, S., Longhin, E., Priola, M., Camatini, M., Mantecca, P. 2019. In vitro pulmonary and vascular effects induced by different diesel exhaust particles. TOXICOLOGY LETTERS, 306, 13-24. DOI: 10.1016/j.toxlet.2019.01.017".*

Graphical abstract

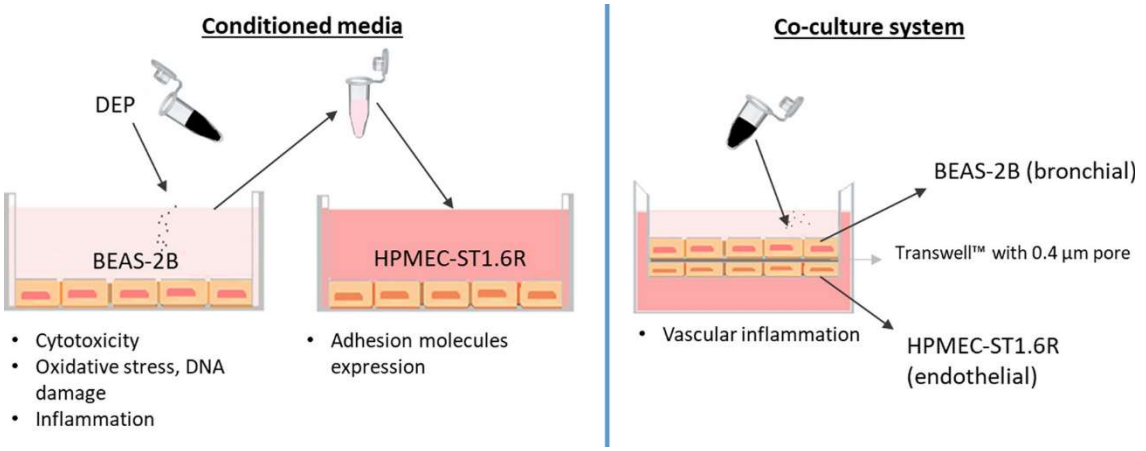

1. Introduction

Air pollution is a growing public health concern, estimated to cause over 3 million premature deaths worldwide, especially attributable to cardiovascular diseases (CVD) (Lelieveld et al., 2015). Ambient particulate matter (PM) is a mixture of solid and liquid particles suspended in air with different size, chemical composition, physical and biological properties. Air pollution is a complex mixture of different compounds that can cause adverse health effects, however the cardiovascular effects are largely attributed to the particulate components (Brook et al., 2010), comprising road dust, vehicle and exhaust particles. Based on aerodynamic diameter particles are divided into PM_{10} (<10 µm), $PM_{2.5}$ (<2.5 µm) and ultrafine particles (UFPs <100 nm). Furthermore, in urban cities, traffic emissions, together with biomass burning, are the major contributors (approximately 26% and 33% respectively) to the average contribution of PM10 and $PM_{2.5}$ sources, especially during high pollution days (PM10 > 50 µg/m^3) (Amato et al., 2016). One of the main source of UFPs is incomplete combustion of diesel engine and the consequent emissions of diesel exhaust particles (DEP), which are composed of agglomerate of solid carbonaceous material and ashes, volatile organic compounds (VOCs) and sulphur compounds (Kittelson, 1998). There is a persuasive evidence that living close to highly trafficked roads increases the risk of developing systemic inflammation, with consequent endothelial dysfunction,

atherosclerosis, and thrombosis (Lanki et al., 2015; Miller et al., 2012). Nevertheless, the biological mechanisms behind the effects of air pollution on CVD remain poorly defined. According to the European automobile manufacturers' association (ACEA), during the last decade there has been a large increase in the percentage of diesel-fuelled vehicles with pre-EURO 5 technologies in Europe as a means to cut CO_2 emission from transport (Schwarze et al., 2013). Therefore, increased level of diesel exhaust particles (DEP) emissions has been observed compared to gasoline-fuelled vehicles. Although the recent efforts in many western countries to reduce or even ban the diesel-fuelled vehicles, DEP emission still remains a great concern for public health and may even worsen in the still growing megalopolis of developing countries.

Oxidative stress, inflammation, cytotoxicity, genotoxicity and cell-to-cell contacts disruption are some of the several pathways involved in the response to PM and ultrafine particles (UFPs) exposure. DEP exposure induces both cytotoxic and pro-inflammatory effects on vascular endothelial cells (Klein et al., 2017; Lawal et al., 2016) with consequent endothelial dysfunction and development of CVD such as ischemia, myocardial infarction, and atherosclerosis (Miller et al., 2012; Robertson and Miller, 2018; Törnqvist et al., 2007). Furthermore, it has been demonstrated that there is a higher incidence of ischemia in smokers chronically exposed to diesel emissions exposure (Finkelstein et al., 2004) and persons with pre-existing CVD are at highest risk. *In vivo* studies have also shown the increased atherosclerotic plaque size and plasma lipid peroxidation in mice exposed to DEP (Miller et al., 2013).

Three main hypotheses have been proposed by which air pollution can promote endothelial activation: i) particle induced inflammatory responses in the lungs, leading to the release of inflammatory and oxidative mediators from the epithelial lung cells to the alveolar capillaries and blood circulation; ii) activation of airway sensory nerves by pollutants; iii) translocation of particles across the air-blood barrier (ABB) and direct entry of pollutants into the pulmonary circulation.

In the presence of cardiovascular risk factors, the endothelium is activated from the quiescent state to host defence response state (Lawal et al., 2016). During endothelial activation, also referred as endothelial dysfunction, cells activate a molecular process that stimulate the production of cytokines, chemokines and adhesion molecules, which interact with leukocytes and platelets to promote inflammation and ROS production, events that

can lead to the formation of atherosclerotic plaques (Eckers and Haendeler, 2015; Vitiello et al., 2014).

As a consequence of an inflammatory status, characterized by the release of cytokines such as interleukin-6 (IL-6), monocytes chemoattractant protein-1 (MCP-1), vascular endothelial growth factor (VEGF) and tumour necrosis factor-alpha (TNF-α), there is an overexpression of adhesion molecules in endothelial cells, including intercellular and vascular adhesion molecules (ICAM-1 and VCAM-1) and E-selectin (Mudau et al., 2012; Sprague and Khalil, 2009). VCAM-1 and ICAM-1 are members of the immunoglobulin superfamily, able to recruit and bind leukocytes and monocytes and involved in the vascular inflammatory pathway. Their expression contributes to endothelial activation and pro-angiogenic processes, that can be induced by cytokines and vascular endothelial growth factor (VEGF), a molecule that acts on the endothelium activating proliferation, migration and cell differentiation (Jośko et al., 2000).

Although in the last year there was a transition to engines and fuels with a lower environmental impact, is still unclear if DEPs generated from new technologies have significant lower adverse effects compared with the old ones. The chemical and physical properties of the emitted DEP, especially the content of metals and polycyclic aromatic hydrocarbons (PAHs), can be in fact greatly influenced by the engine technology, fuel, load, temperature, filtration devices and operating conditions in general, such as the driving regime. The comparison of the toxicological potential of DEPs from different emission sources may be of high relevance, not only for the comprehension of the adverse outcome pathways activated, but also for contributing to more specific mitigation strategies.

In the present work, we preliminary have studied the effects induced by three different DEPs on the bronchial cells BEAS-2B, in order to investigate the primary response of lung epithelial cells, focusing on cytotoxicity, cytoskeletal arrangement, oxidative stress, genotoxicity and release of inflammatory mediators. Afterward, the endothelial activation was investigated. To this purpose, a conditioned media and a co-culture model were set up by using BEAS-2B and the microvascular lung HPMEC cells. These *in vitro* systems allowed to analyse the DEP-induced responses on the epithelial and endothelial cells separately, as well as their interplay in the resulting inflammatory effects. The differences observed in toxicity have been related to the DEP chemical composition and emission sources.

2. Materials and methods

2.1 Diesel particles: preparation and sampling

Two standard reference materials from the NIST were used: DEP SRM 1650b and 2975 (Diesel Particle NIST® SRM®, Sigma Aldrich), which derive from the combustion of a heavy engine and a light duty respectively. DEP particles were weighed with a microbalance (Sartorius, Goettingen, Germany) and re-suspended in sterile milli-Q water to a final concentration of 2 mg/ml. Two different ultrasonic systems were chosen to disperse DEP in the water, bath-type sonicator (SONICA Soltec) and a probe-type sonicator (Bandelin Sonoplus, 3 kJ). The DEP suspension was stored at -20 C°.

DEP Euro 4 was sampled on Teflon filters (Whatman, Maidstone, UK) from a Euro 4 light duty vehicle without DPF (Diesel Particulate Filter) fuelled by commercial gasoline and run over a chassis dyno, as previously reported (Longhin et al., 2016). After sampling, filters were preserved at -20 °C, until particles extraction that was performed by sonication in the bath-type sonicator. Particle suspensions were then dried into a desiccator, weighed and stored at - 20°C. Samples were re-suspended in sterile water (final concentration 2 μg/μL) before use, following the same procedure used for NIST samples.

2.2 Diesel particles characterization

Particles morphology and size were analysed by transmission electron microscopy (TEM). A drop of 5 μl of DEP suspension (50 μg/mL) was deposited on Formvar® coated 200-mesh copper grids. Excess water was gently blotted, then the grids were left to dry in the air and finally inserted into a Jeol JEM-1220 TEM, operating at a voltage of 80kV and equipped with a CCD camera.

The hydrodynamic size of DEPs was analyzed through Dynamic Light Scattering (DLS). DEP particulates were prepared using the method as previously described, then suspended in culture medium LHC-9, milliQ water and PBS at a concentration of 50 μg/mL and analyzed at DLS (Malvern Zetasizer), using a scattering angle $\theta = 90$ °.

Chemical characterization of PAHs through GC-MS was obtained by NIST data sheets for the two SRMs DEP and from a previous work (Longhin et al., 2016) for DEP Euro 4 (Supplementary materials, Table S1). Selected metals were analyzed after mineralization in HNO_3/H_2O_2 (2:1 ratio v/v) of the samples and final dilution with ultrapure water. Metals were quantified by ICP-MS (Perkin Elmer SCIEX mod. ELAN 9000). Data are shown in Supplementary materials, Table S2.

2.3 Cells culture maintenance and treatments.

BEAS-2B cells (ATCC® CRL9609™), derived from human bronchial epithelium, and the cell line HPMEC-ST1.R, derived from the pulmonary microvascular circulation (received from Dr. Ronald E. Unger, Institute of Pathology, Medical University of Mainz, Johannes Gutenberg University, Mainz, Germany) were maintained and treated as previously described (Bengalli et al., 2017). Briefly, BEAS-2B cells (used from passage 13 to 27) were seeded at a concentration of 2.7 x 10^5 cells/well in 6-well plates and the day after treated with DEP (5 µg/cm^2) for 20h. Particles were directly added in the cellular medium. After 20h, supernatants were collected and centrifuged at 1200 rpm for 6min in order to discharge cells debris. The 40% of this conditioned medium was diluted in 60% of HPMEC fresh medium and then added to HPMEC-ST1.6R cells for further 24h.

All the *in vitro* experiments were performed at least in triplicate, and when parallel tests were performed at least a duplicate of samples were used.

2.4 *In vitro* model of lung barrier.

Co-culture of BEAS and HPMEC on Transwell inserts HPMEC-ST1.6R (9×10^4/cm^2) cells were cultured on the lower surface of Transwell® inserts (polyester; 0.4 μm pore size; Costar) coated with 0.2% gelatine and incubated for 2 h at 37°C and 5% CO_2. The filter membranes were then turned upside down and placed in a 12-well plate filled with 1.5 mL M199 complete medium and let grow for 72h. After that, BEAS-2B (5×10^4/cm^2) cells were cultured on the top surface of the Transwell® inserts (that was previously collagen-coated) with LHC-9 medium and let grow for 48h. Before particles exposure, both apical and basal compartment were washed with PBS and filled respectively with 250 µL and 1.5 mL of cellular media. Finally, when BEAS-2B cells reached the confluency (after 2-3 days), 5 µg/cm^2 DEPs were added in the apical compartment for 24h.

To assess confluency preliminary experiments with different seeding densities were made and then Alamar Blue test was performed (data not shown) to choose the appropriate density. We adjust our protocol according to the literature (Stewart et al., 2012).

2.5 Cells viability: Alamar Blue and H/PI

The AlamarBlue® (Life Technologies, Monza, Italy) assay was used to check the viability of BEAS-2B cells according to manufacturer's instruction and as previously described (Bengalli et al., 2017). Briefly, following incubation with DEPs for 20h, BEAS-2B supernatants were collected for conditioned media experiments and a solution containing 1:10 of AlamarBlue® reagent and cell medium was added into each well. After 1-2 h incubation the absorbance of the culture medium was read to the spectrophotometer (TECAN Infinite Pro) at 570 and 630 nm wavelengths. The Alamar Blue reagent was used also to assess the cells viability of both apical and basal compartments of the 3D *in vitro* co-culture model.

Moreover, Hoechst 33342/Propidium Iodide (H/PI) staining was used in order to determine the amount of viable, necrotic and apoptotic cells. Briefly, supernatants of control and treated cells were removed and centrifuged in order to keep floating cells pellets. Cells were washed twice with PBS, trypsinized, mixed to the previous cell suspension and suspended in 500 µL of cell medium and stained with H/PI solution (10 µL of 2: 1 solution of H/PI) (Sigma Aldrich). Samples were stored in the dark for 15 to 30 minutes at room temperature. Cells were centrifuged for 6 minutes at 1200 rpm, and re-suspended in 20 µL of FBS. 3 drops (about 4 µL) of cell suspension were put on the slide. The slide was observed with a fluorescence microscope (Zeiss-Axioplan) with UV filter (365 nm).

At least 300 cells per sample were scored according to nuclei staining and plasma membrane integrity as viable normal cells (H positive and PI negative, without special nuclear characteristic and an intact plasma membrane), necrotic cells (non-apoptotic and PI positive), apoptotic cells (bright H or PI positive stained with condensed or fragmented nuclei), mitotic cells (H positive with chromosome condensation).

2.6 Cell morphology: haematoxylin/eosin and immunostaining

For morphological analysis, cells were seeded on collagenated (PureColl, Advanced BioMatrix, Inc., San Diego, CA, US) cover slide at a concentration of 2.7x 10^5 cells/well, cultured for 24h and exposed to 5 µg/cm^2 for 20h. At the end of the treatment, cells were fixed in formalin 10% for 20 min and then washed with PBS. Cells were stained with Mayer's haematoxylin solution and alcoholic eosin (haematoxylin-eosin staining, HE), dehydrated, clarified in xylene and mounted with Eukitt on a slide. The slides were observed under the

optical microscope (Zeiss-Axioplan). The pictures were acquired using an AxioCam MRc5 digital camera and processed using the AxioVision Real 4.8 software.

For immunostaining, BEAS-2B cells were fixed with 4% paraformaldehyde and, after washing with PBS, non-specific sites were blocked by incubating cells with cold PBST (PBS 1X with 0.1% Tween20; Sigma Aldrich) containing BSA 2%. Then coverslips were incubated with the primary antibody Rabbit anti-ZO-1 (1: 200; Cell signaling) prepared in PBS 1X. After two washes, cells were incubated with the secondary antibody Goat anti-Rabbit Alexa Fluor 488 (1: 500, Life Technologies). In addition, cytoskeleton actin was marked with phalloidin-TRITC (1:150, Cytoskeleton Inc.). Nuclei were counterstained with DAPI (4', 6-diamino-2-phenylindole, 1:100, Molecular Probes, Life Technologies, Monza, Italia). Finally, the slides were mounted with Prolong-antifade (Life Technologies). The images were acquired with a Zeiss AxioObserver Z1 Reverse Microscope and processed with the AxioVision Real 4.8 software.

2.7 Flow cytometry

The potential of DEPs to induce oxidative stress was analysed through flow cytometry by measuring ROS formation and the expression of yH2AX as marker of DNA double-strands breaks (DSBs).

For ROS detection, BEAS-2B cells were pre-incubated for 20 min with the probe Carboxy-2´,7´-Dichlorofluorescein Diacetate (carboxy-DCFDA, 5 µM, Life Technologies) and then treated with DEPs for 90 min. After treatments, cells were detached, centrifuged at 1200 rpm for 6min and re-suspended in PBS. The intensity of fluorescence, in the FITC channel, was examined by flow cytometry (CytoFLEX, Beckman Coulter) and analysed by the program CytoExpert.

The autofluorescence of cells and DEPs was evaluated analysing the signal from unloaded samples (cells not stained with carboxy-DCFDA). These values were then subtracted from the values to DCFDA stained samples.

For measuring DNA DSBs, cells were probed with the phospho-histone H2AX (Ser139) rabbit mAb Alexa Fluor 488 Conjugate (Cell Signaling). After 24h treatment with DEPs, cells were detached, washed once in PBS, fixed in 1% paraformaldehyde in PBS for 15 min on ice and re-suspended in 90% cold methanol and stored overnight at -80 °C prior to analysis.

After discharging methanol, cells were washed two times with 0.5% bovine serum albumin (BSA) in PBS and incubated with primary antibody in PBS with 5% BSA, 0.2% Triton X-100 (dilution 1:200) for 4h at 4°C in the dark. After washing twice with 5% BSA in PBS cells were resuspended in PBS and analysed at the CytoFLEX (Beckman Coulter) in the FITC channel.

2.7 Western blot

After exposure, BEAS-2B and HPMEC-ST1.6R cells monolayers were scraped and lysed on ice in RIPA buffer (150 mM NaCl, 1% TritonX-100, 0.5% sodium deoxycholate, 0.1% SDS, 50 mM Tris pH 8.0 and 0.1% of protease inhibitors). The total protein content was evaluated by the bicinchoninic acid assay (Sigma Aldrich). The same amounts of proteins were loaded onto 10% SDS-PAGE gels, separated and transferred electrophoretically on nitrocellulose membrane. After blocking for 1 h with blocking buffer TBS-T (TBS, 0.1% Tween20, 5% (w/v) BSA) the membranes were incubated at 4 °C overnight with specific primary antibody: HO-1 and NF-kB for BEAS-2B and ICAM-1 and VCAM-1 for HPMEC-ST1.6R (antibodies dilution 1:1000, Cell Signaling). Monoclonal anti-β-Actin antibody (Cell Signaling, 1:1000) was used as loading control. The membranes were then rinsed with TBS-T and incubated with anti-rabbit IgG secondary antibody (1:2000 Cell Signaling Technology) for 1 h. After rinsing with TBS-T three times, the proteins-bound were measured with LiteAblot Plus Chemiluminescent Substrate (Euroclone) by using a UVP machine and a dedicated software (VisionWorks LS). Data were normalized to the β-actin content and expressed as fold increase over control.

2.8 ELISA

After exposure, the supernatants from BEAS-2B and HPMEC-ST1.6R cells and the supernatants from the apical and basal compartments of the *in vitro* co-culture model were collected and stored at -20 °C until analysis. Protein levels were detected by sandwich ELISA according to the manufacturer's instructions (IL-6, IL-8, sIL-6R, VEGF, Life Technologies). The absorbance of each sample was measured by Multiplate Reader Ascent (Thermo Scientific, USA) at the wavelength of 450 nm and the amount of proteins in pg/mL calculated on the basis of standard curves.

2.9 Statistical analysis

The data represent the mean and standard errors (SE) of at least three independent experiments. Statistical analyses were performed using Sigma Stat 3.2 software, using unpaired t-test or One-Way ANOVA and relative post-hoc analysis. Values of $p<0.05$ were considered statistically significant.

3. Results

3. 1 Diesel particles characterization

TEM analysis showed that the three DEPs, when in solution (50 µg/mL in milliQ water), tend to form aggregates, typical of *soot* particles. DEP 1650b (Fig. 1A and B) tend to form bigger aggregates with respect to DEP 2975 (Fig. 1C and D) and Euro 4 (Fig. 1E and F), as also confirmed by DLS analyses of DEPs suspended in distilled water and in medium (Table 1). The single particles have similar morphology and size lower than 50 nm, in all the three DEP samples. DLS analysis showed that particles have a different behaviour according to the suspension medium, forming less aggregates when in milli-Q water. Nevertheless, even when in cell culture media (LHC-9), particles aggregates relied in the nanometric range, in particular DEP 1650b (471 ± 28 nm) and Euro 4 (388 ± 4 nm) showed a mean hydrodynamic diameter higher than DEP 2975 (336 ± 22 nm). Results about the chemical characterization of the three different DEPs are summarized in Supplementary Materials (Table S1).

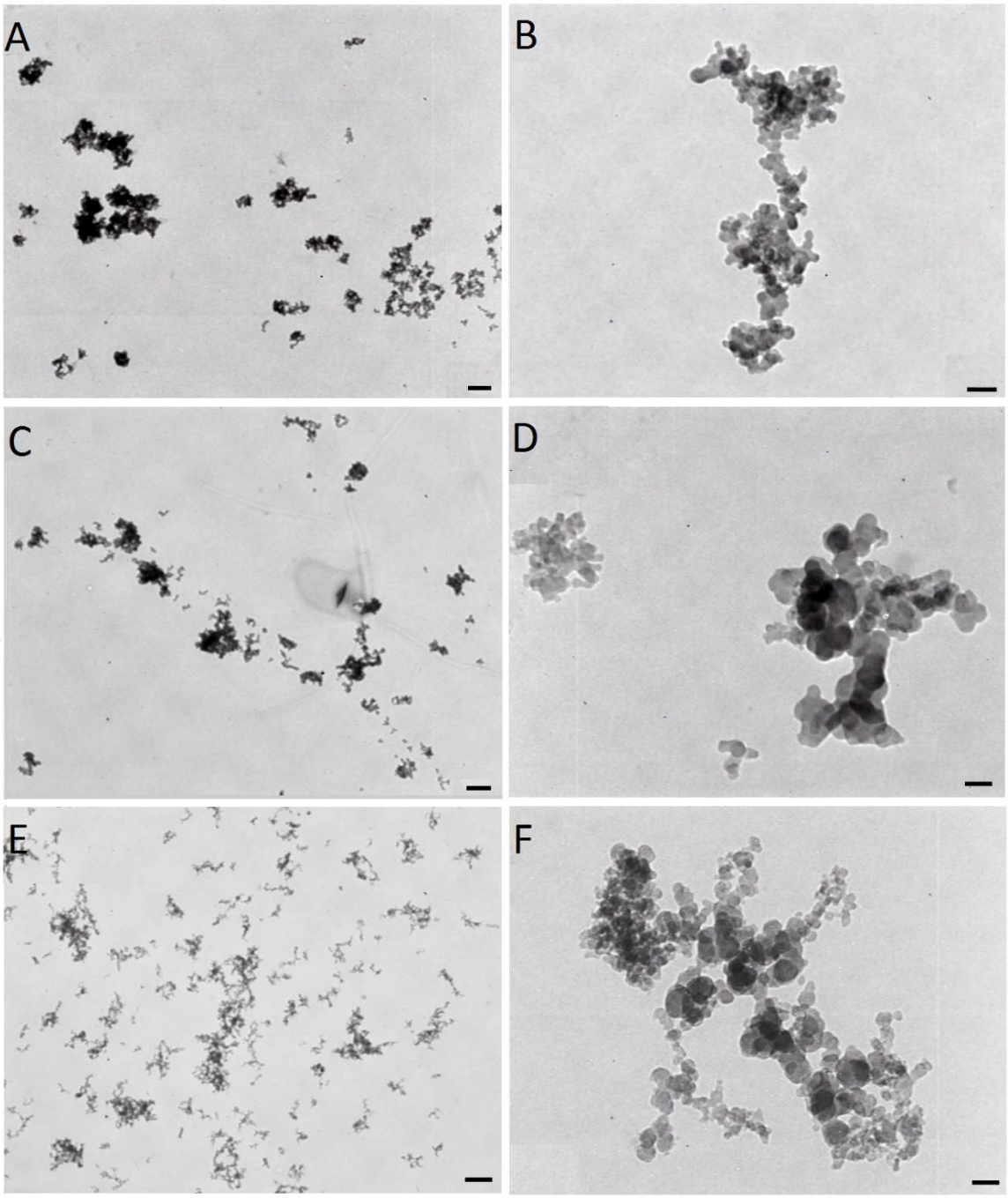

Fig. 1. Morphological characterization of DEPs**.** TEM images of DEP particles: A, B) DEP 1650b; C, D) DEP 2975; E, F) DEP Euro 4. Scale bars= 500nm (A, C, E), 100nm (B), 50 nm (D, F).

	1650b	2975	Euro 4
MilliQ water			
Z-Average (nm)	425.90 ± 34.15	221.56 ± 1.23	421.6 ± 38.63
PdI	0.461	0.172	0.580
PBS 1X			
Z-Average (nm)	618.76 ± 106.75	808.73 ± 298.14	311.16 ± 43.2
PdI	0.460	0.338	0.466
LHC-9 medium			
Z-Average (nm)	471.33 ± 50	336.13 ± 38.89	388.4 ± 7.07
PdI	0.329	0.279	0.358

Table 1. DEP characterization: DLS analysis

3.2 DEP effects on BEAS-2B cells

3.2.1 Cell viability

BEAS-2B cells viability was assessed by Alamar Blue metabolic test and H/PI staining and presented in Fig. 2. Data obtained by the enzymatic test show that the three DEPs did not induce significant effects on cell viability (Fig. 2A). On the contrary, an increased viability was observed after exposure to DEP SRM 2975. H/PI staining instead revealed that there is an increase of necrotic cells of 14% in BEAS-2B cells treated with 5 µg/cm^2 DEP Euro 4, while the other DEPs did not significantly affect cell viability (Fig. 2B).

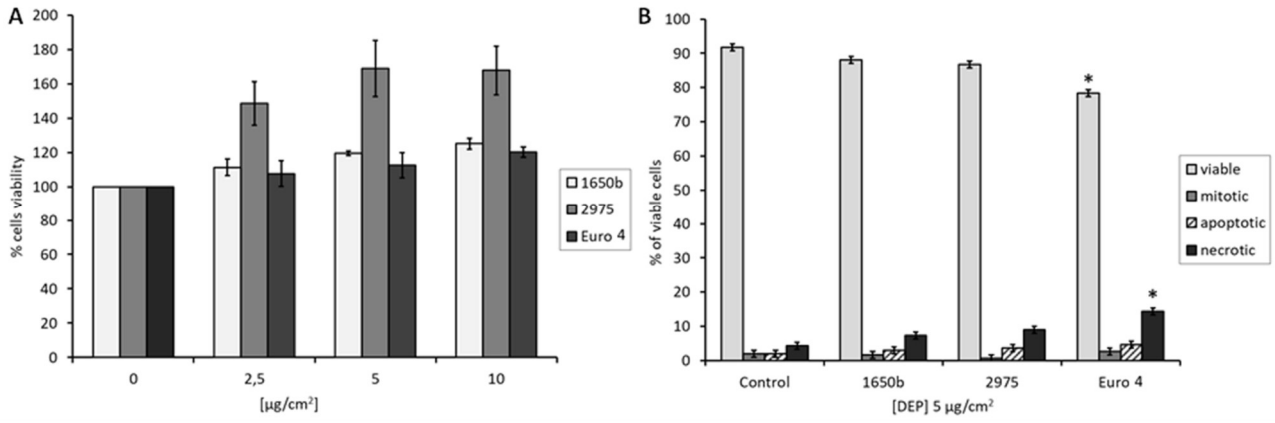

Fig. 2. Cell viability. A) Alamar Blue test: histograms represent the percentage respect to control cells (100%) of viable cells after the exposure to 0, 2,5, 5 and 10 µg/cm^2 to DEP 1650b (light grey bars), 2975 (grey bars) and Euro 4 (black bars). Data show the mean ± SE (n=4). B) H/PI staining: the histograms represent the percentage of viable (light grey bars), mitotic (grey bars), apoptotic (dashed bars) and necrotic (black bars) cells after the exposure to DEP (5 µg/cm^2) observed by fluorescent microscopy. Data show the mean ± SE of at least three independent experiments. *Statistically significant respect to control according to unpaired t-test, $p < 0.05$.

3.2.2 Cell morphology

Cell morphology and particles deposition was investigated through microscopic analysis after BEAS-2B cells exposure to the three different DEPs (5 µg/cm^2). DEPs interact with cells as well as aggregates and single particles. The HE staining showed that diesel particles came in contact with cells (Fig. 3), especially after DEP 2975 exposure (Fig. 3C), and sometimes they were inside cytoplasmic vacuoles (Supplementary materials S1). Compared to control cells, no evident morphological changes were observed after DEP exposure, except for a slight increase in elongated cell morphologies with emission of longer filopodia (Fig. 3; Supplementary materials S1).

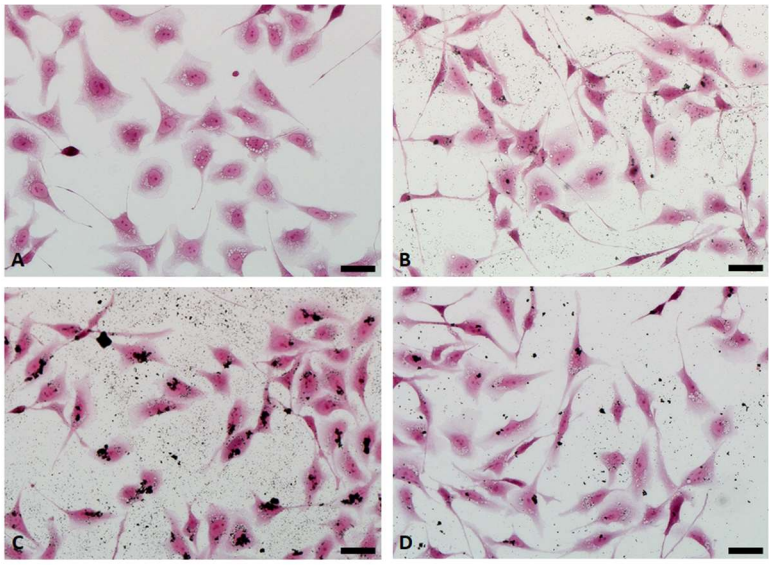

Fig. 3. Morphological analysis. Microscope images of BEAS-2B cells, stained with hematoxylin/eosin, show the slight morphological changes in respect to Control (A) after exposure for 20 h to 5µg/cm^2 DEP 1650b (B), 2975 (C) and Euro 4 (D). Scale bar= 20 µm.

The interference with the expression/organization of cytoskeletal and junctional proteins was qualitatively investigated by *zonula occludens-1* (ZO-1) and actin immunostaining. It is has been reported that BEAS-2B cells are able to form apical localised tight junction at the Air-Liquid Interface (ALI) with a Transepithelial resistance (TEER) > 100 Ω*cm^2 (Stewart et al., 2012). Here we observed the expression of ZO-1 at the cell-to-cell contact points in subconfluent submerged cultures. Under these conditions ZO-1 expression and actin cytoskeleton appeared almost not affected by DEP exposure (Fig. 4).

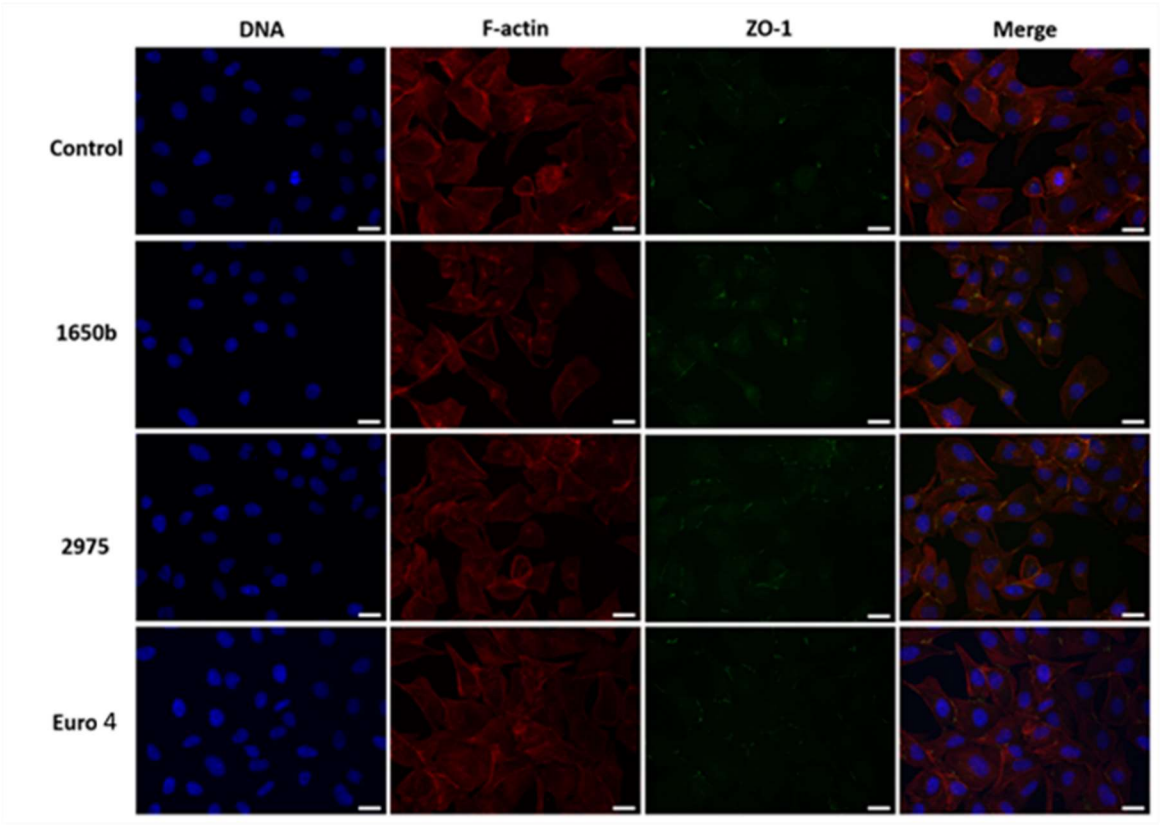

Fig. 4. Fluorescence imaging of BEAS-2B cells exposed to DEPs. The nuclei were stained with DAPI (blue), tight junction proteins with rabbit anti-ZO1 antibody (green) and actin cytoskeleton with rhodamine phalloidin (red). Scale bars= 20 µm.

3.2.3 Oxidative stress and DNA damage

The induction of an oxidative stress response was evaluated with different approaches: 1) ROS detection at early time points, 2) expression of the protein heme oxygenase-1 (HO-1) and nuclear factor-kB (NF-kB) as downstream protein of the oxidative pathway and 3) analysis of the expression of the oxidative DNA damage marker yH2AX. A significant

increase of ROS production was observed in BEAS-2B cells after exposure to DEP Euro 4 (Fig. 5A) and DEP 1650b, while DEP 2975 did not. These data were also confirmed by Western blot analysis of the anti-oxidant protein HO-1 (Fig. 5C). HO-1 expression was significantly increased after exposure to DEP 1650b and Euro 4 with a fold increase of about 5 times compared to unexposed cells. DEP 2975 did not induce a significant increase in HO-1 expression. The expression of NF-kB was evaluated in order to show the effects of different DEPs on oxidative stress pathways. Data showed that only DEP Euro 4 induced a significant higher expression of NF-kB protein, while DEP 1650b seems to induce a slight, but yet not significant induction of the protein (Fig. 5D).

Since oxidative stress can lead to DNA double strand breaks, as expected yH2AX was significantly increased after exposure to DEP Euro 4, and only slightly after exposure to DEP 1650 (Fig. 5B). All together these results evidenced that DEP is able to promote cell oxidative stress, but the importance of the oxidative response and damage may depend by the DEP properties.

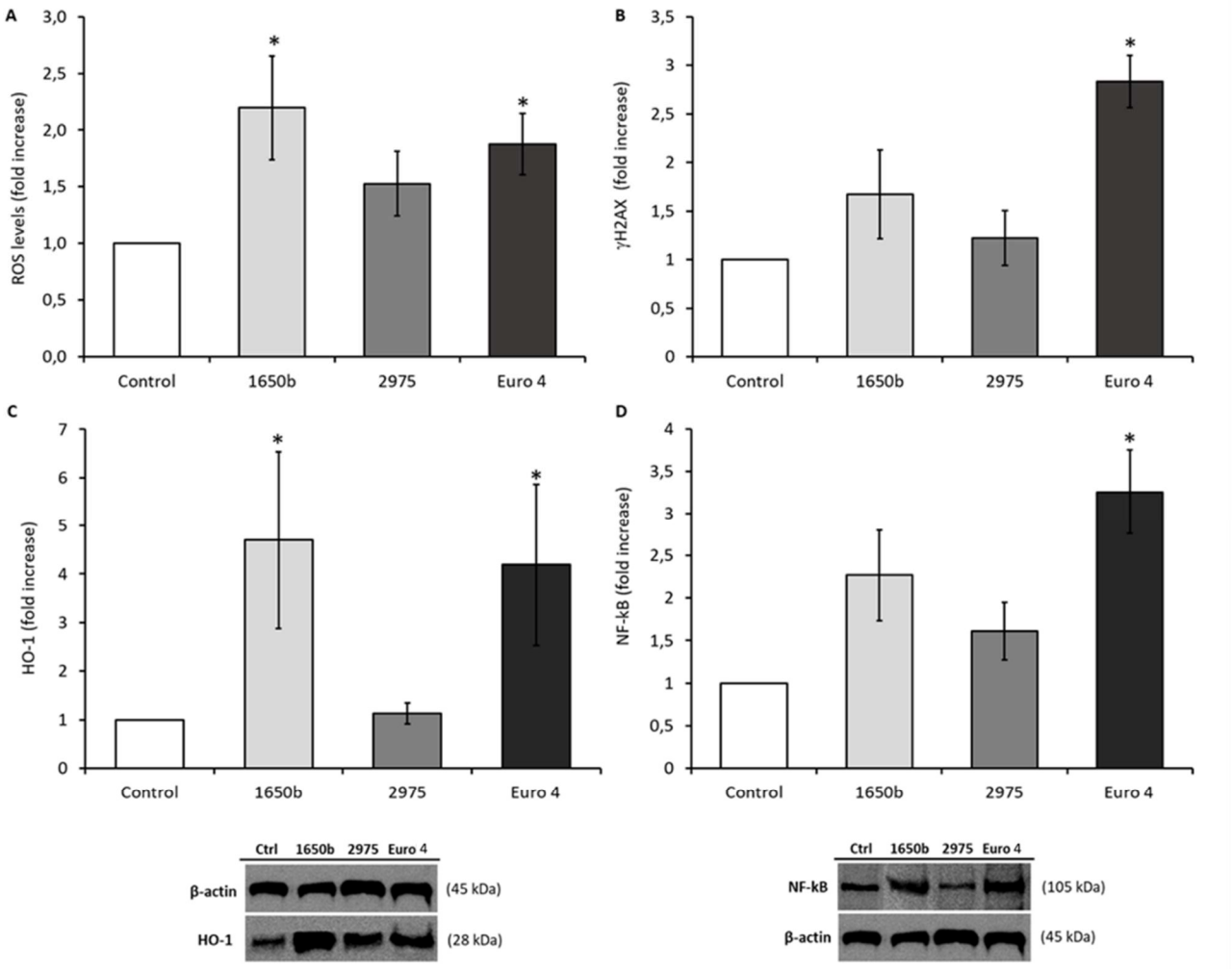

Fig. 5. Oxidative stress and DNA damage. A) ROS levels after 90 min of exposure to 5 µg/cm^2 were detected by DCFDA fluorescent probe; B) DNA oxidative damage was investigated after 20h of exposure to three different DEPs by measuring with cytofluorimetric analysis the expression of yH2AX; C) The expression of HO-1 was evaluated in BEAS-2B cells after the exposure for 20h to three different DEPs through Western Blot analysis; D) NF-kB protein expression. Data represent the mean ± SE of at least three independent experiments. *Statistically significant respect to control according to unpaired t-test, $p < 0.05$.

3.2.4. Release of inflammatory mediators

Since HO-1 is a protective enzyme that activates the secretion of pro-inflammatory proteins, including IL-6 and VEGF, which also contribute to the destruction of cell-cell

contacts, the release of such proteins was therefore investigated, together with sIL-6R and IL-8.

The quantification was carried out on the supernatant of BEAS cell cultures treated with 5 µg/cm^2 DEPs for 20 h. Data showed a significant increase in the release of IL-6 and sIL-6R only after exposure to DEP Euro 4 (Fig. 6A e B), with a 1.87 and 1.5 fold change than control respectively. No significant results were observed after exposure to the SRM DEPs. The expression of the chemokines IL-8 was not affected by any DEP (Fig. 6C). Moreover, although all DEPs seem to promote the release of VEGF by BEAS-2B exposed cells, only DEP Euro 4 determined a statistically significant increase in VEGF secretion compared to untreated cells (Fig. 6D).

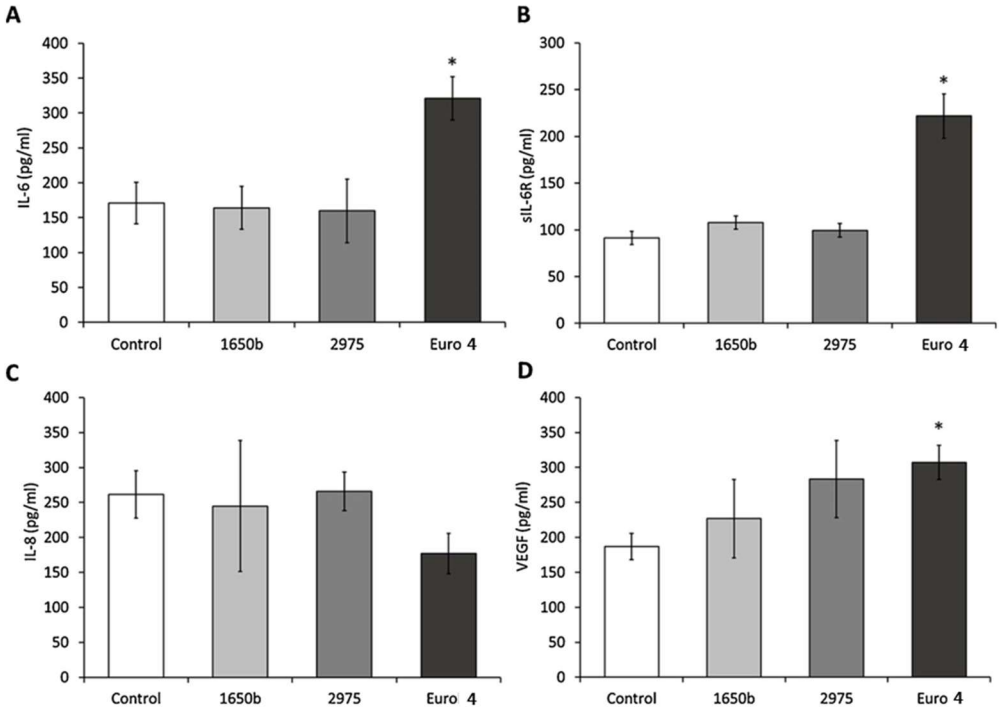

Fig. 6. Release of soluble mediators. The release of IL-6 (A), sIL-6R (B), IL-8 (C) and VEGF (D) was evaluated in BEAS-2B supernatants after the exposure for 20h to 5 µg/cm^2 of three different DEPs. Data are presented as pg/ml and they represent the mean ± SE of at least three independent experiments. *Statistically significant respect to control according to unpaired t-test, $p < 0.05$.

3.3 DEP-induced endothelial activation

To investigate the possible mechanism of the lung endothelium activation, in response to lung epithelial cells stimulation by DEPs, two *in vitro* models, consisting in treatments with conditioned media and 3D co-culture of epithelial and endothelial cells, were used. The results are summarized in the following sections.

3.3.1 Conditioned media experiments

Since endothelial activation is characterized by an increased expression of cellular adhesion molecules, such as ICAM-1 and VCAM-1, the expression of these two proteins was evaluated in endothelial cells after treatment with conditioned media derived from BEAS-2B cells previously exposed to DEPs. As expected, only DEP Euro 4 was able to induce ICAM-1 and VCAM-1 expression in HPMEC-ST1.6R (Fig. 7 A and B), since DEP 1650b and 2975 were not able to induce soluble mediators IL-6 complex release.

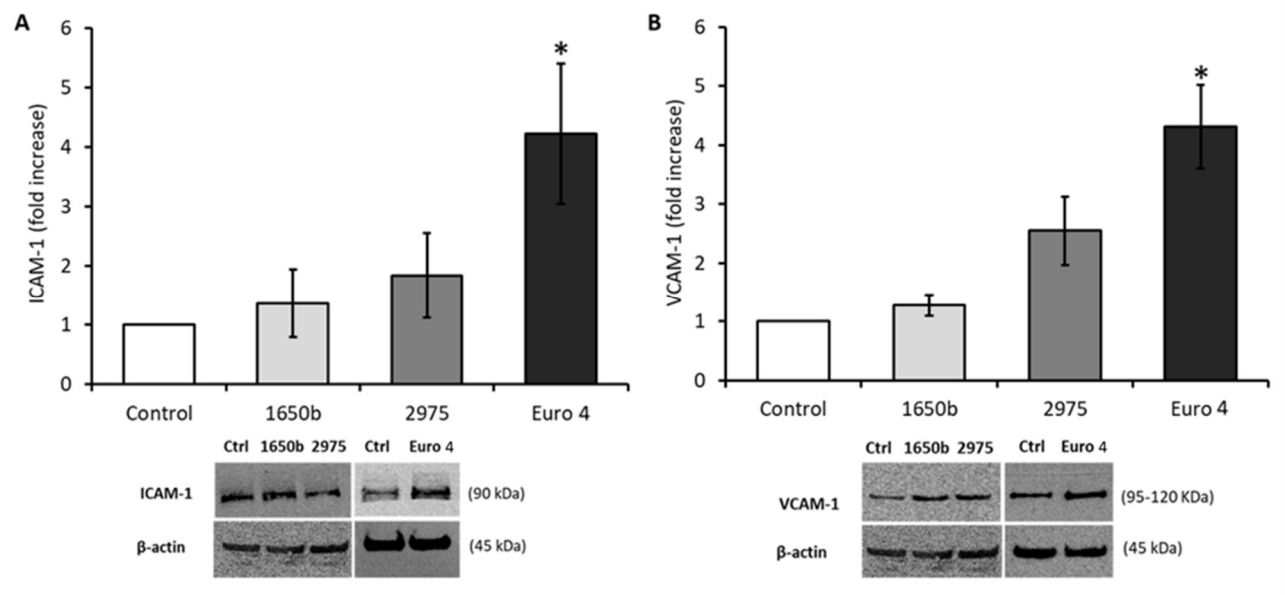

Fig. 7. Endothelial activation. The expression of ICAM-1 (A) and VCAM-1 (B) was evaluated in HPMEC-ST1.6R cells after the exposure for 24 h to conditioned media deriving from BEAS-2B treated with DEPs. Data represent the mean ± SE of at least three independent experiments. *Statistically significant respect to control sample according to ANOVA on Ranks+Dunn's, $p < 0.05$.

3.3.2 Co-culture system

In order to confirm the endothelial activation in a model that more closely mimic the *in vivo* situation, we set up an *in vitro* 3D co-culture model of BEAS-2B cells and HPMEC-ST1.6R. No effects on both apical and basal cell viability was observed after the exposure to the three different DEPs (Fig. 8A). With this system we confirmed that the apical exposure to DEP Euro 4 was able to induce an endothelial response, consisting in an increased release of IL-6 (Fig. 8B) and IL-8 in the basal (endothelial) compartment (Fig. 8C) of the model. An increase of IL-6 release in the apical compartment after DEP Euro 4 was also observed, confirming the data from the conditioned media model. No effects were observed in the endothelial cells after exposure to DEP 1650b and 2975.

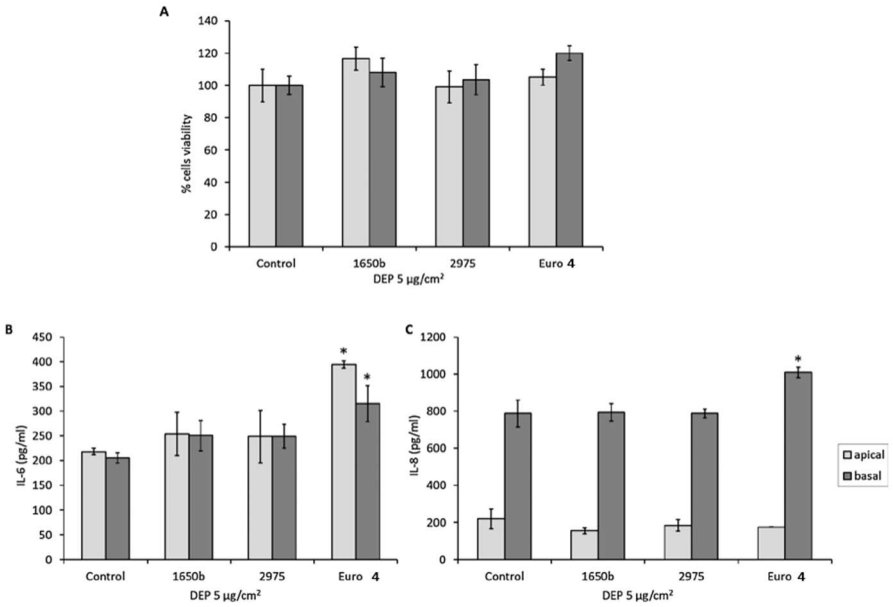

Fig. 8. Effects of DEPs in the co-culture system. Cell viability (A) and IL-6 (B) and IL-8 (C) release were evaluated after apical exposure for 24h to DEP. Data represents the mean ± SE of at least three independent experiments. *Statistically significant respect to control sample according to unpaired t-test, $p < 0.05$.

4. Discussion

DEP is a complex mixture of compounds, whose physico-chemical characteristics are highly dependent on fuel and engine. Studies on the effects of DEP are frequently conducted using standard reference materials (SRMs). Although a well-characterized material can be very useful for investigating the role of soot particles on the biological effects, not always SRMs are representative of real emissions.

In this research, low doses were used for *in vitro* toxicology screening, and the dose of 5 $\mu g/cm^2$ was chosen for inflammatory and endothelial activation endpoints, since it may be considered representative of realistic exposure conditions in large urban centres, where during winter the daily PM concentrations may exceed 70 $\mu g/m^3$ (Li et al., 2003).

Regarding the DEPs tested, the SRMs have been produced under controlled conditions and are representative of the emission of a heavy engine (SRM 1650b) and a light engine (SRM 2975). For this reason, also a DEP from a Euro 4 light duty engine was tested. It was sampled from a vehicle run according to an urban ARTEMIS driving cycle, representative of real average STOP&GO driving conditions characteristic of an European city.

According to our results, the three DEPs are constituted of soot ultrafine particles with very similar primary size (c.a. 50 nm) and tendency toward aggregation (Fig. 1). The hydrodynamic behaviour was in fact comparable, with SRM 2975 showing the lowest hydrodynamic diameter in both pure water and cell culture medium (Table 1). According to previous studies (Braun et al., 2007; Longhin et al., 2016), significant differences in the chemical composition among the three DEPs exist. In the two SRMs the most abundant organic compounds are fluoranthene, pyrene, phenanthrene, and 9-fluorenone and both of them show a graphitic structure (Braun et al., 2006). The chemical speciation of the Euro 4DEP showed a typical PAHs composition with high levels of pyrene, phenanthrene, benzo[a]anthracene and dibenzo(a,h)anthracene (Longhin et al., 2016). Furthermore, the content of PAHs was higher in Euro 4 DEP, respectively 3 and 7 fold respect to SRM 1650b and 2975 (see Supplementary Table S1).

It is well known that the biological effects of nano-sized particles may depend on their primary size and shape, as well as to their aggregation state (Stone et al., 2017), but according to the results cited above, these properties do not justify the variable toxicity responses we observed in the lung epithelial and endothelial cells when exposed to the

three DEPs. It is more likely that the different chemical composition, mainly the differences in PAH species and total content, played a major role.

The main contributors of PM and UFPs-induced biological effects are both PAHs and metals adsorbed on the particles carbonaceous core (Sørensen et al., 2003; Totlandsdal et al., 2015), however there are evidences in literature that PAHs themselves can determine inflammatory response (Totlandsdal et al., 2015) and consequent endothelial activation. Furthermore, for what concern metals levels, our data showed that the DEP Euro 4 has significantly higher amounts of metals compared to the two SRM DEPs, in particular with respect to Al, Ca, Zn and Fe (see Supplementary Table S2). The amount of metals such as Fe, Ca and Zn derives from the diesel engine and from diesel oil. The induction of oxidative stress and release of IL-6 has been associated to the higher amount of metals adsorbed in DEP Euro 4, and it has been reported that Fe, Al and Mn levels are crucial for the pro-inflammatory effects on the respiratory system (Shao et al., 2018). Moreover, Van De Heuvel and colleagues have demonstrated that increased Cu, Ni and Zn induce cytokines release in BEAS-2B cells (Van Den Heuvel et al., 2016).

Our results in fact support the thesis that DEPs with higher content of PAHs and metals are more effective and are responsible of the pulmonary and vascular effects observed. A sequence of events, linking UFPs exposure to oxidative stress and inflammation with consequent indirect activation of the vascular endothelium has been demonstrated. A statistically significant increase in the expression of ICAM-1 and VCAM-1 was observed only after exposure to DEP Euro 4, the only material able to induce oxidative and inflammatory response in lung epithelial cells. These data agree with the work of Hemmingsen and colleagues in which the effects of different DEPs on endothelial cells activation were investigated. Their results in fact showed that the exposure to DEP generated by a conventional diesel Euro 4 engine induced a significantly increased expression of ICAM-1 and VCAM-1 in HUVEC cells, while DEP SRM 2975 did not generate the same response (Hemmingsen et al., 2011).

The existence of a link between endothelial dysfunction and inflammation is supported by diverse clinical and experimental data in which atherosclerosis is associated to the expression of adhesion molecules induced by pro-inflammatory cytokines such as IL-1β, TNF-α and C-reactive protein (CRP) produced by the liver in response to IL-6 (Zhang, 2008).

In our research, the correlation between the release of the pro-inflammatory mediators, such as IL-6, and the increased expression of ICAM-1 and VCAM-1 in endothelial cells was confirmed since treatments with DEP SRMs did not induce epithelial release of IL-6 (Fig. 6) and did not even promote an endothelial response.

These data are in contrast with other works in which the same SRM induced inflammation and cytotoxicity in BEAS-2B cells, nevertheless in those works cells were exposed to higher doses of DEP, up to 60 μg/cm^2 for DEP 1650b and 10 μg/cm^2 for DEP 2975 (Schwarze et al., 2013; Totlandsdal et al., 2015). Here, DEP 1650b was able to induce the formation of ROS and the expression of the anti-oxidant protein HO-1. Nevertheless, this did not activate the downstream oxidative stress pathway (NF-kB expression) and no release of inflammatory mediators, especially IL-6 and its soluble receptor, was detected, with the consequent any activation of the endothelium. These data seem to confirm that this complex has a role in the stimulation of endothelial cells in promoting adhesion molecules expression and a consequent endothelial dysfunction and possible induction of atherosclerotic processes.

Furthermore, we also have observed that DEP Euro 4 is able to induce the phosphorilation of 2AX histone (Fig. 5B), suggesting an activation of the mechanism of DNA repair. Several studies show that global histone phosphorylation levels can be indirectly influenced by oxidative stress that leads to the formation of DNA double-strand breaks, which induce the phosphorylation of H2AX to activate DNA repair (Ye et al., 2016).

Previously Li and colleagues have demonstrated that organic DEP extracts, which are enriched in PAHs, induce different biological effects in bronchial cells and macrophages related to the generation of ROS and that HO-1 expression is the most sensitive marker for oxidative stress (Li et al., 2002). In concordance with occurrence of a limited genotoxic stress after DEP exposure, a recent *in vivo* study showed a slight induction of H2AX phosphorylation and formation of bulky adducts (Douki et al., 2018).

The airway epithelium represents the first point of contact in the respiratory system for particulate matter, and the ways in which it protects against toxic agents include a barrier with tight junctions and early local inflammatory response. The capability of particle to translocate across the epithelial barrier was indirectly investigated through the observation of ZO-1 expression in BEAS-2B cells, as well as actin filaments which are strictly related to cell-to-cell contacts. Tight junctions in BEAS epithelial cells does not appear to be compromised following exposure to the three DEPs, as demonstrated by the unaltered ZO-

1 expression and actin cytoskeleton filaments (Fig. 4). Even if further investigations on this aspect are needed, our results suggest that the exposure to DEPs mostly result in the activation of oxidative and inflammatory responses, instead of morphological and structural cellular changes.

Development of an efficient *in vitro* model of the cardiopulmonary system is a fundamental starting point for testing the effects of different particles. In this work, for the first time, we have developed a co-culture model of BEAS-2B and HPMEC cells in which bronchial epithelial cells, while being exposed to DEP, were allowed to communicate with microvascular endothelial cells through a porous membrane. This model was set up in order to understand if the interaction with different cells modulates the response to diesel particles, even compared to the conditioned media system in which cells do not really 'communicate' since only endothelial cells receive the soluble mediators coming from bronchial cells.

In this research, the response obtained in monoculture and conditioned media are congruent with the results of the co-culture experiments towards early phase inflammation. The complexity of this *in vitro* system is important for the stimulation of endothelial cells in promoting adhesion molecules since they more closely mimic realistic and physiological conditions with respect to monocultures.

In the *in vivo* situation cells communicate to each other through direct contact and secreted soluble mediators. The communication between bronchial epithelial cell cytokine products and other cell types in the surrounding tissue environment allows the tissues to orchestrate specific inflammatory and immune responses. Therefore, an exogenous stimulus is not restricted to the epithelium alone but can be transported to other cells via soluble mediators. In this perspective, the endothelium of the microvascular circulation plays an important role thanks to its ability to respond to inflammatory mediators and express adhesion molecules involved in the recruitment of inflammatory cells. Such a mechanism stands at the base for the development of several vascular diseases (Mögel et al., 1998).

Furthermore, in the conditioned media system it is quite difficult to understand the role of the different cells in inducing inflammation in response to the particles. In fact, we observed a slight not significant increase of IL-6 release from endothelial cells (Supplementary materials S3). Endothelial activation with this model was instead confirmed by the expression of adhesion molecules ICAM-1 and VCAM-1, as shown in

Figure 7. On the other side, in the co-culture system, we observed a significant release of cytokines from the endothelial (basal) compartment of the model. With this model the release by endothelial cells of IL-6 and IL-8 resulted increased after DEP Euro 4 exposure (Fig. 8B and C), suggesting that the cross-talk between cells contributes to the inflammatory response to particles. The cytofluorimetric analysis of VCAM-1 expression in endothelial cells in the co-culture system revealed that the apical (epithelial) exposure to DEP did not induce the expression of this adhesion molecule (see Supplementary materials S4), in contrast to what we have observed in the conditioned media system. This may be due to the high level of released IL-8 from endothelial cells that may reduce VCAM-1 expression. It has been reported that a reduction of VCAM-1 can derives from increased IL-8 levels when endothelial cells are co-cultured with smooth muscle cells (Zhang et al., 2011). In this model, the crosstalk between the two different cell lines was mediated by an augmented secretion of IL-8, which inhibited the expression of VCAM-1 on smooth muscle cells through the ERK signalling pathway.

Nevertheless, the release of IL-8 in the basal compartment is a marker of endothelial activation, as it has crucial roles in chemotaxis, vascular inflammation, arrest of leukocyte and pro-atherogenesis (Sprague and Khalil, 2009; Zhang, 2008). Basing on these findings, the communication between bronchial and endothelial cells should be considered responsible for the amplification of the induced inflammatory effects.

In conclusion, studies on the effects of exposure to different sources of UFPs, including DEP, are of crucial importance in order to define new emission reduction strategies based on the properties, number and sources of UFPs, rather than exclusively on atmospheric concentration in terms of mass. The reduction of particles environmental emissions could lead to an increase of air quality with a consequent lower personal exposure and an improvement in living conditions, above all for people genetically predisposed to the onset of CVD or living in urban centres with intense traffic. In this work it was highlighted that using *in vitro* models that involve the use of conditioned media and co-cultures of lung epithelial and endothelial cells, it is possible to investigate the response in endothelial cells indirectly exposed to UFPs. In particular, the epithelial secretion of IL-6 and its soluble receptor sIL-6R form a complex that causes the increase in adhesion molecules through receptor gp130 as we have previously reported (Bengalli et al., 2017). Here we have further confirmed that, since SRM DEPs did not induce the release of such soluble complex, the

consequent endothelial activation does not occur. This approach can be useful for investigating local mediators involved in endothelial activation. In these experiments the low doses used, and the limited exposure times might be responsible of the weak response to the SRM DEPs, with lower PAH and metals content.

The biological mechanisms activated at the endothelial level provide useful information to understand the correlation between the DEP exposure and increase in respiratory and cardiovascular diseases, related to the different physico-chemical characteristics of the UFPs and to their source of emission (Fig. 9). Since the exposure to air pollution and living in high trafficked areas is a risk factor for the development of several CVD, the analysis of the different pathways can provide new insights and useful tools for identifying specifically targeted pharmacological treatments, such as those against adhesion molecules (VCAM-1 and ICAM-1) and inflammatory cytokines (IL-6 and IL-8).

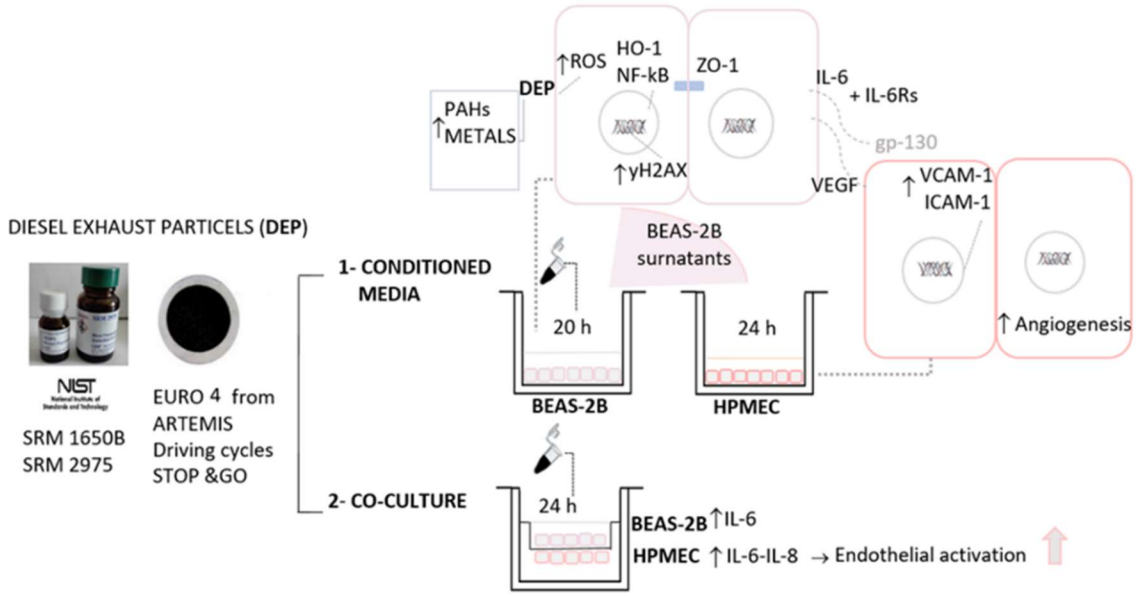

Fig. 9. Graphical scheme of experimental design and of the mechanisms involved in the response to DEP ultrafine particles.

5.1 BIBLIOGRAPHY

Adams, K., Greenbaum, D.S., Shaikh, R., van Erp, A.M., Russell, A.G., 2015. Particulate matter components, sources, and health: Systematic approaches to testing effects. J. Air Waste Manag. Assoc. 65, 544–558. https://doi.org/10.1080/10962247.2014.1001884

Kittelson, D.B., 1998. Engines and nanoparticles: a review. J. Aerosol Sci. Vol. 29, 575–588. https://doi.org/10.1016/S0021-8502(97)10037-4

Shao, J., Wheeler, A.J., Chen, L., Strandberg, B., Hinwood, A., Johnston, F.H., Zosky, G.R., 2018. The pro-inflammatory effects of particulate matter on epithelial cells are associated with elemental composition. Chemosphere 202, 530–537. https://doi.org/10.1016/j.chemosphere.2018.03.052

Van Den Heuvel, R., Den Hond, E., Govarts, E., Colles, A., Koppen, G., Staelens, J., Mampaey, M., Janssen, N., Schoeters, G., 2016. Identification of PM10 characteristics involved in cellular responses in human bronchial epithelial cells (Beas-2B). Environ. Res. 149, 48–56. https://doi.org/10.1016/j.envres.2016.04.029

Amato, F., Alastuey, A., Karanasiou, A., Lucarelli, F., Nava, S., Calzolai, G., Severi, M., Becagli, S., Gianelle, V.L., Colombi, C., Alves, C., Custódio, D., Nunes, T., Cerqueira, M., Pio, C., Eleftheriadis, K., Diapouli, E., Reche, C., Minguillón, M.C., Manousakas, M.-I., Maggos, T., Vratolis, S., Harrison, R.M., Querol, X., 2016. AIRUSE-LIFE+: a harmonized PM speciation and source apportionment in five southern European cities. Atmos. Chem. Phys. 16, 3289–3309. doi:10.5194/acp-16-3289-2016

Bengalli, R., Longhin, E., Marchetti, S., Proverbio, M.C., Battaglia, C., Camatini, M., 2017. The role of IL-6 released from pulmonary epithelial cells in diesel UFP-induced endothelial activation. Environ. Pollut. 231, 1314–1321. doi:10.1016/j.envpol.2017.08.104

Braun, A., Mun, B.S., Huggins, F.E., Huffman, G.P., 2007. Carbon speciation of diesel exhaust and urban particulate matter NIST standard reference materials with C(1s) NEXAFS spectroscopy. Environ. Sci. Technol. 41, 173–8.

Brook, R.D., Rajagopalan, S., Pope, C.A., Brook, J.R., Bhatnagar, A., Diez-Roux, A. V., Holguin, F., Hong, Y., Luepker, R. V., Mittleman, M.A., Peters, A., Siscovick, D., Smith, S.C., Whitsel, L., Kaufman, J.D., American Heart Association Council on Epidemiology and Prevention, Council on the Kidney in Cardiovascular Disease, and Council on Nutrition, Physical Activity

and Metabolism, 2010. Particulate Matter Air Pollution and Cardiovascular Disease: An Update to the Scientific Statement From the American Heart Association. Circulation 121, 2331–2378. doi:10.1161/CIR.0b013e3181dbece1

Douki, T., Corbière, C., Preterre, D., Martin, P.J., Lecureur, V., André, V., Landkocz, Y., Pottier, I., Keravec, V., Fardel, O., Moreira-Rebelo, S., Pottier, D., Vendeville, C., Dionnet, F., Gosset, P., Billet, S., Monteil, C., Sichel, F., 2018. Comparative study of diesel and biodiesel exhausts on lung oxidative stress and genotoxicity in rats. Environ. Pollut. 235, 514–524. doi:10.1016/j.envpol.2017.12.077

Eckers, A., Haendeler, J., 2015. Endothelial cells in health and disease. Antioxid. Redox Signal. 22, 1209–11. doi:10.1089/ars.2015.6323

Finkelstein, M.M., Verma, D.K., Sahai, D., Stefov, E., 2004. Ischemic heart disease mortality among heavy equipment operators. Am. J. Ind. Med. 46, 16–22. doi:10.1002/ajim.20036

Hemmingsen, J.G., Møller, P., Nøjgaard, J.K., Roursgaard, M., Loft, S., 2011. Oxidative stress, genotoxicity, and vascular cell adhesion molecule expression in cells exposed to particulate matter from combustion of conventional diesel and methyl ester biodiesel blends. Environ. Sci. Technol. 45, 8545–51. doi:10.1021/es200956p

Jośko, J., Gwóźdź, B., Jedrzejowska-Szypułka, H., Hendryk, S., 2000. Vascular endothelial growth factor (VEGF) and its effect on angiogenesis. Med. Sci. Monit. 6, 1047–52.

Adams, K., Greenbaum, D.S., Shaikh, R., van Erp, A.M., Russell, A.G., 2015. Particulate matter components, sources, and health: Systematic approaches to testing effects. J. Air Waste Manag. Assoc. 65, 544–558. https://doi.org/10.1080/10962247.2014.1001884

Kittelson, D.B., 1998. Engines and nanoparticles: a review. J. Aerosol Sci. Vol. 29, 575–588. https://doi.org/10.1016/S0021-8502(97)10037-4

Shao, J., Wheeler, A.J., Chen, L., Strandberg, B., Hinwood, A., Johnston, F.H., Zosky, G.R., 2018. The pro-inflammatory effects of particulate matter on epithelial cells are associated with elemental composition. Chemosphere 202, 530–537. https://doi.org/10.1016/j.chemosphere.2018.03.052

Van Den Heuvel, R., Den Hond, E., Govarts, E., Colles, A., Koppen, G., Staelens, J., Mampaey, M., Janssen, N., Schoeters, G., 2016. Identification of PM10 characteristics involved in cellular responses in human bronchial epithelial cells (Beas-2B). Environ. Res. 149, 48–56. https://doi.org/10.1016/j.envres.2016.04.029

Klein, S.G., Cambier, S., Hennen, J., Legay, S., Serchi, T., Nelissen, I., Chary, A., Moschini, E., Krein,

A., Blömeke, B., Gutleb, A.C., 2017. Endothelial responses of the alveolar barrier in vitro in a dose-controlled exposure to diesel exhaust particulate matter. Part. Fibre Toxicol. 14, 7. doi:10.1186/s12989-017-0186-4

Lanki, T., Hampel, R., Tiittanen, P., Andrich, S., Beelen, R., Brunekreef, B., Dratva, J., De Faire, U., Fuks, K.B., Hoffman, B., Imboden, M., Jousilahti, P., Koenig, W., Mahabadi, A.A., Künzli, N., Pedersen, N.L., Penell, J., Pershagen, G., Probst-Hensch, N.M., Schaffner, E., Schindler, C., Sugiri, D., Swart, W.J.R., Tsai, M.-Y., Turunen, A.W., Weinmayr, G., Wolf, K., Yli-Tuomi, T., Peters, A., 2015. Air Pollution from Road Traffic and Systemic Inflammation in Adults: A Cross-Sectional Analysis in the European ESCAPE Project. Environ. Health Perspect. 123, 785–91. doi:10.1289/ehp.1408224

Lawal, A.O., Davids, L.M., Marnewick, J.L., 2016. Diesel exhaust particles and endothelial cells dysfunction: An update. Toxicol. Vitr. 32, 92–104. doi:10.1016/J.TIV.2015.12.015

Lelieveld, J., Evans, J.S., Fnais, M., Giannadaki, D., Pozzer, A., 2015. The contribution of outdoor air pollution sources to premature mortality on a global scale. Nature 525, 367–371. doi:10.1038/nature15371

Li, N., Hao, M., Phalen, R.F., Hinds, W.C., Nel, A.E., 2003. Particulate air pollutants and asthma. A paradigm for the role of oxidative stress in PM-induced adverse health effects. Clin. Immunol. 109, 250–65.

Li, N., Wang, M., Oberley, T.D., Sempf, J.M., Nel, A.E., 2002. Comparison of the pro-oxidative and proinflammatory effects of organic diesel exhaust particle chemicals in bronchial epithelial cells and macrophages. J. Immunol. 169, 4531–41.

Longhin, E., Gualtieri, M., Capasso, L., Bengalli, R., Mollerup, S., Holme, J.A., Øvrevik, J., Casadei, S., Di Benedetto, C., Parenti, P., Camatini, M., 2016. Physico-chemical properties and biological effects of diesel and biomass particles. Environ. Pollut. 215, 366–375. doi:10.1016/j.envpol.2016.05.015

Miller, M.R., McLean, S.G., Duffin, R., Lawal, A.O., Araujo, J.A., Shaw, C.A., Mills, N.L., Donaldson, K., Newby, D.E., Hadoke, P.W., 2013. Diesel exhaust particulate increases the size and complexity of lesions in atherosclerotic mice. Part. Fibre Toxicol. 10, 61. doi:10.1186/1743-8977-10-61

Miller, M.R., Shaw, C.A., Langrish, J.P., 2012. From particles to patients: oxidative stress and the cardiovascular effects of air pollution. Future Cardiol. 8, 577–602. doi:10.2217/fca.12.43

Mögel, M., Krüger, E., Krug, H.F., Seidel, A., 1998. A new coculture-system of bronchial epithelial

and endothelial cells as a model for studying ozone effects on airway tissue. Toxicol. Lett. 96–97, 25–32.

Mudau, M., Genis, A., Lochner, A., Strijdom, H., 2012. Endothelial dysfunction: the early predictor of atherosclerosis. Cardiovasc. J. Afr. 23, 222–31. doi:10.5830/CVJA-2011-068

Robertson, S., Miller, M.R., 2018. Ambient air pollution and thrombosis. Part. Fibre Toxicol. 15, 1. doi:10.1186/s12989-017-0237-x

Schwarze, P.E., Totlandsdal, A.I., Låg, M., Refsnes, M., Holme, J.A., Øvrevik, J., 2013. Inflammation-related effects of diesel engine exhaust particles: studies on lung cells in vitro. Biomed Res. Int. 2013, 685142. doi:10.1155/2013/685142

Shao, J., Wheeler, A.J., Chen, L., Strandberg, B., Hinwood, A., Johnston, F.H., Zosky, G.R., 2018. The pro-inflammatory effects of particulate matter on epithelial cells are associated with elemental composition. Chemosphere 202, 530–537. https://doi.org/10.1016/j.chemosphere.2018.03.052

Sørensen, M., Autrup, H., Møller, P., Hertel, O., Jensen, S.S., Vinzents, P., Knudsen, L.E., Loft, S., 2003. Linking exposure to environmental pollutants with biological effects. Mutat. Res. 544, 255–71.

Sprague, A.H., Khalil, R.A., 2009. Inflammatory cytokines in vascular dysfunction and vascular disease. Biochem. Pharmacol. 78, 539–52. doi:10.1016/j.bcp.2009.04.029

Stewart, C.E., Torr, E.E., Mohd Jamili, N.H., Bosquillon, C., Sayers, I., 2012. Evaluation of Differentiated Human Bronchial Epithelial Cell Culture Systems for Asthma Research. J. Allergy 2012, 1–11. doi:10.1155/2012/943982

Stone, V., Miller, M.R., Clift, M.J.D., Elder, A., Mills, N.L., Møller, P., Schins, R.P.F., Vogel, U., Kreyling, W.G., Alstrup Jensen, K., Kuhlbusch, T.A.J., Schwarze, P.E., Hoet, P., Pietroiusti, A., De Vizcaya-Ruiz, A., Baeza-Squiban, A., Teixeira, J.P., Tran, C.L., Cassee, F.R., 2017. Nanomaterials Versus Ambient Ultrafine Particles: An Opportunity to Exchange Toxicology Knowledge. Environ. Health Perspect. 125, 106002. doi:10.1289/EHP424

Törnqvist, H., Mills, N.L., Gonzalez, M., Miller, M.R., Robinson, S.D., Megson, I.L., MacNee, W., Donaldson, K., Söderberg, S., Newby, D.E., Sandström, T., Blomberg, A., 2007. Persistent Endothelial Dysfunction in Humans after Diesel Exhaust Inhalation. Am. J. Respir. Crit. Care Med. 176, 395–400. doi:10.1164/rccm.200606-872OC

Totlandsdal, A.I., Låg, M., Lilleaas, E., Cassee, F., Schwarze, P., 2015. Differential proinflammatory responses induced by diesel exhaust particles with contrasting PAH and

metal content. Environ. Toxicol. 30, 188–196. doi:10.1002/tox.21884

Van Den Heuvel, R., Den Hond, E., Govarts, E., Colles, A., Koppen, G., Staelens, J., Mampaey, M., Janssen, N., Schoeters, G., 2016. Identification of PM10 characteristics involved in cellular responses in human bronchial epithelial cells (Beas-2B). Environ. Res. 149, 48–56. https://doi.org/10.1016/j.envres.2016.04.029

Vitiello, L., Spoletini, I., Gorini, S., Pontecorvo, L., Ferrari, D., Ferraro, E., Stabile, E., Caprio, M., la Sala, A., 2014. Microvascular inflammation in atherosclerosis. IJC Metab. Endocr. 3, 1–7. doi:10.1016/J.IJCME.2014.03.002

Ye, B., Hou, N., Xiao, L., Xu, Y., Xu, H., Li, F., 2016. Dynamic monitoring of oxidative DNA double-strand break and repair in cardiomyocytes. Cardiovasc. Pathol. 25, 93–100. doi:10.1016/j.carpath.2015.10.010

Zhang, C., 2008. The role of inflammatory cytokines in endothelial dysfunction. Basic Res. Cardiol. 103, 398–406. doi:10.1007/s00395-008-0733-0

Zhang, Z., Guang, M., Msc, C., Wu, H.-X., Ni, M., Msc, Z., Sun, B.-G., Dai, Q.-Y., n.d. IL-8 reduces VCAM-1 secretion of smooth muscle cells by increasing pERK expression when 3-D cocultured with vascular endothelial cells.

5.2 SUPPLEMENTARY DATA CHAPTER V

Supplementary Tables

Table S1: Chemical composition of DEP (PAHs)

PAHs	1650b[(a)]	2975[(b)]	Euro 4[(c)]
	ng/mg	ng/mg	ng/mg
Fluorene	1,27	2,88	19,54
Phenanthrene	65,60	20,70	256,73
Anthracene	1,56	0,05	6,20
Fluoranthene	48,10	30,90	44,37
Pyrene	44,10	1,52	100,04
Benzo[a]anthracene	6,45	0,97	14,75
Chrysene	13,40	5,73	11,79
Benzo[k]fluoranthene	2,30	1,75	3,97
Benzo[a]pyrene	1,25	0,77	18,73
Indeno[1,2,3-cd]pyrene	4,48	2,13	21,81
Benzo[e]pyrene	6,36	2,28	32,63
Benzo[b]fluoranthene	6,77	11,50	27,65
Dibenzo[a,h]anthracene	0,37	0,52	33,92
Total	**202,1**	**81,69**	**592,13**

Table S1. Total PAHs concentraton (ng/mg) of the three DEP. (a) Certificate of Analysis Standard Reference Material®1650b, National Institute of Standards & Technology Reference Mass Fraction Values for PAHs in SRM 1650b Based on Extraction Method and Condition (PFE at 200 °C); (b) Certificate of Analysis Standard

Reference Material®2975, National Institute of Standards & Techno Reference Mass Fraction Values for PAHs in SRM 2975 Based on Extraction Method and Condition (PFE at 200 °C); (c) Longhin et al. Physico-chemical properties and biological effects of diesel and biomass particles. 2016 Aug. PAHs were evaluated by GC/MS (HRGCMS Agilent 5973 Agilent Technologies, CA) after Accelerated Solvent Extraction (ASE) using a mix hexane/acetone (ratio 4:1 v/v). A reduced volume of the extraction solution was injected in the GC/MS and analyzed in a 30 m 250 mm DB-5 capillary with helium carrier gas and a final line temperature of 300°C.

Based on previous work form Braun and colleagues the most abundant organic compounds found in the two DEP SRM are for both fluoranthene, pyrene, phenanthrene, and 9-fluorenone. In addition, the Carbon Speciation with (NEXAFS) spectroscopy show that both diesel soot SRM samples contain basic graphitic structures, with SRM 1650 having a more a more graphitic structure (Braun et al., 2006). The characterization of the DEP Euro 4 showed a typical PAHs composition with high levels of pyrene, phenanthrene, benzo[a]anthracene and dibenzo[a, h]anthracene (Longhin et al., 2016). Comparing the speciation of Euro 4 with compounds quantify in the SRM certificate of analysis, Euro 4 results as the DEP with the highest content of PAHs.

Table S2: Metal content of DEP

	ng/µg		
	1650b	**2975**	**Euro 4***
Al	0,142	0,724	133,900
Ca	0,729	4,635	196,750
Cd	ND	0,008	ND
Co	ND	0,003	0,040
Cr	ND	ND	ND
Cu	0,004	0,079	ND
Fe	0,356	1,049	3,980
K	0,051	0,083	48,510
Mn	ND	0,021	0,030
Ni	ND	ND	0,020
P	0,410	1,365	0,370
Pb	0,003	0,041	0,020
Ti	ND	ND	0,040
V	0,002	0,004	0,050
Zn	0,315	1,441	59,870
Total	2,011	9,454	443,580

Table S2: Metals concentration (ng/µg) detected in DEPs sample by ICP-MS. *Longhin et al., 2016.

Table S3: Endotoxin content in DEP samples

The endotoxin content in DEP samples was determined by a quantitative chromogenic Limulus Amebocyte Lysate (LAL) test (ToxinSensorTM Chromogenic LAL Endotoxin Assay Kit, GeneScript) following the manufacturer's instructions. Briefly, DEP extracts were diluted in apyrogenic water to the concentration of 10 ug/mL, mixed with pyrochrome LAL reagent and incubated at 37°C for 9 minutes. The reaction was then stopped with stop solution (color-stabilizer) and the absorbance of the samples was determined by a spectrophotometer microplate reader (Tecan Infinite Pro) at 545 nm. The content of endotoxin in DEP Euro 4 is below the detection limit of the kit (0.1 EU/ml), while the amount of endotoxin in DEP samples SRM were expressed in EU/mg and are shown in Table S3. In a previous work (Longhin et al., 2013). the content of endotoxin in different seasonal PMs was evaluated in order to understand the role of endotoxin in inducing the release of interleukins. In that work, the only PM sample able to activate the inflammatory response was summer PM10, which had the highest content of endotoxin (25 EU/mg), while winter fine and ultrafine PM, which had lower content of endotoxin, were not able to induce the release of IL-6.

	EU/mg
DEP SRM 1650b	9.63 ± 0.23
DEP SRM 2975	10 ± 0.0003
DEP Euro 4	n.d.*

Tables S3: The content of endotoxin in DEP Euro 4is below the detection limit of the kit (0.1 EU/ml).

Supplementary data S1: Cell morphology

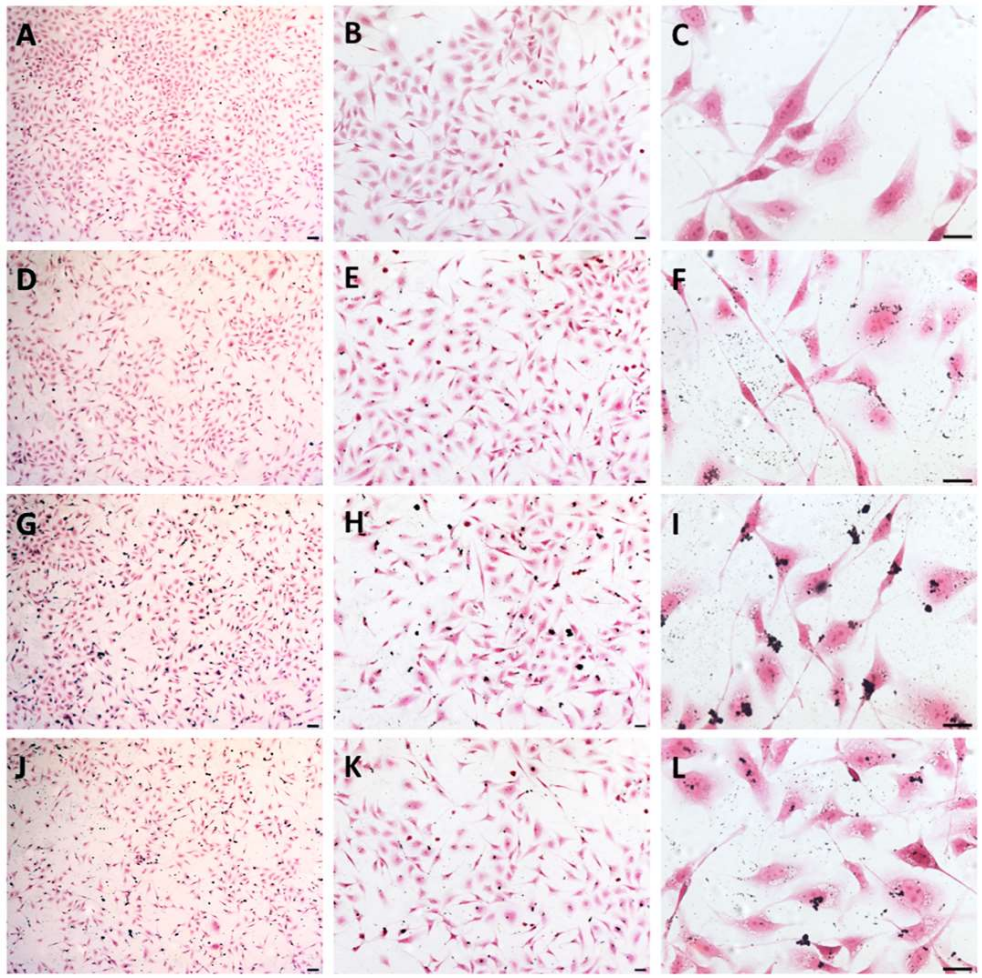

Fig. S1: Morphological analysis. Microscope images of BEAS-2B cells, stained with hematoxylin/eosin, show the slight morphological changes in respect to Control (A, B, C) after exposure for 20 h to 5µg/cm^2 DEP 1650b (D, e, F), 2975 (G, H, I) and Euro 4 (J, K, L). Scale bars= 100 µm (A, D, G, J), 50 µm (B, E, H, K), 20 µm (C, F, I, L).

Supplementary data S2: Endothelial release of IL-6 and IL-8 after exposure to conditioned media

The release of IL-6 and IL-8 by endothelial cells after exposure to BEAS-2B conditioned media was evaluated in order to investigate if there was a vascular inflammatory response. A slight, even if not significant, release of IL-6 was observed but it is not possible to determine if it is due only from HPMEC release or also from BEAS-2B cells.

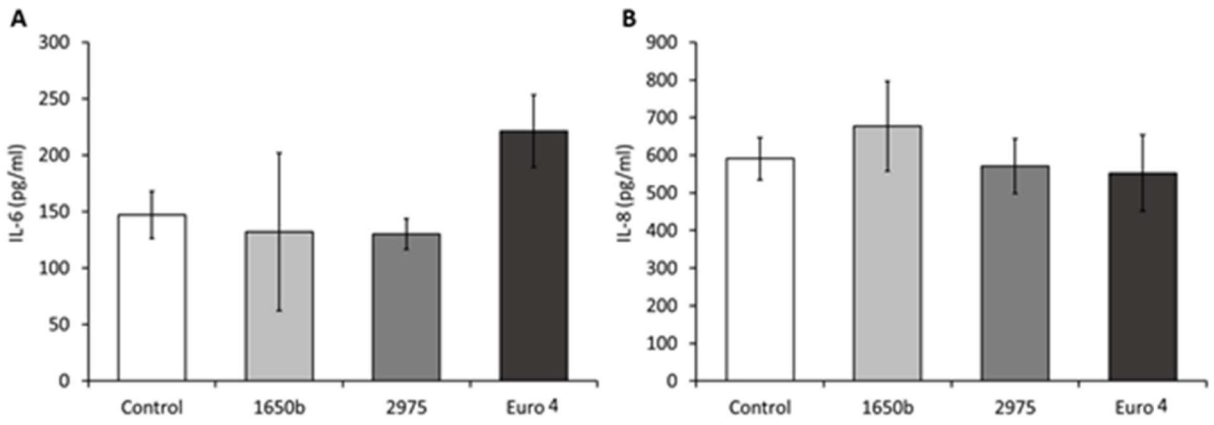

Fig. S2 Release of IL-6 and IL-8 from HPMEC cells. The release of IL-6 (A) and IL-8 (B) from endothelial cells treated with BEAS-2B conditioned medium was evaluated after 24h and for the three different DEP. Data represents the mean ± SEM of at least three independent experiments.

Supplementary data S3: VCAM-1 expression in the co-culture system

The expression of VCAM-1 in the basal level of the co-culture system was evaluated after the exposure to DEP at the apical level for 24h. Data showed that DEPs did not induce the expression of VCAM-1 in this system.

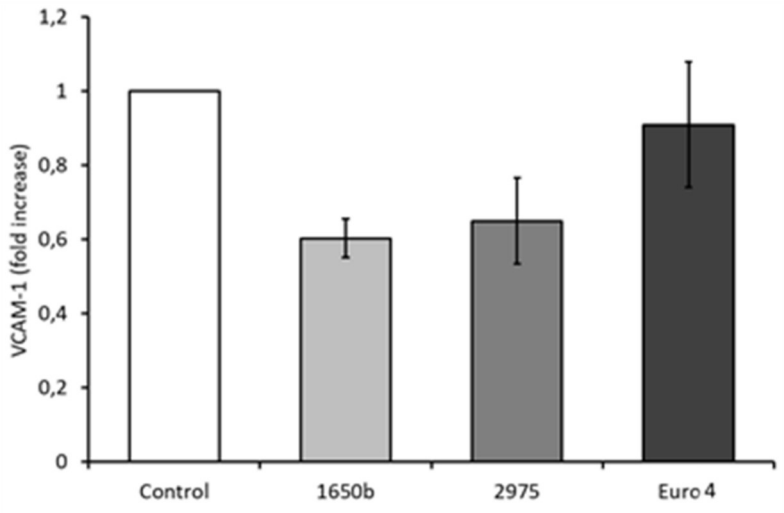

Fig. S3: VCAM-1 expression: co-culture system. The expression of VCAM-1 in the endothelial cells form the co-culture system was evaluated with cytofluorimetric analysis. Data represents the mean ± SEM of at least three independent experiments.

BIBLIOGRAPHY SUPPLEMENTARY

Braun, A., Mun B.S., Huggins F.E., Huffman, G.P., 2006. Carbon Speciation of Diesel Exhaust and Urban Particulate Matter NIST Standard Reference Materials with C(1s) NEXAFS Spectroscopy. doi:10.1021/ES061044W

Longhin, E., Pezzolato, E., Mantecca,P., Holme, J.A., Franzetti, A., Camatini, M., Gualtieri, M. Season linked responses to fine and quasi-ultrafine Milan PM in cultured cells, Toxicology in Vitro, Volume 27, Issue 2, 2013: 551-559. https://doi.org/10.1016/j.tiv.2012.10.018.

Longhin, E., Gualtieri, M., Capasso, L., Bengalli, R., Mollerup, S., Holme, J.A., Øvrevik, J., Casadei, S., Di Benedetto, C., Parenti, P., Camatini, M., 2016. Physico-chemical properties and biological effects of diesel and biomass particles. Environ. Pollut. 215, 366–375. doi:10.1016/j.envpol.2016.05.015

CHAPTER VI

COMPARATIVE EVALUATION OF PARTICULATE EMISSION AND BIOLOGICAL EFFECTS FROM AN OLD GENERATION DIESEL VEHICLE AND LATEST GENERATION (EURO 6) ONE OVER DIESEL PARTICULATE FILTER (DPF) REGENERATION

The incomplete combustion processes in diesel engines produce a big amount of the total Particulate Matter (PM) that contribute to air pollution. In this work we compared the PM emissions and related biological effects of an old generation diesel vehicle (or Euro 3) with the latest generation vehicle during the regeneration of diesel particulate filter (DPF). To collect the two types of Diesel exhaust particles (DEP), different driving cycles were used, and the particles size distribution was monitored using an Engine Exhaust Particle Sizer (EEPS) Spectrometer and an Electrical Low-Pressure Impactor (ELPI). Although the latest generation engine emits particulates only during the regeneration of DPF, which mainly occurs for few minutes at high speeds, the emissions from Euro 6 during regeneration of DPF are characterized of a higher number of ultrafine particles (< 0,1 µm) compared to the old generation diesel vehicle. The emitted particles present different physico-chemical composition, with Euro 6 showing less PAHs content than Euro 3, but resulting enriched in some metals, not or poorly detected in Euro 3. The comparative biological effects of the two DEPs were investigated using human bronchial BEAS-2B cells exposed to 5 µg/cm^{2}PM, which reflects a possible daily exposure dose in a polluted urban area. The in vitro analysis shows that Euro 3 DEP activated the typical inflammatory and pro-carcinogenic pathways induced by combustion-derived particles, while Euro 6 DEP is less powerful in activating such biological responses, even if it induced a significant increase of a DNA damage marker, IL-24 release, and changes in microtubular cytoskeleton that require further investigations. The different in vitro effects could be correlated with a different chemical composition of

the emitted particles, like metals and PAHs content, which are recognised to play a pivotal role in the toxicological outcomes.

This chapter is a paper submitted to Science of the Total Environment:" A.Zerboni; T.Rossi; R.Bengalli; T.Catelani; C.Rizzi; M.Priola; S.Casadei and P.Mantecca. Comparative evaluation of particulate emission and biological effects from an old generation diesel vehicle and latest generation (Euro 6) one over Diesel Particulate Filter (DPF) regeneration. Science of the Total Environment. (Under review Ref. No: STOTEN-D-20-31150)."

Graphical abstract

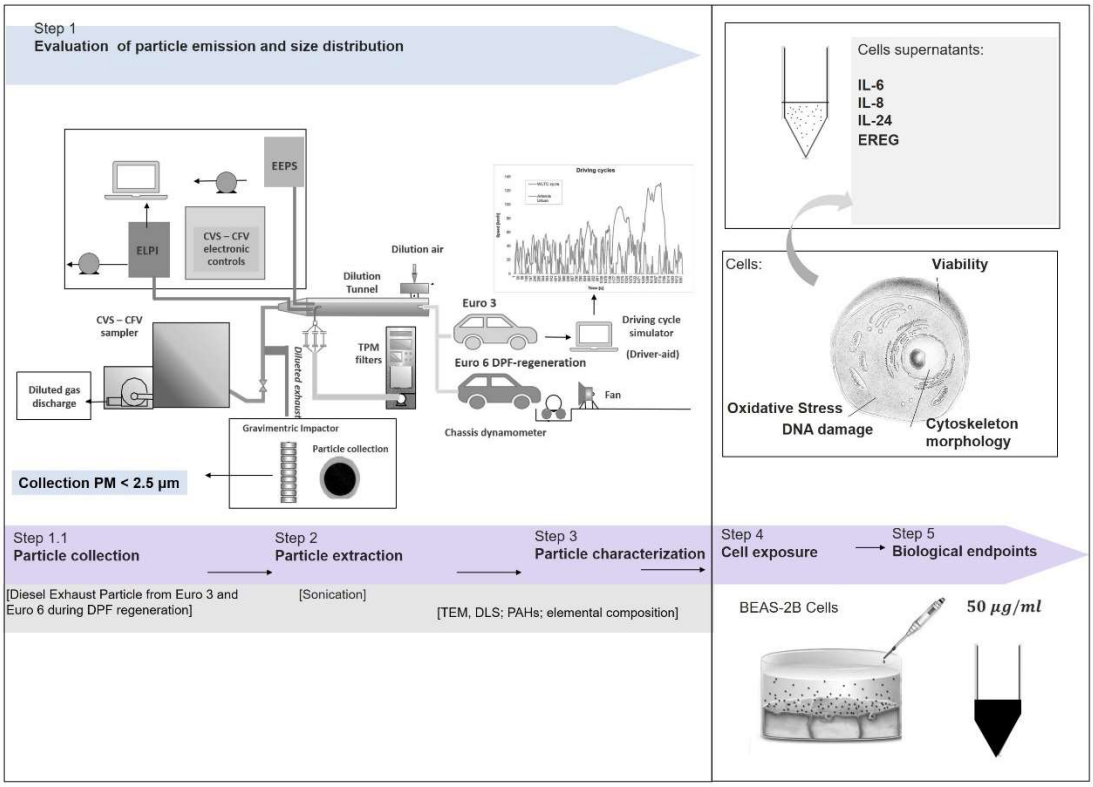

1-Introduction:

Due to cardiovascular and respiratory diseases, air pollution remains a global issue for the 21st century. Adverse outcomes seem to be evident both in long and short-term studies (Dockery et al. 1993) (Brunekreef and Holgate 2002), with also consequent costs of hospital admission associated with exposure to particulate (Wei et al. 2019). Particulate matter (PM) is a complex mixture of different sizes particles dispersed in the air. PM with a diameter less than 2.5 µm ($PM_{2.5}$) passes easily into the deepest area of the lungs. The

toxicity of PM increase with the smaller size and the ultrafine particles (UFPs), less than 0.1 µm, easily pass into other organs through the lung vasculature. The respiratory tract has a large internal surface area that results directly exposed to 10,000 to 20,000 liters of air every day. After inhalation, particles may have different fates: retention in the lung, clearance from the airways or translocation through the air-blood-barrier (ABB) and reach secondary organs (Watson et al. 1988). Understanding the effects on the respiratory apparatus of particles derived from different sources is fundamental for the improvement of risk management policies and pollution mitigation strategies, since fine and ultrafine particles emission has a close connection with human activities. Thus, there is an urgent need to define the real impact of UFPs on human health, and a thorough understanding on UFPs should include the analysis of sources, size distribution, composition, and toxicological mechanisms. It is commonly known that daily $PM_{2.5}$ and PM_{10} pollution determined as mass concentrations (µg m^{-3}) cannot reflect the real spatial variation of UFPs (Chen et al. 2016). It is more advisable to evaluate UFPs through measurements of particle number concentration (PNC), due to their negligible mass compared with the largest particles (Kumar et al. 2014). Combustion is a direct source of UFPs, and the incomplete combustion processes in diesel engines produce a big amount of the total fine and ultrafine particles. In 2012 Diesel Exhaust Particles (DEP) were classified as carcinogen by the International Agency for Research on Cancer (IARC 2012) and this emission has been regulated, due to their involvement in both the health effects and the climate-warming potential. In 1991 the first Euro standards were promulgated and over time were introduced more stringent exhaust emission standards for new vehicles. According to the directive of European Parliament and the Council (2008/50/EC), in 2014 a new stringent regulation was introduced in Europe for new diesel passenger cars, called Euro 6 standards, which confirmed the particulate number emission limit of 6.0×10^{11} solid particles per km and the particulate mass limit of 0.005 g/km, already introduced for Euro 5b diesel vehicles. In order to meet Euro 6 standards, new diesel vehicles must be equipped with after-treatment systems (ATS), such as Diesel Particulate Filter (DPF) and selective catalyst reduction (SCR) systems for the reduction of exhaust NO_x emissions (Pirjola et al. 2019). However, in real conditions, total particulate exhaust emissions from diesel vehicles are still dominated by the presence in the circulating fleet of old generation diesel vehicles (Euro 1, 2, 3, 4 without DPF) beside the new generation vehicles, especially in poor countries. Indeed, there is a

growing international trade of old second hand vehicles from high-developed countries to less-developed countries (Cervero 2013).

In this work, the particulate exhaust emissions derived from an “old” diesel vehicle were compared to the emissions from a “latest” generation one. DEPs were collected from two different diesel vehicles, a EURO 3 (without DPF) and a EURO 6, sampled in a controlled laboratory environment driving vehicles on a chassis dynamometer. In order to collect the two type of DEP, two different driving cycles were driven: “URBAN” Artemis (Assessment and Reliability of Transport Emission Models and Inventory System)(André 2004), driving cycle, which well represents the urban driving behaviour (frequent stop and go and average vehicle speed below 40 km/h), was used for Euro 3, while the DPF-equipped Euro 6 vehicle was driven on the standard homologation Worldwide harmonized Light vehicles Driving Cycle (WTLC) since DPF regeneration needs deep acceleration and especially high-speed conditions to be activated by the vehicle Electronic Control Unit (ECU). DPF has been shown to lead to a very efficient reduction in the emissions of total PNC and PM mass (Karjalainen et al. 2019), (Preble et al. 2015). Since DPF effectively removes most of particulate matter, particles from the exhaust derived from the Euro 6 vehicle were sampled only over the DPF regeneration starting by its activation. Indeed, as reported by Transport & Environment (Transport & Environment, 2020) new, generation diesel vehicles can represent an important health hazard as well. DPF require to be regenerated regularly to clean the filter, which causes diesel vehicles to ‘spill out’ large amounts of particulate matter in the environment. Moreover, according to the results reported in this report, during the “regeneration” of the DPF the emissions of particle exceed over 1,000 times their normal rate. The total exhaust particle number and the size distribution of the two different DEP were determined with an Engine Exhaust Particle Sizer (EEPS) Spectrometer and an Electrical Low-Pressure Impactor (ELPI). An important aspect in the evaluation of exposure to diesel emissions and of the consequent human effects is the respiratory tract deposition of inhalable particles. Size distribution of particles according to their mobility diameter is a useful parameter employed to predict the deposition rate along the respiratory tract, assuming diffusion as the dominating deposition mechanism (Rissler et al. 2012). The PNC and the lung-deposited surface area (LDSA) can be used for predicting pulmonary deposition and inflammation of insoluble and poorly soluble UFPs (Geiss et al. 2016).

Although many studies on the toxicity of DEP have been conducted using standard DEP, such as SRM2975 (Schwarze et al. 2013) (Klein et al. 2017), which represents a well characterized and widely used model for DEP, the possibility of using material sampled by different vehicles in realistic conditions allows to better evaluate how the toxicity of DEP may vary in relation to the sources and the characteristics of the emitted particles. Furthermore, as previously demonstrated, the *in vitro* effects of standard DEP and DEP sampled from a Euro 4 vehicle can be significantly different (Bengalli et al. 2019). Several in vitro studies had proved that DEP trigger various cell signalling pathways that may cause the release of inflammatory markers, oxidative stress, DNA damage directly or indirectly by causing cell death (Schwarze et al. 2013)(K.Jantzen et al. 2012), and also damage to cytoskeleton. The upregulation of specific inflammatory markers, such as interleukin-6 and 8 (IL-6,IL-8), after exposure to DEP, was verified in several previous studies (Steerenberg et al. 1998) (Kim et al. 2016), and also recently, Grilli et al. (2018) reported upregulated levels of trascripts and proteins of IL-24 and epiregulin (EREG), involved in inflammation and carcinogenic processes.

Since we live in a global public health crisis due to the COVID-19 viral pneumonia, it cannot be ignored that the same markers related to PM exposure, with special reference to IL-6, have been identified in studies on the mechanism of action of SARS-CoV-2 infection (McGonagle et al. 2020). Moreover specific cytokines, IL-6 included, are found to be predictive of disease severity (Han et al. 2020).The role of IL-6 and other cytokines in inflammation driven pulmonary vascular disease require further investigation, but some authors hypothesize an association between short-term exposure to air pollution and COVID-19 exacerbation (Zhu et al. 2020). The hypothesis that exposure to air pollutants may contribute to increasing the vulnerability of a population to SARS-CoV-2 infection needs to be considered and, in this context, the knowledge of the contribution of diesel emissions and related hazard could help in designing future preventive and mitigation strategies.

In the present study, in addition to monitoring the particles numbers emissions, *in vitro* studies, which represent simplified and convenient systems to predict the health effects of environmental contaminants, have been used in order to understand the toxicity of DEP from different sources on human terminal airways epithelial cells. After DEP collection on

Teflon filters, monocultures of bronchial epithelium BEAS-2B cells, frequently used for studying the toxicity of fine and ultrafine PM (Raudoniute et al. 2018)(Badran et al. 2020), (Grilli et al. 2018), were exposed to DEP derived from the tested Euro 3 vehicle without DPF and from the tested Euro 6 vehicle over DPF regeneration process, as described above. Besides *in vitro* experiments, the morphology of the particles was analysed with Transmission Electron Microscopy (TEM), the metal content by Energy-dispersive X-ray spectroscopy and Inductively Coupled Plasma Mass Spectrometry (ICP-MS). Polycyclic aromatic hydrocarbons (PAHs) were analysed by Gas Chromatography-Mass Spectrometry (GC-MS). The oxidative potential, cytotoxicity, inflammatory response, cellular DNA damage and morphological cellular changes modulated by the two different DEPs were evaluated in order to investigate their mechanisms of toxicity on lung cells.

One of the main aims of this work is to understand if the evolution of diesel engines and the technologies of after-treatment systems have led to a real reduction of human health risk for the exposure to DEP emission. Furthermore, studies regarding how particles elicit their effects at cellular and molecular level may contribute at identifying biomarkers of effects and susceptible groups in the population, which is important especially when considering the possible concomitant effects of other abiotic or biotic atmospheric contaminants. Today more than ever it is required to have more detailed pictures of the biological effects of the atmospheric pollutants from different sources, as part of an integrated approach for human health safety in a long-term perspective.

2. Methods:

2.1 Particulate Sampling methods and emission measurements.

DEPs were sampled on Teflon filters (Whatman, Maidstone, UK) using a high sample flow rate cascade impactor (Dekati® DGI-1570, Finland), that allows to collect particles basing on the mass size distribution of the PM fraction. Teflon filters were placed in the last stage of the impactor (stage cut-point of 2.5 μm) in order to collect as many particles as possible, suitably for biological tests. DEPs were collected from the diluted exhaust of a Euro 3 light

duty vehicle without DPF fuelled with commercial diesel and driven on a chassis dynamometer, following a research driving cycle named “URBAN” Artemis Driving Cycle (André 2004)showed in Figure 1, which was chosen being well representative of real average stop-and-go driving conditions typical of a European urban context where light commercial vehicles are used. DEP from a Euro 6 d-temp-evap passenger car, fuelled with commercial diesel were also sampled on the Teflon filters, but over a DPF regeneration phase. Euro 6 vehicle was driven on a chassis dynamometer, following the (WLTC) (COMMISSION REGULATION (EU) 2017/1151 2017)(Figure 1). DPF regenerations for most vehicles occur when the ECU detects, for few consecutive minutes, high speed conditions, which are for example foreseen in the third and fourth phases of WLTC, named “High” and “Extra-high” phase, respectively.

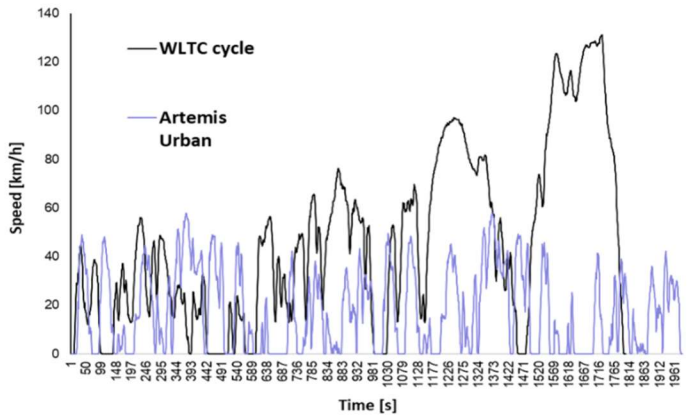

Figure 1. Speed chart of WLTC and a double Artemis Urban driving cycle: The graph shows the different speeds (km/h) over time (s) for the different driving cycles adopted: WLTC cycle (black line) for Euro 6 DEP from regeneration and an Artemis Urban (purple line, repeated twice), typical of a STOP&GO driving cycle, for Euro 3 DEP.

Several tests were carried out in repeatability conditions for each vehicle in order to collect enough particles required for biological tests. The two testing vehicles were checked to meet all gaseous and particulate European emission standards, and moreover they were regularly maintained and passed every periodical technical inspection. Over the two testing cycles, the exhaust was collected, diluted through the Constant Volume Sampler – Constant Flow Venturi (CVS-CFV) system of the laboratory and analysed with a couple of

particle analysers: an Electrical Low-Pressure Impactor (ELPI) to measure particles with average aerodynamic diameter within 0.007 and 10 µm range and an Engine Exhaust Particle Sizer (EEPS) to measure particles with diameter within 5.6 and 560 nm range.

2.2 Particles preparation

After sampling, filters were preserved at −20 °C until particles extraction, that was performed by sonication in the bath-type sonicator (SONICA). Particle suspensions were then dried into a desiccator, weighed with a microbalance (Sartorius, Goettingen, Germany) and stored at - 20 °C until use for experiments.

2.3 Characterization of Particles Suspensions

The analysis of particles morphology and size was conducted by TEM. A drop of 5 µL of DEP suspension in ultrapure water (50 µg/mL) was deposited on Formvar® coated 200-mesh copper grids. Excess water was gently blotted, then the grids were left to dry in the air and finally inserted into the TEM. TEM micrographs were acquired by means of JEOL JEM 2100 Plus Transmission Electron Microscope (JEOL, Japan) operating with an acceleration voltage of 200kV, and equipped with an 8-megapixel Gatan (Gatan, USA) Rio Complementary Metal-Oxide-Superconductur (CMOS) camera. TEM/STEM EDX maps and spectra were acquired by means of 80mmq Oxford (Oxford, UK) UltimMax detector. Metals were also quantified by ICP-MS (Perkin Elmer SCIEX mod. ELAN 9000). The filters were digested in a microwave oven (Multiwave Pro by Anton Paar) with a mixture of 4 mL of nitric acid (HNO_3), 2 mL of hydrogen peroxide (H_2O_2) and 1 mL of hydrofluoric acid (HF). The solution obtained, suitably diluted, was analysed using an external calibration line with internal standards (Ge, In and Lu), used to compensate plasma fluctuations.

The particles hydrodynamic size was measured using a dynamic light scattering (DLS) (Malvern Zetasizer, Malvern, UK) technique, at a scattering angle of 90°. DEP suspensions were prepared using the method previously described, then diluted in culture medium (LHC-9, Gibco, Life Technologies, Monza, Italy) at a final concentration of 50 µg/mL.

Following the procedure reported in (Ferrero et al. 2019), 13 PAHs (fluorene, phenanthrene, anthracene, fluoranthene, pyrene, benzo(a)anthracene, chrysene, benzo(b)fluoranthene, benzo(k)fluoranthene, benzo(a)pyrene, indeno(1,2,3,c,d)pyrene, dibenzo(a,h)anthracene and benzo(g,h,i)perylene) were analyzed in samples by GC-MS. Briefly, samples were extracted with 2 mL of dichloromethane (purity≥99.8%, Chromasolv Honeywell) in an ultrasonic bath at 40°C-over 1 hour. The extract was filtered with a PTFE syringe filter (cut 0.22 µm) to remove any particles. The extraction solvent was then evaporated under a gentle nitrogen stream until dryness and dissolved in n-hexane. The extracts were analysed by gas chromatography-mass spectrometry (GC/MS, Agilent Technologies, CA, USA) in single ion monitoring (SIM) mode.

A SGE BPX50 column (60 m length, 0.25 mm internal diameter, 0.25 µm film thickness) was used for the separation. The oven program was: 80 °C kept for 1 min; 25 °C min−1 up to 140 °C; 15 °C min−1 up to 250 °C; 2 °C min−1 up to 270 °C; 4 °C min−1 up to 310 °C ; 310 °C for 8 min; 30 °C min−1 up to 320 °C; 320 °C for 20 min. The MS transfer line temperature was set at 280°C and the injector at 250°C.

2.4 Oxidative potential of DEP

The oxidative potential of the two DEPs was evaluated by measuring the reduction of cytochrome-C as previously described (Longhin et al. 2016). The reaction mix was prepared using 10 µg/mL of particles, 100 µM TCEP (tris (2-carboxyethyl) phosphine) and 50 µM cytochrome-C in 50 mM Tris-HCl buffer at pH 7.5. Absorbance was immediately measured at 550 nm with a multiplate spectrophotometer reader (Infinite 200Pro, TECAN, Männedorf, Switzerland) with a kinetic program (10 s interval, 96 readings). Rates of cytochrome-C reduction were determined from absorbance curves by calculating the ΔA/min (linear equation of the curves × 60).

2.5 Cells culture maintenance and treatments

BEAS-2B (ATCC® CRL9609™) cells were maintained in LHC-9 medium (Gibco, Life Technologies, Monza, Italy) at suitable grow condition (37 °C with 5% of CO_2). Cells

(passages 20 to 45) were seeded at a density of 2.7×10^5 cells/well in 6-well plates and treated after 24 h of incubation with 50 µg/mL of UFPs, corresponding to 5 µg/cm^2. This concentration of diesel DEP has been chosen because it is sub-toxic, and it is also the lower tested dose that induces effect in the in vitro system here used after a single exposure. After 24 h of exposure, media were collected, and cellular responses were analysed. Particles were directly added in the cellular medium. All the in vitro experiments were performed at least in triplicate (three independent experiments).

2.6 Cell viability

The effect of the two DEPs on cell viability was analysed using two different tests: 3-(4,5-Dimethylthiazol-2-yl)-2,5-Diphenyltetrazolium Bromide (MTT) assay and trypan blue exclusion test.

For MTT test, BEAS-2B cells were treated with 50 µg/mL Euro 3 particles and Euro 6 DPF regeneration particles. After 24 h of exposure, the medium was substituted with phosphate-buffered saline (PBS) and then MTT (Sigma Aldrich) solution, prepared in LHC-9 medium at a concentration of 0.3 mg/mL, and incubated over 3 h. After the formation of MTT formazan crystals, the medium was removed and the crystals were solubilized with dimethyl sulfoxide (DMSO, Euroclone, Pero, Italy). The absorbance of each sample was measured with a multiplate reader spectrophotometer (Infinite 200Pro, TECAN, Männedorf, Switzerland) at 570 nm, using 690 nm as a reference wavelength. Cell viability was reported as relative decrease compared to the absorbance resulting from the control, indicated as 100% of viable cells. Trypan Blue staining can discriminate between viable and non-viable cells. BEAS-2B cells were treated with 50 µg/mL Euro 3 and Euro 6 DPF regeneration particles. After 24 h of exposure, cells were washed twice with PBS, trypsinized, centrifuged at 1200 rpm for 6 min and suspended in 500 µL of Trypan-Blue solution 0.4% (Sigma) in PBS (1:1), for 5 to 10 minutes. The haemocytometer chamber was filled with cells suspension. The cells were counted by the microscope in four 1 x 1 mm squares of one chamber and determined the average number of cells per square. The stained cells (blue) were considered dead, the unstained cells were considered vital.

2.7 Quantification of Cytokines

After exposure, the supernatants from BEAS-2B cells were collected and stored at −80 °C until analysis. Protein levels were detected by sandwich ELISA kit specific for IL-6 and IL-8, provided by Life Technologies (Monza, Italy), and IL-24 and EREG (Epiregulin) provided by Elabscience Biotechnology Co., Ltd (Elabscience, Houston, Texas, US). The experiments were conducted according to the manufacturer's instructions. The absorbance of each sample was measured by mean of a multiplate reader (Infinite 200Pro, TECAN, Männedorf, Switzerland) at the wavelength of 450 nm and the total amount of proteins was calculated in pg/mL by mean of standard curves.

2.8 Endotoxin quantification

For the detection of endotoxin content in the two DEP samples (Euro 3, Euro 6 DPF) used for the in vitro test, a LAL Chromogenic Endotoxin Quantitation Kit (Thermo Scientific™ Pierce™) was used following the manufacturer's instructions, working in sterile condition and with endotoxin-free materials. The absorbance of each sample was measured by a multiplate spectrophotometer (Infinite 200Pro, TECAN, Männedorf, Switzerland) at the wavelength of 405-410nm. The developed colour intensity is proportional to the amount of endotoxin present in the sample and can be calculated using a standard curve and express as EU/mL.

2.9 Flow cytometry: detection of DNA double strand breaks and reactive oxygen species

The capability of UFPs, from both Euro 3 and Euro 6 DPF regeneration, to induce the expression of phospho-histone H2AX (y-H2AX), as marker of DNA double-strands breaks (DSBs) and to trigger intracellular reactive oxygen species generation was analysed through flow cytometry, as previously described (Bengalli et al. 2019) . Briefly for measuring DNA DSBs, BEAS-2B cells were probed with the rabbit mAb anti-yH2AX Alexa Fluor 488 Conjugate (Cell Signalling, Leiden, The Netherlands). After 24 h of exposure cells were detached, washed in PBS, fixed in 1% paraformaldehyde in PBS, suspended in 90% cold methanol and stored overnight at −20 °C before the analysis. Samples were then stained for y-H2AX following manufacturers' instructions and analysed at the CytoFLEX (Beckman Coulter, Milan, Italy) in the FITC channel (Excitation wavelength= 488 nm; Emission Wavelenght= 525 nm). To analyse the production of intracellular ROS, BEAS-2B cells were

pre-incubated over 30 min with the probe Carboxy-2´,7´-Dichlorofluorescein Diacetate (carboxy-DCFDA, 5 µM, Life Technologies) and then treated with DEPs over 3 h. The signal from unloaded samples (cells not stained with carboxy-DCFDA) were subtracted from the values to DCFDA stained samples. The intensity of fluorescence, in the FITC channel, was examined by flow cytometry (CytoFLEX, Beckman Coulter) and analysed using the program CytoExpert.

2.10 Cell morphology

For immunostaining, BEAS-2B cells were fixed with 4% paraformaldehyde and, after washing with PBS, cells were incubated over 60 min with PBST (BSA 2%, PBS 1X with 0.1% Tween20; Sigma Aldrich, Pero, Italy) which allows the blocking of non-specific sites. The coverslips were incubated with the Rabbit mAb anti-β-Tubulin (9F3) conjugated to Alexa Fluor 488 (Cell Signaling). Cytoskeleton actin was marked with phalloidin-rodhamine (1:150, Cytoskeleton Inc.). Slides were mounted with VECTASHIELD ® Antifade Mounting Medium (Vector Laboratories Inc., Burlingame, CA, US). The images were acquired with a Zeiss AxioObserver Z1 Reverse Microscope and processed with the Zeiss ZEN (Blue edition) software.

2.11 Statistical analysis

The data represent the mean and standard errors (SE) of at least three independent experiments. Statistical analysis was applied using Graph Pad Software, using un-paired t-test or One-Way ANOVA and relative post-hoc analysis. Values of $p < 0.05$ were considered statistically significant.

3- Results and discussion

3.1 Particulate sampling and emission measurements

Modal particle exhaust emission detected with ELPI and EEPS was initially considered to analyse the whole number of particles emitted for both testing vehicles over both test cycles. Figures 2 A.1 and A.2 shows particle number (PN) modal exhaust emission detected for Euro 3 vehicle over the Artemis Urban Cycle. PN emission detected with EEPS is on average just slightly higher than PN detected with ELPI, as EEPS is generally more sensitive

for UFPs and nanoparticles measurement, which are typically the most emitted ones by diesel engines (Kittelson 1998).

Figure 2 B.1 and B.2 show PN exhaust emission detected for Euro 6 vehicle over the WLTC. The DPF regeneration approximately started at the second 880 of WLTC and was detected by both PN analyzers. Coherently with PN exhaust emission detected for Euro 3, EEPS measurements for Euro 6 show higher PN values here as well, compared with ELPI.

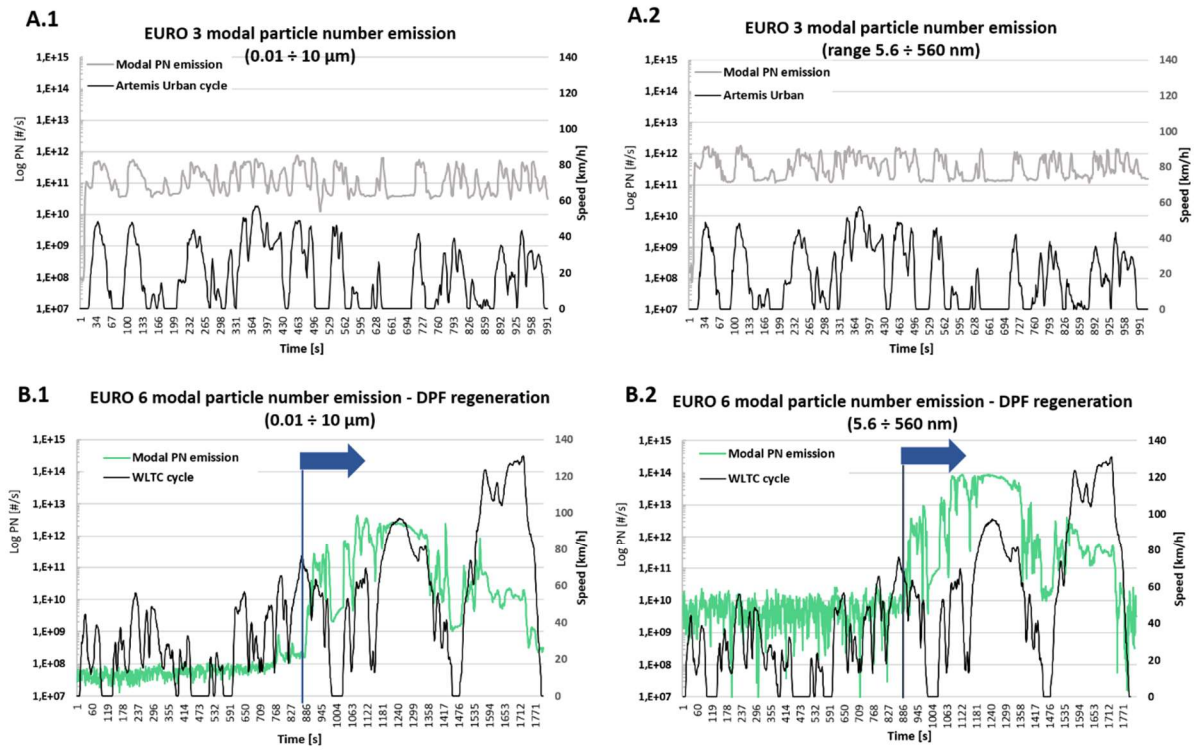

Figure 2. Particle Number (PN): modal exhaust emission from Euro 3 (A.1;.A.2, reported in grey) and from Euro 6 vehicle also over regeneration (B.1; B.2, reported in green), were detected respectively over Artemis Urban and WLTC cycle and measured with ELPI (A.1;B.1) and EEPS (A.2;B.2). The speed profile of both cycles is reported in black. Blue arrow indicates the beginning of the DPF regeneration.

As long as the DPF works regularly, it is clear that Euro 6 exhaust particle emission, even at higher speeds, is much lower than the Euro 3 one, as DPF very efficiently reduces the solid particle emission (Giechaskiel 2020)(Fiebig et al. 2014). When the DPF regeneration occurs

(blue arrows in Figure 2) the total particle emission increases, with similar speeds, on average up to four order of magnitude compared to DPF normally working.

Data from Euro 6 with DPF regeneration are compared to EURO 3 in Figure 3, in which the particle number size distributions were obtained by averaging the whole tests values measured with EEPS and ELPI. These were related to the typical trimodal distribution (Kittelson 1998), nuclei, accumulation and coarse mode, whose size ranges are here represented within arrows.

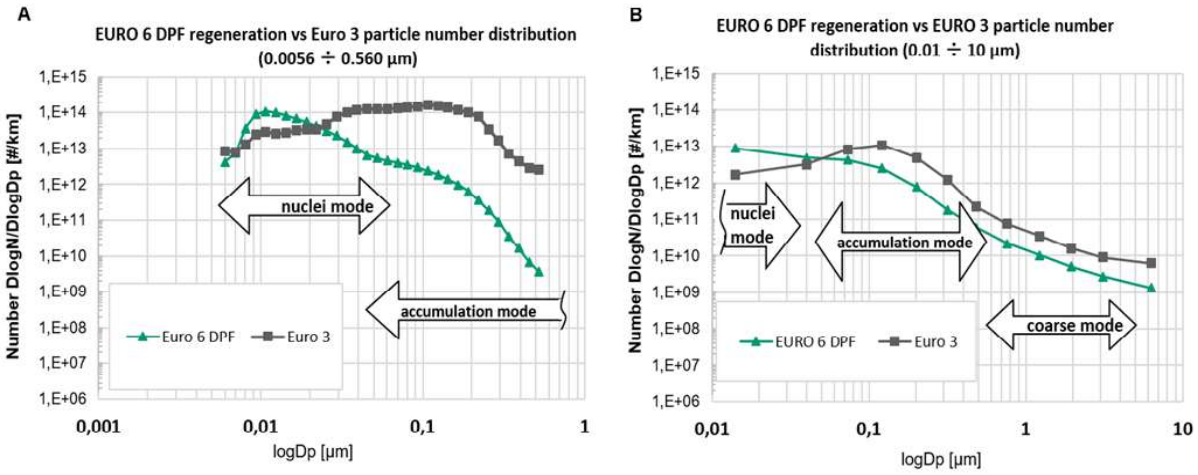

Figure 3. PN size distributions obtained from EEPS (A) and from ELPI (B). Typical engine exhaust particles formation processes related to their diameter are showed by the arrows.

Size distributions could be well described by using a log-normal function (Rissler et al. 2012). Figure 3 shows that Euro 3 exhaust particle emission is higher over Artemis Urban than the Euro 6 one over WLTC (with the occurrence of DPF regeneration), in the ranges corresponding to accumulation and coarse modes. As Kittelson reported, most of the diesel exhaust particulate mass corresponds to the accumulation mode, whose particles are known to be composed of carbonaceous agglomerates and adsorbed materials (Seigneur 2009) (Zeraati-Rezaei et al. 2020). In Figure 3 it is also showed that, although the 2.5 µm cut point stage was used to collect DEP, most particles measured with ELPI, can be classified as UFPs since they are smaller than 0.1 µm for both testing vehicles.

The nuclei mode particles are identified in the range of 0.005—0.05 μm of aerodynamic diameter, and typically consist of sulphur and volatile organic compounds, solid carbon and metals (Kittelson 1998). Nuclei mode was not accurately detected by ELPI, due to its low sensitivity for nanoparticles measurement (Dp < 50 nm), but EEPS measurements well complemented this deficiency: Euro 6 over WLTC, with DPF regeneration occurring, emitted higher nuclei particles number than Euro 3 did over Artemis Urban cycle. For Diesel exhaust, the nuclei mode typically covers <10% of the particle mass but >90% of the total particle number (Kittelson 1998).

The percentage of solid particles was not investigated in this work, therefore volatile and non-volatile exhaust particles were taken into account as a whole and showed with charts in Figure 2 and 3. Due to the amount of particles emitted from Euro 3 tests and from the regeneration phase of Euro 6 tests, the particle analysers were found to measure the highest particle emission peaks over their suitable measuring range, which should advice to carefully interpret their absolute values, as measurement artefacts may have occurred. However, these particulate emission data suggest a possible different impact on human health given by a constant high emission from a Euro 3 vehicle compared to a limited (strictly when the DPF regeneration occurs) high emission from a DPF-equipped Euro 6 one, defining a remarkably different human health risk exposure for the two vehicles. Considering PM10, as the widest used parameter for atmospheric particulate pollution, the number size distributions of particles less than 10 μm of the two vehicles are shown in Figure 4, as estimated from the ELPI results, in combination with respiratory deposition fraction curves. The LDSA values are considered as a relevant metric for the negative health effects of aerosol particles since the side effects and the reactivity of the particles within the lung is related to the surface area and number of particles (Kuuluvainen et al. 2016). The aerodynamic number size distribution of particles less than 0.1 μm shows that Euro 3 emitted less UFPs than Euro 6 during regeneration of DPF. While the number of fine fraction (< 2.5 μm) of PM results to be higher in EURO 3 respect to EURO 6 during DPF regeneration (Supplementary S.1). Deposition in the human respiratory tract can be predicted using the ICRP model (ICRP 1994) and the respiratory deposition fraction curves could be useful in understanding how the deposition of the particles changes in the

different area of the respiratory system based on particles diameter. For the construction of the curves, the value referred to an adult male was used (Supplementary S.2).

Particles smaller than 0.1 µm can reach the deeper area of respiratory system (tracheobronchial, alveolar region). UFPs can also translocate from the epithelial surface into the interstitium, enter the pulmonary blood circulation and consequently reach other organs, causing endothelial dysfunction, systemic inflammation, and also coagulation alterations that can induce cardiovascular disease (Schraufnagel 2020). As reported in a study on the deposition of DEP in the human respiratory tract, an aerosol with a high number of nucleation mode particles lead to a higher number of lung deposited particles (Rissler et al. 2012). In evaluating the health risk associated to the exposure to Euro 6 particle emission, it must be considered that a DPF has to be emptied regularly, but this is usually done during "regeneration" when the exhaust temperature's high enough, on highways or fast roads, instead of Euro 3 without DPF whose PM emissions are steadily higher also in the traffic condition in an urban area. This means that the Euro 6 contribution to primary particulate pollution is usually limited in the urban areas. Although DPF regeneration tends to occur at high speed, in a recent work it has been reported that regeneration could occur also in a stop-and-go traffic condition (Valverde and Giechaskiel 2020).

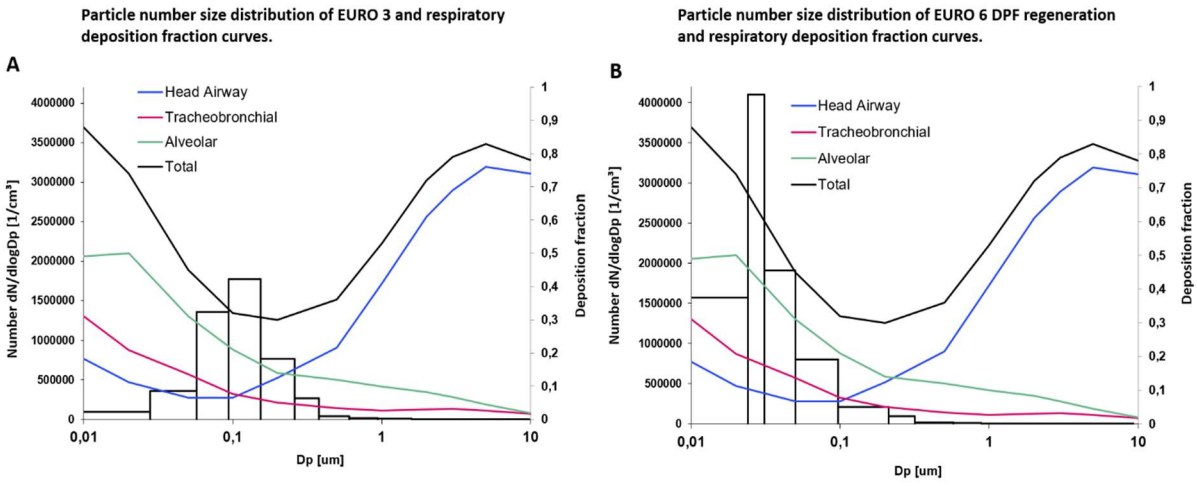

Figure 4. Histograms of the particle number size distributions (flow rate 10L/min) compared to the respiratory deposition fraction curves for alveolar (AL), tracheobronchial (TB), head airway (HA) regions and total deposition in an adult male (Breathing rate =1.50 $m^3 h^{-1}$)(Hinds, 1999). Figure A represent Euro 3 particles distribution and Figure B Euro 6 DPF particles distribution.

3.2 DEPs characterization

The chemical and physical properties of the emitted DEP depend on the engine technology, filtration devices and driving regime (Wang et al. 2019). The structure and size of particles are associated to their properties and determine their atmospheric residential time as well as their deposition pattern in the respiratory apparatus. The most used technique to characterize the structure of particles is TEM, which provides projected two dimensional properties of particles (Park, Kittelson, and McMurry 2004). TEM analysis showed that the two DEPs tend to form agglomerates. The single particles collected from Euro 3 (Fig.5 A.1; A.2) have similar morphology and the typical shape of soot particles, whereas particles derived from Euro 6 DPF regeneration (Fig.5 B.1; B2) have a more heterogeneous electron density and irregular shape and they present some filamentous structure (Figure Supplementary S.4), not observed in DEP Euro 3. As reported by Jung and colleagues diesel combustion might unintentionally lead to the necessary condition for carbon nanotube (CNTs) formation. In fact TEM analysis show DEPs having CNT-like structures , and the authors also supposed that Fe can act as catalytic metals require for CNTs formation (Jung et al. 2013).

Metals and Polycyclic aromatic hydrocarbons (PAHs) are known to play a considerable role in promoting cellular oxidative reactions and thus adverse health effects upon inhalation of combustion-derived particulate (Chen and Lippmann 2008). In this work metals content of the two samples was first analysed using EDX (Figure 5.C). Euro 3 particles seem to have a lower concentration of metals; Cu was excluded from the analysis because of the influence of the Copper grid where the sample is deposited. Euro 6 DEP present a higher concentration of Al, Fe, Ca, Mg, Si, S, Zn compared to Euro 3 ones. In a previous work (R.Bengalli et al. 2019) Al and Ca were also identified as predominant element in Euro 4 DEP. This was also reported by Wang and colleagues (Wang et al. 2003), indeed they noted that the concentrations of “crust elements” (including Al, Ca, Fe) was much higher than those of anthropogenic elements (including Cd, Co, Cr, Cu, Mn, Ni, Pb, Ti, V, and Zn) in DEP release under the transient-cycle condition. Moreover, clusters of crustal material (containing Ca, Al, Fe) were predominantly associated with measures for inflammation and acute toxicity (Chen and Lippmann 2008). An additional EDX analysis suggests that Euro 6 DPF presents some particles richer in metals (Fe, Zr) (Supplementary S.6), which are among

the additives used for the coating of DPF for the promotion of soot oxidation (Choi 2006). The elemental composition of the more electron dense particles from Euro 6 was analysed by EDX and compared with that of the lighter particles in the same sample. The results showed a higher content of Fe and Zr in the darker particles (Supplementary S.6). Similar results were obtained by comparing the EDX results coming from selected wider areas of the two DEPs. In fact, Euro 6 particles showed Fe peaks, which were not observed in Euro 3 ones. Considering these results, more attention should be payed to the presence of Fe in the exhaust of latest diesel vehicles, its possible catalytic role in CNTs formation, as well as in intracellular ROS formation. ICP-MS elemental analysis of the two DEPs was also carried out, and the results reported in the Supplementary figure S.3, showed that among the 15 elements analysed, Fe is the most abundant one in Euro 3, followed by Al and P. The limit of this analysis is related to the small amount of particles collected on the filters and the consequent possible underestimation of some elements. This is especially true for the Euro 6 DEP sample due to sampling difficulty during regeneration of DPF, in fact the ICP-MS analysis indicates a high concentration of only three metals: Cu, Al and K. The other elements are under the detection limits.

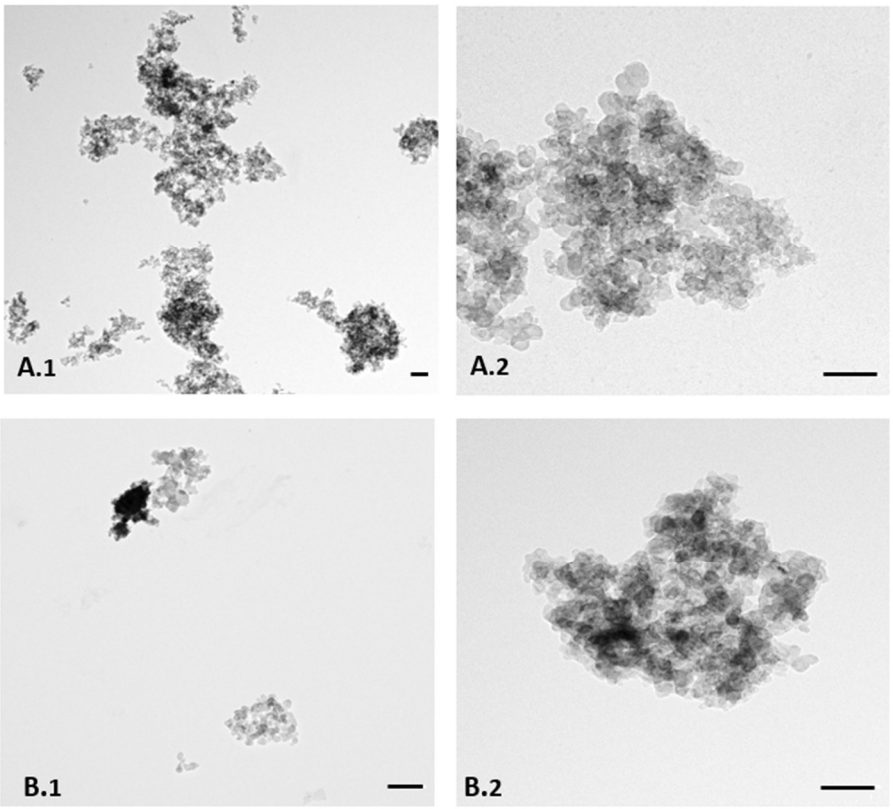

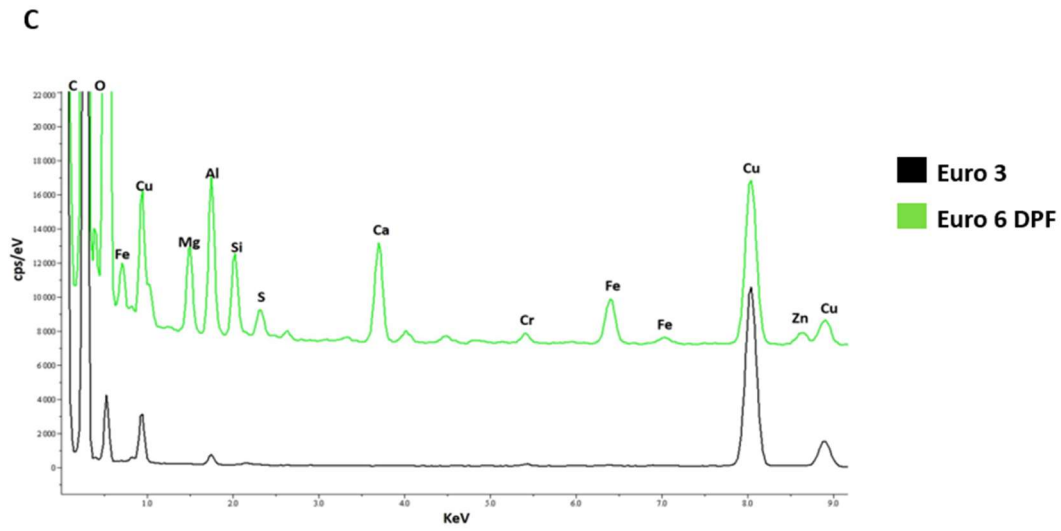

Figure 5: Morphological characterization of DEP. TEM images of Euro 3 DEP (A.1; A.2); DEPs Euro 6 over DPF regeneration (B.1; B.2). Scale bars: 100 nm (A.1; B1); 200 nm (A.2; B.2). EDX Spectrum (C), of Euro 6 DPF (Green line) and Euro 3 ones (Black line).

Besides metals and other trace elements, on the carbonaceous core of DEP organic compounds can also be absorbed, including PAHs and nitro-PAHs. PAHs present in diesel fuel are mainly retained or destroyed before being emitted, however the PAHs present in diesel have an important contribution to total emissions of PAHs (de Souza and Corrêa 2016). Since the same type of fuel was used for both testing vehicles, the difference in PAHs concentration might depend on the type of engine and sampling condition. The determination of PAHs concentrations reveals that in both samples the most abundant PAH is Phenanthrene, which was previously identified as the PAH present in higher concentration in DEP organic extract compared with other chemicals (Holme et al. 2019). Euro 3 particles result to be more enriched in total PAHs (394 ng/mg) compared to EURO 6 ones (261 ng/mg). Due to the limited amount of samples available for the chemical characterization, some PAHs (Dibenzo[a,h]anthracene; Indeno[1,2,3-cd]pyrene; Benzo[g.h.i]perylene) resulted to be under the detection limit.

Polycyclic aromatic hydrocarbons (ng/mg)

	EURO 3	**EURO 6 DPF**
Fluorene	10	9
Phenanthrene	135	106
Anthracene	22	6
Fluoranthene	70	25
Pyrene	81	33
Benzo[a]anthracene	26	36
Chrysene	10	11
Benzo[b]fluoranthene	16	11
Benzo[k]fluoranthene	10	16
Benzo[a]pyrene	14	9
Dibenzo[a,h]anthracene	/	/
Indeno[1,2,3-cd]pyrene	/	/
Benzo[g.h.i]perylene	/	/
Total	**394**	**261**

Table 1: PAHs concentration (ng/mg) in Euro 3 particulate and Euro 6 DPF one.

Analysing the particles behaviour in the cell culture medium by DLS, the results showed that both DEPs form agglomerates of similar size, with mean hydrodynamic size of 328.87 ± 4.7 nm and 317.47 ± 1.9 nm for Euro 3 and Euro 6 respectively, confirming that almost all the sampled particles can be classified as ultrafine.

The analysis of cytochrome-c reduction in a cell-free system after the exposure to the DEP extracted from the filters showed that particles from Euro 3 possess a slightly higher oxidative potential (1.8-fold increase) in respect to Euro 6 from DPF regeneration ones (1.5-fold increase) (Figure 6) (Supplementary S.5). It is known that free radicals cause oxidative damage to biological macromolecules and are involved in the activation of different intracellular signalling pathway that could lead to toxicity (Leikauf, Kim, and Jang 2020).

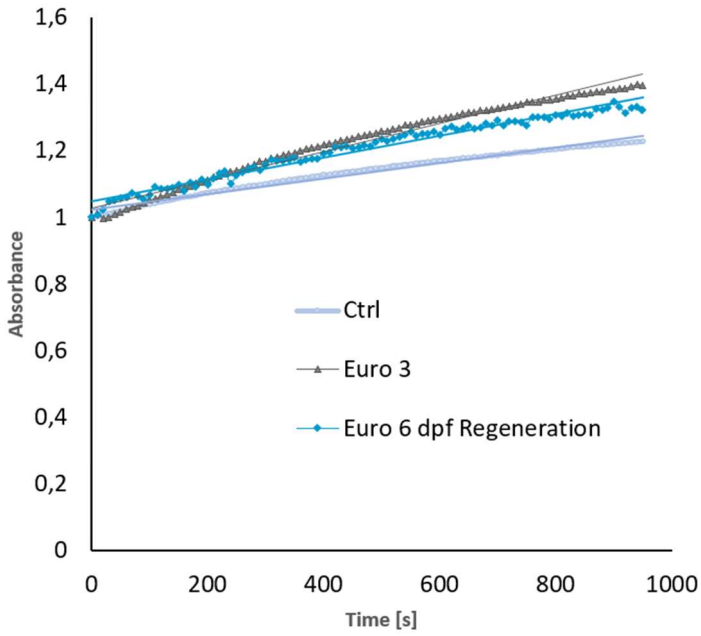

Figure 6: Progress curves of cytochrome C reduction of Euro 3 particles, Euro 6 DPF Regeneration ones and Ctrl (Water) normalized on time point 0.

3.3 Biological assays

In the present study we decided to use a single subtoxic DEP concentration of 50 μg/mL to compare the biological effects of the two DEPs. Moreover, a critical aspect in the *in vitro* studies is working with concentrations representative of a real exposure condition to PM in an urban centre. For this reason, it is necessary to reconcile the in vivo PM exposures, measured as ($\mu g/m^3$), with the DEP concentrations in cell cultures, measured as μg/mL. This was previously done by Li and colleagues proving that the in vivo dose of DEP ranges from 0.2 to 20 $\mu g/cm^2$ (Li et al. 2003). This evidence supports the choice to expose cells with a concentration of 50 μg/mL, which corresponds to 5 $\mu g/cm^2$ in the cell culture conditions here used.

BEAS-2B cells viability was assessed by MTT assay and Trypan Blue. The data obtained revealed that the two DEPs do not significantly affect cell viability. A slight decrease in cell viability was observed only after exposure to Euro 3 particles (Fig.7 A, B), confirming that the exposure conditions used may be considered as able to induce sub-acute toxic effects. Similar results were obtained in previous *in vitro* studies on DEP toxicity, where the vascular effects, possibly involved in aetiology and exacerbation of pulmonary and cardio vascular diseases or the autoimmune and carcinogenic ones, have been considered (Bengalli et al. 2019) (Pierdominici et al. 2014). On the contrary, in another study (Nakamura et al. 2012) it was found out that mouse-derived splenic mononuclear cells co-cultured with environmental nanoparticles generated from a diesel engine significantly reduced cell viability at 50 μg/mL.

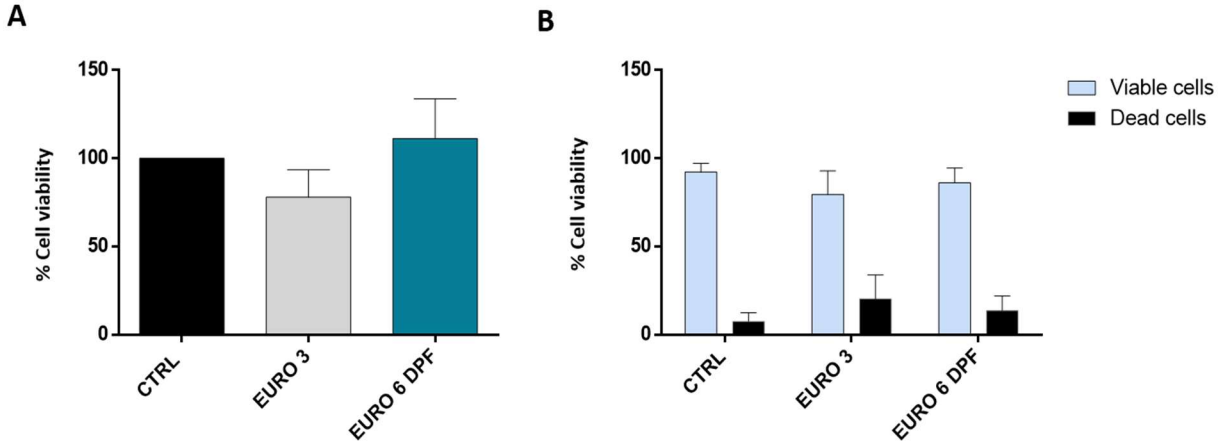

Figure 7. Cell viability. MTT assay (**A**) histograms represent the percentage, respect to control cells (Ctrl, 100%), of viable cells after the exposure to 50 µg/mL of UFPs from Euro 3 and Euro 6 DPF regeneration. Data show the mean ± SE (n = 3). Trypan Blue assay (**B**) histograms represent the percentage of viable cells and dead cells after the exposure to 50 µg/mL of UFPs from Euro 3 and Euro 6 DPF regeneration; data show the mean ± SE (n = 3).

To exclude that the release of proinflammatory mediators could have been determined by the presence of bacterial contamination in DEP samples, the levels of endotoxins were quantified and resulted below 1 EU/ml (Supplementary S.7), which can be considered negligible and suggesting that the inflammatory response observed after exposure to DEP was due to other compounds rather than biological contamination.

Many studies have indeed suggested that ambient PM in general, including DEP, initiates an inflammatory response that is associated with upregulation of different cytokines and chemokines and finally causes cellular injury. Among them, commonly secreted proteins measured *in vitro* studies are the cytokines IL-6 and IL-8 (Carter et al., 1997;). Moreover, it has been recently demonstrated that BEAS-2B cells exposed to DEP overexpressed and released other key inflammatory mediators, like IL-24 and EREG (Grilli et al., 2018). The deregulation of the latter marker is also known to contribute in the progression of the carcinogenic process.

For the reasons mentioned above, in our study we selected four biomarkers (IL-6, IL-8, IL-24 and EREG) to compare the inflammatory effects of DEP from Euro 3 and Euro 6 vehicles.

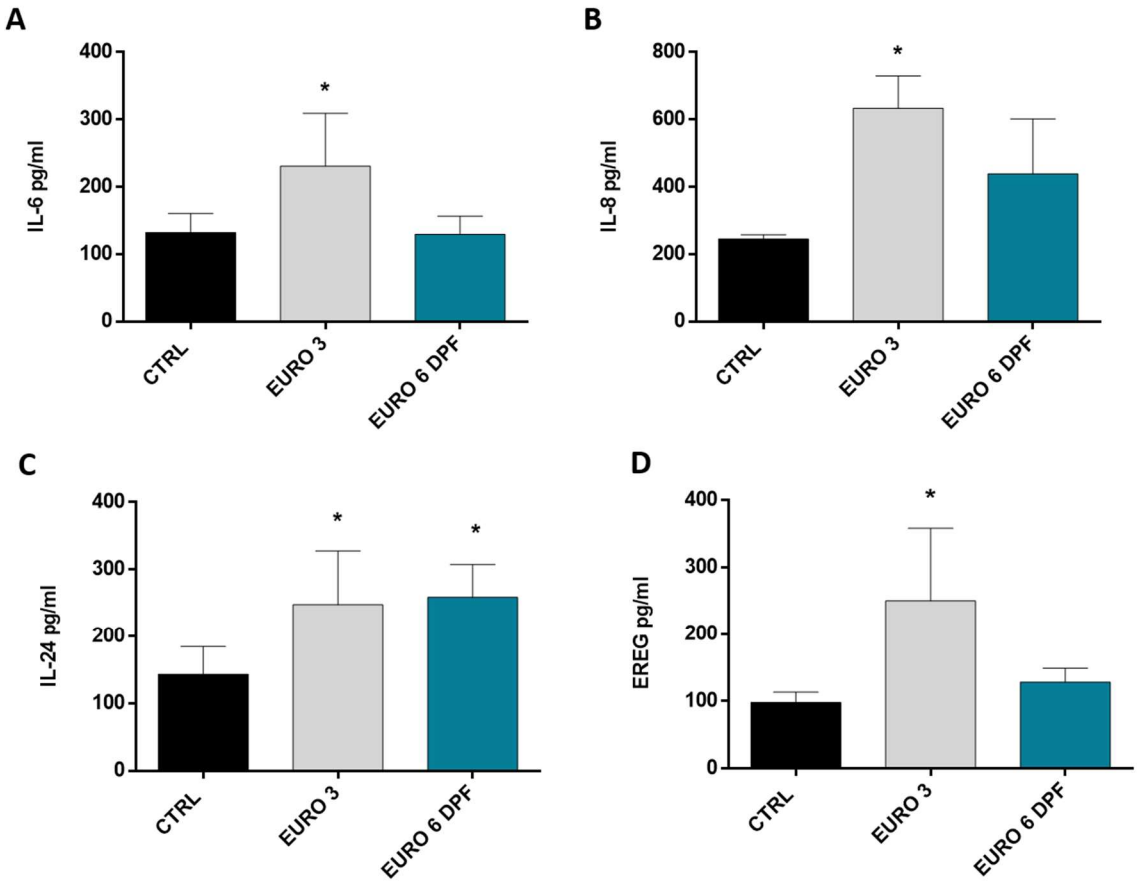

Figure 8: Inflammatory response. The release of the pro-inflammatory cytokine IL-6 (**A**); IL-8 (**B**); IL-24 (**C**) and EREG (**D**) was evaluated in BEAS-2B supernatants after the exposure for 24 h 50 µg/mL to the two different DEP. Data are presented as pg/mL and the histograms represent the mean ± SE of at least three independent experiments. * Statistically significant according One-Way ANOVA; $p < 0.05$. Post hoc test: Dunnett's Test.

Figure 8 shows that a significant increase in the release of IL-6, IL-8, IL-24 and EREG occurred after exposure to Euro 3 DEP compared to the control, while the exposure to Euro 6 DPF regeneration DEP only induced a significant increase of IL-24. The results on IL-6 and IL-8 are in line with other studies investigating the inflammatory response of lung cells after exposure to PM 2.5 (Longhin et al. 2018) and to DEP (Mazzarella et al. 2007)(Skuland et al.

2017)(Takizawa et al. 2000). IL-8 is a key chemoattractant chemokine involved in the activation and recruitment of neutrophils (Bickel 1993). Tal and colleagues demonstrated that the exposure to a low organic-containing DEP stimulates IL-8 expression trough a NF-kB-dependent pathway, while exposure to high organic-containing DEP induced IL-8 expression by a mechanism that requires the activity of the transcription factor AP-1 (Tal et al. 2010). IL-6 is a multifunctional cytokine involved in the regulation of the immune response, inflammation expression and haematopoiesis (Tanaka et al. 2014); this interleukin is also involved in endothelial activation after exposure of lung alveolar cells to DEP (Bengalli et al. 2017). In our results both DEPs resulted effective in inducing an increase in Interleukin-24 (IL-24), which is a protein of the IL-10 family of cytokines, selectively inducing apoptosis in various cancer cells, and with a role in cell growth and differentiation, thus playing as antitumor signal (Emdad et al. 2009). Another biomarker here evaluated is EREG, which is a protein involved in the development of cancer. Data showed that only Euro 3 DEP did increase EREG secretion, while Euro 6 ones did not. EREG modulation has been reported before in BEAS-2B cells exposed to Euro 4 DEP and PM (Grilli et al. 2018) (Gualtieri et al., 2012).

All in all, when considering the above markers of inflammation and carcinogenicity, EURO 3 DEP appeared to induce a stronger biological response respect to DEP from Euro 6 DPF regeneration. The higher increase of the inflammatory biomarkers after exposure to Euro 3 might be the consequence of the higher PAHs concentration, which in turn may trigger an aryl hydrocarbon receptor (AhR)-mediated cell response (Holme et al. 2019).

Due to their chronic exposure to PM, epithelial cells of respiratory tract are at greater risk of DNA damage induced by oxidative stress and carcinogens (Risom, Møller, and Loft 2005). The presence of DNA damage triggers cell cycle arrest, a mechanisms that allows cells to correct potential genetic defects (Pellegata et al. 1996). DNA damage was here evaluated with the analysis of the expression of the biomarker for DNA double-strand breaks, γ-H2AX. The results show an increased expression of γ-H2AX after 24 h of exposure to Euro 3 DEP (2.2-fold increase) and a slight, but statistically significant, increase (1.5-fold increase) after the exposure to DEP from Euro 6 DPF regeneration (Fig. 9). As reported by Kowalska and colleagues the exposure to DEP induces genotoxicity with increased frequencies of micronuclei, or deregulated expression of genes involved in DNA damage in BEAS-2B and

A549 cells, but do not significantly induces γ-H2AX- detectable double-strand breaks (Kowalska et al. 2017), while Douki and colleagues reported that in the lungs of diesel-exposed rats can occur a limited induction of γ-H2AX (Douki et al. 2018) and Bengalli and colleagues have reported that DEP from a Euro 4 vehicle induces a significant increase of this marker in BEAS-2B cells (Bengalli et al. 2019).

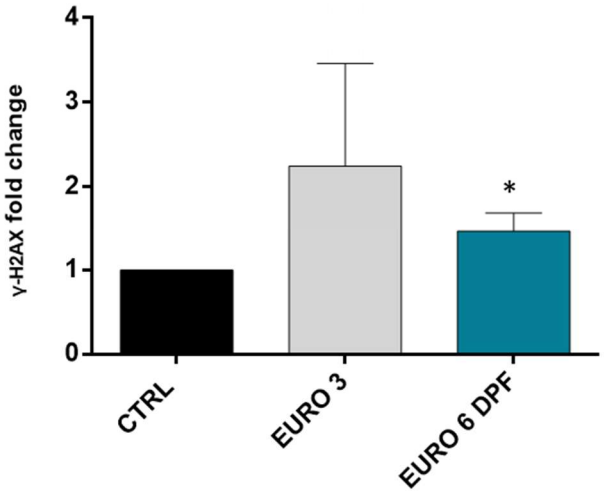

Figure 9. DNA damage: DNA damage was investigated after 24 h of exposure to three different UFPs by measuring with cytofluorimetric analysis the expression of γH2AX. Data represent the mean ± SE of at least three independent experiments. *Statistically significant respect to control according to un-paired t test; $p < 0.05$.

Moreover, DEP is recognised to induce free radicals, which may lead to an increase in cell oxidative stress. Indeed previous studies have proved that the increased ROS after DEP exposure may trigger other cell responses, like the inflammatory ones (Ji et al. 2018), by activating specific mechanisms involving Nuclear factor-κB (NF-κB), activation protein-1 (AP-1), nuclear factor erythroid 2 related factor 2 (Nrf2), and CREB-binding proteins (CBPs)(Leikauf, Kim, and Jang 2020) (Bhargava A.; 2019). In our study DEP Euro 3 was able to induce the formation of ROS, with a fold increase of 1.7 with respect to the untreated control cells (Supplementary S.8), even if the data is not statistically significant. In addition, Euro 3 showed a higher oxidative potential in a cell free condition (Figure 6) compared to Euro 6 DPF. However, as shown in Supplementary data S.6 , Euro 6 emitted Fe-enriched particles during regeneration of DPFs, which in turn might contribute to increase the

oxidative stress risk over prolonged period of exposure, since it has been demonstrated that inhaled iron oxide particles induce mild pulmonary inflammation and lead to altered alveolar epithelial integrity, upon the oxidative injury catalysed by transition metals and the consequent acute pulmonary inflammation effects (Lay et al. 2001).

The interference with the organization of cellular cytoskeleton was qualitatively investigated by the evaluation of the morphological changes of both actin filaments and microtubules, by mean of F-actin and β-tubulin staining respectively (Figure 10). In normal BEAS-2B cells, polymerized actin filaments appeared well-defined and brightly red fluorescent, while microspikes of actin were evident in cells exposed to Euro 3 DEP. The presence of microspikes in BEAS-2B was observed also after exposure to PM (Longhin et al., 2018). Cells exposed to Euro 6-DPF regeneration show remarkable changes in the cytoskeletal organization, especially considering β-tubulin. Microtubules in fact appeared poorly organized, with evident foci of β-tubulin in almost all cells, in contrast with control cells, where the microtubular network appears well-organized. Such effect might be attributed to an inhibition in tubulin polymerization, which is known to be associated with G2/M cell cycle arrest (Kanthou et al. 2004). This evidence could be positively related to the increased level of the γH2AX expression, since it was previously reported that an increase of this DNA damage marker occurs in parallel to the mitotic arrest in G2/M (Tu et al. 2013).

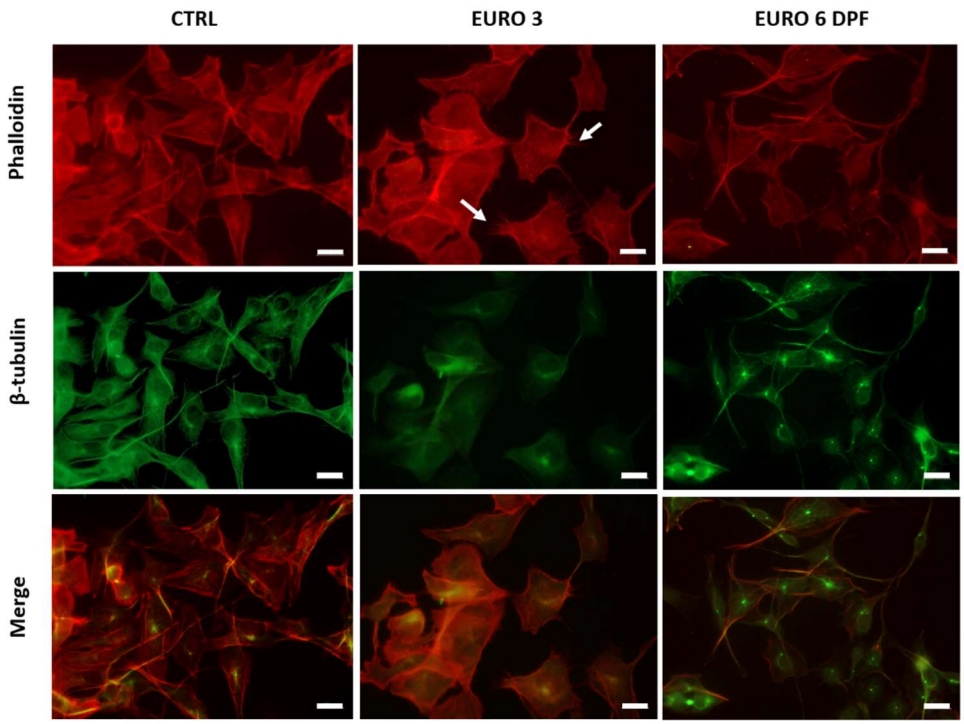

Figure 10. Cell morphology. Fluorescence images of unexposed BEAS-2B cells (CTRL) and cells exposed to DEP from Euro 3 and from Euro 6 DPF regeneration. White arrows indicate microspikes of actin. Microtubules were stained with Ab β-Tubulin (green) and actin cytoskeleton filaments with rhodamine phalloidin (red). Scale bars = 20 µm.

4-Conclusions

Differences in engine and emission-cleaning technologies may change the ratio of elemental carbon and the nucleation mode particles of condensed hydrocarbons and sulphate of the emitted DEP, and also the composition and amount of chemicals adhered to the surface of the particles (Hesterberg et al. 2011). Due to the requirement to force the DPF regeneration, the sampling activity turned out to be a limitation which partly affected the particles amount needed to both carry out chemical characterization and biological assay evaluations. In this work we show that although the latest generation diesel vehicle emits particulates only during regeneration, which generally occurs at high speeds, therefore mainly on highways and not in urban centres, the emission from Euro 6 during regeneration of DPF are characterized of a higher number of ultrafine particles compared to the old generation diesel vehicle ones. The emitted particles also resulted differing in physico-chemical composition, with Euro 6 showing less PAHs content than Euro 3, but

resulting enriched in some metals (e.g., Fe, Zr according to EDX-analyses). The *in vitro* biological analyses show that Euro 3 DEP activate the typical pathways (inflammation, carcinogenicity) induced by combustion-derived particles, while Euro 6 DPF regeneration DEP are less powerful in activating such biological responses, even if its physico-chemical peculiarities might have been responsible for the sub-acute effects registered in this work, like the induction of DNA-repair enzymes and the alteration of the microtubular dynamics. These preliminary evidences suggest that further investigations are required to better address the toxicological risk of the emissions during Euro 6 DPF regeneration. It should indeed be considered that our study might have been affected by the protocols required for sampling and preparing UFPs for the biological analyses and that more advanced in vitro models, directly exposed to the engine emission as a whole, are required for improving the relevance for human health impact.

The new diesel vehicles are approaching to reduce emissions and the consequent health effects of the exposed population, although it would be interesting to further investigate our preliminary results and deeper understand the difference between DEP emitted from old and new generation vehicles. The regulation of new diesel vehicles and pollution mitigation policies have been supported over the last years by several studies on the adverse effects induced by exposure to diesel exhaust which have led to incentives for the development of promising new technologies. In a future prospective of human health risk assessment, all impacts along life cycles of a vehicle should be considered and in the next years new generation diesel vehicles should be compared with alternative powered vehicles (electric, hybrid). Our results could help to clarify how the contribution to the health risk of diesel vehicle emissions over the last years has changed and to clarify the role of new generation diesel vehicles in urban pollution.

6.1 BIBLIOGRAPHY

André, Michel. 2004. “The ARTEMIS European Driving Cycles for Measuring Car Pollutant Emissions.” *Science of the Total Environment* 334–335: 73–84. https://pubmed.ncbi.nlm.nih.gov/15504494/

Badran, Ghidaa et al. 2020. “Toxicological Appraisal of the Chemical Fractions of Ambient Fine (PM2.5-0.3) and Quasi-Ultrafine (PM0.3) Particles in Human Bronchial Epithelial BEAS-2B Cells.” *Environmental Pollution* 263: 114620.

Bengalli, R. et al. 2019. “In Vitro Pulmonary and Vascular Effects Induced by Different Diesel Exhaust Particles.” *Toxicology Letters* 306.

Bengalli, Rossella et al. 2017. “The Role of IL-6 Released from Pulmonary Epithelial Cells in Diesel UFP-Induced Endothelial Activation.” *Environmental Pollution* 231: 1314–21.

Bickel, M. 1993. “The Role of Interleukin-8 in Inflammation and Mechanisms of Regulation.” *Journal of periodontology* 64(5 Suppl): 456–60. http://www.ncbi.nlm.nih.gov/pubmed/8315568 (April 27, 2020).

Cervero, Robert. 2013. “Linking Urban Transport and Land Use in Developing Countries.” *Journal of Transport and Land Use* 6(1): 7–24.

“COMMISSION REGULATION (EU) 2017/1151 of 1 June 2017 Supplementing Regulation (EC) No 715/2007 of the European Parliament and of the Council on Type-Approval of Motor Vehicles with Respect to Emissions from Light Passenger and Commercial Vehicles (Euro 5 A.” http://publications.europa.eu/resource/cellar/7d1c640d-62d8-11e7-b2f2-01aa75ed71a1.0006.02/DOC_1

Douki, Thierry et al. 2018. “Comparative Study of Diesel and Biodiesel Exhausts on Lung Oxidative Stress and Genotoxicity in Rats.” *Environmental Pollution* 235: 514–24.

Emdad, Luni et al. 2009. “Historical Perspective and Recent Insights into Our Understanding of the Molecular and Biochemical Basis of the Antitumor Properties of Mda-7/IL-24.” *Cancer Biology and Therapy* 8(5): 402–11.

Ferrero, Luca et al. 2019. “Chemical Composition of Aerosol over the Arctic Ocean from Summer

ARctic EXpedition (AREX) 2011–2012 Cruises: Ions, Amines, Elemental Carbon, Organic Matter, Polycyclic Aromatic Hydrocarbons, n-Alkanes, Metals, and Rare Earth Elements." *Atmosphere* 10(2): 54. http://www.mdpi.com/2073-4433/10/2/54

Fiebig, Michael, Andreas Wiartalla, Bastian Holderbaum, and Sebastian Kiesow. 2014. "Particulate Emissions from Diesel Engines: Correlation between Engine Technology and Emissions." *Journal of Occupational Medicine and Toxicology* 9(1): 6. http://occup-med.biomedcentral.com/articles/10.1186/1745-6673-9-6 .

Geiss, Otmar, Ivana Bianchi, and Josefa Barrero-Moreno. 2016. "Lung-Deposited Surface Area Concentration Measurements in Selected Occupational and Non-Occupational Environments." *Journal of Aerosol Science* 96: 24–37. http://dx.doi.org/10.1016/j.jaerosci.2016.02.007.

Giechaskiel, Barouch. 2020. "Particle Number Emissions of a Diesel Vehicle during and between Regeneration Events." *Catalysts* 10(5): 587. https://www.mdpi.com/2073-4344/10/5/587 .

Grilli, Andrea et al. 2018. "Transcriptional Profiling of Human Bronchial Epithelial Cell BEAS-2B Exposed to Diesel and Biomass Ultrafine Particles." *BMC Genomics* 19(1): 1–15.

Han, Huan et al. 2020. "Profiling Serum Cytokines in COVID-19 Patients Reveals IL-6 and IL-10 Are Disease Severity Predictors." *Emerging Microbes and Infections* 9(1): 1123–30.

Hesterberg, Thomas W et al. 2011. "Journal of the Air & Waste Management Association Particulate Matter in New Technology Diesel Exhaust (NTDE) Is Quantitatively and Qualitatively Very Different from That Found in Traditional Diesel Exhaust (TDE)." *Journal of the Air & Waste Management Association* 61(9): 894–913. https://www.tandfonline.com/action/journalInformation?journalCode=uawm20.

Holme, Jørn A. et al. 2019. "Potential Role of Polycyclic Aromatic Hydrocarbons as Mediators of Cardiovascular Effects from Combustion Particles." *Environmental Health: A Global Access Science Source* 18(1): 1–18. https://doi.org/10.1186/s12940-019-0514-2.

Ji, Jie et al. 2018. "Multi-Cellular Human Bronchial Models Exposed to Diesel Exhaust Particles: Assessment of Inflammation, Oxidative Stress and Macrophage Polarization." *Particle and Fibre Toxicology* 15(1): 1–16.

Jung, Heejung S., Art Miller, Kihong Park, and David B. Kittelson. 2013. “Carbon Nanotubes among Diesel Exhaust Particles: Real Samples or Contaminants?” *Journal of the Air and Waste Management Association* 63(10): 1199–1204.

K, Jantzen et al. 2012. “Oxidative Damage to DNA by Diesel Exhaust Particle Exposure in Co-Cultures of Human Lung Epithelial Cells and Macrophages.” *Mutagenesis* 27(6). https://pubmed.ncbi.nlm.nih.gov/22869610/

Kanthou, Chryso et al. 2004. “The Tubulin-Binding Agent Combretastatin A-4-Phosphate Arrests Endothelial Cells in Mitosis and Induces Mitotic Cell Death.” *American Journal of Pathology* 165(4): 1401–11.

Karjalainen, Panu et al. 2019. “Strategies to Diminish the Emissions of Particles and Secondary Aerosol Formation from Diesel Engines.” *Environmental Science and Technology* 53(17): 10408–16.

Kim, Jin Ah et al. 2016. “Diesel Exhaust Particles Upregulate Interleukins IL-6 and IL-8 in Nasal Fibroblasts” ed. Thomas H Thatcher. *PLOS ONE* 11(6): e0157058. https://dx.plos.org/10.1371/journal.pone.0157058 .

Kittelson, David B. 1998. 29 J. Aerosol Sci *ENGINES AND NANOPARTICLES: A REVIEW*.

Kowalska, Magdalena et al. 2017. “Genotoxic Potential of Diesel Exhaust Particles from the Combustion of First- and Second-Generation Biodiesel Fuels—the FuelHealth Project.” *Environmental Science and Pollution Research* 24(31): 24223–34. http://link.springer.com/10.1007/s11356-017-9995-0 .

Kuuluvainen, Heino et al. 2016. “Lung Deposited Surface Area Size Distributions of Particulate Matter in Different Urban Areas.” *Atmospheric Environment* 136: 105–13.

Lay, J. C., K. L. Zeman, A. J. Ghio, and W. D. Bennett. 2001. “Effects of Inhaled Iron Oxide Particles on Alveolar Epithelial Permeability in Normal Subjects.” *Inhalation Toxicology* 13(12): 1065–78. https://pubmed.ncbi.nlm.nih.gov/11696874/.

Leikauf, George D., Sang Heon Kim, and An Soo Jang. 2020. “Mechanisms of Ultrafine Particle-Induced Respiratory Health Effects.” *Experimental and Molecular Medicine* 52(3): 329–37. https://doi.org/10.1038/s12276-020-0394-0 .

Li, Ning et al. 2003. “Particulate Air Pollutants and Asthma. A Paradigm for the Role of Oxidative Stress in PM-Induced Adverse Health Effects.” *Clinical immunology (Orlando, Fla.)* 109(3): 250–65. http://www.ncbi.nlm.nih.gov/pubmed/14697739 .

Longhin, Eleonora et al. 2016. “Physico-Chemical Properties and Biological Effects of Diesel and Biomass Particles.” *Environmental Pollution* 215: 366–75.

Longhin, Eleonora et al. 2018. “Milan Winter Fine Particulate Matter (WPM2.5) Induces IL-6 and IL-8 Synthesis in Human Bronchial BEAS-2B Cells, but Specifically Impairs IL-8 Release.” *Toxicology in Vitro* 52: 365–73.

Mazzarella, G. et al. 2007. “Effects of Diesel Exhaust Particles on Human Lung Epithelial Cells: An in Vitro Study.” *Respiratory Medicine* 101(6): 1155–62.

McGonagle, Dennis, Kassem Sharif, Anthony O’Regan, and Charlie Bridgewood. 2020. “The Role of Cytokines Including Interleukin-6 in COVID-19 Induced Pneumonia and Macrophage Activation Syndrome-Like Disease.” *Autoimmunity Reviews* 19(6): 102537. https://doi.org/10.1016/j.autrev.2020.102537.

Nakamura, Ryosuke et al. 2012. “Effects of Nanoparticle-Rich Diesel Exhaust Particles on IL-17 Production in Vitro.” *Journal of Immunotoxicology* 9(1): 72–76.

Park, Kihong, David B. Kittelson, and Peter H. McMurry. 2004. “Structural Properties of Diesel Exhaust Particles Measured by Transmission Electron Microscopy (TEM): Relationships to Particle Mass and Mobility.” *Aerosol Science and Technology* 38(9): 881–89.

Pellegata, Natalia S., Ronald J. Antoniono, J. Leslie Redpath, and Eric J. Stanbridge. 1996. “DNA Damage and P53-Mediated Cell Cycle Arrest: A Reevaluation.” *Proceedings of the National Academy of Sciences of the United States of America* 93(26): 15209–14.

Pierdominici, Marina et al. 2014. “Diesel Exhaust Particle Exposure in Vitro Impacts T Lymphocyte Phenotype and Function.” *Particle and Fibre Toxicology* 11(1).

Preble, Chelsea V. et al. 2015. “Effects of Particle Filters and Selective Catalytic Reduction on Heavy-Duty Diesel Drayage Truck Emissions at the Port of Oakland.” *Environmental Science and Technology* 49(14): 8864–71.

Raudoniute, Jovile et al. 2018. “Pro-Inflammatory Effects of Extracted Urban Fine Particulate

Matter on Human Bronchial Epithelial Cells BEAS-2B." *Environmental Science and Pollution Research* 25(32): 32277–91.

Risom, Lotte, Peter Møller, and Steffen Loft. 2005. "Oxidative Stress-Induced DNA Damage by Particulate Air Pollution." In *Mutation Research - Fundamental and Molecular Mechanisms of Mutagenesis*, Elsevier, 119–37.

Rissler, Jenny et al. 2012. "Experimental Determination of Deposition of Diesel Exhaust Particles in the Human Respiratory Tract." *Journal of Aerosol Science* 48: 18–33.

Schraufnagel, Dean E. 2020. "The Health Effects of Ultrafine Particles." *Experimental and Molecular Medicine* 52(3): 311–17. https://doi.org/10.1038/s12276-020-0403-3 .

Schwarze, P. E. et al. 2013. "Inflammation-Related Effects of Diesel Engine Exhaust Particles: Studies on Lung Cells in Vitro." *BioMed Research International* 2013.

Seigneur, Christian. 2009. "Current Understanding of Ultrafine Participate Matter Emitted from Mobile Sources." *Journal of the Air and Waste Management Association* 59(1): 3–17.

Skuland, Tonje S. et al. 2017. "Proinflammatory Effects of Diesel Exhaust Particles from Moderate Blend Concentrations of 1st and 2nd Generation Biodiesel in BEAS-2B Bronchial Epithelial Cells—The FuelHealth Project." *Environmental Toxicology and Pharmacology* 52: 138–42.

de Souza, Carolina Vieira, and Sergio Machado Corrêa. 2016. "Polycyclic Aromatic Hydrocarbons in Diesel Emission, Diesel Fuel and Lubricant Oil." *Fuel* 185: 925–31.

Steerenberg, P. A. et al. 1998. "Diesel Exhaust Particles Induced Release of Interleukin 6 and 8 by (PRIMED) Human Bronchial Epithelial Cells (BEAS 2B) in Vitro." *Experimental Lung Research* 24(1): 85–100. https://www.tandfonline.com/doi/abs/10.3109/01902149809046056.

Takizawa, Hajime et al. 2000. "Diesel Exhaust Particles Activate Human Bronchial Epithelial Cells to Express Inflammatory Mediators in the Airways: A Review." *Respirology* 5(2): 197–203.

Tal, Tamara L. et al. 2010. "Differential Transcriptional Regulation of IL-8 Expression by Human Airway Epithelial Cells Exposed to Diesel Exhaust Particles." *Toxicology and Applied Pharmacology* 243(1): 46–54.

Tanaka, Toshio, Masashi Narazaki, and Tadamitsu Kishimoto. 2014. “Il-6 in Inflammation, Immunity, And Disease.” *Cold Spring Harbor Perspectives in Biology* 6(10): a016295.

New Diesels , new problems. Transport & Environment 2020. www.transportenvironment.org .

Tu, Wen Zhi et al. 2013. “Γh2AX Foci Formation in the Absence of DNA Damage: Mitotic H2AX Phosphorylation Is Mediated by the DNA-PKcs/CHK2 Pathway.” *FEBS Letters* 587(21): 3437–43.

Valverde, Victor, and Barouch Giechaskiel. 2020. “Assessment of Gaseous and Particulate Emissions of a Euro 6d-Temp Diesel Vehicle Driven >1300 Km Including Six Diesel Particulate Filter Regenerations.” *Atmosphere* 11(6).

Wang, Xiaochen et al. 2019. “An Overview of Physical and Chemical Features of Diesel Exhaust Particles.” *Journal of the Energy Institute* 92(6): 1864–88.

Zeraati-Rezaei, Soheil et al. 2020. “Size-Resolved Physico-Chemical Characterization of Diesel Exhaust Particles and Efficiency of Exhaust Aftertreatment.” *Atmospheric Environment* 222: 117021.

Zhu, Yongjian, Jingui Xie, Fengming Huang, and Liqing Cao. 2020. “Association between Short-Term Exposure to Air Pollution and COVID-19 Infection: Evidence from China.” *Science of the Total Environment* 727. https://pubmed.ncbi.nlm.nih.gov/32315904/ (October 4, 2020).

6.2 SUPPLEMENTARY DATA CHAPTER VI

Supplementary S.1 Particles Number divided in dimensional range emitted from EURO 3 and EURO 6 during DPF regeneration engines (Data from ELPI).

		Dp < 0.1µm	**0.1µm < Dp <2.5µm**	**Dp > 2.5µm**
Euro 3	Number dN/dlogDp [1/cm³]	541.5 x 10^4	396.1 x 10^4	0.2 x 10^4
Euro 6 DPF	Number dN/dlogDp [1/cm³]	1698.6 x 10^4	48.3 x10^4	0.2 X 10^4

Table S.1: Number of particles, divided in three-dimensional range (Dp< 0.1; 0,1µm < Dp <2.5µm and Dp > 2.5µm) counted using ELPI during the sampling of Euro 3 and Euro 6 DEP.

Supplementary S.2 Respiratory deposition data.

Deposition fraction

Particles (nm)	**Head Airway**	**Tracheobronchial**	**Alveolar**	**Total**
10	*0,183*	*0,31*	*0,49*	*0,88*
20	*0,112*	*0,208*	*0,5*	*0,74*
50	*0,066*	*0,1362*	*0,31*	*0,45*
100	*0,066*	*0,0774*	*0,21*	*0,32*
200	*0,124*	*0,0508*	*0,14*	*0,3*
500	*0,215*	*0,0344*	*0,12*	*0,36*
1000	*0,41*	*0,0272*	*0,099*	*0,53*
2000	*0,61*	*0,0304*	*0,083*	*0,72*
3000	*0,69*	*0,0311*	*0,067*	*0,79*
5000	*0,76*	*0,0272*	*0,045*	*0,83*
10000	*0,74*	*0,0172*	*0,019*	*0,78*

Table S2: Respiratory deposition data taken from (Hinds, 1999), in an adult male (Breathing rate =1.50 m3 h^{-1}).

Supplementary S.3 Trace Elemental Quantification.

Metals	EURO 3	EURO 6 DPF
V	*3,9*	*nd*
Cr	*37,2*	*nd*
Mn	*283,3*	*nd*
Co	*12,4*	*nd*
Ni	*580,5*	*nd*
Cu	*nd*	*8058,9*
Zn	*85,9*	*nd*
Cd	*nd*	*nd*
Pb	*14,7*	*nd*
P	*1676,5*	*nd*
Ti	*390,1*	*nd*
Al	*2611,5*	*181998,3*
K	*nd*	*52113,6*
Ca	*1592,9*	*nd*
Fe	*4017,0*	*nd*

Table S.3. Metals concentration (ppm) of Euro 3 and Euro 6 analyse in ICP-MS.

*nd: non detected.

Supplementary S.4 Characterization of Euro 6 DEP.

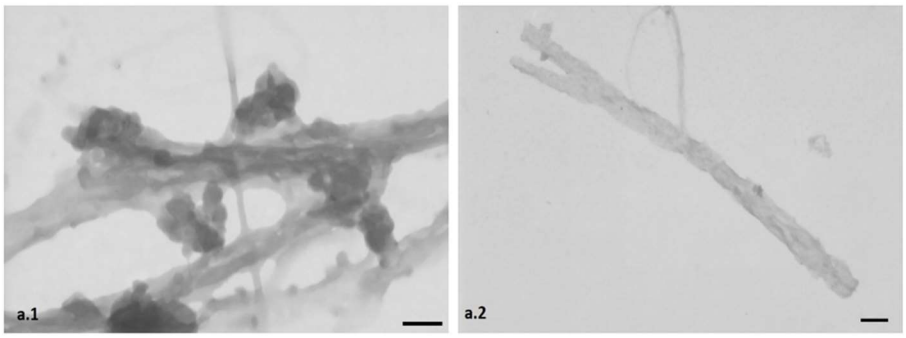

Figure S.4. Morphological characterization of DEP EURO 6 DPF (Scale bars a.1 100 nm; a.2 200 nm).

Supplementary S.5 Cytochrome-C

	ΔA/min ± SD	Fold change ± SD
Blank	0.012 ± 0	1 ± 0
Euro 3	0.022 ± 0.0035	1.83 ± 0.29
Euro 6 DPF regeneration	0.018 ± 0	1.5 ± 0

Table S.5 ΔA/min and Fold change of sample compared to control (Water), mean of three curves ± Standard deviation.

Supplementary S.6 EDX spectrum of Euro 6 DEP.

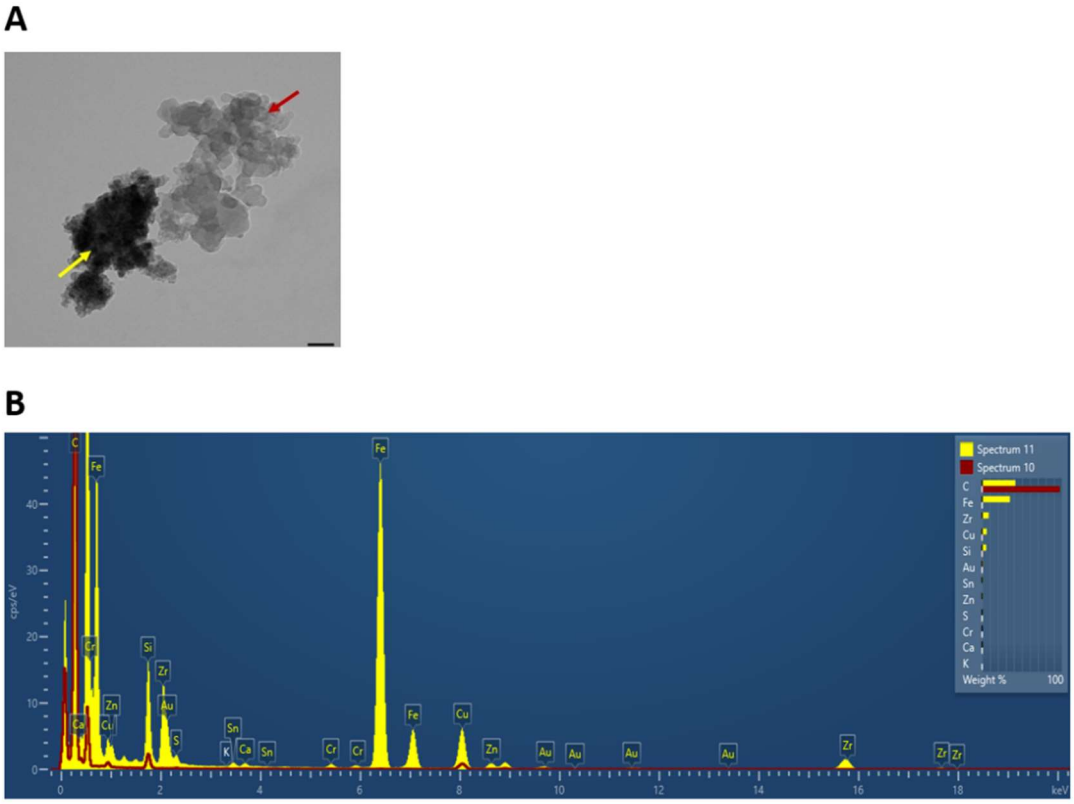

Figure S. 6: TEM images of Euro 6 DEPs (A) and respective EDX Spectrum (**B**), of dark particles (yellow arrow and line) and light particles (red arrow and line).

Supplementary S.7 Endotoxin quantification

Particles	EU/ml
EURO 3	0,857848
EURO 6 DPF	0,1143

Table S.7 : Endotoxin quantification (EU/ml) of Euro 3 and Euro 6.

Supplementary S.8 Oxidative Stress

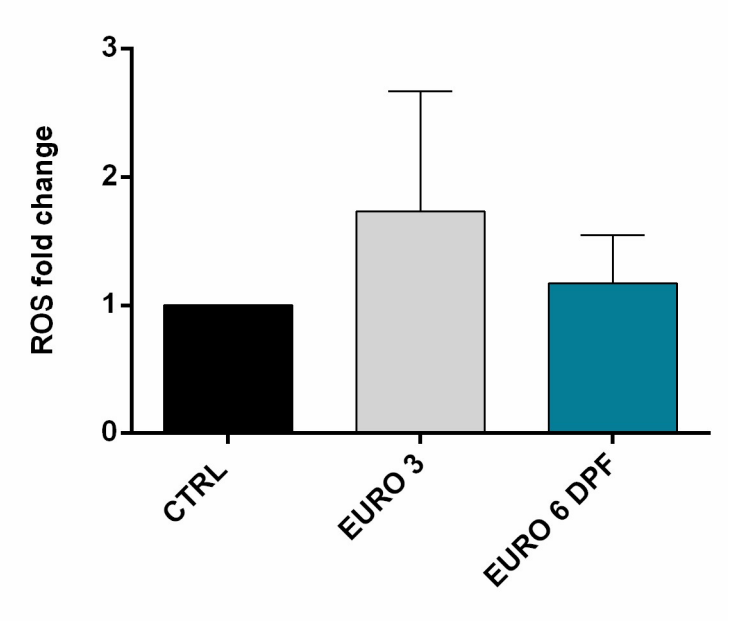

Figure S.8: Fold change of Reactive oxygen species (ROS) analysed in cytofluorimet

CHAPTER VII

COMPARISON BETWEEN THE TOXICOLOGICAL EFFECTS OF EURO 3 DIESEL EXHAUST PARTICLES AND BIOMASS COMBUSTION DERIVED PARTICLES ON BEAS-2B HUMAN BRONCHIAL CELLS

Combustion derived particles (CDPs) have been linked to several adverse health effects, including lung cancer. Diesel exhaust particles (DEP) and particles derived from biomass burning are two of the major exhaust-sources of fine and ultrafine CBPs in urban areas. The aim of the present study was to characterise and compare the PM emitted from a mobile (diesel vehicle) and a fixed (wood burning) exhaust source, with respect to their physicochemical properties and biological effects on human bronchial cells. Transmission electron microscopy (TEM) was used in order to characterize the particles morphology, while metal and polycyclic aromatic hydrocarbon (PAHs) content were determined through Inductively Coupled Plasma Mass Spectrometry (ICP-MS) and as chromatography with mass spectrometry (GC-MS), respectively. The effects on bronchial cells were studied, including cellular-uptake, cells cycle progression, inflammatory response, genotoxic effects and modulation of genes involved in several PM-activated pathways. The present study proved that biomass particles, produced by a modern stove propelled with beech wood, had a lower biological impact on bronchial cells compared to DEP derived from an old diesel engine (Euro 3). DEP was confirmed as a very hazardous component of the urban PM, since it is able to induce inflammation, genotoxicity and modulation of several genes involved in relevant cellular toxic responses. However, consequences on human health from a chronic exposure to wood particles cannot be excluded and need further investigations.

1-Introduction

In residential areas, anthropogenic sources of airborne particles are often more important than natural one in contributing to air pollution and quality. Diesel exhaust particles (DEP) and particles derived from biomass burning are among the main exhaust-sources of fine and ultrafine combustion derived particles (CBPs) in urban area (Longhin et al., 2016). Fine particulate matter (PM < 2.5 μm; $PM_{2.5}$) and ultrafine particles (UFPs) can be primary emitted from various sources or derived by gas-to-particle conversion of secondary products from atmospheric oxidation of SO_2, NOx, and hydrocarbons (Wolf & Hidy, 1997). Despite the technological progress and the improvement of environmental policies, in many urban areas in the European Union (EU), $PM_{2.5}$ concentrations still exceed European and WHO guidelines, resulting to an increase in premature mortality (WHO, 2013). Diesel engine has found widespread use in on-road vehicles and its exhaust contains a high number of fine particles and UFPs that causes adverse health effects and severe impact on the environment (Sydbom et al., 2001). Scientific evidences support the existence of a correlation between DEP exposure and the development of cancer in humans (IARC, 2012) (Risom et al; 2005a). DEP is known to induce inflammation and oxidative stress and an important portion of the mutagenic potential of traffic related particles is attributable to polycyclic aromatic hydrocarbons (PAHs) and metals absorbed on the carbonaceous core of particles (Pashin et al; 1979). Another important source of $PM_{2.5}$ and UFPs in residential areas itis constituted by biomass combustion. Therefore, there is an urgent need to comprehend whether the health implications that may occur following exposure to biomass-derived PM are comparable to those observed for PM originated from other sources (e.g., traffic). In the last years, in Europe many efforts have been made to reduce DEP emissions, with a consequent mitigation of pollution, thanks to emission abatement technology (Alozie and Ganippa; 2019). On the contrary, biomass combustion emissions are still poorly regulated, indeed there is a large difference of this emissions across EU Member States, due to diverse climatic conditions, regulations, technological standards and climate policies regarding the use of biomass (Amann; 2018). Exposure to wildfire and other biomass burning for residential heating is recognized as a relevant public health concern (Johnston et al., 2019). Although the most employed solid fuels are wood and other biomass sources, few epidemiological studies have analyzed their carcinogenic

potential yet. The importance to design additional researches in this field is also urged by the high concentrations of emissions that can be reached and by evidences showing that wood smoke is mutagenic in humans (WHO, 2010). Moreover, emissions from biomass fuels combustion has been classified as “probably carcinogenic to humans” (WHO, 2010). Studies on the toxicity of biomass CDPs have been focused on the cellular induction of reactive oxygen species (ROS) and the consequent oxidative damage, which trigger a signalling cascade that could lead to cytotoxicity, inflammatory responses and genotoxic effects (Pardo et al., 2020).

Moreover, precise knowledge about particle size, morphology and chemical composition is fundamental in order to understand the mechanisms by which particles could affect human health.

The aim of present study was to compare $PM_{2.5}$ emitted from a mobile (diesel vehicle Euro 3) and a fixed (wood burning stove) exhaust source, focusing on the physicochemical properties that may affect the toxicological profile of the tested particles.

The collected particles, hereafter called Euro 3 DEP and wood particles, were morphologically characterized by transmission electron microscopy (TEM) and particles metal was determined by Inductively Coupled Plasma Mass Spectrometry (ICP-MS). The amount and type of PAHs adsorbed on the two different kind of particles were analyzed in the two samples by gas chromatography with mass spectrometry (GC-MS). The effects on bronchial cells (BEAS-2B) were studied and focused on cellular-uptake, cells cycle, inflammation, genotoxic effects and modulation of genes involved in several PM-activated processes. The present research points out the importance of understanding the potential human health risk associated to CDPs exposure, through the comparison of the biological outcomes and the physicochemical characteristics of two different typical urban exhaust sources.

2-Materials and methods

2.1 CDPs collection and extraction

Euro 3 DEPs were sampled from a Euro 3 light duty vehicle without DPF run over a chassis dyno according to the "URBAN" Artemis Driving Cycle, as previously described (Chapter VI). Beech wood particles emissions, derived from a stove (Piazzetta Model e920, 8 kW) were sampled on Teflon filters after dilution of emitted gases with clean air. Both DEP and biomass particles were collected on Teflon filters (Whatman pure teflon filters), using a DGI-1570 (Dekati Gravimetric Impactor, Finland) to remove bigger aggregates (stage cut-point of 2.5 µm). Filters from diesel and wood combustion, were preserved at −20 °C after sampling and until particles extraction for chemical characterization or biological tests. Particles were extracted in pure sterile water by repeated cycle of 20 minutes of sonication in an ultrasound bath (Sonica Soltec). Particle suspensions were then dried into a desiccator, weighed with a microbalance and stored at - 20 °C until use for experiments, as reported before (Bengalli et al., 2019).

2.2 Characterization of particles suspensions

Characterization of particles suspensions was performed as previously described (Chapter VI). Briefly particles morphology was characterized by transmission electron microscopy (TEM), using a JEOL JEM 2100 Plus (JEOL, Japan) operating with an acceleration voltage of 200kV, and equipped with an 8-megapixel Gatan (Gatan, USA) Rio Complementary Metal-Oxide-Superconductur (CMOS) camera. Particles hydrodynamic size was measured by using dynamic light scattering (DLS) (Malvern Zetasizer, Malvern, UK) technique. DEP and Wood CDPs suspensions were diluted in culture medium (LHC-9, Gibco, Life Technologies, Monza, Italy) at a concentration of 50 µg/mL. PAHs were evaluated by GC/MS (GC/MS, Agilent Technologies, CA, USA in single ion monitoring (SIM) mode.). Metals were quantified by ICP-MS (Perkin Elmer SCIEX mod. ELAN 9000).

2.3 Cell culture and treatments

Bronchial cells were directly exposed to particles in a submerge condition for the biological experiments. BEAS-2B (ATCC® CRL9609™) cells were maintained in LHC-9 medium (Gibco, Life Technologies, Monza, Italy) at suitable grow condition (37 °C with 5% of CO_2). Cells were seeded at a density of 2.7×10^5 cells/well in 6-well plates and treated for 24 or 48 h with 50 μg/mL of CDPs, corresponding to 5 μg/cm^2. After the exposure times, media were collected and stored for cytokines release analyses, and cellular responses were evaluated.

2.4 Transmission Electron Microscopy

For transmission electron microscopy analysis, cells were cultured in 6-well plates and exposed either to Euro 3 DEP and wood CDPs for 24 h and then processed as previously described (Zerboni et al., 2019). Briefly, cells were fixed for 45 min in a 2% glutaraldehyde solution, subsequently, cells were centrifuged for 10 min at 13,000 rpm to obtain the pellet, and post-fixed for 1 h in 1% Osmium Tetroxide solution prepared in phosphate buffer (PB) 0.1 M. Samples were stained with 1% Uranyl Acetate and then dehydrated, transferred in a final concentration of propylene oxide, and embedded in Epon resin. After resin polymerization at 60 ◦C for 48 h, samples were cut with Rickert-Jung ultramicrotome and ultra-thin sections (70 nm) were collected on TEM grids. Samples were observed with JEOL JEM 2100 Plus Transmission Electron Microscope (JEOL, Japan) operating with an acceleration voltage of 200kV, and equipped with an 8-megapixel Gatan (Gatan, USA) Rio Complementary Metal-Oxide-Superconductur (CMOS) camera.

2.5 Cytokines release

After 24 and 48 h exposure to DEP and wood particles, the supernatants from BEAS-2B cells were collected and stored at −80 °C until analysis. Protein levels were detected by sandwich ELISA according to the manufacturer's instructions (IL-6 and IL-8, Life Technologies, Monza, Italy). The absorbance of each sample was measured by a multiplate reader (Infinite200Pro, TECAN, Männedorf, Switzerland) at the wavelength of 450 nm and the amount of proteins in pg/mL calculated.

2.6 Cell cycles analyses

The cell cycle progression of cells exposed to CDPs was investigated after 24 h of exposure by DNA-staining, as previously reported. Briefly cells were trypsinized, collected and pooled with the harvested medium, centrifuged at 1200 rpm for 6 min, fixed in 90% ethanol and stored at −20 °C until analysis. Cells were incubated with RNAse DNAse-free (1 mg/mL, Sigma-Aldrich, Italy) for 30 minutes. Finally, the fluorescent dye PI was added to stain DNA of cells for 7 min in the dark. Fluorescence was measured by flow cytometer (CytoFLEX 13/3) using 617 nm band pass filters (ECD-A filter). Data were processed with the CytoExpert software.

2.7 Cytofluorimetric detection of γ -H2AX

A marker of DNA double-strands breaks (DSBs) was analysed through flow cytometry, as previously described (Bengalli et al., 2019) . Briefly for measuring DNA DSBs, BEAS-2B cells were probed with the rabbit mAb anti-yH2AX Alexa Fluor 488 Conjugate (Cell Signaling). After 24 and 48 h of exposure cells were fixed in 1% paraformaldehyde, suspended in 90% cold methanol and stored overnight at −20 °C before the analysis. Cells were then stained for y-H2AX following manufacturers' instructions and analysed at the CytoFLEX (Beckman Coulter) in the FITC channel (Excitation wavelength= 488 nm; Emission Wavelenght= 525 nm).

2.8 Cytokinesis-Block Micronucleus Assay

BEAS-2B cells were seeded on a 6-well plate at the density of 1,2 x 10^5 cells/well; on the 2nd day cells were treated with the two CDPs for 48 h; Mitomycin C (MMC) (Sigma-Aldrich) was used as a positive control at a final concentration of 0.7 µM . After 48 h of exposure, cell medium was removed and cells were washed twice with pre-warmed PBS, then Cytochalasin B (Sigma-Aldrich) was added to each well at a final concentration of 1.5 µg/ml and cells were incubated for an additional 26 h. At the end of incubation in the presence of Cytochalasin B, the medium was removed and each well gently washed twice with pre-warmed PBS. Then cells were harvested with Trypsin-EDTA solution (Life Technologies) and centrifuged for 5 minutes at room temperature (RT), at 1000 rpm (Eppendorf 5810R centrifuge, rotor A-4-62). After the removal of the supernatant, a pre-fixing solution of ethanol: glacial acetic acid (6:1) was added to the cells and incubated for 2 minutes at RT.

Then, after centrifugation, ice-cold ethanol was added to the cells and incubated for 1h at -20°C. This procedure was repeated three times. The fixed cells were then re-suspended gently with a glass Pasteur pipette and dropped on cold microscope slides. The slides were let dry for at least 6 h and then stained with a solution of 2% Giemsa. Samples were then processed and analysed according to the criteria of Fenech (Fenech, 2007).Three biological replicates for each sample were prepared for Cytokinesis-Block Micronucleus (CBMN)analysis with two technical replicates each. For each experimental condition, the cytokinesis block proliferation index (CBPI) was calculated using the following formula: ((N◦ mononucleated cells) + (2 × N◦ binucleated cells) + (3 × N◦ multinucleated cells))/ (total number of cells). Furthermore, for each experimental condition the number of micronuclei (MN) and nuclear buds (NBUDs) in 1000 binucleated cells was evaluated.

2.9 Gene expression

After exposure for 48 h to CDPs, BEAS-2B cells were washed with cold PBS and lysed in 350 µl RLT lysis buffer (Qiagen, Germantown, MD, USA). Samples were stored at −80 °C until RNA extraction was carried out. RNA was extracted from cells and purified using the RNeasy Plus kit (Qiagen, Germantown, MD, USA). The RNA quantification was done by a ND-1000 UV–Vis Spectrophotometer (NanoDrop Technologies). 1 µg of total RNA was reverse transcribed using the High-Capacity RNA to c-DNA kit (Applied Biosystem) SYBR™, according to the manufacturer's protocol. Real-Time PCR was performed with a total of 5 ng of cDNA for each reaction, using SYBR™ Green Master Mix (Applied Biosystem) reaction was performed on 7900HT Fast Real-Time PCR System, according to the manufacturer's instructions. The amount of target cDNA in each sample was calculate using comparative Ct methods (2-ΔCt method)., normalized to the GAPDH and expressed as fold change relative to control cells. Primer sequences and thermal cycling conditions are reported in supplementary data (Supplementary S.1).

2.10 Statistical Analysis

The data represent the mean ± standard error of the mean (SE) of at least three independent experiments. Statistical analyses were performed using GraphPad 6.0v software, using unpaired *t*-test or One-way ANOVA and Bonferroni's post hoc analysis, if not elsewhere specified in the figure captions. Values of $p < 0.05$ were considered statistically significant.

3-Results and discussion

3.1 Characterization of physico-chemical properties

TEM microscopy and analytical techniques were used to study the Euro 3 DEP and Wood CDPs physico-chemical properties that may be relevant in determining their biological outcomes. Euro 3 DEP were previously characterized (Data show in chapter VI), here the data are reported in comparison to Wood CDPs.

TEM images of both DEP and biomass samples showed aggregates of soot particles, with dimensions of single particles below 50 nm. DLS analyses show that both DEP and Wood CDPs form agglomerates when suspended in cell medium, with a mean hydrodynamic size of 328.87 ± 4.7 nm and 564.9 ± 2.3 nm respectively, means that almost all the sampled particles can be classified as quasi-ultrafine particles. Trough the combustion process, the surfaces of the carbon particles become chemically activated. CDPs present, absorbed on their surface or embedded in the carbon particles, metals and metal-oxides that participate in Fenton-type reactions contributing to the induction of oxidative stress process in biological system (Steiner et al.2016). ICP-MS analyses showed a different composition between the two type of particles. The emission of the metals in vehicle exhausts could be related to the consumption of metal contents in diesel fuel (Bharathi et al; 2006) and a high content of Fe, Mn, Ni, Zn was found in Euro 3 DEP samples. The principal trace elements found in Wood CDPs are Al, K and Ca. Al is originated mainly from soil dust, K is derived from vegetation biomass and Ca from mixed sources (Novakov et al., 1997).

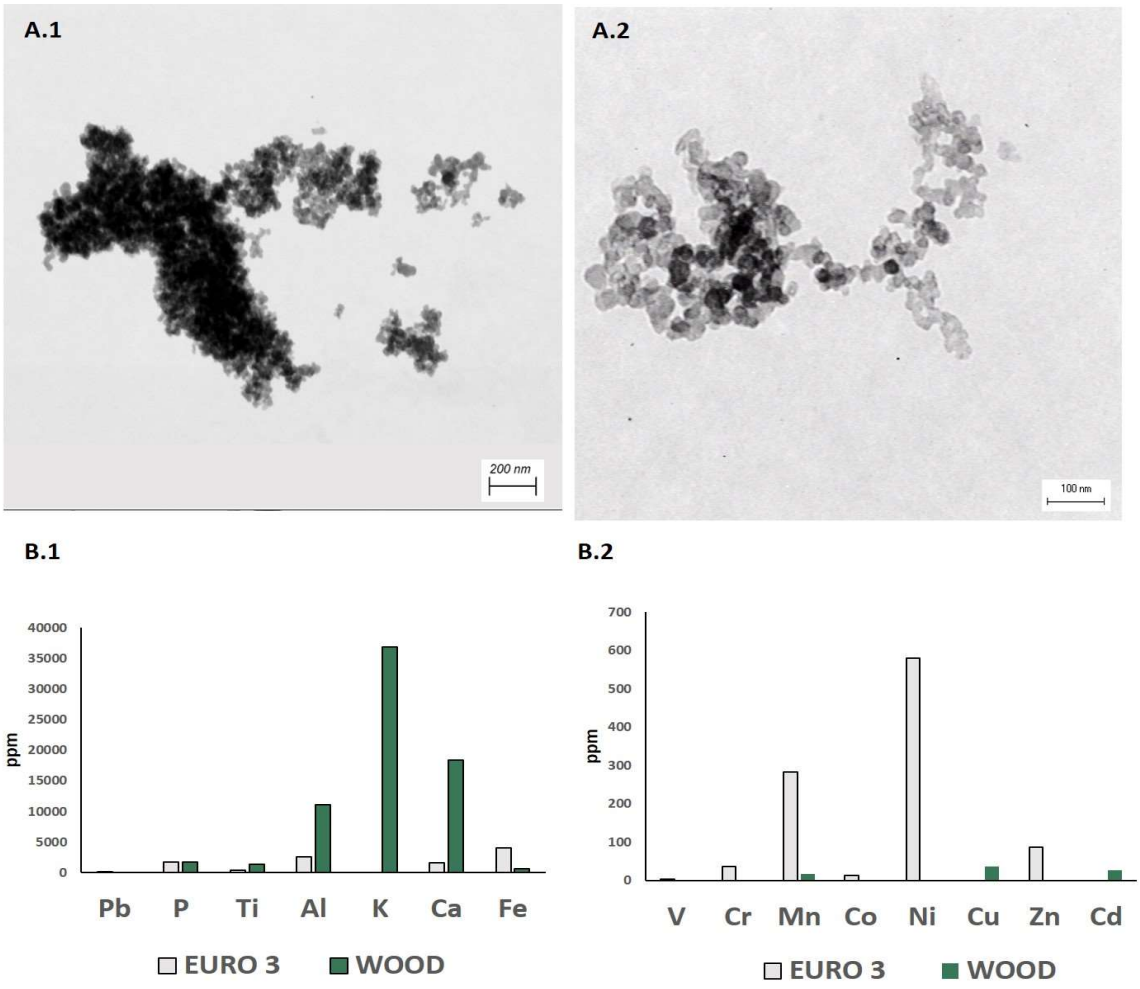

Figure 1: Physico-chemical characterization of particles. TEM images of DEP (A.1) and wood (A.2) samples. In panels B.1 and B.2 metal concentrations are reported, data are presented as part per million (ppm).

Chemical speciation presented a typical composition of PAHs, with diesel soot with high levels of phenanthrene, pyrene, fluoranthene, while pyrene, fluoranthene and benzo[b]fluoranthene were the most abundant PAHs in wood CDPs (Table 1). The total amount of PAHs in Wood CDPs is almost two times the concertation of PAHs in Euro 3 DEP. However, to better evaluate the toxic effects of PAHs in particles, the organic compound extracted from particles should be evaluated separately since the bioavailability of PAHs could occur after a longer time of exposure. The use of organic extracts augments the bioavailability of PAHs respect to the use of whole particles (Libalova et al., 2016), therefore it would provide a more complete evaluation of toxic effects of PAHs associated to the CDPs. DEP toxic effects are known to be dependent on PAHs content (Gilmour et al; 2015). Adverse health effects of biomass-smoke PM (i.e., wood CDPs) are also highly dependent

on organic composition, which varies across distinct size fractions and results in different toxicity pathway.

Polycyclic aromatic hydrocarbons (ng/mg)

	EURO 3	WOOD
Fluorene	10	/
Phenanthrene	135	34
Anthracene	22	10
Fluoranthene	70	132
Pyrene	81	148
Benzo[a]anthracene	26	100
Chrysene	10	89
Benzo[b]fluoranthene	16	118
Benzo[k]fluoranthene	10	56
Benzo[a]pyrene	14	47
Dibenzo[a,h]anthracene	/	10
Indeno[1,2,3-cd]pyrene	/	23
Benzo[g.h.i]perylene	/	42
Total	**394**	**809**

Table 1: Chemical characterization of CDPs. PAHs concentrations are reported as ng/mg.

3.2 Biological effects

Previous studies comparing diesel and biomass CDPs described stronger toxicological outcomes from one or the other source alternatively (Longhin et al., 2016)(Kocbach et al; 2008)(Totlandsdal et al., 2014). These differences could be explained in relation to the characteristics of emitted particles, which are mainly determined by combustion conditions, fuels and technologies employed. However, the biological responses strongly

depend also on the exposure conditions and the interaction among cells and particles, including the capability of lung cells to internalize CDPs. Some studies proved the *in vitro* uptake of DEP by lung epithelial cells (Saxena et al. 2008)(Boland et al., 1999). In the present study, the ultrastructure of cells exposed to the two different particles was evaluated by TEM (Figure 2). The images evidenced that both types of CDPs were up taken by bronchial cells. In general, a greater uptake of DEP particles compared to Wood particles was noticed, probably due to the different mean diameter of the particles, which, according to DLS analyses, results smaller in DEP sample. Anyway, according to Penn and colleagues, the uptake of airborne ultrafine particles by cells is not essential for the transport of toxicants from the particles to the target cells (Penn et al. 2005). No relevant alterations in the cellular ultrastructure were highlighted after exposure to particles.

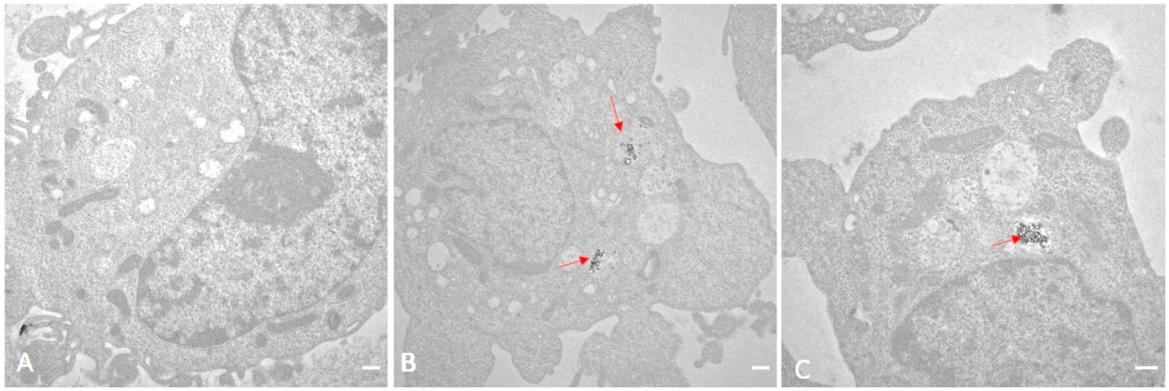

Figure 2: Euro 3 DEP and wood CDPs cellular uptake. TEM images of BEAS-2B after 48 h of exposure to 50 µg/ml of particles: (A) CTRL; (B) DEP; (C) Wood. Red arrows indicate the internalized particles. Scale bar: 500 nm

Fine and especially ultrafine particles are known to induce more pulmonary inflammation and to be retained longer in the lungs respect to coarse particles (Qing et al., 2019)(Arias-Pérez et al., 2020). In epidemiological studies, several biomarkers of systemic inflammation, included proinflammatory cytokines, were monitored in a population exposed to PM (Li et al., 2017). The exposure to chronic biomass-burning smoke was correlated with systemic alterations in the levels of the immune markers of inflammation, that may cause eosinophil-derived inflammatory response (Falfán-Valencia et al., 2020).

Despite the evidences linking biomass CDPs exposure to lung diseases, the experimental studies conducted on the impact of biomass smoke on airway epithelial cells are still limited, while a high number of studies reported the *in vitro* effects of DEP. Here interleukins secretion (IL-6 and IL-8) was investigated after 24 h and 48 h exposure to particles in order to evaluate a possible activation of inflammatory response (Figure 3). Euro 3 DEP induced a significant increase of both cytokines after 24 h of exposure, although this response was not observed after 48 h of treatment, while wood CDPs induced an increased release of IL-6 after 48h. A significant secretion of IL-6 and IL-8 from BEAS-2B after 24 h respect to 48 h of exposure to DEP was previously reported (Steerenberg et al., 1998). The effectiveness of wood CDPs to induce an inflammatory response may depend on combustion conditions and consequent particles properties, as previously reported by Bølling and colleagues. Indeed, particles emitted during a process of medium-temperature combustion are more cytotoxic than particles derived from high-temperature incomplete combustion and they also induced a higher production of IL-6 (Bølling et al., 2012). Moreover, airborne endotoxin produced during combustion of biomass may play a significant role in inducing health effects associated with biomass smoke (Black, 2010). In order to exclude that the increased level of cytokines could be promoted by the presence of endotoxins in the tested samples, the levels of endotoxins were quantified by LAL assay and they resulted below 1 EU/mL for DEP sample and higher than 1 EU/mL for Wood CDPs sample (1.57 EU/ml) (Supplementary S.2). However, in the present study the higher presence of endotoxins observed in wood samples with respect to DEP did not seem to promote a strong induction of inflammatory response. The increased release of IL-6 after 48 h of treatment with Wood CDPs may be determined by particles properties more than by endotoxin presence.

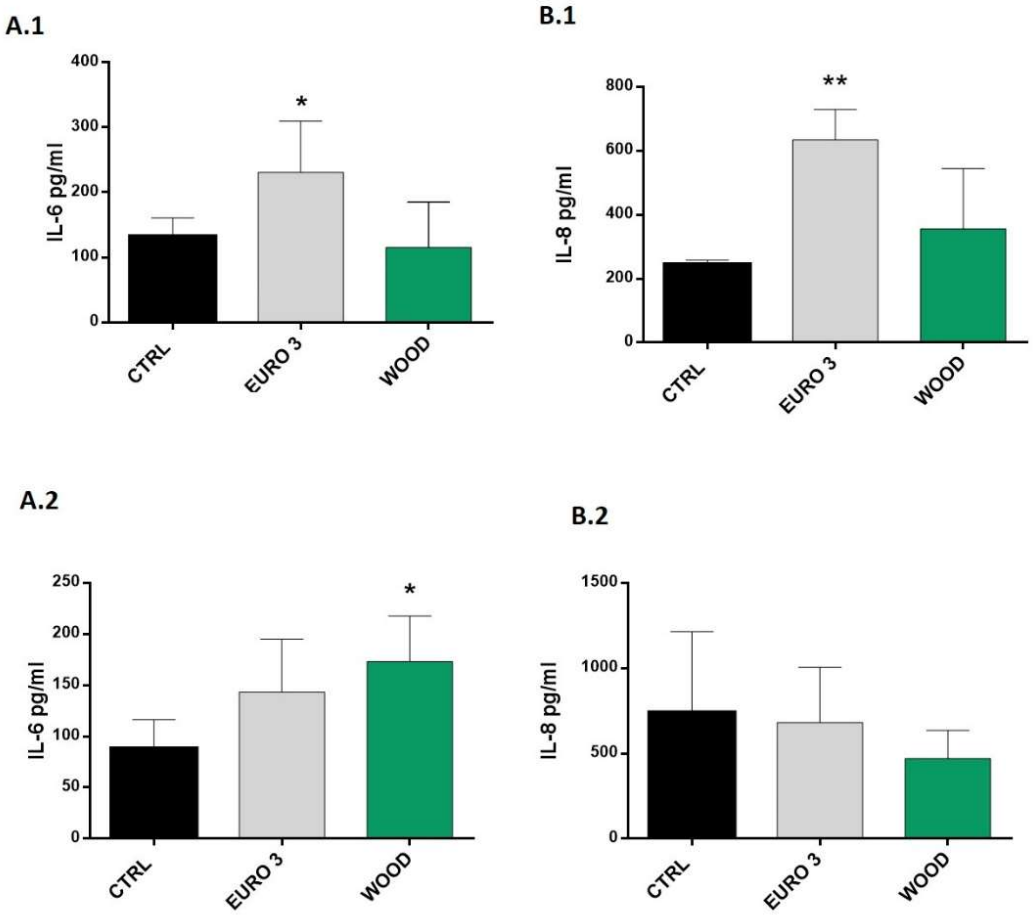

Figure 3: Inflammatory response: Release of IL-6 and IL-8 from BEAS-2B exposed for 24 (A.1; B.1) and 48 h (A.2; B.2) to 50 µg/mL of Euro 3 DEP and Wood CDPs (n=3). *Statistically significant according to unpaired t-test; ***p*<0.01 and **p*<0.05 vs control cells.

Euro 3 DEP and wood CDPs capability to induce DNA damage and genotoxic insult were evaluated by the quantification of γ-H2AX expression and micronucleus test (MNT) respectively.

Oxidative stress can lead to DNA double-strand breaks (DSBs) and subsequently to the formation of micronuclei. DNA DSBs could also be indirectly caused by the formation of DNA adducts. The formation of DSBs is always followed by the phosphorylation of the histone, H2AX(Ward & Chen, 2001), which is considered a biomarker of DNA oxidative

damage. The quantification of γ-H2AX is showed in Figure 4. Only the exposure for 48 h to DEP induced increased expression of the γ-H2AX marker (Figure 4, A.2).

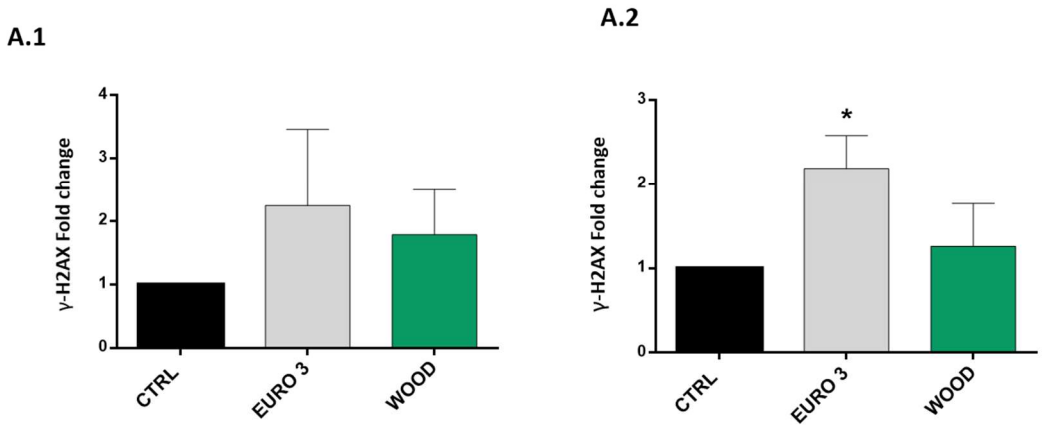

Figure 4: DNA damage: expression of γ-H2AX. BEAS-2B cells expression of γ-H2AX after 24 (A.1) and 48 h (A.2) exposure to 50 µg/mL Euro 3 DEP and Wood CDPs (n=3). Data represent the mean ±SE of the fold change of γ-H2AX expression in treated samples (EURO3 and WOOD) compared to control (CTRL) ones. *Statistically significant according to unpaired t-test; *p<0.05 vs control cells.

The MNT is a well-established *in vitro* genotoxic assay and is an accepted standard method to evaluate the genotoxic hazard of chemicals (OECD, 2016). Micronuclei are caused by DNA damage or mitotic errors (Spektor et al; 2014). A significant increase of micronuclei (MN) was observed after 48 h of treatment with DEP, while no significant data was observed after exposure to Wood CDPs (Figure 4, A.1). In addition, we evaluated the presence of NBUDs (Figure 4, A.2), which is a micronucleus-like bodies attached to the nucleus by a thin nucleoplasmic bridge. Our results show a significant increase after exposure to DEP of NBUDs. From the data obtained, CBPI index "Cytokinesis Block Proliferation Index" was calculated in order to evaluate the cellular proliferation progression. CBPI obtained from cells exposed to the two CDPs, are not statistically significant compared to the control condition (Figure 4; B.1). However, data from MNT

acquire an importance if we consider the fact that both MN and NBUDs are indices of genomic instability and they have been correlated with augmented risk of cancer development (El-Zein et al., 2006).

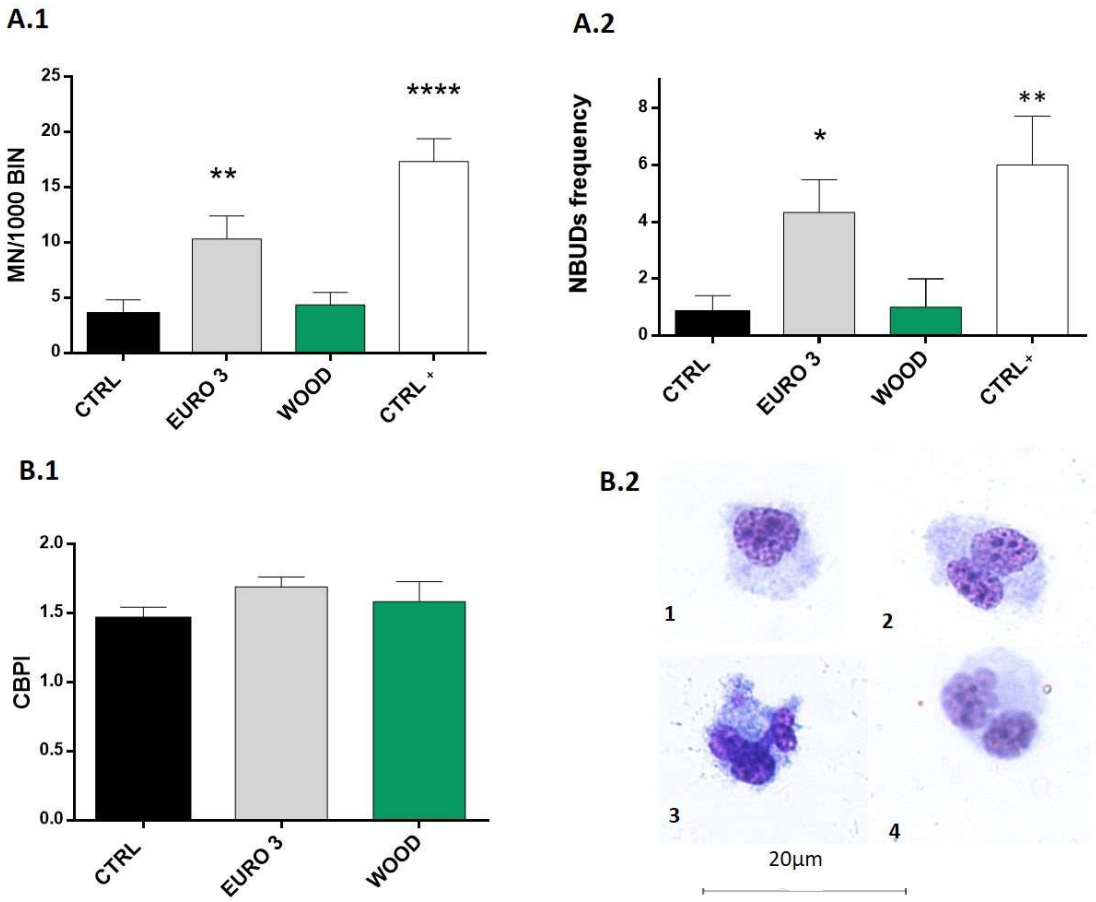

Figure 5: *Micronucleus analysis.* BEAS-2B cells exposure to 50 µg/mL of Euro 3 DEP and Wood CDPs were evaluate for MN (A.1), NBUDs (A.2) frequency and CBPI (B.1) (n=3). In figure B.2 are reported images of a mononucleate cell (1); binucleated cell (2); binucleated cell with NBUDs (3) and binucleated with MN (4). *Statistically significant according to unpaired t-test; ****p<0.0001, ***p<0.001, **p<0.01 and *p<0.05 vs control cells.

Genotoxic potential of DEP was studied in the past and it is recognised that the major contributors to the mutagenicity of DEP are the PAHs and nitro-PAHs adsorbed onto the particle (Kowalska et al., 2017). Despite in a previous study was reported that Wood CDPs generated more DNA damage than standard DEP (SRM 2975) in human cells (Danielsen et al. 2009), the present results evidence a higher genotoxic potential of DEP representative of STOP&GO urban driving cycle with respect to Wood CDPs. Moreover cell cycle

checkpoints are part of DNA repair mechanisms (El-Zein et al., 2006). Cell cycle progression can be blocked or delayed in response to exposure to PM (Qin et al., 2017). Longhin and colleagues reported that exposure to $PM_{2.5}$ in BEAS-2B cells produce an early arrest in G2 phase, followed by an arrest in M/A (Metaphase/anaphase transition point) with a consequence inhibition of cytokinesis and an increased number of MN, associated with a rapid DNA damage response (Longhin et al., 2013). Therefore, the cell cycle progression was evaluated in control cell (untreated) and in cells exposed to 50 µg/mL Euro 3 DEP and Wood CDPs after 48h of treatment, data are shown in Supplementary (Figure S.3) and no significant changes in the cell cycle progression were noted.

In addition to elucidate biological potential of Euro 3 DEP and Wood CDPs after 48 h of exposure, the modulation of genes involved in several CDPs-activated pathways were investigated. The transcriptional profiling of BEAS-2B cells after exposure to DEP and Biomass derived UFPs was analysed before by Grilli and co-workers and results showed that the exposure to diesel UFPs induces the activation of genes implicated in TNFα signalling via NF-kB, inflammatory response, and hypoxia, while the exposure to biomass UFPs led to less definite modifications of the gene expression profiles(Grilli et al., 2018). In Figure 6 the expression of eleven genes (CCD1; ki-67; CYP1A1; MMP1; HMOX-1; HIF-1α; NF-kB; SERPIN-B2; EREG; IL-1β; IL-24) are presented as a fold change respect to the control cells. CCND1 (Cyclin D1) and Ki-67 are genes involved in cell proliferation and cycle progression (Miller et al., 2018), and in accordance with the results from cell cycle analyses no changes at this level were appreciable, despite the Wood CDPs induce a downregulation of Ki 67 expression (0.4-Fold change) that need further investigation. CYP1A1 (Cytochrome P450 Family 1 Subfamily A Member 1) and MMP1 (Matrix Metalloproteinase 1) are gene activated in response to xenobiotic metabolism (Ono et al., 2013). Both DEP and Wood CDPs induced a strong up-regulation of CYP1A1 (Fold change >10 and 9.7 respectively) and of MMP1 (Fold change >10 and 2.6 respectively). CYP1A1 are highly activated by PAHs via aryl hydrocarbon receptor (AhR), and the potency of DEP and Biomass CDPs to promote CYP1A1 upregulation has previously been demonstrated (Totlandsdal et al; 2010)(Longhin et al., 2016). It has been previously reported that the CYP1A1 metabolism play a pivotal role in detoxifying foreign chemicals and metabolic activation, leading to oxidative damage (Nebert et al. 2004). MMP-1 has been implied as a pathogenic factor in human respiratory

diseases. The expression of MMP enzymes in the respiratory tract seems to cause the degradation of the basement membrane and interstitial extracellular matrix and has been previously identify after exposure to DEP and Wood CDPs (Amara et al., 2007) (Ramos et al., 2009). Oxidative stress, with consequence oxidative DNA damage, has been correlated with the transition metals leaching from DEP or by their adhesion on particle surfaces, as well as by PAHs (Risom et al. 2005). Downregulation of HMOX-1gene has been reported to potentially promote apoptosis and autophagy, despite these has not been evaluated in the present work (Zhu et al., 2015). HMOX-1 is a gene encoding for Heme oxygenase (HO-1), which is an oxidative stress marker but is also a cytoprotective enzyme (Amara et al., 2007). Overexpression of HMOX-1 can be implied in the detoxification of ROS generated by PM. The present result showed that while Euro 3 DEP induced an upregulation of HMOX-1 (4.6-Fold change), the Wood CDPs determined a downregulation of this gene (0.7-Fold change). Furthermore $PM_{2.5}$ may induce cardiac hypoxia and it has been proved that exposure to $PM_{2.5}$ promotes inflammation that lead to an increase of hypoxia-inducible factors (HIF) in vascular endothelium cells (Dai et al., 2016). In the present study the two type of CDPs do not determined an increase expression of HIF-1α, which expression should be evaluated also on pulmonary endothelial cells rather than on epithelial cells. $PM_{2.5}$ have been implicated also as potential Epithelial-mesenchymal transition (EMT) mediators. EMT refers to the conversion of epithelial cells to mesenchymal phenotype, and this process is involved in cancer progression with metastatic expansion. SERPIN-B2 is a gene connected to EMT and its expression was strongly modulated after the exposure to Euro 3 DEP, but also, to a lower extent, to Wood CDPs (fold change respectively >10 and 2). As reported by Longhin and colleagues, the over-expression of SERPINB2 in PM-exposed samples might be evaluated as an initial protective mechanism of EMT (Longhin et al; 2018). The exposure to the two CDPs also induce a modulation of gene involved in inflammation process (IL-1β) and carcinogenesis (EREG; IL-24). Euro 3 DEP have been confirmed as the particles able to induce a higher gene upregulation, except for IL-24 which result stronger modulated by Wood CDPs (7.8-Fold change). NF-kB/IκB activation after exposure to PM play a pivotal role in generation of oxidative damage, in the modulation of the gene expression and the secretion of pro-inflammatory mediators (Dagher et al., 2007). In this work the upregulation of NFKb was confirmed only after exposure to Euro 3 DEP. The present data,

in accordance with the work of Grilli and colleagues, suggest that gene modulation is stronger after exposure to DEP respect Biomass CDPs (Grilli et al., 2018).

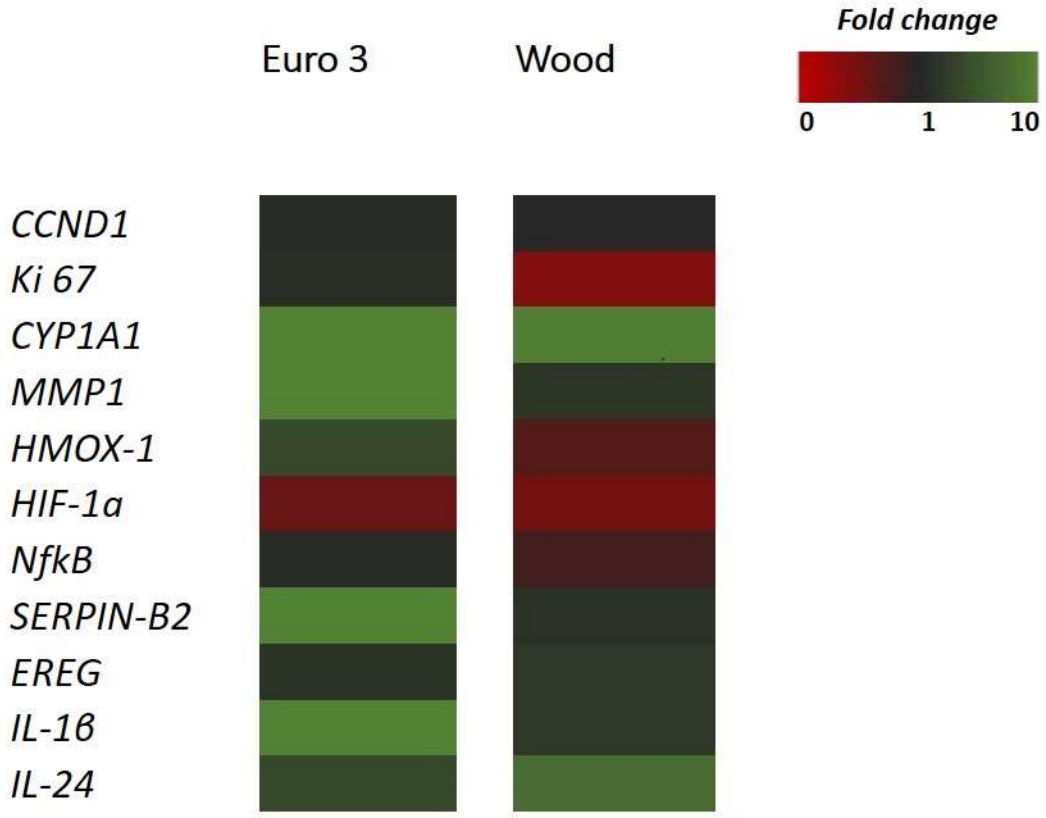

Figure 6: Gene expression. Modulation of genes after 48 h of exposure to DEP and Wood CDPs (50 µg/mL) in BEAS-2B cells. Data are reported as Fold change relative to control cells.

4-Conclusions

Exhaust emissions have been linked to adverse health effects and global climate change. Here we compared the chemical properties and biological effects of two different types of particulates produced by combustion process: diesel exhaust and wood burning. Wood combustion is an important source of air pollution, especially during the winter, and together with particles derived from traffic contribute to the worsening of air quality in

residential areas. The present study confirmed that biomass particles produced by a modern stove propelled with beech wood had low hazardous toxic effects compared to DEP emitted from an old diesel engine. DEP was confirmed as a very harmful component of the urban PM able to induce inflammation, genotoxicity and modulation of several genes involved in relevant cellular toxic responses: xenobiotic metabolism (CYP1A1; MMP1); oxidative stress (HMOX-1); inflammatory response (IL-1β); carcinogenesis (IL-24; EREG) and EMT (SERPIN-B2). However, since an important modulation of CYP1A1 genes and other genes (e.g. IL-24) occurred also in cells exposed to Wood CDPs, consequences on human health from a chronic exposure to the Wood CDPs cannot be excluded, as also suggested by the induction of IL-6 production at a later endpoint of exposure (48 h). The stronger biological effects of DEP could be explained by the physic properties, in fact diesel particles from Euro 3 vehicle are smaller particles compared to Wood, easily internalized by cells. Moreover, the typical chemical composition of DEP (prevalent presence of phenanthrene, pyrene and fluoranthene as PAHs and the presence of Zn and Fe as trace elements) has been previously associated with important toxicological outcomes (Bengalli et al., 2019). Despite Wood CDPs present a higher content of total PAHs respect to DEP Euro 3, this characteristic did not determine a higher genotoxic effect as expected. In order to better evaluate the potential hazard of PAHs in Wood particles, the toxic effects of the organic compound extracted from particles should be evaluated separately. The results here presented suggest the necessity to investigate all the potential sources of fine and ultrafine particulate in an urban area, with specific focus towards the combustion processes. A better comprehension of how the emission source determines the toxicity and physico-chemical properties of PM, as well as exposure patterns, could be useful in the future to orient intervention strategies that should be adopted to improve air quality.

7.1 BIBLIOGRAPHY

Amann, M. (2018). *Measures To Address Air Pollution From Small Combustion*. 1–51.

Amara, N., Bachoual, R., Desmard, M., Golda, S., Guichard, C., Lanone, S., … Boczkowski, J. (2007). Diesel exhaust particles induce matrix metalloprotease-1 in human lung epithelial cells via a NADP(H) oxidase/NOX4 redox-dependent mechanism. *American Journal of Physiology - Lung Cellular and Molecular Physiology*, *293*(1). https://doi.org/10.1152/ajplung.00445.2006

Arias-Pérez, R. D., Taborda, N. A., Gómez, D. M., Narvaez, J. F., Porras, J., & Hernandez, J. C. (2020, December 1). Inflammatory effects of particulate matter air pollution. *Environmental Science and Pollution Research*, Vol. 27, pp. 42390–42404. https://doi.org/10.1007/s11356-020-10574-w

Bengalli, R., Zerboni, A., Marchetti, S., Longhin, E., Priola, M., Camatini, M., & Mantecca, P. (2019). In vitro pulmonary and vascular effects induced by different diesel exhaust particles. *Toxicology Letters*, *306*. https://doi.org/10.1016/j.toxlet.2019.01.017

Bharathi, K. V. L., Dwivedi, D., Kumar Agarwal, A., & Sharma, M. (2006). *DIESEL EXHAUST PARTICULATES CHARACTERIZATION FOR HEAVY METALS*.

Black, H. (2010). Endotoxin from biomass burning: an underestimated health hazard? *Environmental Health Perspectives*, Vol. 118, p. A304. https://doi.org/10.1289/ehp.118-a304b

Boland, S., Baeza-Squiban, A., Fournier, T., Houcine, O., Gendron, M. C., Chévrier, M., … Marano, F. (1999). Diesel exhaust particles are taken up by human airway epithelial cells in vitro and alter cytokine production. *American Journal of Physiology - Lung Cellular and Molecular Physiology*, *276*(4 20-4). https://doi.org/10.1152/ajplung.1999.276.4.l604

Bølling, A. K., Totlandsdal, A. I., Sallsten, G., Braun, A., Westerholm, R., Bergvall, C., … Herseth, J. I. (2012). Wood smoke particles from different combustion phases induce similar pro-inflammatory effects in a co-culture of monocyte and pneumocyte cell lines. *Particle and Fibre Toxicology*, *9*(1), 1–15. https://doi.org/10.1186/1743-8977-9-45

Dagher, Z., Garçon, G., Billet, S., Verdin, A., Ledoux, F., Courcot, D., … Shirali, P. (2007). Role of nuclear factor-kappa B activation in the adverse effects induced by air pollution particulate matter (PM2.5) in human epithelial lung cells (L132) in culture. *Journal of Applied Toxicology*, *27*(3), 284–290. https://doi.org/10.1002/jat.1211

Dai, J., Sun, C., Yao, Z., Chen, W., Yu, L., & Long, M. (2016). Exposure to concentrated ambient fine particulate matter disrupts vascular endothelial cell barrier function via the IL-6/HIF-1α signaling pathway. *FEBS Open Bio*, *6*(7), 720–728. https://doi.org/10.1002/2211-5463.12077

El-Zein, R. A., Schabath, M. B., Etzel, C. J., Lopez, M. S., Franklin, J. D., & Spitz, M. R. (2006). Cytokinesis-blocked micronucleus assay as a novel biomarker for lung cancer risk. *Cancer Research*, *66*(12), 6449–6456. https://doi.org/10.1158/0008-5472.CAN-06-0326

Falfán-Valencia, R., Ramírez-Venegas, A., Pérez Lara-Albisua, J. L., Ramírez-Rodriguez, S. L., Márquez-García, J. E., Buendía-Roldan, I., … Ortiz-Quintero, B. (2020). Smoke exposure from chronic biomass burning induces distinct accumulative systemic inflammatory cytokine alterations compared to tobacco smoking in healthy women. *Cytokine*, *131*, 155089. https://doi.org/10.1016/j.cyto.2020.155089

Fenech, M. (2007). Cytokinesis-block micronucleus cytome assay. *Nature Protocols*, *2*(5), 1084–1104. https://doi.org/10.1038/nprot.2007.77

Gilmour, M. I., Kim, Y. H., & Hays, M. D. (2015). Comparative chemistry and toxicity of diesel and biomass combustion emissions. *Analytical and Bioanalytical Chemistry*, *407*(20), 5869–5875. https://doi.org/10.1007/s00216-015-8797-9

Grilli, A., Bengalli, R., Longhin, E., Capasso, L., Proverbio, M. C., Forcato, M., … Camatini, M. (2018). Transcriptional profiling of human bronchial epithelial cell BEAS-2B exposed to diesel and biomass ultrafine particles. *BMC Genomics*, *19*(1), 1–15. https://doi.org/10.1186/s12864-018-4679-9

Health Organization, W., & Office for Europe, R. (2013). *Review of evidence on health aspects of air pollution – REVIHAAP Project Technical Report*. Retrieved from http://www.euro.who.int/pubrequest

IARC. (2012). *DIESEL ENGINE EXHAUST CARCINOGENIC*. https://doi.org/10.1093/jnci/djs034

Johnston, H. J., Mueller, W., Steinle, S., Vardoulakis, S., Tantrakarnapa, K., Loh, M., & Cherrie, J. W. (2019, December 1). How Harmful Is Particulate Matter Emitted from Biomass Burning? A Thailand Perspective. *Current Pollution Reports*, Vol. 5, pp. 353–377. https://doi.org/10.1007/s40726-019-00125-4

Kocbach, A., Namork, E., & Schwarze, P. E. (2008). Pro-inflammatory potential of wood smoke and traffic-derived particles in a monocytic cell line. *Toxicology*, *247*(2–3), 123–132. https://doi.org/10.1016/j.tox.2008.02.014

Li, W., Dorans, K. S., Wilker, E. H., Rice, M. B., Ljungman, P. L., Schwartz, J. D., … Mittleman, M. A. (2017). Short-Term Exposure to Ambient Air Pollution and Biomarkers of Systemic Inflammation: The Framingham Heart Study. *Arteriosclerosis, Thrombosis, and Vascular Biology*, *37*(9), 1793–1800. https://doi.org/10.1161/ATVBAHA.117.309799

Libalova, H., Rossner, P., Vrbova, K., Brzicova, T., Sikorova, J., Vojtisek-Lom, M., … Topinka, J. (2016). Comparative analysis of toxic responses of organic extracts from diesel and selected alternative fuels engine emissions in human lung BEAS-2B cells. *International Journal of Molecular Sciences*, *17*(11). https://doi.org/10.3390/ijms17111833

Longhin, E., Camatini, M., Bersaas, A., Mantecca, P., & Mollerup, S. (2018). The role of SerpinB2 in human bronchial epithelial cells responses to particulate matter exposure. *Archives of Toxicology*, *92*(9), 2923–2933. https://doi.org/10.1007/s00204-018-2259-z

Longhin, E., Gualtieri, M., Capasso, L., Bengalli, R., Mollerup, S., Holme, J. A., … Camatini, M. (2016). Physico-chemical properties and biological effects of diesel and biomass particles. *Environmental Pollution*, *215*, 366–375. https://doi.org/10.1016/j.envpol.2016.05.015

Longhin, E., Holme, J. A., Gutzkow, K. B., Arlt, V. M., Kucab, J. E., Camatini, M., & Gualtieri, M. (2013). Cell cycle alterations induced by urban PM2.5 in bronchial epithelial cells: Characterization of the process and possible mechanisms involved. *Particle and Fibre Toxicology*, *10*(1), 63. https://doi.org/10.1186/1743-8977-10-63

Miller, I., Min, M., Yang, C., Tian, C., Gookin, S., Carter, D., & Correspondence, S. L. S. (2018). *Ki67 is a Graded Rather than a Binary Marker of Proliferation versus Quiescence*. https://doi.org/10.1016/j.celrep.2018.06.110

Nebert, D. W., Dalton, T. P., Okey, A. B., & Gonzalez, F. J. (2004, June 4). Role of aryl hydrocarbon

receptor-mediated induction of the CYP1 enzymes in environmental toxicity and cancer. *Journal of Biological Chemistry*, Vol. 279, pp. 23847–23850. https://doi.org/10.1074/jbc.R400004200

Novakov, T., Cachier, H., Clark, J. S., Gaudichet, A., Macko, S., & Masclet, P. (1997). Characterization of Particulate Products of Biomass Combustion. In *Sediment Records of Biomass Burning and Global Change* (pp. 117–143). https://doi.org/10.1007/978-3-642-59171-6_6

OECD. (2016). *OECD/OCDE 487 OECD GUIDELINE FOR THE TESTING OF CHEMICALS*. Retrieved from http://www.oecd.org/termsandconditions/.

Ono, Y., Torii, K., Fritsche, E., Shintani, Y., Nishida, E., Nakamura, M., … Morita, A. (2013). Role of the aryl hydrocarbon receptor in tobacco smoke extract-induced matrix metalloproteinase-1 expression. *Experimental Dermatology*, *22*(5), 349–353. https://doi.org/10.1111/exd.12148

Pardo, M., Li, C., He, Q., Levin-Zaidman, S., Tsoory, M., Yu, Q., … Rudich, Y. (2020). Mechanisms of lung toxicity induced by biomass burning aerosols. *Particle and Fibre Toxicology*, *17*(1), 4. https://doi.org/10.1186/s12989-020-0337-x

Pashin Yu., V., & Bakhitova, L. M. (1979). Mutagenic and carcinogenic properties of polycyclic aromatic hydrocarbons. *Environmental Health Perspectives*, *Vol. 30*, 185–189. https://doi.org/10.1289/ehp.7930185

Penn, A., Murphy, G., Barker, S., Henk, W., & Penn, L. (2005). Combustion-derived ultrafine particles transport organic toxicants to target respiratory cells. *Environmental Health Perspectives*, *113*(8), 956–963. https://doi.org/10.1289/ehp.7661

Qin, Z., Hou, H., Fu, F., Wu, J., Han, B., Yang, W., … Chen, Y. (2017). Fine particulate matter exposure induces cell cycle arrest and inhibits migration and invasion of human extravillous trophoblast, as determined by an iTRAQ-based quantitative proteomics strategy. *Reproductive Toxicology*, *74*, 10–22. https://doi.org/10.1016/j.reprotox.2017.08.014

Qing, H., Wang, X., Zhang, N., Zheng, K., Du, K., Zheng, M., … Bachert, C. (2019, November 15). The effect of fine particulate matter on the inflammatory responses in human upper airway mucosa. *American Journal of Respiratory and Critical Care Medicine*, Vol. 200, pp. 1315–

1318. https://doi.org/10.1164/rccm.201903-0635LE

Ramos, C., Cisneros, J., Gonzalez-Avila, G., Becerril, C., Ruiz, V., & Montaño, M. (2009). Increase of Matrix Metalloproteinases in Woodsmoke-Induced Lung Emphysema in Guinea Pigs. *Inhalation Toxicology*, *21*(2), 119–132. https://doi.org/10.1080/08958370802419145

Risom, L., Møller, P., & Loft, S. (2005a). Oxidative stress-induced DNA damage by particulate air pollution. *Mutation Research*, *592*, 119–137. https://doi.org/10.1016/j.mrfmmm.2005.06.012

Risom, L., Møller, P., & Loft, S. (2005b). Oxidative stress-induced DNA damage by particulate air pollution. *Mutation Research - Fundamental and Molecular Mechanisms of Mutagenesis*, *592*(1–2), 119–137. https://doi.org/10.1016/j.mrfmmm.2005.06.012

Sabinus Alozie, N., & Christopher Ganippa, L. (2019). Diesel Exhaust Emissions and Mitigations. In *Introduction to Diesel Emissions*. https://doi.org/10.5772/intechopen.85248

Saxena, R. K., Ian Gilmour, M., & Hays, M. D. (2008). Isolation and quantitative estimation of diesel exhaust and carbon black particles ingested by lung epithelial cells and alveolar macrophages in vitro. *BioTechniques*, *44*(6), 799–805. https://doi.org/10.2144/000112754

Spektor, A., Liu, S., Jackson, E., & Pellman, D. (2014). Micronuclei-Induced DNA Damage and Mutagenesis in Cancer. *International Journal of Radiation Oncology*Biology*Physics*, *90*(1), S781. https://doi.org/10.1016/j.ijrobp.2014.05.2259

Steerenberg, P. A., Zonnenberg, J. A. J., Dormans, J. A. M. A., Joon, P. N. T., Wouters, I. M., Van Bree, L., … Van Loveren, H. (1998). Diesel exhaust particles induced release of interleukin 6 and 8 by (PRIMED) human bronchial epithelial cells (BEAS 2B) in vitro. *Experimental Lung Research*, *24*(1), 85–100. https://doi.org/10.3109/01902149809046056

Steiner, S., Bisig, C., Petri-Fink, A., & Rothen-Rutishauser, B. (2016, July 1). Diesel exhaust: current knowledge of adverse effects and underlying cellular mechanisms. *Archives of Toxicology*, Vol. 90, pp. 1541–1553. https://doi.org/10.1007/s00204-016-1736-5

Sydbom, A., Blomberg, A., Parnia, S., Stenfors, N., Sandström, T., & Dahlén, S. E. (2001). Health effects of diesel exhaust emissions. *European Respiratory Journal*, *17*(4), 733–746. https://doi.org/10.1183/09031936.01.17407330

Totlandsdal, A. I., Cassee, F. R., Schwarze, P., Refsnes, M., & Låg, M. (2010). Diesel exhaust particles induce CYP1A1 and pro-inflammatory responses via differential pathways in human bronchial epithelial cells. *Particle and Fibre Toxicology*, *7*, 41. https://doi.org/10.1186/1743-8977-7-41

Totlandsdal, A. I., Øvrevik, J., Cochran, R. E., Herseth, J. I., Bølling, A. K., Låg, M., … Kubátová, A. (2014). The occurrence of polycyclic aromatic hydrocarbons and their derivatives and the proinflammatory potential of fractionated extracts of diesel exhaust and wood smoke particles. *Journal of Environmental Science and Health - Part A Toxic/Hazardous Substances and Environmental Engineering*, *49*(4), 383–396. https://doi.org/10.1080/10934529.2014.854586

Ward, I. M., & Chen, J. (2001). Histone H2AX Is Phosphorylated in an ATR-dependent Manner in Response to Replicational Stress. *Journal of Biological Chemistry*, *276*(51), 47759–47762. https://doi.org/10.1074/jbc.C100569200

WHO. (2010). *VOLUME 95 Household Use of Solid Fuels and High-temperature Frying IARC Monographs on the Evaluation of Carcinogenic Risks to Humans WORLD HEALTH ORGANIZATION INTERNATIONAL AGENCY FOR RESEARCH ON CANCER*.

Wolf, M. E., & Hidy, G. M. (1997). Aerosols and climate: Anthropogenic emissions and trends for 50 years. In *JOURNAL OF GEOPHYSICAL RESEARCH* (Vol. 102). https://doi.org/10.1029/97JD00199

Zerboni, A., Bengalli, R., Baeri, G., Fiandra, L., Catelani, T., & Mantecca, P. (2019). Mixture effects of diesel exhaust and metal oxide nanoparticles in human lung A549 cells. *Nanomaterials*, *9*(9), 1–21. https://doi.org/10.3390/nano9091302

Zhu, X. F., Li, W., Ma, J. Y., Shao, N., Zhang, Y. J., Liu, R. M., … Wang, S. M. (2015). Knockdown of heme oxygenase-1 promotes apoptosis and autophagy and enhances the cytotoxicity of doxorubicin in breast cancer cells. *Oncology Letters*, *10*(5), 2974–2980. https://doi.org/10.3892/ol.2015.3735

7.2 SUPPLEMENTARY DATA CHAPTER VII

Supplementary data S.1

Gene	Primer sequences *5'-forward-3'* *5'-reverse-3'*		Thermal cycling conditions
CCND1	CGTGGCCTCTAAGATGAAGGA	CGGTGTAGATGCACAGCTTCTC	45 cycles of 95°C for 10 minute, 95°C for 15 minutes 60°C for 1 minutes + dissociation stage.
Ki 67	CCCGTGGGAGACGTGGTA	TTCCCGTGACGCTTCCA	
CYP1A1	TGAGAACGCCAATGTCCAGC	GCCGTGACCTGCCAATCA	
MMP1	GGGAGATCATCGGGACAACTC	GGGCCTGGTTGAAAAGCAT	
HMOX-1	TACCACATCTAT GTGGCCCTG	TGGCTGGTGTGTA GGG GAT	
HIF 1α	GCTGATTTGTGAACCCATTCC	TTCATATCCAGGCTGTGTCG	
NfkB	AAGTGCAGAGGAAACGTCAGAAG	CTACCACCGCCGAAACTATCC	
SERPIN-B2	TGTGGGTTCATGCAGCAGAT	AAGCTCGCAGACTTCTCACC	
EREG	ATCACAGTCGTCGGTTCCAC	AGGCACACTGTTATCCCTGC	
IL-1β	ACGATGCACCTGTACGATCACT	CACCAAGCTTTTTTGCTGTGAG	
IL-24	AGG CGG TTT CTG CTA TTC C	GAG CTG CTT CTA CGT CCA ACT	
GAPDH	TGGACTCCACGACGTACTCAG	TGGACTCCACGACGTACTCAG	

Table S.1: Primers used for rt-PCR and Therma cycling condition

Supplementary data S.2

For the detection of endotoxin in the two samples was used a LAL Chromogenic Endotoxin Quantitation Kit (Thermo Scientific™ Pierce™), following the manufacturer's instructions and working in sterile condition and with endotoxin-free materials. The absorbance of each sample was measured by a multiplate reader (Infinite200Pro, TECAN, Männedorf, Switzerland) at the wavelength of 405-410nm. The developed colour intensity is proportional to the amount of endotoxin present in the sample and can be calculated using a standard curve and express as EU/mL.

	EU/ml
EURO 3	0,86
Wood	1,57

Table S.2: LAL test.

Supplementary data S.3

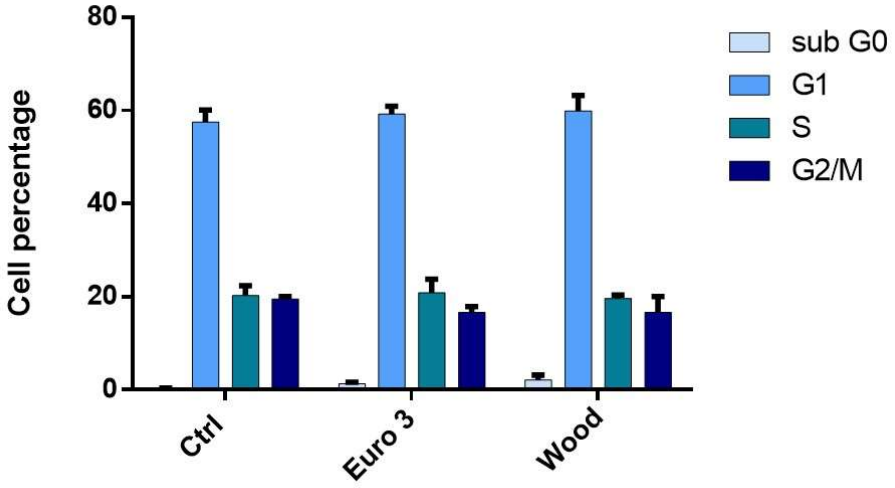

Figure S.3: Cell Cycle.: Samples were analysed through cytofluorimeter and are data represent the mean +/- SE of three independent experiments.

CHAPTER VIII

SUMMARY OF MAJOR FINDINGS

The aim of this research was to analyse and compare the in vitro effects of particles emitted from different sources using human lung cells, focusing on the relationship between the particles P-chem properties and the cellular and molecular pathways that drive the biological health effects of specific PM sources. The work was focus also on the analysis of emissions from old and latest-generation diesel vehicles. The research presented emphasized the role of particle physical and chemical composition in triggering significant biological outcomes.

In this chapter the major findings of the research are synthesized.

In the first part of the study (Chapter III and IV), A549 alveolar cells were used to test the effects of a standard DEP (SRM 2975), representing the traffic exhaust contribution to the urban emissions. Since in real conditions the population is exposed to a mixture of different particles, it is possible that the co-exposure to different co-contaminants can lead to a distinct toxicity compared to the well-known biological responses induced by the single compounds. For this reason, DEP has been tested alone and in co-exposure with metal oxide nanoparticles (MeO NPs), which in an urban pollution scenario are normally present as a product of brake wear, tire and road wear and which constitute the non-exhaust component of fine and ultrafine PM. In fact, in high traffic areas, non-exhaust emissions represent a major source of a number of metals into ambient air, specifically Zn and Cu. In order to understand the possible mixture's effects of DEP and non-exhaust particles, we chose CuO NPs and ZnO NPs as representative MeO NPs. In this work, the pivotal role of ions release from NPs in their toxic outcomes, and how the bioavailability of this metals can change in the presence of DEP, have been demonstrated. Extra- and intra-cellular release of Cu ions from the surface of soluble CuO NPs might have been limited by a sort of passivation effect exerted by DEPs, which can justify the lower toxicity of DEP + CuO

mixture. ZnO NPs trigger their cytotoxic effects in lung cells mainly thanks to the massive release of zinc ions, which seemed to be almost unaffected by the presence of DEP. The enhanced toxicity observed for the DEP + ZnO mixture was largely attributable to an increased NPs uptake by the lung epithelial cells. Moreover, the co-exposure to MeO NPs and DEP highly increases the toxicity of DEP. The analysis of cells death confirmed that CuO are the most cytotoxic NPs, and that they induced apoptosis at the lowest concentration (10 μg/mL) and necrosis at the highest concentration (20 μg/mL) of exposure. We demonstrated that NP-mixture exposure can result in different cellular toxicity than the single counterparts: NPs can either reduce the toxicity of DEP (CuO) or enhance it (ZnO) through a mechanism that may involve autophagy as cellular response to these stressors. In fact, CuO and DEP+ZnO treatments showed a possible activation of the autophagy pathway, as consequence of particles sequestration in lysosomes for degradation of harmful compounds. On the other hand, a modification of cell-cell interaction among adjacent epithelial cells inside A549 colonies has been evaluated after exposure to particles in order to investigate whether key hallmarks of colonies' phenotype have been changed. Here we proposed a method based on colonies' classification (4 types of colonies) to evaluate the cell-cell interaction within the colonies. CuO individual particles and in mixtures with DEP, but at a lower extent also ZnO and its mixtures, induced severe modifications in cell-cell interaction, on adhesion molecules (E-cadherin) and consequentially on colonies formation, morphology and dimensions. In particular, exposure to CuO NPs strongly affected the interaction between cells inside the colonies, leading to an increased number of colonies here denominated as type D, characterized by less adhesive cells with augmented motility and invasiveness capability. This evidence suggests that a repeated exposure to such particles could lead to the activation of the epithelial-to-mesenchymal transition (EMT) pathway, contributing to the progression and metastasizing of lung cancer.

Overall, the results from this study showed that MeO NPs in mixture with airborne DEP could differently affect lung cell toxicity, evidencing the importance to test the possible synergistic or antagonistic effects of different environmental particles.

In chapter V a study on the *in vitro* pulmonary and vascular effects induced by different diesel exhaust particles was reported. The effects of three DEPs, two standard reference

materials (SRM 1650b and 2975) and one DEP directly sampled from a Euro 4 vehicle without Diesel Particulate Filter (DPF) have been compared. The SRMs DEPs have been produced under controlled conditions and are representative of the emission of a heavy engine (SRM, 1650b) and a light engine (SRM, 2975), while DEP Euro 4 was collected from a light duty engine run over a chassis dyno, following an Artemis STOP&GO driving cycle, typic of a high traffic area. In the present work, the effects induced by the three different DEPs on the bronchial cell line BEAS-2B were preliminary studied, in order to investigate the primary response of the respiratory epithelium. Afterward, endothelial pulmonary cells activation was investigated. To this purpose, a conditioned media and a co-culture model were set up by using BEAS-2B and the microvascular lung HPMEC cells. A sequence of events, linking DEP exposure to pulmonary oxidative stress and inflammation with consequent indirect activation of the vascular endothelium has been demonstrated. A statistically significant increase in the expression of ICAM-1 and VCAM-1 was observed only after exposure to DEP Euro 4, which was the only sample able to induce oxidative and inflammatory response in lung epithelial cells. In our research, the correlation between the release of the pro-inflammatory mediators, such as IL-6 and its soluble receptor sIL-6R and VEGF, and the increased expression of ICAM-1 and VCAM-1 in endothelial cells was confirmed, since treatments with DEP SRMs did not induce the epithelial release of IL-6 and consequently did not promote an endothelial response. Furthermore, we have also observed that Euro 4 DEP is able to induce the phosphorylation of the Histone H2AX, suggesting an activation of DNA repair machinery. In this research, the responses obtained from monocultures and conditioned media are congruent with the results from co-culture experiments towards early phase inflammation. Moreover, this study proved that it is possible to investigate the response in endothelial cells indirectly exposed to UFPs. The data obtained have shown that only DEP Euro 4, which had the major content of polycyclic aromatic hydrocarbons (PAHs) and metals, were able to induce oxidative stress, inflammation, and consequent endothelial activation, as demonstrated by the expression of adhesion molecules and the release of inflammatory markers from endothelial cells. SRMs, which have a lower content of PAHs and metals were not effective under our experimental conditions.

In chapter VI, PM emissions and related biological effects of an old generation diesel vehicle (or Euro 3) with the latest generation vehicle (Euro 6) during the regeneration of diesel particulate filter (DPF) were compared using BEAS-2B cells as *in vitro* model. Exhaust particles emission from a Euro 6 vehicle (with DPF) is much lower than emission from Euro 3 vehicle (without DPF), as DPF very efficiently reduces the solid particles emission. When the DPF regeneration occurs the total particle emission increases, with similar speeds, on average up to four order of magnitude compared to DPF normally working. Although the latest generation engines emit particulates only during the regeneration of DPF, which mainly occurs for few minutes at high speeds, the emissions from Euro 6 during regeneration of DPF are characterized of a higher number of ultrafine particles (< 0,1 µm) compared to the old generation diesel vehicle. The emitted particles also resulted different in their physico-chemical composition, with Euro 6 DEP showing less PAHs content with respect to Euro 3 ones, but resulting enriched in some metals (e.g., Fe, Zr according to EDX-analyses). Different biomarkers (IL-6, IL-8, IL-24, EREG and γ-H2AX) were study with the aim to compare the inflammatory, carcinogenic and genotoxic effects of DEP from Euro 3 and Euro 6 vehicles. The biological analyses showed that Euro 3 DEP activates the typical pathways (inflammation, carcinogenicity) induced by combustion-derived particles, while Euro 6 DPF regeneration DEP modulates such toxicological responses at lower extent. However, the physico-chemical peculiarities of Euro 6 DEP might have been responsible of the sub-acute effects registered in this work, like the induction of DNA-repair enzymes and the alteration of the microtubular dynamics. The higher increase of the inflammatory biomarkers after exposure to Euro 3 might be the consequence of the higher PAHs concentration, which in turn may trigger an aryl hydrocarbon receptor (AhR)-mediated cell response. These preliminary evidences suggest that further investigations are required to better address the toxicological risk of the emissions during Euro 6 DPF regeneration.

In chapter VII the properties and biological effects of diesel exhaust from an Euro 3 vehicle was compared to that of wood burning derived CDPs on BEAS-2B bronchial cells. These results proved that biomass particles produced by a modern stove propelled with beech wood had lower biological effects compared to DEP from an old diesel engine. DEP was confirmed as a very hazardous component of the urban PM, able to induce inflammation, genotoxicity and modulation of several genes involved in relevant cellular toxic responses:

xenobiotic metabolism (CYP1A1; MMP1); oxidative stress (HMOX-1); inflammatory response (IL-1β); carcinogenesis (IL-24; EREG) and EMT (SERPIN-B2). However, since an important modulation of CYP1A1 genes and other genes (e.g., IL-24) occurred also in cells exposed to Wood CDPs, consequences on human health from a chronic exposure to the Wood sample cannot be excluded, as also suggested by the induction of IL-6 production at a later endpoint of exposure (48 h). The stronger biological effects of DEP particles could be explained by the physic properties, in fact diesel particles from Euro 3 vehicle are smaller in size compared to Wood ones, and they can be easily internalized by cells. Moreover, the chemical properties of DEP particles (higher content of phenanthrene, pyrene and fluoranthene as PAHs and the presence of Zn and Fe as trace elements) has been previously found in Euro 4 emitted DEP, as reported in Chapter VI, and their composition has been associated with relevant toxicological effects. Despite Wood CDPs present a higher content of total PAHs with respect to DEP Euro 3, this does not determine a higher genotoxic effect as it would be expected, suggesting once more that for wood CDPs long term exposure or repeated doses are needed to induce adverse biological outcomes.

A schematic representation of the p-chem of the particles analysed in this work of thesis is shown in Figure 1, while the major findings regarding the biological outcomes are summarized in Figure 2.

CHARACTERIZATION OF PARTICLES

	Elemental composition (Most abundant metal)	**Tot PAHs (ng/mg)**	**Size** (Z-Average (nm) in cell medium)
SRM 2975	Low metals content	81,69	336.13 ± 38.89
SRM 1650b	Low metals content	202	471.33 ± 50
Euro 3	Fe, Al, P, Ca	394	328.87 ± 4.7
Euro 4	Ca, Al, Zn, K, Fe	592	388.4 ± 7.07
Euro 6 (DPF regeneration)	DEP presents some particles richer in Fe, Zr.	261	317.47 ± 1.9
Wood CDPs	K, Al, Ca	809	564.9 ± 2.3

Figure 1: A schematic representation of the p-chem of the carbonaceous particles analysed in this work of thesis, included the most abundant metals, the total PAHs and the Z-average of each particles analyzed in culture medium.

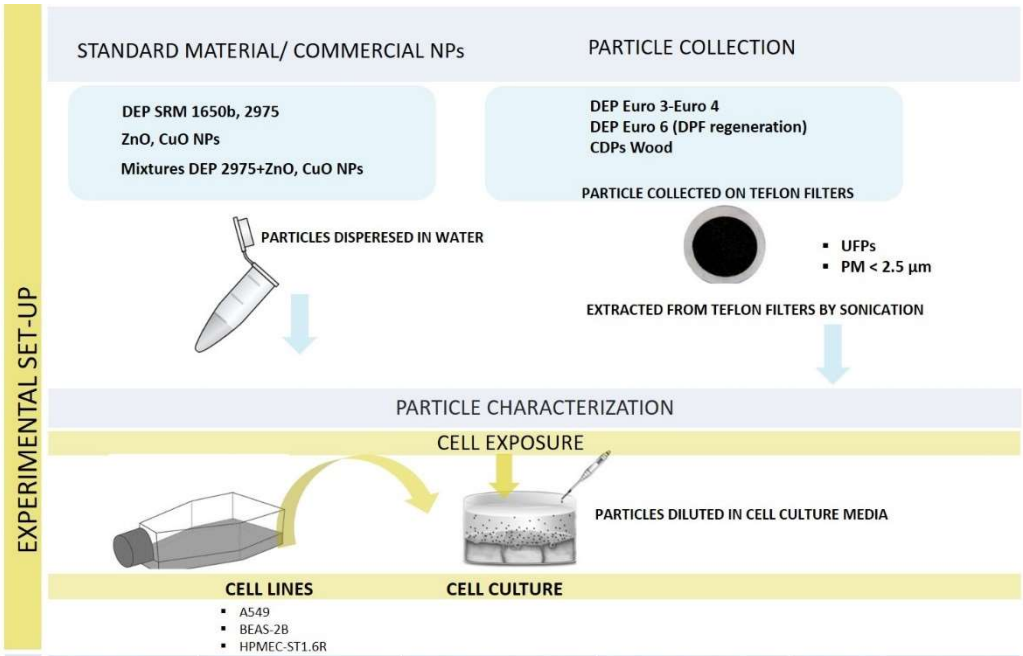

RESULTS

PARTICLES STUDIED	IN VITRO MODEL	CONCENTRATION USED*	TIME OF EXPOSURE	BIOLOGICAL EFFECTS
SRM DEP 2975	A549 BEAS-2B, HPMEC-ST1.6R (monoculture, conditioned media-co-culture)	5 µg/cm² 10 µg/cm²	3-24-48-72 h	No significant effects
SRM DEP 1650b	BEAS-2B, HPMEC-ST1.6R (monoculture, conditioned media-co-culture)	5 µg/cm²	24 h	↑ ROS HO-1
DEP+ZnO	A549 (monoculture)	10 µg/cm² of DEP+ 1, 1.5; 2; 2.5 µg/cm² ZnO	3-24-48-72 h	Cytotoxic effects Cytostatic effects ↓ E-cadherin LC3B ↑
ZnO	A549 (monoculture)	10 µg/cm² of DEP+ 1, 1.5; 2; 2.5 µg/cm² ZnO	3-24-48-72 h	Cytotoxic effects Cytostatic effects ↓ E-cadherin IL-8 ↑
DEP+ CuO	A549 (monoculture)	10 µg/cm² of DEP+ 1, 1.5; 2; 2.5 µg/cm² CuO	3-24-48-72 h	Cytotoxic effects Cytostatic effects Cell cycle block at G1-S ↑ LC3B
CuO	A549 (monoculture)	1, 1.5; 2; 2.5 µg/cm²	3-24-48-72 h	Cytotoxic effects Cytostatic effects ↑ IL-8 Cell cycle block at G1-S ↓ E-cadherin LC3B ↑
DEP Euro 3	BEAS-2B (monoculture)	5 µg/cm²	24-48 h	↑ IL-6; IL-8; EREG; IL-24; γ- H2AX MN NBUDs ↑ CYP1A1 MMP1 HMOX-1 SERPIN-B2 IL-1β
DEP Euro 4	BEAS-2B, HPMEC-ST1.6R (monoculture, conditioned media-co-culture)	5 µg/cm²	24 h	↑ γ- H2AX NF-Kb IL-6; sIL-6R; IL-8; VEGF VCAM-1; ICAM-1 ↑ ROS HO-1
DEP Euro 6 (DPF regeneration)	BEAS-2B (monoculture)	5 µg/cm²	24 h	↑ γ- H2AX; IL-24
Wood CDPs		5 µg/cm²	24-48 h	↑ IL-6 ↑ CYP1A1 IL-24 ↓ HMOX-1

Figure 2: Schematic presentation of the experimental set-up and main results from toxicological studies. *The concentration used in experimental studies has been converted in µg/cm^2 corresponding to the µg/mL presented in the chapters.

Altogether the different approaches enlighten that after exposure to inhaled fine and ultrafine particles some biological pathways are usually involved and should be investigated, including:

- Oxidative stress (ROS formation and HMOX-1 expression) and consequent DNA damage (γ-H2AX expression)
- Inflammation (IL-6, IL-8) and soluble markers release (sIL-6r, IL-24, EREG)
- Endothelial dysfunction at vascular level (ICAM-1 and VCAM-1 upregulation)
- Genotoxic effects (MNs upregulation) and EMT progression (E-cadherin downregulation)
- Autophagy (LC3B expression and autophagosome formation)

CHAPTER IX

GENERAL CONCLUSIONS AND FUTURE PERSPECTIVES

Air pollution constitutes a major risk to human health in the 21st century in both developed and developing countries (Kumar et al. 2014). The World Health Organisation (WHO) estimates that air pollution is accountable for 7 million deaths every year globally, ascribable to the joint effects of household and ambient air (WHO 2014). Reducing the health effects from urban air pollution is mainly above the control of single individual and requires action by public authorities at national and international levels, through the development and implementation of long-term policies and programs aimed to mitigate air pollution and improve public health. Furthermore, considering the economic costs of air pollution, public policies aimed at controlling and reducing pollution entail also large economic benefits (Dechezleprêtre et al.2020). The chemical properties and toxicological profiles of air pollutants mainly depend on the emitting sources (Hime et al. 2018), and several studies have generally demonstrated a great impact of PM on health (WHO, 2013). The European Union's air quality directives (2008/50/EC Directive on Ambient Air Quality and Cleaner Air for Europe and 2004/107/EC Directive on heavy metals and polycyclic aromatic hydrocarbons in ambient air) establish the pollutant concentrations limits value that shall not be exceeded in a defined number of days per years. However, authorities should improve air quality management programs, in order to keep PM concentrations below the defined limit values. Premature deaths attributable to $PM_{2.5}$ are expected to decline by 54 % from 2005 to 2030, if European Union legislations will be entirely implemented (EEA 2020). Interdependence exists between toxicological studies and regulatory process. Toxicological studies could be useful in orienting environmental policies, indeed the aim of toxicity testing is to provide information about PM properties and biological interactions, so that the health and environmental risks associated to PM exposure can be fully evaluated. Information from toxicity testing should be employed by

national and international agencies to define an acceptable concentration of environmental agents and to protect public health (Persad 2009). Moreover, the knowledge improvement related to the molecular and cellular mechanisms leading to adverse health effects derived from PM exposure, should be used to identify biomarkers for epidemiological and clinical studies, and to recognize susceptible individuals in the population (Yang et al. 2017).

Despite many studies have been performed to investigate the inhalation toxicity profile of PM, the correlation between physical and chemical composition of particles with the biological outcomes have not yet been totally understood. Furthermore, the influence of the different emission sources and the consequent biological effects of the emitted particles is still unclear.

The present work provides a focus on the toxic effects induced by exhaust and non-exhaust particulates sources and by a mixtures condition of both, testing particles representative relevant sources of fine and ultrafine PM in urbanized areas.

The SRM DEPs are well characterized and widely used in toxicological studies. Two types of standard DEPs were used in this work: 2975 and 1650b SRM. Both SRM DEPs showed more limited *in vitro* effects than DEP collected from diesel vehicles exhaust emission. This suggests that the use of sampled particles is a preferable choice, as it provides a more realistic picture of the toxicological profile of the emitted particles. However, the standard DEP 2975 proved to be very useful in the study of mixture effects with metal oxide nanoparticles of CuO and ZnO. In these studies, the suggestion that NP-mixture exposure can lead to different cellular toxicity than the single counterpart was confirmed. The co-exposure with DEP can either reduce the toxicity of NPs or enhance it. This finding indicates that, in the light of providing experimental results more strictly reflecting real-life environmental conditions, the possible interaction of different hazardous airborne particles, and the final toxicity deriving from the mixture effects should be evaluated. DEPs collected from old diesel vehicle without DPF (Euro 3 and Euro 4) were confirmed as a very hazardous element of ultrafine fraction of urban PM, able to induce inflammation, oxidative stress, genotoxicity, endothelial activation, and modulation of several genes

involved in relevant cellular toxic responses. Both samples (Euro 3 and Euro 4 DEPs) present a similar chemical-physical profile, which seem to be effective in inducing important toxicological outcomes. In recent years, the latest generation diesel engines equipped with after-treatment system (DPF) have started to circulate in the developed countries. New diesel vehicles (Euro 6) with DPF are approaching to reduce emissions. Although the latest generation diesel vehicle emits particulates only during regeneration, which generally occurs at high speeds, therefore mainly on highways and not in urban centres, the exhaust emissions from Euro 6 during regeneration of DPF presents a higher number of UFPs compared to the old generation diesel vehicle. Moreover, the emitted particles show different physico-chemical composition compared with DEP emitted from an old vehicle without DPF, with Euro 6 showing less PAHs content but enriched in some metals (e.g Fe). The effects and the physico-chemical characteristics of the DEP Euro 3 were also compared with Wood CDPs. This study proved that biomass particles produced by a modern stove propelled with beech wood had lower toxic effects compared to DEP. Despite Wood CDPs present a higher content of total PAHs respect to DEP Euro 3, this does not induce a higher genotoxic effect as expected. However, in the light of these results, possible consequences on human health from a chronic exposure to the Wood CDPs should not be excluded.

The results presented in this thesis offer a contribution to the understanding of the physic-chemical properties and biological outcomes of particulate mostly relevant to public health. This thesis highlights three main aspects that should be considered in the evaluation of risk from exposure to airborne particulate matter:

- The use of particles collected and derived from different emission sources are representative of a more realistic exposure scenario, compared to the standard reference material.
- Exposure to mixtures of different particles should be assessed in order to better understand the risk derived from a co-exposure scenario from multiple sources.
- The biological mechanisms involved in the response to different particles are related to their physicochemical properties, which finally depend on the emission source, operating conditions, and eventual treatment processes.

The future improvement of air quality limit values in highly polluted urban and industrialized areas will require an accurate evaluation of the biological impact of particulate from different emission sources, with a specific focus on the most important UFPs sources, from both exhaust and non-exhaust sources. In fact, there are not enough scientific evidences that limiting only particle mass emissions (PM_{10}, $PM_{2.5}$), as the existing legislation does, will finally lead to a significant reduction of UFPs emissions (Cassee et al. 2019). This underlines the need to establish more strict regulatory strategies and measures to mitigate the concentration and impacts of high UFPs, considering their high health risks.

In the next future new approaches and methods should be implemented to assess the effects of inhaled particles on human health. These approaches will be established on mechanisms of toxicity and by adopting the use of *advanced in vitro* and exposure models.

Considerable challenges remain in the evaluation of toxicological outcomes and consequent health effects of PM, and these include:

- *Creating a validated lung in vitro models based on realistic physiological exposure conditions*: the evolution of *in vitro* models for toxicological studies is greatly supported by the principles of 3Rs (Replacement, Reduction and Refinement). Respect to the two-dimensional (2D) *in vitro* models, the new advanced models such as organ-on-a-chip technologies (OOC) or three-dimensional (3D) *in vitro* models may replace experiment on animals and reduce the gap between in vivo and in vitro studies(Alépée et al. 2014). New models for the respiratory system have been developed in the last years consisting of 3D airway models usually composed of a respiratory epithelium cultured on air-liquid-interface (ALI)(Hufnagel et al. 2020).

- *Identifying more in detail developed adverse outcome pathways (AOPs) from PM inhalation:* AOP framework is a systematic process which defines mechanistic connections between a molecular initiating event, intermediate key events and the final adverse outcome. This approach facilitates the studies of health effects resulting from exposure to PM and air pollution mixtures, because it is focused on the ability of pollutants to impact on a common clinical endpoint that is valuable in humans (Halappanavar et al. 2020).

- *Deeper investigating long-term chronic toxicological effects of PM:* epidemiological and toxicological studies on the chronic effects of PM components is limited, in contrast to numerous short-term studies. There is a requirement for further researches in this area and to design experimental studies that are able to tease out the effects of long-term exposure to PM (Wyzga and Rohr 2015).

- *Investigating the effects of mixtures and the cumulative, synergistic, and antagonistic interactions of the different component of PM:* traditional risk assessment methods assume that the components of a mixture adhere to the concentration addition model. Thus, mixture toxicity can be evaluated by the summation of the individual component toxicities. Nevertheless, interactions can occur between particles into a mixture condition, which can modify the toxicity so that it could be more or less than expected from the single constituents (Heys et al. 2016). Therefore, in a perspective of cumulative-risk assessment it is necessary to evaluate the mixture effects of the different component of PM.

9.1 BIBLIOGRAPHY

Alépée, Natalie et al. 2014. “State-of-the-Art of 3D Cultures (Organs-on-a-Chip) in Safety Testing and Pathophysiology.” In *Altex*, Elsevier GmbH, 441–77. /pmc/articles/PMC4783151/?report=abstract (January 4, 2021).

Cassee, Flemming R., Lidia Morawska, and Annette Peters. 2019. “Ambient Ultrafine Particles : Evidence for Policy Makers.” : 1–23.

Dechezleprêtre, Antoine, Nicholas Rivers, and Balazs Stadler. 2020. *THE ECONOMIC COST OF AIR POLLUTION: EVIDENCE FROM EUROPE JT03464647 OFDE*. www.oecd.org/eco/workingpapers (December 28, 2020).

EEA. 2020. “The European Environment — State and Outlook 2020 — European Environment Agency.” https://www.eea.europa.eu/publications/soer-2020 (December 28, 2020).

Halappanavar, Sabina et al. 2020. “Adverse Outcome Pathways as a Tool for the Design of Testing Strategies to Support the Safety Assessment of Emerging Advanced Materials at the Nanoscale.” *Particle and Fibre Toxicology* 17(1): 16. http://creativecommons.org/licenses/by/4.0/.TheCreativeCommonsPublicDomainDedicationwaiver (January 4, 2021).

Heys, Kelly A. et al. 2016. “Risk Assessment of Environmental Mixture Effects.” *RSC Advances* 6(53): 47844–57. www.rsc.org/advances (January 4, 2021).

Hime, Neil, Guy Marks, and Christine Cowie. 2018. “A Comparison of the Health Effects of Ambient Particulate Matter Air Pollution from Five Emission Sources.” *International Journal of Environmental Research and Public Health* 15(6): 1206. http://www.mdpi.com/1660-4601/15/6/1206 (December 29, 2020).

Hufnagel, Matthias et al. 2020. “Toxicity and Gene Expression Profiling of Copper- And Titanium-Based Nanoparticles Using Air-Liquid Interface Exposure.” *Chemical Research in Toxicology* 33(5): 1237–49. https://dx.doi.org/10.1021/acs.chemrestox.9b00489 (January 4, 2021).

Kumar, Prashant et al. 2014. “Ultrafine Particles in Cities.” *Environment International* 66: 1–10.

Persad, Amanda S. 2009. “Regulatory Toxicology.” In *Information Resources in Toxicology*, Elsevier Inc., 401–6.

WHO. 2014. “WHO | 7 Million Premature Deaths Annually Linked to Air Pollution.” *WHO*.

WHO Regional Office for Europe. 2013. “Health Effects of PM.” https://www.ncbi.nlm.nih.gov/books/NBK361803/ (December 29, 2020).

Wyzga, R.E., and A.C. Rohr. 2015. “Long-Term Particulate Matter Exposure: Attributing Health Effects to Individual PM Components.” *Journal of the Air & Waste Management Association* 65(5): 523–43. https://www.tandfonline.com/doi/full/10.1080/10962247.2015.1020396 (January 4, 2021).

Yang, Lixin et al. 2017. “Biomarkers of the Health Outcomes Associated with Ambient Particulate Matter Exposure.” *Science of the Total Environment* 579: 1446–59.

LIST OF PUBLICATIONS

This thesis is based on the following publications:

- **Zerboni A**, Bengalli R, Baeri G, Fiandra L, Catelani T, Mantecca P. Mixture Effects of Diesel Exhaust and Metal Oxide Nanoparticles in Human Lung A549 Cells, **Nanomaterials** (Basel). 2019;9(9):1302. Published 2019 Sep 11. doi:10.3390/nano9091302. *(Chapter III)*

- Bengalli, R.*, **Zerboni, A***., Marchetti, S., Longhin, E., Priola, M., Camatini, M., Mantecca, P. 2019. In vitro pulmonary and vascular effects induced by different diesel exhaust particles. **TOXICOLOGY LETTERS**, 306, 13-24. DOI: 10.1016/j.toxlet.2019.01.017
  (*Equal contributors: Rossella Bengalli, Alessandra Zerboni). *(Chapter V)*

- **A.Zerboni**; T.Rossi; R.Bengalli; T.Catelani; C.Rizzi; M.Priola; S.Casadei and P.Mantecca
  Comparative evaluation of particulate emission and biological effects from an old generation diesel vehicle and latest generation (Euro 6) one over Diesel Particulate Filter (DPF) regeneration.
  Science of the Total Environment. (Under review Ref. No: STOTEN-D-20-31150). *(Chapter VI)*

LIST OF ABBREVIATIONS

ABB: air-blood-barrier

AOPs: adverse outcome pathways

BSA: bovine serum albumin

CAM-1: intercellular adhesion molecule-1

CBPI: Cytokinesis Block Proliferation Index

CDPs: combustion derived particles

CFE: Colony forming efficiency

COPD: chronic obstructive pulmonary disease

CVD: cardiovascular diseases

CYP1A1: Cytochrome P450 Family 1 Subfamily A Member 1

Dae: aerodynamic equivalent diameter

DEP: diesel exhaust particles

DLS: dynamic light scattering

DPF: Diesel Particulate Filter

ECU: Electronic Control Unit Engine

EEPS: Exhaust Particle Sizer

ELPI: Spectrometer and an Electrical Low-Pressure Impactor

EREG: Epiregulin

FBS: fetal bovine serum

GC-MS: Gas Chromatography-Mass Spectrometry

HMOX-1: heme oxygenase 1

HO-1: heme-oxygenase-1

ICP-MS: Inductively Coupled Plasma Mass Spectrometry

IL-1β: interleukin 1-β

IL-24: Interleukin-24

IL-6: interleukin-6

IL-8: interleukin-8

LDSA: lung-deposited surface area

MMP1: Matrix metalloproteinase 1

MN: micronucleus

MTT: 3-(4,5-Dimethylthiazol-2-Yl)-2,5-Diphenyltetrazolium Bromide.

NBUDs: nucelar buds

NIST: National Institute of Standard and Technology

NPs: nanoparticles

OECD: Organisation for Economic Co-operation and Development

PAHs: polycyclic aromatic hydrocarbons

PBS: Phosphate-buffered saline

PM: particulate matter

PN: Particle Number

PNC: particle number concentration

ROS: reactive oxygen species

SRMs: Standard Reference Materials

TEM: transmission electron microscope

TSP: total suspended particles

UFPs: ultrafine particles

VCAM-1: vascular cellular adhesion molecule-1

VEGF: vascular endothelial growth factor:

WTLC: Worldwide harmonized Light vehicles Driving Cycle

y-H2AX: phospho-histone H2AX

ZO-1: zonula occludens-1

ACKNOWLEDGMENTS

This project was made possible thanks to the scholarship granted by Innovhub, Stazioni Sperimentali per l'Industria (SSI) and by the project Protect (EU-H2020, project n.720851).